Greenwich Academic Literature Archive (GALA)
– the University of Greenwich open access repository
http://gala.gre.ac.uk

Citation:

Bernasko, Peter Kojo (2012) Study of intermetallic compound layer formation, growth and evaluation of shear strength of lead-free solder joints. PhD thesis, University of Greenwich.

Please note that the full text version provided on GALA is the final published version awarded by the university. “I certify that this work has not been accepted in substance for any degree, and is not concurrently being submitted for any degree other than that of (name of research degree) being studied at the University of Greenwich. I also declare that this work is the result of my own investigations except where otherwise identified by references and that I have not plagiarised the work of others”.

Bernasko, Peter Kojo (2012) Study of intermetallic compound layer formation, growth and evaluation of shear strength of lead-free solder joints. ##thesis_type##, ##institution##

Available at: http://gala.gre.ac.uk/9452/

Contact: gala@gre.ac.uk

Study of Intermetallic Compound Layer Formation, Growth and Evaluation of Shear Strength of Lead-Free Solder Joints

By

Peter Kojo Bernasko

Electronics Manufacturing Engineering Research Group (EMERG)
School of Engineering
University of Greenwich, UK

A thesis submitted in partial fulfilment of the requirements of the University of Greenwich for the Degree of Doctor of Philosophy

May 2012

DECLARATION

I certify that this work has not been accepted in substance for any degree, and is not currently submitted for any degree other than that of Doctor of Philosophy (PhD) being studied at the University of Greenwich. I also declare that this work is the result of my own investigation except where otherwise identified by references and that I have not plagiarised the work of others.

Signed by the Student:

Date:

Signed by 1st Supervisor:

Date:

Signed by 2nd Supervisor:

Date:

ACKNOWLEDGEMENT

I would like to take this opportunity to express my sincerest gratitude and appreciation to my supervisors, Professor Ndy Ekere and Dr. Sabuj Mallik for their great support and guidance through the course of my PhD research. I also would like to express my sincerest thanks to my colleagues in the MERG Group for the discussions, valuable suggestions and help in experimental work through the past four years.

I would like to thank Dr Ian Slipper in School of Sciences, University of Greenwich, for his kindness and help in access of laboratory facilities. I wish to give my special acknowledgement to Dr. Alam Ohid a post doctoral fellow with EMERG for help with the Dage bond tester. Thanks are also extended to Dr. Shefui Zachariah for his advice on the thesis write-up.

I am most grateful to Mrs Nicola Cox and Mrs Sharon Wood for arranging MERG meetings and sending feedbacks. Finally, I am forever indebted to my family for their great love, support and encouragement.

ABSTRACT

Solder joints play a very important role in electronic products as the integrity of electronics packaging and assembly rests on the quality of these connections. The increasing demands for higher performance, lower cost, and miniaturisation in hand-held and consumer electronic products have led to the use of dense interconnections. This miniaturization trend means that solder joint reliability remains an important challenge with surface mount electronics assembly, especially those used in hostile environments, and applications such as automobile, aerospace and other safety critical operations.

One of the most important factors which are known to affect solder joint reliability is the thickness of intermetallic compound (IMC) layer formed between the solder and the substrate. Although the formation of an IMC layer signifies good bonding between the solder and substrate, its main disadvantage is that it is also known to be the most brittle part of the solder joint. Thus as the miniaturisation trend continues, and solder joints become even smaller in size, the nature and impact of IMC layer thickness on solder joint reliability becomes even more of a concern with the introduction of new lead-free soldering. Other factors which are known to affect solder joint reliability include the bonding strength, the voiding percentage in joints, the size of the voids and their location within the joint.

The work reported in this thesis on formation and growth of intermetallic compound layer, and evaluation of the shear strength of lead-free solder joints is divided into four main parts. The first part of the study is concerned with understanding of the effect of pad sizes on Inter-metallic compound layer formation and growth for lead-free solder joints. The second part concerns the study of the effect of temperature cycling and reflow profiles on intermetallic growth between Sn-Ag-Cu alloy and Cu substrate. The third part of the study concerns the investigation of the effect of reflow soldering profile optimization on solder volumes using design of experiment technique. The focus of the final part of the study is the investigation of the effect of Inter-metallic Compound thickness on shear strength of 1206 surface mount chip resistor.

The results from the experimental work showed that the pad size has very little influence on the growth of the IMC. The result also shows that the growth of IMC

depends on diffusion rate, temperature and time according to the power-law model; and that the IMC layer thickness is independent of pad size. The significance of this result is that with further reductions in joint size (with IMC layer thickness remaining the same), the ratio of the IMC layer thickness to solder joint size will increase and adversely impact the joint reliability. The work carried out on ageing temperatures and reflow profiles of Sn-Ag-Cu alloy and Cu substrate also showed the reaction-diffusion mechanism of intermetallic compound formation and growth in solder joints. The study also showed that the most significant factor in achieving lower IMC layer thickness and fine microstructures is the time to peak temperature of the reflow soldering process. The effect of IMC layer thickness on the shear strength of Sn-Ag-Cu solder joints was investigated. The relationship of shear strength, interfacial microstructures and fracture surfaces was considered. It is clear that formation of continuous Cu-Sn and SnNiCu layers are the reason for the weak interface strength. The results show that the shear strength of solder joints decreases with increasing ageing time. The results of this study have been disseminated through journal and conference publications and will be of interest to R&D personnel working in the area of high temperature electronics and in particular those working in the field of automotive electronics.

TABLE OF CONTENTS

CHAPTER I: INTRODUCTION

1.1 Surface mount technologies assembly process 1

1.1.2 SMT chip components in electronic packaging 3

1.1.3 Increasing I/O, in flip chip 5

1.1.4 Sn-Ag-Cu solder alloy 5

1.1.5 Intermetallic formation during assembly 6

1.1.6 Thermal cycling and isothermal ageing of electronic assembly 7

1.1.7 Solder joints reliability 8

1.2 **Scope of this research study** 9

1.2.2 Problem statement 9

1.2.3 Research objectives 11

1.3 Structure of thesis 11

CHAPTER II: LITERATURE REVIEW

2.1 Introduction 13

2.2 Previous properties of Lead and Lead-free Solder Alloys 13

2.2.1 Previous studies on lead-bearing solders 13

2.2.2 Previous studies on Lead- free solders 14

2.2.2.1 Previous studies on Sn-Ag-Cu lead-free solder 16

2.3 Previous studies on Solder Alloy Microstructures 23

2.3.1 Previous studies on modification of Pb-free alloy microstructure With the addition of RE elements 29

2.4 Previous Studies on Intermetallic Compound (IMC) 31

2.4.1 Dissolution rate of a metal substrate into molten solder 32

2.4.2 Intermetallic compounds formed between the solder alloy and substrate and within the solder alloy matrix 32

2.5 Previous Studies on Solid State Growth 40

2.6 Previous studies on Reflow Profile 48

2.7 Gaps identified from literature review 55

2.8 Summary 56

CHAPTER III: SOLDER JOINT METALLURGY AND MICROSTRUCTURE

3.1 Introduction 57
3.2 Intermetallic Compound Formation 57
3.2.1 Diffusion 58
3.2.2 Formation of IMC layers 61
3.2.3 Solid state growth 63
3.3 Solidification Process 64
3.3.1 Nucleation and growth 65
3.3.2 Homogeneous Nucleation 66
3.3.3 Heterogeneous Nucleation 67
3.3.4 Activation Energy 68
3.4 Summary 72

CHAPTER IV: EXPERIMENTAL PROCEDURE AND METHODOLOGY

4.1 Introduction 73
4.2 Description of Test Vehicles used in the study 73
4.2.1 Type 1 Test vehicle for evaluation of pad size on IMC 74
4.2.2 Type 2 Test vehicle for ageing temperatures and Reflow profiles on IMC 74
4.2.3 Type 3 Test vehicle for reflow profile optimization for Sn-Ag-Cu Solder bumps 75
4.2.4 Type 4 Test vehicle for IMC and shear strength of solder joint 76
4.3 Experimental Equipment 77
4.3.1 Stencil printing of solder paste 77
4.3.2 Reflow soldering 80
4.3.3 Temperature profiles 81
4.4 Isothermal and Temperature cycling ageing 82
4.5 Evaluation of solder joint shear strength 84
4.6 Metallographic preparation of solder joint test samples 84
4.6.1 Cutting 85
4.6.2 Mounting 85

4.6.3 Grinding 85
4.6.4 Polishing 86
4.7 Assessment of IMC Layer Thickness 86
4.7.1 Measuring with Reichert microscope 87
4.7.2 Measuring with Scanning Electron Microscope (SME) 88
4.8 **Experimental procedures** 90
4.8.1 Experimental procedure of the effect of pad size on IMC layer formation and growth in Sn-Ag-Cu solder joint 90
4.8.2 Experimental procedure of cycling temperatures and reflow profiles on inter-metallic growth between Sn-Ag-Cu solder alloy and Cu. 91
4.8.3 Experimental procedure of reflow soldering profiles using full factorial design for Sn-Ag-Cu solder bumps on Cu substrate 94
4.8.3.1 Factorial design of experiments 95
4.8.3.2 Assigned parameters of (2^4) full factorial design 96
4.8.4 Experimental procedure of the effect of inter-metallic compound layer thickness on the shear strength of 1206 surface mount chip resistor 99
4.9 Summary **100**

CHAPTER V: EFFECT OF PAD SIZES ON IMC LAYER FORMATION AND GROWTH

5.1 Introduction 101
5.2 Experimental Details 102
5.3 Results 102
5.3.1 Evolution of intermetallic compound microstructures 102
5.3.2 Evolution of microstructure during reflow 103
5.3.3 Microstructures of IMC after Isothermal ageing 106
5.3.4 Analysis of IMC layer composition 109
5.3.5 Effect of ageing time and temperature on IMC 114
5.4 **Discussion of Results** 124

5.5 **Summary** 126

CHAPTER VI: EFFECT OF AGEING TEMPERATURES AND REFLOW PROFILES ON THE INTERMETALLIC GROWTH

6.1 **Introduction** 127
6.2 Experimental details 127
6.3 **Results** 128
6.3.1 Effect of reflow profiles on intermetallic formation and growth 128
6.4 Discussion of Results 136
6.5 **Summary** 138

CHAPTER VII: EFFECT OF REFLOW PROFILES FOR Sn-Ag-Cu SOLDER BUMPS ON CU SUBSTRATE

7.1 Introduction 139
7.2 Full factorial design of experiments (DOE) 139
7.3 Results 140
7.3.1 Analysis of normal probability plot of factor effects 142
7.3.2 Pareto plot analysis 144
7.3.3 Optimiser plot 146
7.3.4 Minitab optimiser parameters reflowed profile 148
7.3.5 Analysis of variance in the reflow soldering parameters 151
7.4 Discussion of Results 153
7.4 Summary 155

CHAPTER VIII: EFFECT OF IMC LAYER THICKNESS ON THE SHEAR STRENGTH OF 1206 CHIP RESISTOR JOINTS

8.1 Introduction 156
8.1.2 Reliability of solder joints 156
8.1.3 Effect of reflow and isothermal ageing on solder joints shear strength 157
8.1.4 Effect of ageing temperatures on Cu-Sn intermetallic compound 158
8.2 Experimental details 159

8.3 Results 159

8.3.1 IMC during reflow process 159

8.3.2 Interfacial reaction between component surface finish and solder deposit during isothermal ageing 162

8.3.3 Interfacial reaction between substrate and solder deposit 163

8.3.4 Evaluation of voids percentage in solder deposit 166

8.3.5 Fracture surface of FR-4 PCB pad and component termination 171

8.4 **Discussion of Results** 175

8.5 **Summary** 178

CHAPTER IX: CONCLUSIONS AND RECOMMENDATION FOR FUTURE WORK

9.1 Conclusions 179

9.2 Suggestion for future work 180

9.3 Publications 182

REFERENCES 183

LIST OF FIGURES

Figure 1.1 Examples of Area Array SMT Packages 3

Figure 1.2 Example of flip-chip on board 4

Figure 1.3 IMC formation in assembly of flip-chip 8

Figure 2.1 Schematic diagram Sn-Pb phase diagram 23

Figure 2.2 Schematic of isothermal section at 400°C (Top View) of the Sn-Ag-Cu phase diagram 25

Figure 2.3 Schematic of isothermal section at 219°C of the Sn-Ag-Cu phase diagram 25

Figure 2.4 Schematic of mass fractions of phases vs. temperature of Sn-3.24wt%Ag-0.57wt%Cu alloy 26

Figure 2.5 Bulk microstructure of eutectic Sn-Ag-Cu Alloy 26

Figure 2.6 Microstructures of Sn-Ag-Cu alloys aged 12 days at 175°C 27

Figure 2.7 Schematic diagram of intermetallic growth during reflow in a joint with low area-to-volume (A:V) Ratio 33

Figure 3.1 Diffusion mechanisms of an atom in solids 59

Figure 3.2 Schematic diagram illustrating the growth of an intermetallic compound 62

Figure 3.3 The total free energy of solid-liquid system changes with the size of the solid 65

Figure 3.4 Schematic of energy changes from the un-reacted to the reacted state 70

Figure 3.5 Illustration of the variation of the free energy during growth competion between a stable compound and metastable compound 71

Figure 4.1 Type 1. Test Vehicle – For Effect of Pad Sizes on IMC layer Formation and Growth 74

Figure 4.2 Type 2. Test Vehicle – Used for Effect of Ageing Temperatures and Reflow Profiles on Formation and Growth IMC 74

Figure 4.3 Type 3 Test Vehicle – Used for Reflow profile Optimization for Sn-Ag-Cu solders bumps on Cu substrate 75

Figure 4.4 Type 3 Test Vehicle - Used for Effect of inter-metallic compound thickness on mechanical strength of 1206 surface mount

chip resistors with nickel termination 77
Figure 4.5 Stencil printing machine (DEK 260 SERIES) 78
Figure 4.6 Pick and place machine (Gold-Plea L20) 78
Figure 4.7 Novastar 2000HT Convection Reflow Oven 79
Figure 4.8 Raddish Electronics SM500CXE Batch Reflow Oven 79
Figure 4.9 Sample of Reflow Profile of Novastar Oven 81
Figure 4.10 Sample Reflow Profile of Raddish Electronics SM500CXE 82
Figure 4.11 Heraeus 4020 Temperature Cycling Chamber 83
Figure 4.12 Dage-4000PXY Bond tester 83
Figure 4.13 Reichert Microscope 87
Figure 4.14 JSM5310LV Scanning Electron Microscope 89
Figure14.15a Temperature cycle profile, T25 (20°C - 25°C) 83
Figure 14.15b Temperature cycle profile, T40 (20°C – 40°C) 93
Figure 14.15c Temperature cycle profile, T60 (20°C - 60°C) 94
Figure 5.1a Solder joint microstructure of pad (B1) after reflow 104
Figure 5.1b Solder joint microstructure of pad (B2) after reflo 104
Figure 5.1c Solder joint microstructure of pad (B3) after reflow 105
Figure 5.1d Solder joint microstructure of pad (B4) 105
Figure 5.1e Solder joint microstructure of Pad Area (B5) 106
Figure 5.2a Representative of SEM micrograph showing microstructure of B1 after 100 hours isothermal ageing 107
Figure 5.2b Representative of SEM micrograph showing microstructure of B1 after 200 hours isothermal ageing 108
Figure 5.2c Representative of SEM micrograph showing microstructure of B1 after 300 hours isothermal ageing 108
Figure5.3a. SEM micrograph showing five spotted locations on sample B1 used for elemental and atomic weight percent analysis after 100 hours isothermal ageing 110
Figure 5.3b. SEM micrograph showing five spotted locations on sample B1 used for elemental and atomic weight percent analysis after 200 hours isothermal ageing 110

Figure 5.3c SEM micrograph showing five spotted locations on
sample B1 used for elemental and atomic weight percent analysis
after 300 hours isothermal ageing 111

Figure 5.4a EDS spectrum of B1 after 100 hours aging showing intensities
of Cu and Sn on IMC form near to the substrate 111

Figure 5.4b EDS spectrum of B1 after 200 hours aging showing intensities
of Cu and Sn on IMC form near to the substrate 112

Figure 5.4c .EDS spectrum of B1 after 300 hours aging showing intensities
of Cu and Sn on IMC form near to the substrate 112

Figure 5.5 Variation of average thickness of IMC as a function of
time during solid-state interfacial reactions of Sn-Ag-Cu solder
of different Cu pad sizes 118

Figure 5.6a. Cu_5Sn_6 and Cu_2Sn intermetallic component layers growth
for sample B1 aged at 175°C 120

Figure 5.6b Cu_5Sn_6 and Cu_2Sn intermetallic component layers growth
for sample B2 aged at 175°C 120

Figure 5.6c Cu_5Sn_6 and Cu_2Sn intermetallic component layers growth
for sample B3 aged at 175°C 121

Figure 5.6d Cu_5Sn_6 and Cu_2Sn intermetallic component layers growth
for sample B4 aged at 175°C 121

Figure 5.6e Cu_5Sn_6 and Cu_2Sn intermetallic component layers growth
for sample B5 aged at 175°C 122

Figure 5.7 Variation of average IMC layer thickness of the samples
after reflow soldering and isothermal ageing of 175°C 123

Figure 6.2a IMC layer aged at 24 hours with T25 temperature
cycle for paste samples P1 128

Figure 6.2b IMC layer aged at 24 hours with T25 temperature cycle for paste samplesP2 129
Figure 6.3a IMC layer aged at 24 hours with T40 temperature cycle for paste samples P1 129
Figure 6.3b IMC layer aged at 24 hours with T40 temperature cycle for paste samplesP2 130
Figure 6.4a IMC layer aged at 24 hours with T60 temperature cycle for paste samplesP1 130
Figure 6.4b IMC layers aged at 24 hours with T60 temperature cycle for paste samplesP2 131
Figure 6.5a IMC thickness for paste P1 as a function of reflow profile and temperature cycle 132
Figure 6.5b IMC thickness for paste P2 as a function of reflow profile and temperature cycle 133
Figure 6.6a Increase in IMC layer thickness of T40 and T60 temperature cycles compared to T25, for paste P1 133
Figure 6.6b Increase in IMC layer thickness of T40 and T60 temperature cycles compared to T25, for paste P2 134
Figure 6.7a IMC layer thickness as a funtion of temperature cycle ageing for different reflow profiles for P1 135
Figure 6.7b IMC layer thickness as a funtion of temperature cycle ageing for different reflow profiles for P2 135
Figure 7.1 Test board with three different sizes of solder bumps 140
Figure 7.2a. Normal probability plots of factor effects of (∅3.1mm) 142
Figure7.2b Normal probability plots of factor effects of (∅3.7mm) 143
Figure 7.2c Normal probability plots of factor effects of (∅4.3mm) 143
Figure 7.3a Pareto chart of effects of (∅3.1mm) 144
Figure 7.3b Pareto chart of effects of (∅3.7mm) 145
Figure 7.3c Pareto chart of effects of (∅4.3mm) 145
Figure 7.4a Response optimizer plot for (∅ 3.1mm) solder bump 146
Figure 7.4b Response optimizer plot for (∅ 3.7mm) solder bump 146
Figure 7.4c Response optimizer plot for (∅ 4.3mm) solder bump 147

Figure 7.5a. Optimal reflow for (∅ 3.1mm) solder bump 149
Figure 7.5b Optimal reflow for (∅ 3.7mm) solder bump 149
Figure 7.5c Optimal reflow for (∅4.3mm) solder bump 150
Figure 8.3a SEM micrographs of the Sn-3.8Ag-0.7Cu solder/1206 joints aged at 175°C as-soldered 159
Figure 8.3b SEM micrographs of the Sn-3.8Ag-0.7Cu solder/1206 joints aged at 175°C for 100 hours isothermal ageing 160
Figure 8.3c SEM micrographs of the Sn-3.8Ag-0.7Cu solder/1206 joints aged at 175°C for 200 hours isothermal ageing 160
Figure 8.3d SEM micrographs of the Sn-3.8Ag-0.7Cu solder/1206 joints aged at 175°C for 300 hours isothermal ageing 161
Figure 8.4a SEM micrographs of the Sn-3.8Ag-0.7Cu solder deposit and substrate aged at 175°C as-reflowed 162
Figure 8.4b SEM micrographs of the Sn-3.8Ag-0.7Cu solder deposit and substrate aged at 175°C for 100 hours 163
Figure 8.4c SEM micrographs of the Sn-3.8Ag-0.7Cu solder deposit and substrate aged at 175°C for 200 hours 163
Figure 8.4d SEM micrographs of the Sn-3.8Ag-0.7Cu solder deposit and substrate aged at 175°C for 300 hours 164
Figure 8.5 IMC thicknesses as a function of ageing time during solid-state interfacial reactions of Sn-Ag-Cu solder with substrate Cu surface finish and component termination of Ni surface finish 165
Figure 8.6a X–Ray, Voids in solder deposits as reflowed 166
Figure 8.6b X–Ray, Voids in solder deposits after 100 hours isothermal ageing 167
Figure 8.6c X–Ray, Voids in solder deposits after 200 hours isothermal ageing 167
Figure 8.6d X–Ray, Voids in solder deposits after 300 hours isothermal ageing 168
Figure 8.7 Evaluation of voids in joints after reflowed and isothermal ageing times 169
Figure 8.8 Average shear strength of samples reflowed, 100hrs, 200hrs and 300hrs ageing. 169

Figure 8.8a Fracture surface of the interface formed between
Sn-3.8Ag-0.7Cu solder alloy and component as-reflowed 170
Figure 8.8b Fracture surface of the interface formed between Sn-3.8Ag-0.7Cu
solder alloy and component at 100 hours of isothermal ageing. 171
Figure 8.8c Fracture surface of the interface formed between Sn-3.8Ag-0.7Cu
solder alloy and component at 200 hours of isothermal ageing. 171
Figure 8.8d Fracture surface of the interface formed between Sn-3.8Ag-0.7Cu
solder alloy and component at 300 hours of isothermal ageing. 172
Figure 8.9a Fracture surface of the interface formed between Sn-3.8Ag-0.7Cu
solder alloy and pad as-reflowed 172
Figure 8.9b Fracture surface of the interface formed between Sn-3.8Ag-0.7Cu
solder alloy and pad at 100 hours of isothermal ageing. 173
Figure 8.9c Fracture surfaces of the interface formed between Sn-3.8Ag-0.7Cu
solder alloy and pad at 200 hours of isothermal ageing. 173
Figure 8.9d Fracture surfaces of the interface formed between Sn-3.8Ag-0.7Cu
solder alloy and pad at 300 hours of isothermal ageing. 174

LIST OF TABLES

Table 2.1 Important properties of solder alloys 15

Table 2.2 Eutectic binary alloys composition and temperatures 15

Table 2.3 Eutectic Sn-Ag-Cu solder composition 17

Table 2.4 Summary of mechanical properties of revelant metals solder alloys and intermetallic compounds 21

Table 2.5a Dissolution of Various Surface Finishes in Different Solder Alloys 36

Table 2.5b Dissolution of Various Surface Finishes in Different Solder Alloys 37

Table 2.6 The Growth Rate of the IMC Layer in the Sn-Pb Solder Alloys 41

Table 2.7 IMC Layer Growth in Various Solder Alloys Aged at 250°C 44

Table 2.8 Reflow profiles used in Skidmore et al (2000) experiments 50

Table 4.1 Reflowed soldering process parameters (IPC/JEDEC) 90

Table 4.2 Pad dimensions of selected components 91

Table 4.3 Reflow profiles used for specimen types P1 and P2 92

Table 4.4 Experimental parameters 96

Table 4.5 High and low signs for the reflow process design 97

Table 4.6 Reflow profile parameter combinations 98

Table 5.1a The (atomic%) compositions of IMC at solder/Cu interface and the solder matrix at 100 hours of isothermal ageing 113

Table 5.1b The (atomic%) compositions of IMC at solder/Cu interface and the solder matrix at 200 hours of isothermal ageing 113

Table 5.1c The (atomic%) compositions of IMC at solder/Cu interface and the solder matrix at 300 hours of isothermal ageing 113

Table 5.2a Measured average values in (µm) of IMC of the five different pad sizes after reflow soldering in (µm) 115

Table 5.2b Measured average values in (µm) of IMC of the five

different pad sizes at 175°C for 100 hours 115

Table 5.2c. Measured average values in (µm) of IMC of the five different pad sizes at 175°C for 200 hours 116

Table 5.2d. Measured average values in (µm) of IMC of the five different pad sizes at 175°C for 300 hours 116

Table 5.3 The coefficient of determinant (R^2) values and power regression model for sample B1, B2, B3, B4 and B5 118

Table 5.4: The coefficient of determinant (R^2) value and power regression model for sample B6 119

Table 5.5. Growth rate constant and time exponent from power regression model of the five samples 119

Table 5.6. Growth rate constant and time exponent d from power regression model of B6 119

Table 5.7 Growth rate constant and time exponent deduced from power regression model of Cu_5Sn_6 122

Table 5.8 Growth rate constant and time exponent deduced from power regression model of Cu_2Sn 123

Table 6.1 Polynomial model fitted data for pastes P1 and P2 136

Table 7.1 Experimental parameters 139

Table 7.2 Average response of ∅ 3.1mm 140

Table 7.3 Average response of ∅ 3.7mm 141

Table 7.4 Average response of ∅ 4.3mm 141

Table 7.5 Minimum values of Minitab optimiser settings 148

Table 7.6 Comparison of Minitab optimiser and recommended IPC IMC response 148

Table 7.7 Analysis of variance for (∅ 3.1mm) 151

Table 7.8 Analysis of variance for (∅ 3.7mm) 151

Table 7.9 Analysis of variance for (∅4. 3mm) 152

Table 8.1 IMC layer thickness during reflow and isothermal ageing 164

CHAPTER I: INTRODUCTION

This study concerns intermetallic compound layer formation, growth and shear strength of lead-free solder joints. The work, which is geared towards lead-free soldering for electronics assembly and packaging used in automotive electronics environment, is part of an urgent world-wide research effort to solve one of the most burning issues affecting solder joint reliability. There is very little research directed towards the understanding of the intermetallic layer formation in Pb-free alloy systems since the implementation of the ban on leaded solder, its effects on long-term solder joint reliability and the understanding of factors associated with long-term in-service behaviour and reliability of the finished solder joints. In many ways, the presence of inter-metallics may indicate that a good metallurgical bond has been achieved, but the main drawback is that such layers are generally brittle and their presence can lead to a loss in shear strength and hence reliability of the joint.

1.1 Surface Mount Technology Assembly Process

Lead-free Surface Mount Technology (SMT) can be achieved reliably if several process requirements are implemented carefully. Some of the important variables include: Melting temperature of alloy, flux chemistry and wetting and surface tension properties of the alloy. The SMT assembly process starts with the deposition of solder paste onto pads on the surface of the PCB, and then the placement of the electronic components onto the PCB. The PCB and components are then reflowed in a reflow soldering oven to form the surface mount solder joints.

The SMT assembly process is so versatile that a variety of SMT packages can be used on the same PCB. SMT components are typically much smaller in size than Through hole technology (THT) components and can be mounted on both sides of the PCB – this means that SMT assemblies can achieve much higher board densities than THT boards. This size and weight advantage meant that SMT

components achieved very widespread usage even though THT components were generally less expensive than SMT components (Jirsa and Dusek, 2011).
SMT has many other benefits. Among the most important design-related benefits are the significant saving in weight and real estate, and the electrical noise reduction. Surface mount components can weigh as little as one-tenth of the through hole components. This leads to a significant reduction in the weight of surface mount assemblies. As a result of this lower weight of components, SMT assembly technique also provides improved shock and vibration resistance, and because of their shorter lead lengths, the SMT packages have easy loading than through-hole packages, resulting in reduced package noise (Zhaozhi et al, 2010).

In addition to the foregoing examples of design benefits of the surface mount assembly method, SMT also provides many manufacturing related benefits. These include reduced board cost, material handling cost, and a reduction in the number of manufacturing proceses as surface mount assembly does not require the drilling of holes, and SMT components are also more amenable to automation than THT ones. The repair of surface mount assemblies is also easier and generally sustains less damage than THT assemblies (Jien-Ming et al 2010).

.

Further benefit of the use of SMT methods relate to the use of the area-array packages such as ball grid array (BGA) and chip scale package (CSP). These packages have no lead and hence no lead compliance problem as with the perimeter I/O packages such as QFP. Also, the package can accommodate higher I/O density. Finally the SMT component pitch (distance between solder joints) is relatively larger, relieving in particular the stringent requirements of pick-and-place equipment and printing performance. (Tseng et al 2010).

The area array packages such as BGA and CSP have evolved by steadily increasing circuit density whilst minimising real estate coverage on the printed circuit board (PCB). However, as the inevitable drive towards miniaturisation continues, the need to completely eliminate the minimum IC chip packaging becomes critical. The introduction of cost effective flip chip technology, whereby interconnection involves the attachment of unpackaged, naked, chips directly onto a supporting PCB, is key to both the IC industry and the future of Surface Mount

Technology (SMT) capabilities. Flip chip solutions enable products to be designed with solder joint geometries similar to those of the semiconductor chips. Fig1.1 shows Area Array of SMT packages.

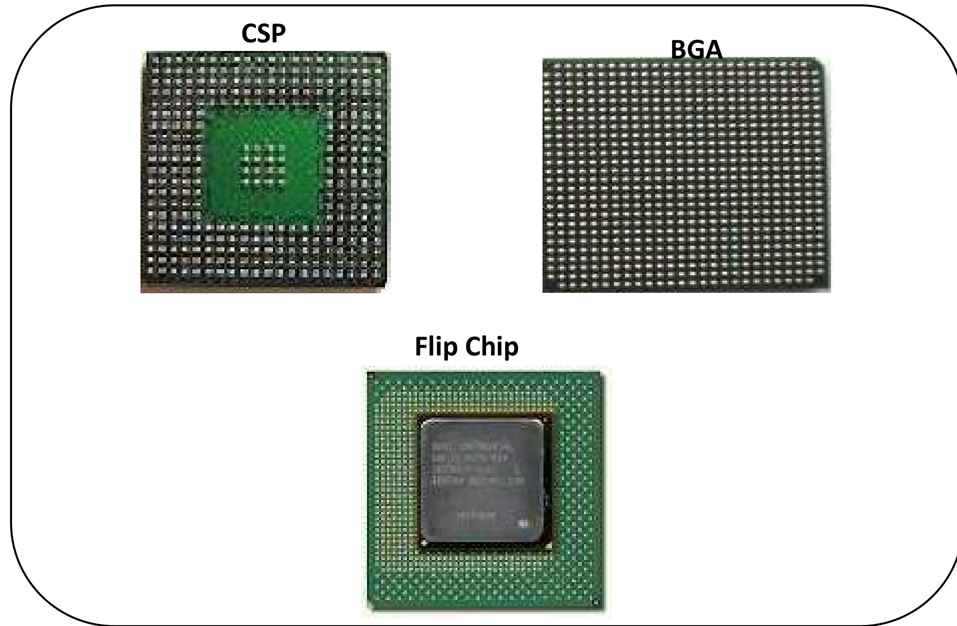

Figure 1.1 Examples of Area Array SMT Packages
(Fairchild Semiconductor Corporation, 2006)

.1.1.2 SMT Chip Components in Electronic Packaging

The Surface Mount Chip components are smaller in sizes, shorter internal leads, and smaller board layouts and less in weight. A typical example is the flip-chip on board (FCOB) as shown in Figure 1.2 The entire interconnection system can be subdivided into four functional areas under-bump metallization (UBM); encapsulation (underfill), solder ball and substrate pad with substrate pad finish or top surface metallurgy (TSM). UBM provides adhesion and acts as a barrier between the solder alloy and the conductor metallization on the chip, such as Au or Cu. It consists of 3-4 different metal layers as shown in Figure 1.2(b).

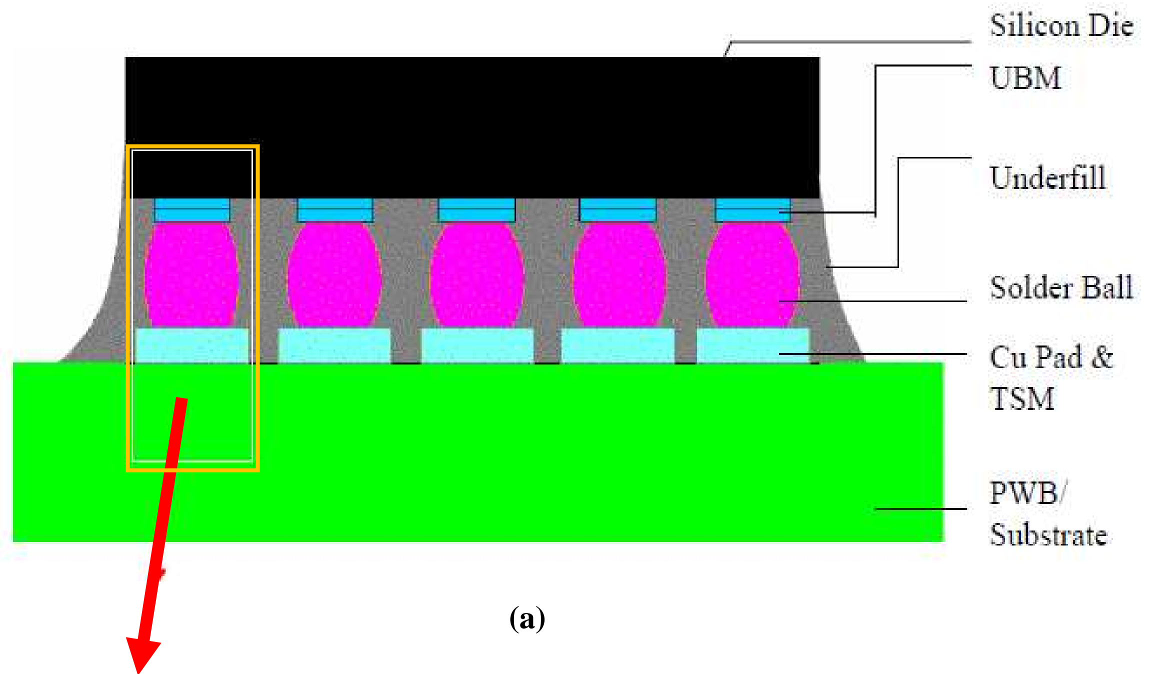

(a)

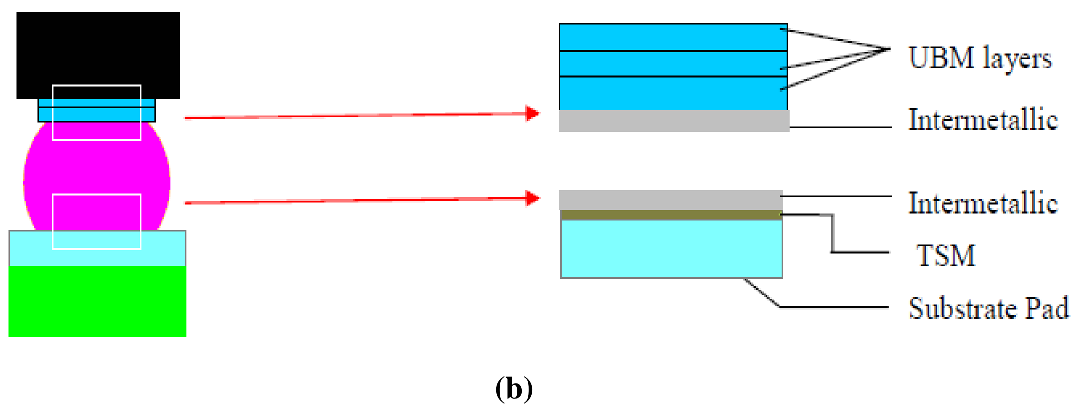

(b)

Figure 1.2 Example of flip-chip on board; (a) Cross section (b) Enlarged view of die/solder and solder/PCB **interface**

Underfill effectively binds the PWB with the die and distributes the stress in the solder joints. The solder ball/bump acts as the mechanical and the electrical connection from the silicon die to the PWB. The substrate pad (Cu) together with the TSM (different metal layers, usually Ni/Au) provides the interface between the solder and the PWB.

1.1.3 Increasing I/O's in Flip-Chip

Although flip-chip technology can achieve a far greater number of I/O than any of the other currently available options, still increasing functionality and decreasing consumer electronic sizes demand for ever increasing I/O's. The number of I/Os are projected to cross 10,000 I/Os with a required pitch (distance between two solder bumps) of 30 to 70µm. Typically the solder ball height is half the pitch of the substrate pads. Increasing I/O's imply decreasing pitch size and eventually decreasing height of the solder bumps as well. This means that the percentage of intermetallic in the joint would increase. Besides as the surface pad finish differs from that of the molten solder, then the pad finish becomes, in fact, a contaminant to the solder in the joint. As the surface pad finish becomes thicker relative to the quantity of solder comprising the solder joint volume, it will have a greater effect on the composition; and therefore, on the properties of the solder once the wetting element from the pad finish has dissolved. (Wong et al 2005)

The compositional change can cause an increase in the solder's liquidus temperature, resulting in premature solidification of the solder before the joint is completely formed. Contaminants may also decrease the solidus temperature of the solder, thus reducing the maximum service temperature to which the joint can be exposed. High contamination levels can lead to reductions in the mechanical strength and ductility properties of the solder after solidification (e.g. Au embrittlement). These problems can be particularly acute for fine pitched solder joints. The small quantities of solder will experience higher contamination levels from the dissolved layer(s), resulting in a greater effect on their properties and that of the joint, before and after solidification. Thus different intermetallics growth, shape and thickness are studied for Pb-free solder.

1.1.4 Sn-Ag-Cu Solder Alloy

The basic properties of solder that are of importance for electronics application are: metallurgical bonding capability with substrate materials, wetting ability during soldering and alloying phenomena between elements alloys (Sriyarunya et

al 2010). The National Centre for Manufacturing Sciences (NCMS) (2001) conducted a survey of approximately 12,000 binary and ternary phase diagrams, which revealed that the cost effective elements that can form alloys with Sn, are Ag, As, Au, Bi, Cd, Cu, In, Sb, Se and Zn. Also, examination of the periodic table shows all these metallic elements are close to Sn (in the same or adjacent period/group). Their closeness in the periodic table explains the reasons for their compatibility with Sn.

The use of Cd, Hg and Sb can be immediately discounted due to their intrinsic toxicity. In addition, Ga and Mg are respectively rare and reactive; thus they were discounted from further consideration. The high cost of Au makes it also an unlikely choice. Bi is also discounted because it is a by-product of Pb mining. This is because when Pb production is decreased, Bi output will decrease which in turn may lead to an increase in Bi costs. Although several elements could not be considered, many alloying combination with Sn have been introduced as possible candidates for replacing the Sn-Pb solder since the first time EC legislation proposing the phase-out of leaded solders in electronic products.

1.1.5 Intermetallic Formation During Assembly

The intermetallic forms during the assembly of the flip-chip on the PWB as is described in figure 1.3. On the chip side, the typical UBM structure consists of three layers (1) adhesion layer such as Al or Ti/Cr , (2) barrier layer such as Ni and (3) wetting layer such as Cu or Au. During the assembly the wetting layer is dissolved completely and an IMC is formed. The intermetallic compound forms due to the dissolution of the UBM wetting **layer** into the molten solder during the reflow. A typical TSM consists of two layers (1) the solderable layer touching the Cu pad and (2) the protective layer over the solderable layer. The purpose of the solderable layer is to provide the surface to which the molten solder will wet and then subsequently adhere on solidification. TSM serves two purposes. The first is to make the underlying Cu pad solderable. Besides solderability, TSM also acts as a barrier layer between the solder and the underlying substrate side pad material (Cu pad).

This solderable layer also prevents the diffusion of the solder to the substrate side base Cu pad. The protective layer, as the terminology implies, protects the solderability of the underlying solderable layer surface from being degraded by exposure to the ambient environment until the actual reflow occurs. During the reflow the solder melts and flows over the PWB pad. During this flowing, the protective layer dissolves and diffuses into the bulk of the solder. The underlying solderable layer is now exposed. Once exposed to the molten solder, the solderable finish is also subjected to dissolution by the molten solder until solidification has occurred. Thus an intermetallic is formed at the interface of solderable finish (the undissolved part) and the solder.

1.1.6 Thermal Cycling and Isothermal Ageing of Electronic Assembly

During thermal cycling or isothermal aging, the assembly's intermetallic layers on the substrate side can grow due to solid/solid reaction between the underlying solderability layer and the solid solder. IMC formed on the chip side can grow due to the solid/solid reaction between and the wetting layer (Cu) and the solid solder. The intermetallic formation and growth is shown in Figure 1.3

The intermetallic layer thickness depends on the solder composition, reflow temperature, duration and the substrate pad finishes. The new Pb–free solder (Sn95.5-Ag3.8-Cu0.7) does not work well with the current set of substrate pad finishes as the intermetallic reaction between copper and tin is particularly rapid (Korhonen et al., 2000) The growth of tin-copper intermetallics has been reported for leads covered with Pb-Sn eutectic solder. However, it is this same tendency of tin to form intermetallics that raises a long term reliability concern with high tin solders. Thus there is a need to explore the effect of IMC on assembly and packaging of electronic components and the reliability of Pb-free solder joints.

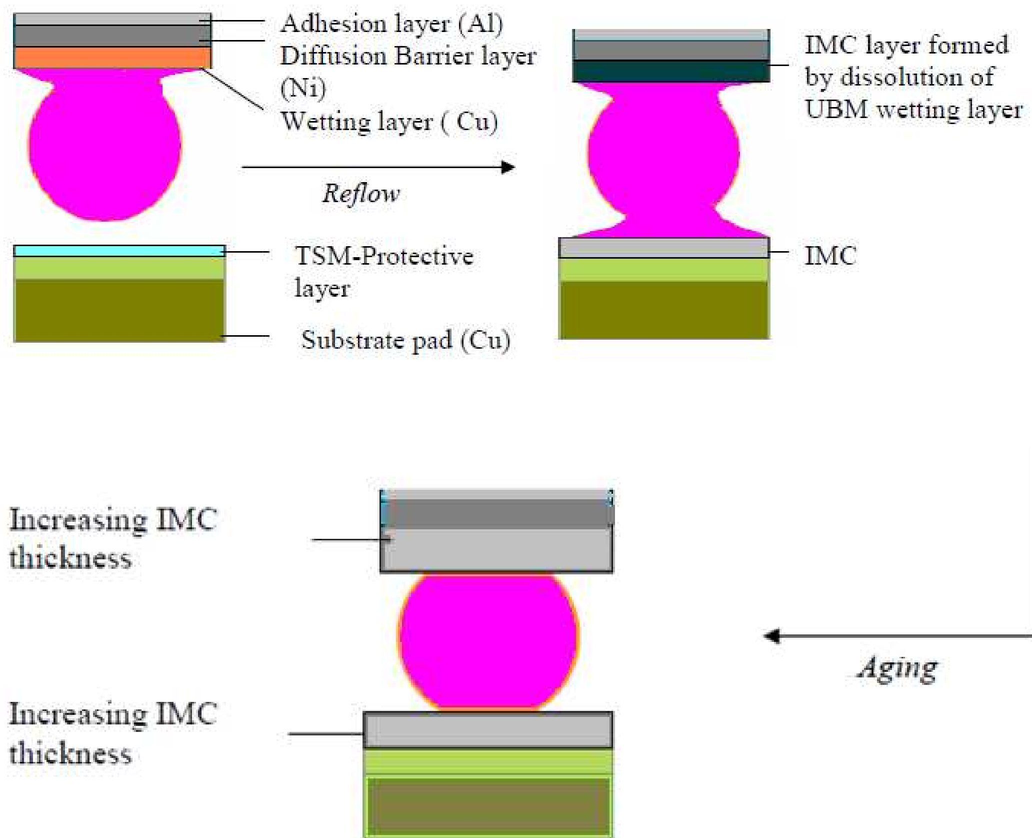

Figure 1.3 IMC formation in assembly of flip-chip. (a) Unassembled UBM and TSM (b) Reflowed assembled chip (c) Aged assembled chip

1.1.7 Solder Joints Reliability.

Solder joints are simply electrical interconnections. As technology advanced, electrical component size decreased and the number of input/output (I/O) interconnections increased; making the function of the solder joint become more critical. In practical terms, as the electronic component dimensions decreased, the number of solder joints increased. There are numerous benefits of shrinking solder joint dimensions for example increased speed and greater density, but concerns about solder joint reliability have also increased. The solder joint reliability is seen as critical in particular, for the electrical and electronic products used for controlling operational and safety critical functions in automotive and aerospace applications.

For an improvement of the solder joint reliability, it is vital to understand the thermodynamic and chemical relationship between the solders and the different metallic substrates. This relationship can be explained briefly as follows: In the soldering process, solders act by (a) wetting the base metal surfaces forming the joint; (b) flowing between these surfaces so as to fill the space between them; and (c) metallurgically bonding to the surfaces when solidified (Steller et al, 2010). The metallurgical bonding between the solder and the base metal surfaces is known as inter-metallic compound (IMC) layer.

The formation of inter-metallic layer by the reaction of the solder with the substrate occurs during the wetting process. The presence of inter-metallic layer signifies good metallic bonding, but the inter-metallic layer is also known to be the weakest part of the joint as it is brittle. A thick inter-metallic layer will weaken the joint, making it less able to withstand the thermal cycling and operating strains imposed on the joint during its life time. Furthermore, the solder joint also become depleted of the elemental constituent used to form the IMC and thereby changing the mechanical properties of the joint in terms of its strength.

1.2 Scope of this Research Study

1.2.1 Problem Statement

As the demand for smaller and miniature hand-held and pocket electronic consumer products such as calculators, camcorders, mobile phones and laptops continues, the drive towards further miniaturisation of electronic devices and solder joints will also continue. The reliability of the solder joints is known to be dependent on the microstructures and the inter-metallic layers of the solder joints. It is also well known that IMCs are brittle (thick IMCs may jeopardise a joint's mechanical integrity), and they also have a higher resistivity than the base metal.

Moreover, with the elimination of hazardous Pb from the composition of solders (used to fabricate electronic joints), other metallic additives were incorporated in the solder alloys to tailor their properties to the requirements of certain applications. Unlike Pb, many of the new metallic additives (Cu, Au, Ag, Ni...

etc) to solder are reactive with Sn and with the elements present at the metallization. These elements also diffuse very fast in Sn- based solders even at room temperature. Their presence in miniaturized electronic joints can alter the behaviour at the solder/metal interface. Instead of binary Sn- metal inter-metallic usually observed in Sn/metal diffusion couples, ternary or quaternary compounds may grow at the solder/metallization interface. This may degrade the mechanical properties of the joints and compromise their reliability.

Although the IMC formation in Sn-Pb alloy systems has been studied extensively and a number of empirical relationships have been developed (Frear *et al* 1994; Ourdjini et al 2006), there are few reports on the Sn-Ag-Cu alloy systems. There is wide agreement that the existing empirical kinetic relationships developed for the Sn-Pb alloys cannot be extrapolated to fit the Sn-Ag-Cu lead-free alloy systems.

There is thus an urgent need to study the formation and growth of IMCs in the Sn-Ag-Cu lead-free alloy at high temperature of 175°C in isothermal ageing, since there is no established data. This will help to provide a better understanding of their effect on the long-term reliability of solder joints. Also, having reviewed various reports on the reflow soldering process, there are different conclusions on the impact of the reflow profile and reflow soldering process parameters. Therefore, determining the optimal reflow profile settings for Sn-Ag-Cu solder volumes and the most significant factor that influences the process were investigated.

Solder joints in an electronic package experiences vibration and thermo-mechanical loading due to coefficient of thermal expansion (CTE) mismatches between the electronic component and substrate, in combination with thermal excursion during service (Ming-Yi et al 2004). The majority of studies in solder joint reliability in terms of shear strength, focused on the effects of the shear speed on the mechanical response of the solder joint. Therefore, the relationship between the shear strength and IMC thickness during reflow and isothermal ageing is investigated. In addition, since the solder joints in application fail along

the soldering interface, the fracture surface and porosity of the solder joints is also studied.

1.2.2 Research Objectives

The objectives of the research work are as follows:

(1) The study of the effect of pad sizes on inter-metallic compound layer formation and growth for lead-free solder joints under isothermal ageing

(2) The study of the cycling temperatures and reflow profiles on inter-metallic growth between Sn-Ag-Cu solder alloy and Cu.

(3) The study of the effect of reflow soldering profile parameters on Sn-Ag-Cu solder bumps using Cu substrate

(4) The study of the effect of inter-metallic compound layer thickness on the shear strength of 1206 surface mount chip resistor with Nickel termination and Sn-3.8Ag-0.7Cu on Cu surface finish.

1.3 Structure of thesis

The thesis is sub-divided into nine chapters. Chapter 1 presents the introduction to the study, a summary of the issues affecting solder joint reliability, the research objectives and overview of the thesis

Chapter 2 presents the literature review on properties of lead and lead-free solder alloys, IMCs and their microstructure, reflow soldering, thermal cycling and isothermal ageing of solder joints and solder joint reliability.

Chapter 3 presents solder joint metallurgy and microstructure. The chapter is divided into four main parts. The first part of the chapter concerns phase diagrams and their use in the study of different alloy systems. The second part presents the basic concepts used in the study of the microstructure of solder joints. The third part of the chapter deals with the concepts used in the study of IMC formation and growth, and in particular the principle of diffusion and solid state growth. The

final part presents some of the important concepts on solidification process including nucleation and growth, and thermodynamics of reaction.
Chapter 4 presents the details of experimental materials, methods and procedures. The first part describes test vehicles used for each experimental investigation. The second part focuses on metallurgical/ metallographic preparation. The final part focuses on the aspects of microstructures and intermetalic compound thickness measurement.

Chapter 5 presents the study of the effect of pad size on inter-metallic compound formation and growth on copper substrate.

Chapter 6 presents the study of the effect of reflow profiles and thermal cycle temperatures on inter-metallic compound formation and growth between Sn-Ag-Cu Solder Alloy and Cu substrate

Chapter 7 presents the study of the effect of reflow soldering profile parameters on Sn-Ag-Cu solder bumps using cu substrate

Chapter 8 presents the study of the effect of inter-metallic compound thickness on the shear strength of 1206 surface mount chip resistor with Nickel termination and Sn-3.8Ag-0.7Cu alloy on Cu surface finish. This chapter also investigates the percentage of voids in the solder joints during isothermal ageing.

Chapter 9 presents summaries and conclusions of work described in this thesis. The chapter concludes with recommendations for future work.

CHAPTER II: LITERATURE REVIEW

2.1 Introduction

The chapter outlines the outcome of a literature review on properties of lead and lead-free solder alloys, IMCs and their microstructure, reflow soldering and temperature profiling, thermal cycling and isothermal ageing of solder joints and solder joint reliability. The chapter is divided into five key sections. The first section gives a review of preceding studies on properties of lead and lead-free solder alloys. The second part is a review of solder alloy microstructures. The third section deals with lead-free alloy microstructure and with additions of rare earth elements. The fourth part is a review on IMC formation and growth. Its main significance is with regard to the previous work on dissolution rates, diffusion and growth kinetics. The final section of the chapter present a review of previous work on the influence of reflow soldering on solder joint microstructure and IMC formation.

2.2 Previous studies on properties of lead and lead-free solder alloys

2.2.1 Previous studies on Lead-bearing solders

Soldering is the most widely used interconnection method for the packaging and assembly of almost all electronic products. Lead-bearing solders, especially the eutectic 63Sn-37Pb or near-eutectic 60Sn-40Pb alloys, have been used extensively in different levels of the electronic assembly, where stringent electrical, mechanical and thermal properties of solder alloys are important. The Sn-Pb binary system has an eutectic temperature of 183ºC. This soldering temperature is compatible with most substrate materials and devices. This solder has many merits, including low melting temperatures, good workability, ductility, ease of handling and excellent wetting on Cu and its alloys. Lead, being one of the primary components of eutectic solders, provides many technical advantages, which include: (i) lowering the surface tension of pure tin and (ii) facilitating wetting (Vianco, 1993).

With lead as an alloying element in tin, it helps to prevent the transformation of white or beta (β) tin to gray or alpha (α) tin. The transformation, if it occurs, leads to an increase in volume which will cause loss of structural integrity to the tin(Reed-Hill, 1994). These factors, coupled with Pb being a low cost and readily available metal, makes it an ideal alloying element with tin.

The physical metallurgy, mechanical properties, flux chemistries, manufacturing processes and reliability of eutectic and near eutectic Sn-Pb solders have been reported by (Tu and Zeng, 2001).They reported that the board level soldering system that is mainly based on eutectic and near eutectic Sn–Pb solders has been well developed and refined. It was pointed out that the good behaviour of Sn–Pb solders has enabled current board level technology to assemble and create small geometry solder joints, approaching 75µm in size, in high volume, and at competitive cost.

2.2.2 Previous studies on Lead-free solders

Sn-Pb solders have been used intensively in the electronics industry due to their unique characteristics such as low cost and ease of manufacturing. It is a challenging task to find suitable alternatives for the lead-containing solders. To-date, although a number of lead-free solders are currently available, there is still no drop-in alternative for eutectic Sn-Pb. Not only must the lead-free alternatives meet health, environment and safety requirements, as well as solder joint reliability and performance expectations, they must also be compatible with the existing soldering processes. When identifying a replacement to the current widely used Sn-Pb solders, it is crucial to ensure that the properties of the replacement solder are comparable to or superior to Sn-Pb solders. Table 2.1 summarizes some of the properties of solders that are of importance from a manufacturing and long-term reliability standpoint (Zeng and Tu, 2002).

Table 2.1 Important properties of solder alloys (Zeng and Tu, 2002)**.**

Properties relevant to reliability and performance	**Properties relevant to manufacturing**
Electrical conductivity	Melting temperature
Thermal conductivity	Wettability to copper
Creep resistance	Availability
Fatigue properties	Cost
Tensile properties	Recyclability
Intermetallic compound formation	Manufacturability using current processes
Coefficient of thermal expansion	Ability to make into balls
Corrosion and oxidation resistance	Ability to make into paste

However to date, the lead-free replacements developed are mostly application specific. There is no specific replacement for everyone's use. For most Pb-free solders, it has been identified that the basic building block element is tin (Sn) and the potential substitutes for lead (Pb) include: silver (Ag), antimony (Sb), zinc (Zn), copper (Cu), bismuth (Bi), indium (In) and gold (Au). There is also a special class of eutectic alloys of Sn and noble metals: Au, Ag and Cu. A eutectic alloy is used as it has a single and low melting point. Hence, partial melting or solidification will not occur and the entire solder joint will melt or solidify at a given temperature. Table 2.2 shows the eutectic temperatures of the binary Pb-free solder systems in comparison with eutectic Sn-Pb (Zeng and Tu, 2002).

System	**Eutectic Temperature (°C)**	**Eutectic composition (wt.% of the second element)**
Sn-Cu	227	0.7
Sn-Ag	221	3.5
Sn-In	120	51
Sn-Bi	139	57
Sn-Zn	198.5	0.9
Sn-Au	217	10
Sn-Pb	183	38.1

The common characteristic of eutectic Sn-noble metal alloys is that they possess a higher melting point as compared to that of eutectic Sn-Pb. This results in the reflow temperature being higher by about 30°C, which in turn may lead to an increase in the dissolution rate and solubility of Cu and Ni in the molten solder as well as the rate of intermetallic compound formation with Cu and Ni. In addition, except for 80Au-20Sn, a high temperature solder which is similar to the high-Pb solder is yet to be developed. This is attributed to Sn-based solder of high-Ag or high-Cu concentration having the tendency of a large temperature separation between the solidus and liquidus points (Hansen and Anderko, 1958). This results in partial melting or solidification which is undesirable application wise. To-date, a relatively large number of lead-free solder has been proposed other than examples of the binary systems (Sn-Ag, Sn-Sb, Sn-In, Sn-Bi alloys) and ternary systems (Sn-Ag-Cu, Sn-Bi-In, Sn-Bi-Cu and Sn-Bi-Ag). Among the most promising lead-free solders, combinations of the Sn-Ag-Cu family of alloys appear to be more popular (Abtew and Selvaduray, 2000; Suganuma, 2001; Foley et al, 2000; Kikuchi et al, 2001; Plumbridge et al, 2001 and Wade et al, 2001).

The studies reported above shows that in the lead-base solder, the Pb lowers the surface and interfacial energies of the solder. Also, the eutectic SnPb solder has a very low wetting angle on Cu. The interfacial energy between the molten solder and the IMC is low. The studies also show that the lead-based solders have been researched for more than three decades and hence, their behaviours are well understood. However, the lead-based solders are now being replaced by lead-free solder alloys because of environmental concerns and health hazards. The introduction of these new lead-free solders means that there is an increasing demand to study and understand the behaviour of these new materials, especially how they react with the substrate and component surfaces and the formation and growth of IMC.

2.2.2.1 Previous studies on Sn-Ag-Cu Lead-free Solder

One popular alloy which is already used for high temperature solder applications is the binary Sn-Ag system, which has a eutectic temperature of 221ºC. Existing literature has reported that this lead-free solder possesses good mechanical and

thermal fatigue properties (Abtew and Selvaduray, 2000; Suganuma, 2001; Foley et al, 2000; Kikuchi et al, 2001; Plumbridge et al, 2001 and Wade et al, 2001). However, this solder has liquidus temperature, which is about 40ºC higher than that for Sn-Pb eutectic alloys. Hence, this hinders manufacturers from switching from lead-containing solder to lead-free solder, due to involvement in high capital investment. Therefore, in order to make Sn-Ag based alloys more compatible with Sn-Pb manufacturing processes, ternary additions like copper (Cu) are introduced to reduce the liquidus temperature. Cu also provides a eutectic point that helps to limit the mushy range. The presence of a eutectic point is desirable for ideal solder system as eutectics, which have a sharp melting point and narrow mushy range, are preferred for their ease of manufacturing and reliability at high temperature. However, the eutectic composition of Sn-Ag-Cu has been a subject of controversy. Investigators have reported different eutectic compositions, which is tabulated in Table 2.3

Table2.3 Eutectic Sn-Ag-Cu solder composition (Zeng and Tu, 2002).

Investigator	Composition	
	Ag	Cu
Senju	3.5	0.75
HUT, Finland	3.4	0.8
Northwestern University, USA	3.5	0.9
Heraeus	3.2	0.5
NIST, USA	3.5	0.9
Multicore	3.8	0.7
Alpha Metals	4.0	0.5

The eutectic and near eutectic compositions of the Sn-Ag-Cu alloy have over the recent years become an industry-wide candidate as a Pb-free alloy in Europe and North America. It is considered to be superior to other Pb-free solder alloy candidates in term of corrosion, availability and toxicity. Furthermore its melting point (217°C) is lower than the eutectic Sn-Ag alloy (221°C). This alloy is also recommended by professional groups such as the Soldertec (1999) and National Electronics Manufacturing Initiative (NEMI, 2000). The alloy composition range

recommended by NEMI and Soldertec are Sn-3.9Ag-0.6Cu and Sn-(3.4-4.1) Ag-(0.45-0.9) Cu respectively.

In a study, Hsin-Chieh (2003) investigated the mechanical properties and low cycle fatigue (LCF) behaviour of Sn-3.5Ag and Sn-3.5Ag-0.5Cu lead-free solders. The properties were compared with those of conventional Sn-37Pb solder in order to evaluate the feasibility of using lead-free solders to replace the Pb-containing solders in the future. It was found that the tensile strength increased with increasing strain rate for all the three types of solder alloys. The Sn-3.5Ag-0.5Cu alloy had the highest tensile strength followed by Sn-3.5Ag alloy and then Sn-37Pb alloy. Also, it was observed that due to the influence of creep mechanism during tensile deformation process, the elongation and the true fracture ductility of lead-free solders decreased with decrease in strain rate. However, the Sn-37Pb alloy exhibited a super- plastic behaviour when tested at lower strain rates. Furthermore it was found that the lead-free solders usually have better low cycle fatigue resistance than the traditional Sn-37Pb solder due to their greater strength and creep resistance. The Sn-3.5Ag-0.5Cu alloy exhibited longer fatigue life than Sn-3.5Ag.

Due to the current restriction on the use of lead and other hazardous substances in consumer electronic products, electronics manufactures have been forced to adopt new technologies. As a result, a substantial amount of research has been carried out in the last fifteen years in different aspects of lead-free soldering technology. In one study, Suganuma (2004) provided a very useful introduction to lead-free soldering technology. The paper discusses the worldwide regulations on restricting the use of lead in electronics manufacturing and presents details of global lead-free solder development projects. It was pointed out that the Japanese electronics manufacturers are the pioneers in adopting lead-free solder for mass production. While outlining the advantages and limitations of different lead-free solder alloys, it was stated that the Sn-Ag-Cu family are the strongest candidates to become the standard lead-free solder, as they are extremely stable and also meets the globally acknowledged standards.

In a study, Wu et al (2004) carried out an investigation on the properties of lead-free solder alloys with rare earth element of mainly cerium (Ce) and lanthanum (La), as additions to address the reliability issues of electromigration, creep, wettability and solderability. The lead-free solder alloy doped with rare earth elements include; Sn-Ag, Sn-Cu, Sn-Zn and Sn-Ag-Cu. It was found that doped solder alloys were better in term of wettability, creep strength and tensile strength. Also, it was found that the creep rate of these tin-based alloys can be represented by a single empirical equation. Again, with the addition of rare elements, solders for bonding on difficult substrates such as semiconductors, diamond and optical material have been developed.

In another study, Price (2005) reported on the important challenges in relation to the transition to lead-free soldering. They specifically identified the challenges posed by the relatively high temperature of lead-free solder alloys and the consequence of using higher melting point lead-free alloys for processes and fpr components originally developed for Sn-Pb soldering. Sn-Ag-Cu (SAC) alloys with the melting points between 215°C-220°C were identified as cost-effective and widely used alternatives to lead-based solders. The study also outlines the issues/challenges in reflow, wave and hand soldering and how the processes can be optimised for lead-free soldering.

The eutectic AuSn solder, widely used in high temperature and high reliability applications due to excellent mechanical and thermal properties (particularly strength and creep resistance) and its ability to be reflowed without flux, have been study by Chromik et al (2005). They showed that other lead-free and traditional lead-based eutectic solders suffer by comparison due to a variety of issues which include the requirement of fluxes, responsible for bond pad corrosion, as well as excessive creep or stress relaxation. The study also concluded that low strength eutectic AuSn is erroneously associated with embrittlement of conventional SnPb and Pb-free solders on Cu.

In another study, Chromik et al (2005) have investigated the mechanical behaviour of solders and intermetallic compounds, especially for use as inputs in finite element analysis (FEA). It was found out that measurements obtained from

bulk samples often produced by arc melting are usually misleading, due to significant differences in grain size, residual stresses, and mechanical constraint compared to typical solder joints, joint geometries, and material combinations. Furthermore, the mechanical properties of solders, metals, and relevant inter-metallic compounds obtained on actual solder joints have been presented in table 2.4.

The thermal properties, wetting and spreading of the eutectic or near eutectic Sn96.5Ag3.5, Sn91Zn9, Sn99.3Cu0.7, Sn95Cu4Ag1, and Sn95.8Ag3.5Cu0.7 solders and compared with the eutectic Sn-Pb solder have been reported by Ozvold et al (2008). In their experiment, Differential Scanning Calorimentry (DSC) was used to determine the thermal properties of solders. Also wettability and surface tension were evaluated by means of goniometric method at temperature of 50°C higher than the melting point solders. Again, they expressed wettability through wetting angle and the size of wetted surfaces for all types of fluxes in the solders on the copper substrate.

Furthermore, the chemical compositions of the phases formed at the interface were determined using electron probe microanalyzer with EDX. The study concluded that Sn91Zn9 solder revealed the melting temperature of 201±2°C and two phase structure consisting of Sn and Zn. The Sn95.8Ag3.5Cu0.7 and Sn95.5Ag4Cu0,5 ternary solders revealed the four phase structure (Sn,a-CuSn,b-CuSn, Ag3Sn) and melting temperatures 220±3 and 216.9 °C, respectively. The Sn95Ag1Cu4 ternary solder revealed the melting temperature of 223 ±5°C and the same phases as stated for the Sn95.8Ag3.5Cu0.7 solder. The surface tension of Sn–40Pb, Sn95.5Ag4Cu0.5 and Sn95.2Ag3.8Cu1 solders was 455, 513 and 588 mN/m, respectively.

In another study, Gao et al (2009) reported on thermal properties of nanosolders. They investigated thermal properties of lead-free nanosolders on nanowires. The thermal properties of nanosolders were characterized by using a temperature-programmable furnace tube under a controlled atmosphere. Again, in their study, it was revealed that nitrogen plays an important role in the nanosolder reflow process. Furthermore, an optimal nanowire nanosolder system with effective

barrier and wetting layers was obtained. Finally a liquid phase-based solder reflow process was developed, in which the nanosolder nanowires were assembled in a liquid medium and solder joints were formed between nanowires.

Table 2.4 Summary of mechanical properties of relevant metals, solder alloys and intermetallic compounds (Chromik *et al,* 2005)

Material	Young Modulus of Elasticity (E) (GPa)	Passion Ratio (v)	Coefficient of Thermal Expansion (CTE) (ppm/C)	Yield Stress (σ_y) (MPa)	Tensile Strength (GPa)
Au	83	0.42	14.4	207	1.03
Sn	41	0.33	28.8	56	0.11
Cu	114	0.34	16.4	52	1.7
Au 80Sn20	74	0.4	16	276	1.3
Sn63Pb37	32	0.4	25	34	
Sn96.5-Ag3.5	53	0.4	22	49	0.16
Au_5Sn (ξ)	76	0.4	-	830	2.5
AuSn (δ)	87	0.3	-	370	1.1
$AuSn_2$ (ε)	103	0.33*	-	970	2.9
$AuSn_4$ (η)	39	0.31	-	400	1.2
Ag_3Sn	88	0.33*	-	970	2.9
Cu_6Sn_5	119	0.33*	-	2200	6.5
Cu_3Sn	143	0.33*	-	2100	6.2

In a recent work, Yu et al (2008) carried out an experiment to determine the reliability of eutectic AuSn solder. In their work, it was found that AuSn solder are extremely stable in a broad range of harsh environments. These include

thermal cycle from -55 to +125C, high temperature storage from 75 to 150C and high humidity environments.

In another recent work, Garcia et al (2009) carried out a comparative experimental work to develop interrelating mechanical properties, solidification thermal parameters and microstructures characteristic of a hypoeutectic Sn–4 wt.% Zn, a hypereutectic Sn–12 wt.% Zn and a eutectic Sn–9 wt.% Zn solder alloys. In their work, they used a water-cooled vertical upward unidirectional solidification system to obtain the samples. It was found that a more homogeneous distribution of the eutectic mixture, which occurs for smaller dendrites spacing in hypoeutectic and hypereutectic alloys, increases the ultimate tensile strength. The resulting microstructure of the eutectic Sn-9 wt.% Zn alloy induced higher mechanical strength than those of the Sn–4 wt.% Zn and Sn–12 wt.% Zn alloys. It was found that the eutectic alloy experiences a microstructural transition from globular-to-needle-like Zn-rich morphologies which depend on the solidification growth rate. It was also shown that a globular-like Zn-rich morphology provides higher ultimate tensile strength than a needle-like Zn-rich eutectic morphology.

The review of the literature on lead free solder alloys revealed that the choice of solder alloy requires a sound knowledge of substrate surface metallurgy and solder alloy melting temperature (to avoid any harmful effect on the components). In the case of lead-free solder, it is clear that the performance of lead-free solder joints will depend on the specific component and operating environment of the application area. The review also that the research and development of lead-free solder alloys is still in the infancy state. Some research also demonstrated that the lead-free solder alloys are not as reliable as the lead-based counterpart. One of the reasons behind this reliability issue is the lack of knowledge and understanding of the IMC formation and growth in lead-free solder alloy applications. The research work reported in this thesis will help to provide a better understanding of the IMC formation (of lead-free solder alloys) and their growth at different temperatures and ageing times.

2.3 Previous studies on solder alloy microstructures

The microstructures of the tin-lead (Sn-Pb) solder alloys have been comprehensively studied by Morris *et al* (1994). In their study the composition of the Sn-Pb solder used is 63wt%Sn-37wt%Pb. It was found that the eutectic Sn-Pb solder joint formed by relatively slow cooling has lamellar microstructures (Morris *et al,* 1994). The lamellar microstructure has a very high surface area per unit volume, and is thermodynamically unstable (Morris *et al* 1994). Thus it has tendency to lower its surface area per unit volume to achieve an equilibrium condition. Therefore the lamellar microstructure in the as-soldered eutectic Sn-Pb solder joint could easily re-crystallize into the equiaxed microstructure after being aged at moderate temperature. This course of action can also be accelerated by plastic deformation. The phase diagram of the eutectic Sn-Pb alloy can be seen in figure 2.1. The equiaxed microstructure of the eutectic Sn-Pb alloy can also be obtained directly during the soldering process by using fast cooling or quench.

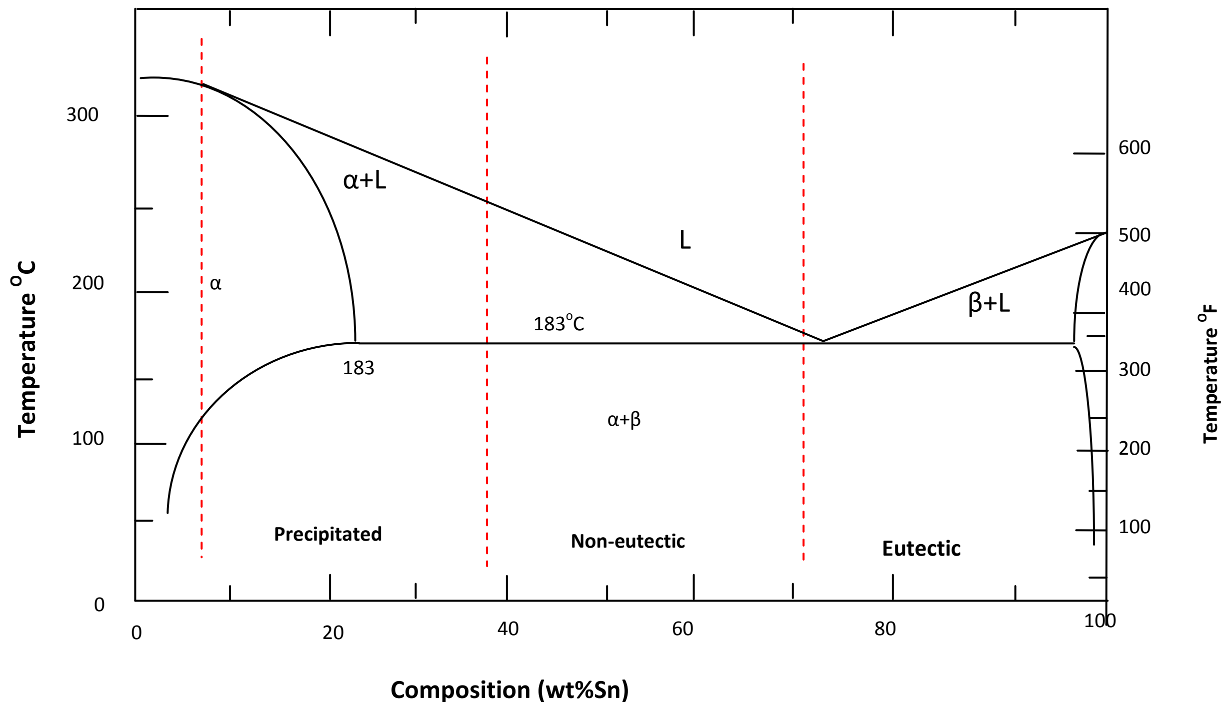

Figure 2.1. Schematic diagram Sn-Pb phase diagram

Adopted from (Askeland 1996)

The microstructure phases of binary and ternary lead-free solder alloys were investigated by (Abtew and Selvandduray 2000). Sn-9Zn, Sn-3.5Ag, Sn-0.7Cu and Sn-Ag-Cu alloys were employed in the investigation. The study showed that Sn-9Zn, Sn-Ag and Sn-Cu alloys exhibited similar microstructures. It was also found that the eutectic and near eutectic binary and ternary alloys microstructures were not uniform when the coarse β-Sn plane formed at cooling rate of 15-20ks^{-1}. Furthermore it was observed that from the melting temperature point-of-view, the eutectic Sn–9Zn alloy is one of the best alternatives to PbSn with a melting temperature of 199 °C, as compared with 183 °C of PbSn. Its microstructure consists of two phases: a body-centred tetragonal Sn matrix phase and a secondary phase of hexagonal Zn containing less than 1 wt. % Sn in solid solution. The solidified microstructure exhibits large grains with a fine uniform two-phase eutectic colony.

The study of solder alloy microstructure and phase equilibria were investigated separately by (Moon *et al*, 2000 and Ohnuma *et al,* 2000). In their study, the phase diagram of the Sn-Ag-Cu ternary system was presented, which is shown in figure (2.2 and 2.3) and figure 2.4 displays the phase fraction of the eutectic Sn-Ag-Cu alloy. The phase fraction indicates that when the liquid eutectic Sn-Ag-Cu alloy solidifies, the ternary reaction is as follows:

Liquid $\rightarrow$ β-Sn + η-Cu_6Sn_5 + Ag_3Sn. In addition, the studies also show that the alloy microstructures consist of primary β-Sn matrix surrounded by rod-like Ag_3Sn intermetallic and rounded or hexagonal shape η-Cu_6Sn_5 intermetallics. The typical microstructure of the eutectic Sn-Ag-Cu alloy can be seen in figure 2.5 and 2.6 .In these figures, the white-island is the Sn-matrix, the rod-like shape is the intermetallic Ag_3Sn and the rounded or hexagonal shape is the intermetallic Cu_6Sn_5.

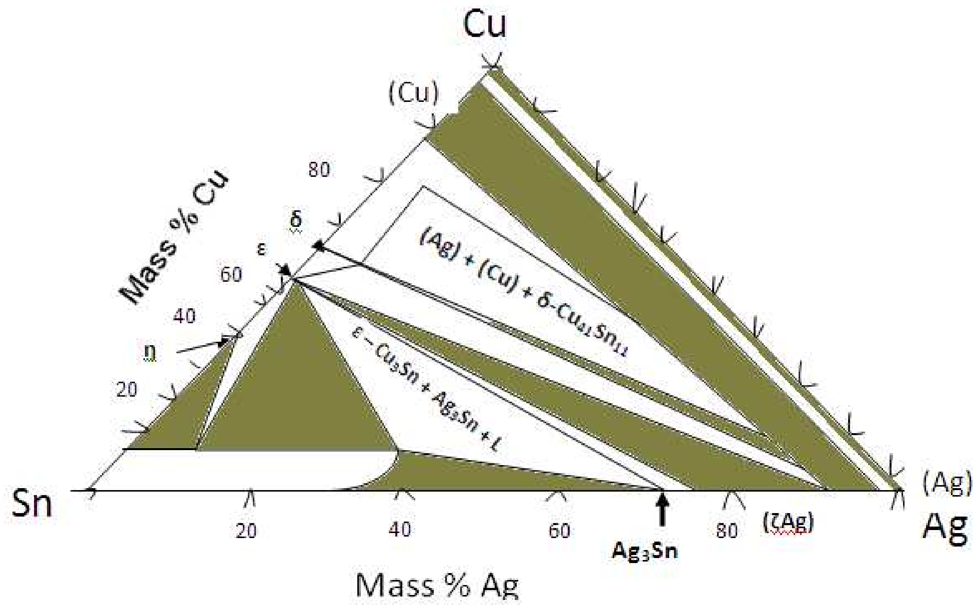

Figure 2.2 Schematic of Isothermal Section at 400°C (Top View) of the Sn-Ag-Cu Phase Diagram (Ohnuma *et al* 2000)

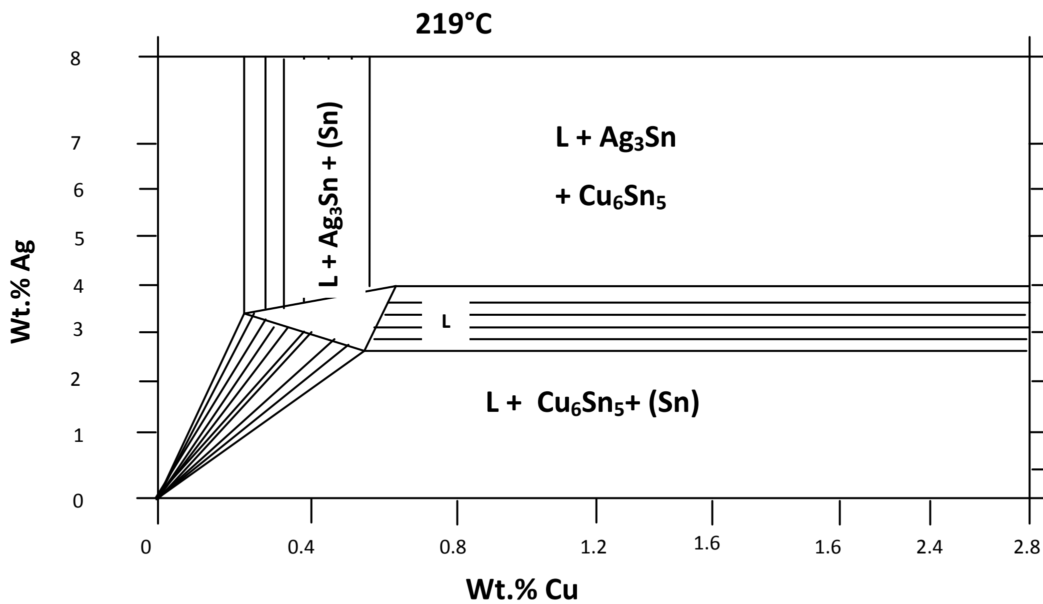

Figure 2.3 Schematic of isothermal section at 219°C of the Sn-Ag-Cu Phase Diagram (adopted from Moon *et al* 2000)

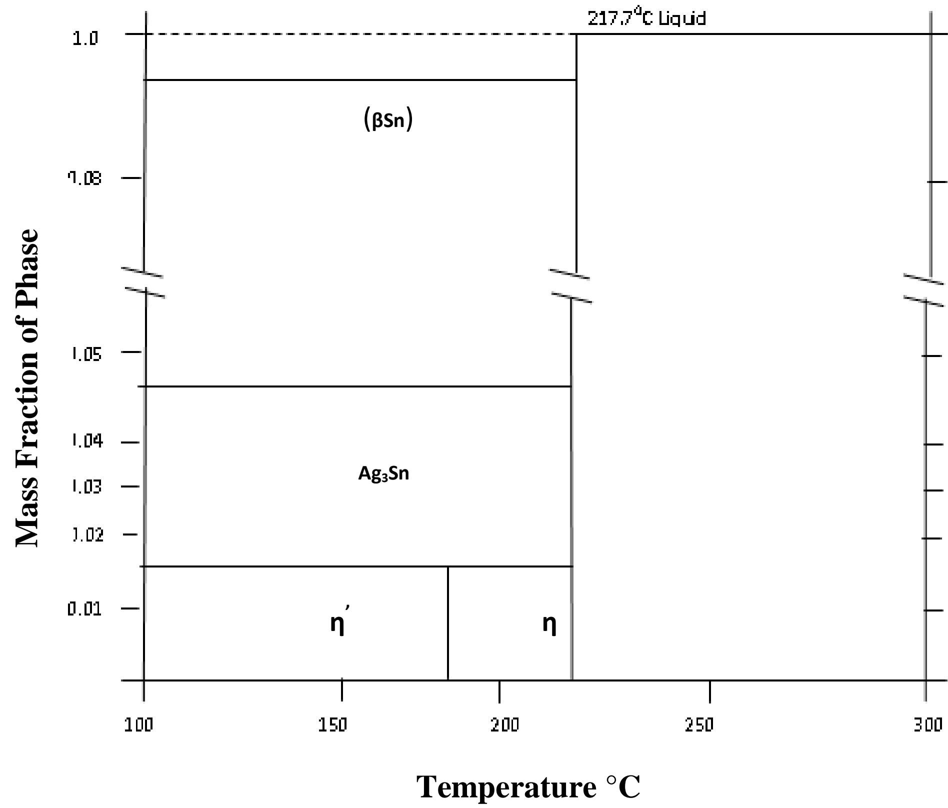

Figure 2.4. Schematic of Mass fractions of phases vs. temperature of Sn-3.24wt%Ag-0.57wt%Cu alloy (adopted from Ohnuma *et al* 2000)

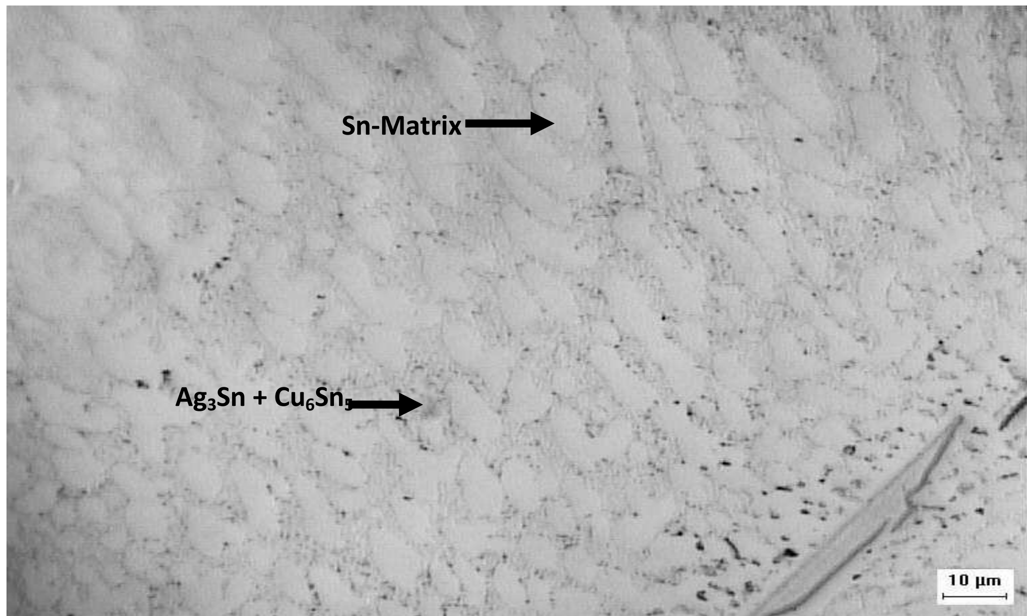

Figure 2.5 Bulk Microstructure of Eutectic Sn-Ag-Cu Alloy

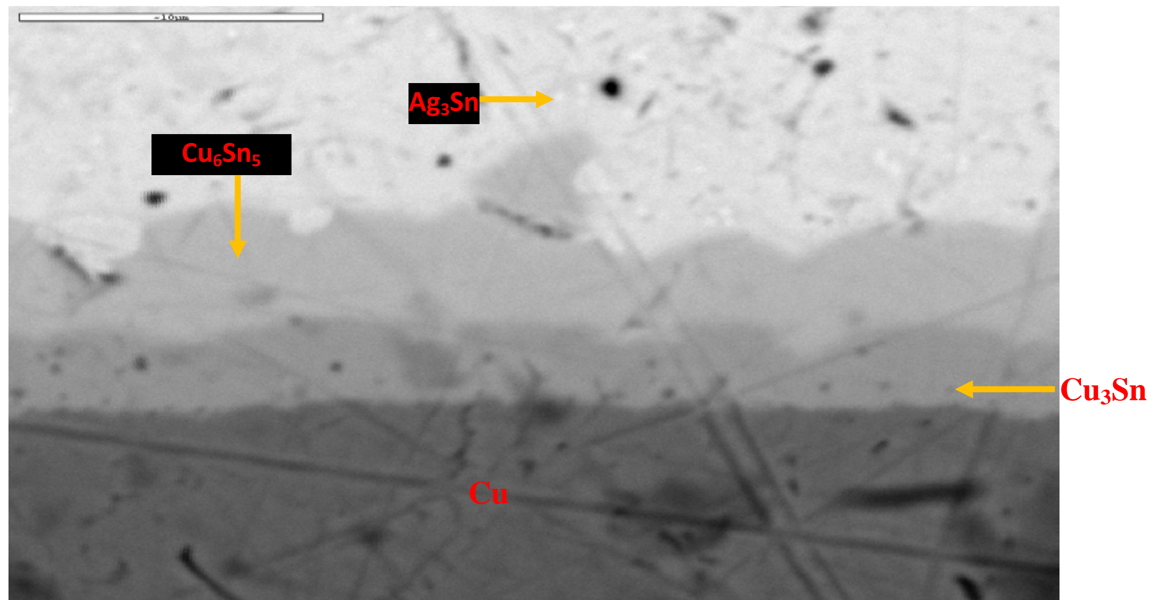

Figure 2.6 Microstructures of the Sn-Ag-Cu alloys aged 12 days at 175°C

In another development, a more detailed study of the Sn-Ag-Cu alloy's microstructure has also been investigated by (Hwang 2001). The composition of the Sn-Ag-Cu alloy investigated is 96.5-92.3% Sn, 3-4.7% Ag and 0.5-3% Cu. It was reported that the Cu_6Sn_5 and Ag_3Sn inter-metallics in the Sn-matrix of the Sn-Ag-Cu alloys effectively strengthen the alloy microstructure and could prevent fatigue crack propagation. In addition, these inter-metallics also act as partition for the Sn-matrix grain, producing a finer microstructure. The study also indicates that the finer the inter-metallics are, the more effectively they partition the Sn-matrix grain, resulting in the overall finer microstructure that can facilitate grain boundary sliding mechanisms, which should in turn extend the fatigue lifetime.

The work of Hwang (2001) also extended to various compositions of the eutectic Sn-Ag-Cu alloy. The study shows that for the solder alloys at 0.5-0.7% Cu, any content of Ag higher than 3% will increase the size of the Ag_3Sn particles, which will lead to higher strength but will not increase the fatigue life. This study showed that when the Cu content of the alloy is around 1-1.7%, the fatigue life will decrease because the size of the Ag_3Sn particles is large. One conclusion from the study is that the optimal composition of the Sn-Ag-Cu alloys is Sn-3.1Ag-1.5Cu because this gives the finest microstructures producing high fatigue life, strength and plasticity.

An experimental study by Wiese *et al* (2001) shows that the microstructure (of the eutectic Sn-Ag-Cu alloy) formed in the flip chip joints is different from that formed in the bulk solder. Weise *et al* (2001) concludes that this is a function of the higher cooling rate during solidification of the smaller flip chip joints. The higher cooling rate gives a microstructure with higher number of very small Ag_3Sn precipitates as compared to the smaller number of large Ag_3Sn precipitates found in bulk solder specimens.

In another study, the microstructures and tensile properties of three different Sn-Ag-Cu alloys namely (Sn-3.0Ag-0.5Cu, Sn-3.5Ag-0.7Cu and Sn-3.9Ag-0.6Cu, at wt%) prepared under three different cooling conditions were investigated (Kim *et al* 2002). The results of the study show that the microstructures of the Sn-Ag-Cu samples prepared with high cooling rate consist of the eutectic phase of β-Sn with fine Ag_3Sn dispersion which surrounds primary beta-Sn grains. In addition the study also indicates that most of the samples prepared with the slow cooling rate exhibit additional large primary Ag_3Sn. One of the conclusions of this study is that lowering the cooling speed decreases the tensile strength and elongation. This degradation effect might be due to the formation of large primary Ag_3Sn intermetallic.

Microstructural coarsening of the Sn-3.2Ag-0.5Cu solder joints during thermal cycling was also investigated by (Ye *et al,* 2000). The study showed that in terms of the average grain size of the Ag_3Sn intermetallic there is very little difference between the as-soldered and thermally cycled samples. In another study by Chi *et al* (2002) the Sn-matrix (in the microstructure of the Sn-3.5Ag-0.7Cu solder ball in a BGA package) was found to be coarsened after the specimens were isothermally aged at 155°C for several days.

2.3.1 Previous studies on modification of Pb-free alloy microstructure with the addition of RE elements

The modification of lead-free alloy microstructure with the addition of rare-earth elements was studied by (Chen *et al*, 2002). In their study, it was outlined that with the addition of the rare-earth elements, the microstructures of all the lead-free solders become more uniform than their respective microstructures without the addition of rare-earth elements. This phenomenon was found in SnZn, SnCu, SnAg, SnBiAg, SnAgCu as well as SnPb alloys. They also stated that with the addition of 0.25% rare-earth elements of mainly cerium (Ce) and lanthanum (La), the coarse β-Sn grains are refined and the IMC particles become finer.

The microstructure indicates that the β-Sn grains are now several micrometers in size and the IMC particles become 0.1 and 0.3 μm. In addition, the width of the eutectic colonies becomes much thinner. The map of Ce element distribution indicates that the rare-earth elements are well dispersed in the alloy and can also be found in the eutectic colonies. Due to the small amount of the RE element additions, there is no clear image obtained when mapping for Ce and La. It is known that the standard Gibbs free energy of formation for Sn–RE intermetallic compounds is lower than those for Cu–RE and Ag–RE. So the RE elements have a higher affinity for Sn, and this explains their effectiveness in the refinement of the Sn-rich microstructure.

The study of cooling rate on lead-free soldering microstructure of Sn-3.0Ag-0.5Cu solder was investigated by (Qiang *et al*, 2005). In their study, it was found that the microstructure of lead free solder Sn-3.0Ag-0.5Cu is more complex as compared to the traditional Sn-Pb solder. It was also outlined that the cooling rate significantly affects the secondary dendrite arm size and the IMC morphology, which influence the solder joint mechanical behaviour. The solder joint microstructure and morphology of three different cooling rates which include air cooling, forced air cooling and water cooling were studied. The morphology of the Ag_3Sn was relatively spherical under water cooling, and had a needle-like morphology under air cooling. The IMC of the joint was a relatively planar

Cu_6Sn_5 layer under water cooling while a nodular Cu_6Sn_5 layer was formed under air cooling.

The impact of the Ag content on the microstructure development of the Sn-xAg-Cu (x= 0.0, 1.2, 2.6, 3.0, 3.5 and 3.9) interconnects was studied in detail by using surface microetching microscopy, cross section microscopy, differential scanning calorimetry and shear test by Lu et al (2006). The thermal treatment was realized by conducting isothermal agieng 150°C for 1000 hours. The study revealed that Ag content had a clear effect on the interconnect microstructure evolution while Ag_3Sn intermetallic compound (IMC) plates were sophisticated microtextures with various morphologies.

The basic microstructure of the Ag_3Sn plates had morphology of a strengthened fan and Ag_3Sn plates grew in central symmetry. Again, it was found that the Cu-Sn IMC microstructures were also influenced by the Ag content, but to a lesser degree. The study also reported that the occurrence of the Ag_3Sn plates did not exactly follow the trend of Ag content increase, but was governed more by the alloy undercooling. Also for a given Cu content, the undercooling of the alloy groups demonstrated a quasi-parabolic behaviour with a minimum apex. Furthermore, it was reported that after ageing, there was size recession and sharp edge smoothening for the Ag_3Sn plates.

In a recent work, Hu *et al* (2008) have systematically investigated the evolution of microstructure and of intermetallic compounds (IMCs), in particular, for lead-free SnAgCuEr solders during isothermal aging tests. The effect of trace amounts of the rare earth element Erbium (Er) on this process has also been studied. The results indicate that diffusion and reassembly occur in the solder matrix during the aging process, and the major influence of the rare earth element Er is concentrated on the nucleation sites.

The $ErSn_3$ (IMCs) formed from the molten solder provide heterogeneous nucleation sites for the IMCs in the soldering and aging process. Subsequently, the Cu-Sn IMCs produced during soldering and Ag-Sn IMCs precipitated during

the aging process have uniform size and distribute evenly in the solder matrix, and the refinement effect has been achieved in Er-containing solder joints. In addition, some cracks can be seen in Er-free solder joints, and the cracks may nucleate and propagate in the structure along the compound/solder boundaries.

2.4 Previous studies on Intermetallic Compound

The IMC layer forms initially as a part of the wetting process by the molten solder, however it can also develop further by solid state diffusion processes of the joint solidification. Moreover the solid state growth rate increases with temperature and time duration. However, the IMC growth rate reduces when the IMC constituents' (eg, Cu-Sn) is saturated during ageing time (Li et al, 2002). The IMC layer indicates that, in fact, a metallurgical bond has formed between the molten solder and the substrate surface.

One of most important factors which influence solder joint reliability is the intermetallic compound (IMC) layer formed between the solder and the substrate interface and within the solder matrix. The presence of intermetallic layer signifies good metallic bonding but the intermetallic layer is also known to be the weakest part of the joint as it is brittle. A thick intermetallic layer will weaken the joint, making it less able to withstand the thermal cycling and operating strains imposed on the joint during its life time. Due to this, there has been a great deal of interest and discussion on the effect of IMC on joint reliability.

The studies reported above on intermetallic compound growth in solder joints revealed that majority of the research have been conducted on dissolution rate of the metal substrate into the molten solder and intermetallic compounds formed between the solder alloy and substrate and within the solder alloy matrix. However, there is not much research work carried out on the effect of pad sizes on intermetallic compound layer thickness (only two research papers have been published in this area – each with opposing views). Therefore, there is an urgent need to study this area of IMC in more detail.

2.4.1 Dissolution rate of a metal substrate into molten solder.

It is important to investigate the dissolution rate of a metal substrate into molten solder because dissolution of the substrate metal may result in de-wetting due to exposure of an unsolderable intermetallic layer on the substrate surface (Romig *et al,* 1991). In addition, the dissolution may also trigger the formation of excessive amounts of intermetallic in the bulk solder joint, which will make a solder joint brittle. Furthermore the dissolution may also trigger the formation of a very thick intermetallic layer, which could reduce the service life of a solder joint. An understanding of the dissolution process is very important in the case of flip-chip solder joints where the dissolution of the metal substrate must be controlled due to limited amount of substrate material (±15 micron thickness).

2.4.2 Intermetallic compounds formed between the solder alloy and substrate and within the solder alloy matrix.

Solid state growth of inter-metallic during service poses a difficult reliability problem. This is because, over the joints service life, inter-metallic layers may grow to significant thicknesses (>20 micron) depending on the kinetics of growth for a particular solder-substrate system and the service condition (Romig *et al* 1991). For this reason, IMC growth continues to be an area of great scientific interest.

One of the early studies of IMCs formation in Sn-Pb solder alloy systems has been reported by (Frear, 1991 and Frear *et al*,1994). The study shows that the most common intermetallic compounds in the Sn-Pb solder joints are Cu-Sn and Ni-Sn compounds that are formed by a reaction between tin in the solder and copper or nickel in the substrate. The intermetallics may be found both in the solder-substrate interface and within the bulk of the solder joints.

At the interface between the solder (Sn-Pb alloys) and the Cu substrate, the intermetallic compositions formed are Cu_6Sn_5 and Cu_3Sn. The Cu_3Sn forms preferentially when there is an excess of copper and the Cu_6Sn_5 forms preferentially when there is an excess of tin. However the Cu_3Sn is also found at

interfaces that are exposed to high tin solder alloys at high temperatures because Cu_3Sn is more stable at high temperatures than the Cu_6Sn_5.

The shape of the inter-metallic layer reflects the crystal structure of the inter-metallic. The Cu_3Sn is orthorhombic in structure and tends to form a tightly coherent layer with nearly equiaxed grain whilst the Cu_6Sn_5 is hexagonal and tends to form a rough layer with knobs or hexagonal prisms that extend into the solder. The inter-metallics formed at the interface may also be found in the bulk of solder joints {after thermal cycling}. The Cu_6Sn_5 forms in bulk solders immediately after solidification.

The formation and growth mechanism of the Cu-Sn intermetallics in the Sn-Pb solder alloys was also studied by Schaefer et al (1997). The growth mechanism can be explained as follows: When the soldering process starts, intermetallic growth into Cu would be rapid and intermetallic dissolution would also be fairly rapid. The net layer growth would occur as long as the growth rate is higher than the dissolution rate. The initial part of the growth curve as seen in Figure 2.7 is the net result of formation of intermetallic and dissolution of intermetallic into the solder.

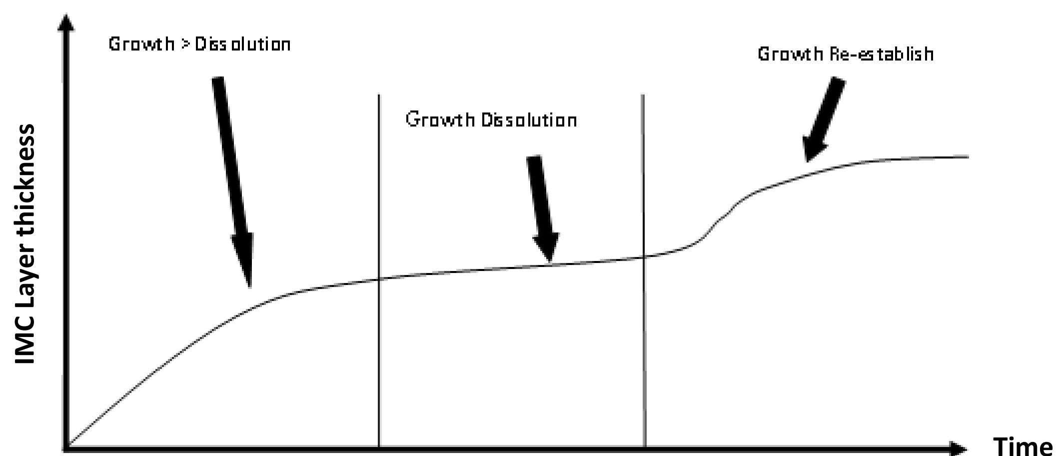

Figure 2.7 Schematic Diagram of Intermetallic Growth during Reflow in a Joint with Low Area-to-Volume (A:V) Ratio (Adopted from Schaefer et al 1997)

As the layer becomes thicker (and if the dissolution rate remains high) these two competing effects will balance out and the net growth will approach zero. During both of these stages the Cu content of the molten solder will increase and eventually the solder would approach saturation. The dissolution would stop and the net layer thickness would begin to grow again. Finally the study indicates that solder joint design (substrate area [A] and solder volume [V] would dictate how rapidly the solder will saturate with Cu; Large A:V ratio saturation will occur rapidly and small A:V ratio saturation will occur slowly.

Harris *et al* (1998) have also carried out a study on inter-metallic layer formation, focusing on the factors which control the morphology and distribution of IMCs within Sn-Pb, eutectic Sn-Ag, and Sn-Cu solder joints. To evaluate the effect of soldering conditions on inter-metallic formation, pellets of the lead-free solder alloys (eutectic Sn-Ag, eutectic Sn-Cu and eutectic Sn-Pb) were reflowed on fluxed copper sheet for different durations.

The study indicates that the factors which affect the quantity of inter-metallic formed during soldering are the substrate materials, temperature/time and volume of solder, nature of solder alloy and morphology of the deposit. In addition the study also shows that the most effective method of minimising the quantity of inter-metallic formed during soldering operation would be to reduce the length of time the molten solder is in contact with the substrate material. Finally the study finds that the factors which affect the morphology of the inter-metallic phase are the quantity of solute, cooling rates, thermal gradients/constitutional undercooling and alternative modes of nucleation.

An experimental study of the dissolution rate of Cu and Cu-Ni alloy into the lead-free solder alloys (Sn-3.5Ag and Sn-3.8Ag-0.7Cu) has been reported by (Korhonen *et al.,* 2000). The experiments were performed by immersing Cu and Cu-Ni alloy metal foil into the solder bath (molten) of Sn-3.5Ag and Sn-3.8Ag-0.7Cu. The results indicates that the dissolution rate of the metals (Cu and Cu-Ni alloys) into the Sn-3.8Ag-0.7Cu alloy was a lot higher than that for the eutectic Sn-Pb alloy. In addition, it was found that the dissolution rate for the Sn-3.8Ag-0.7Cu alloy is slower than that for the Sn-3.5Ag alloy. Finally the study concludes

that a higher Cu content in the Sn-solder alloy results in a decrease in the dissolution rate and an increase in the net intermetallic growth. Similar conclusions have also been reported by (Schaefer *et al*, 1997).

Kang et al (2002) have studied the dissolution rate of electroless Au/Ni(P), electroless Au/Pd/Ni(P), Au/Ni(electroplated) and Cu(electroplated) in Sn-3.5Ag, Sn-3.8Ag-0.7Cu and Sn-3.5Ag-3%Bi solder alloys. The experiment was performed by using known surface finish layers deposited on a Si wafer substrate. Since the initial thickness of the surface finish layer is known, it is then possible to determine amount of the dissolution. The study finds that the dissolution kinetic behaviour in the Sn-3.8Ag-0.7Cu appears to be linear as a function of the reaction time. The dissolution rates of the electroless Au/Ni(P) and electroless Au/Pd/Ni(P) are about half of that of Cu. In addition, the dissolution rate of the substrates in the Sn-3.8Ag-0.7Cu alloy is the slowest. Also, different solder compositions will have different melting temperatures; hence the optimal operating temperature for each alloy will be different, and this temperature change will impact on copper dissolution. Typically the higher the temperature the higher the copper dissolution rate, for two principal reasons: Firstly the saturated copper concentration increases with temperature; secondly the dissolution rate follows Arrhenius behaviour:

$$K = A\exp\left(\frac{-Ea}{RT}\right) \qquad \text{Eqn 2.1}$$

Where K is the dissolution rate, A is a constant independent of temperature, Ea is the activation energy and R is the gas constant (Izuta etal, 2007; Hamilton and Snugovskv, 2007). The detailed results of the study are given in Table 2.5(a and b).

Table 2.5a Dissolution of Various Surface Finishes in Different Solder Alloys. (Kang et al, 2002)

Solder Surface Finish	Substrate Thickness [μm] after 0, 2, 6, 20 min Ageing Time				Total Dissolution	Dissolution Rate (μm/min)
	0 min	2 min	6 min	20 min		
Sn-3.5%Ag						
Cu (4μm)	4.0	1.0-2.3	0.7-1.7	0-1.7	4.0	0.20
Au/Ni(P)/Cu	4.3	3.9	3.4	2.7	1.6	0.08
Au/Pd/Ni(P)/Cu	4.3	3.3	3.0	2.5	1.8	0.09
Sn-3.8%Ag-0.7%Cu						
Au/Ni(P)/Cu	4.3	4.0	3.7	3.3	1.0	0.05
Au/Pd/Ni(P)/Cu	4.3	3.9	3.5	2.8	1.5	0.08
Sn-3.5%Ag-3.0%Bi						
Au/Ni(P)/Cu	4.3	3.7	3.3	2.7	1.6	0.08
Au/Pd/Ni(P)/Cu	4.3	3.5	2.7	2.3	2.0	0.10

Table 2.5b Dissolution of Various Surface Finishes in Different Solder Alloys. (Kang et al, 2002)

Solder Surface Finish	Substrate Thickness [µm] after 0, 2, 6, 20 min Ageing Time				Total Dissolution	Dissolution Rate (µm/min)
	0 min	2 min	6 min	20 min		
Sn-3.5%Ag						
Au/Ni(P)/Cu (electroless)	4.3	3.9	3.4	2.7	1.6	0.08
Au/Ni/Cu (electroplated)	4.7	4.3	3.8	3.6	1.1	0.055
Sn-3.8%Ag-0.7%Cu						
Au/Ni(P)/Cu (electroless)	4.3	4.0	3.7	3.3	1.0	0.05
Au/Ni/Cu (electroplated)	4.7	4.3	4.0	3.8	0.9	0.045
Sn-3.5%Ag-3.0%Bi						
Au/Ni(P)/Cu (electroless)	4.3	3.7	3.3	2.7	1.6	0.08
Au/Ni/Cu (electroplated)	4.7	4.3	4.0	3.7	1.0	0.05

Sharif and Chan (2004) carried out an investigation to compare the dissolution kinetics of the Cu pad of the ball grid array (BGA) substrate into the molten conventional Sn–Pb solder and Sn–3.5Ag solder. In their experiment, a fixed volume of the BGA solder ball (760 µm diameter) was used on the 15–18 µm thick Cu pad having a circular area with a diameter of 650 µm. The dissolution measurement was carried out by measuring the change of Cu pad thickness as a function of time and temperature. A scanning electron microscope (SEM) was

used to observe the microstructure of the solder joint and to measure the consumed thickness of Cu. The result revealed that a fast dissolution of the substrate occurred in the beginning for the molten solder/solid Cu reaction couple. But the dissolution in Sn–Ag was higher than that in Sn–Pb solder. Also the rates of Cu dissolution were measured for different soldering temperatures ranging from 225 to 240 °C and activation energies of 54 and 116 kJ/mol were found for the dissolution reaction in Sn–Ag and Sn–Pb solder, respectively.

The role of Cu content in the dissolution kinetics of Cu in high-Sn solders during the solid/liquid reaction accompanied by interfacial intermetallic compound formation was studied by (Huang *et al,* 2005). Their investigation pointed out that small additions of Cu (0.7%, 1.5%) in high-Sn solders dramatically decrease the dissolution rate of Cu at low temperatures. While Sn-3.5Ag, as expected, has a dissolution rate similar to that of pure Sn. The difference in dissolution rate of Cu in various molten solders is explained in terms of the solubility limit of Cu in molten solders based on the Cu-Sn phase diagram. Furthermore, the study concluded that the correlation between the metallurgical aspects of interfacial (Cu_6Sn_5) phase formation and dissolution kinetics of Cu in molten solders leads to an understanding of the mechanism that controls the dissolution rate of Cu in molten solders.

Dissolution and intermetallic compound (IMC) layer development were examined for couples formed between 99.9 silver (Ag) and molten 95.5Sn-3.9Ag-0.6Cu (wt pct), 99.3Sn-0.7Cu, and 63Sn-37Pb solders, using a range of solder temperatures and exposure times by (Vianco *et a,l* 2006). The investigation reveals that the interface reactions that controlled Ag dissolution were sensitive to the solder composition. The Ag3Sn IMC layer thickness and interface microstructure as a whole exhibited nonmonotonic trends and were controlled primarily by the near-interface solder composition. The kinetics of IMC layer growth were weakly dependent upon the solder composition. The processes of Ag dissolution and IMC layer growth were independent of one another.

The influence of copper concentration, temperature or flow rate of solder on the dissolution of PCB copper electrode was investigated and the methods to control

the copper electrode dissolution were studied by (Izuta *et al,* 2007). The conclusions derived from the experiment revealed that the copper dissolution rate dW/dt for Sn-3.0Ag-xCu can be expressed in an equation parameterized with the temperature (T) and copper concentration in solder (n) and was experimentally validated to be consistent with the tendency predicted by the Nernst-Brunner equation, the amount of copper dissolution in flow solder has a straight-line relationship with the dipping time; within the temperature range practically used in wave soldering, the dissolution rate constant can be regarded as static; the copper dissolution rate for Sn-3.0Ag-1.5Cu solder can be lowered to the equivalent level as that of conventional Sn-Pb eutectic solder, even at 560 K; and the fatigue life of Sn-3.0Ag-0.5Cu and Sn-3.0Ag-1.5Cu solder alloys is almost the same.

In another study, Miao and Hunt (2009) investigated the various factors that influence the dissolution of copper in molten solder, paying particular attention to important parameters such as temperature, solder composition and flow rate. In their study, it was observed that different alloys at the same temperature can have considerably different flow rate, owning to their different viscosities at that temperature. The experiment conducted to determine the dissolution rates of copper in seven lead-free alloys and the Sn-Pb alloy are compared at 255, 275 and 300°C. The findings indicated that generally the samples with a thicker intermetallic layer are those that exhibit a longer dissolution time.

In a recent work, conducted by Madeni and Liu (2011) on effect of thermal aging on the interfacial reactions of tin-based solder alloys and copper substrates and kinetics of formation and growth of inter-metallic compounds revealed that there was migration and dissolution of Cu from the substrate to the solder at lower temperatures (70,100 and 150ºC). The results indicate that the formation of the inter-metallic layer is a diffusion-controlled process. Also the thickness of the layer of inter-metallic compound increases with increasing aging temperature and time. From the review of literature on solder alloy microstructures, it is clear that the microstructural evolution is based on the solder alloys, and that their interactions with the metal (Cu) on the substrate during reflow and solid state during service, are very important but rather complex. It was also revealed that the

microstructural evolution of the solder is affected not only by the process parameters (example, reflow profile) and thermal ageing condition (temperature and time), but also by Cu dissolution into the solder.

2.5 Previous studies on solid-state intermetallic layer growth

A survey of the literature on solid-state intermetallic growth shows that there have been extensive studies on solid-state intermetallic growth in the Sn-Pb solder alloys but there is very little reported on lead-free solder alloys especially Sn-Ag-Cu solder alloys. There is thus a need for further work on the solid-state growth of IMCs in Pb-free alloys, to provide further understanding of the mechanism. The solid state growth of intermetallic compounds could cause more complex engineering problems than intermetallic which form during the soldering process. Another area of concern is the long-term growth of intermetallic layers at the solder-substrate interface during the service life of the solder joint. The solder joint can become more endangered because over long periods of time these layers can grow to significant thickness (>20 micron) and the solder-intermetallic interface may constitute an easy site for crack initiation and propagation.

A review of the previous studies on solid-state intermetallic growth in the Sn-Pb solder joint has been carried out by (Frear, 1991). The report grouped previous work according to the type of metal substrate that was investigated for example Au and Au alloys, Cu and Cu alloys, Ag and Ni. In the report it was revealed that pure Au has linear reaction kinetics with the Sn-Pb solder alloys. The intermetallics formed in the reaction between Sn and Au are AuSn, ASn_2 and $AuSn_4$. For the eutectic Sn-Pb alloys, $AuSn_2$ and $AuSn_4$ were observed but in the Pb-rich layer, only the $AuSn_4$ phase was found.

This is an indication that the layer slows the reaction rate. The $AuSn_4$ was observed to be considerably thicker than the $AuSn_2$. The study concluded that the $AuSn_4$ will dominate in the case of limited amount of Au. The Au based alloy, Pt-Au, has been shown to have a more sluggish intermetallic growth rate. It has also been found that the Pb-rich alloy exhibited considerably lower growth rates,

especially at high temperatures. The solid-state growth kinetics of Cu and Cu base alloys in contact with Sn-Pb solder alloys are much more sluggish than those of Au and Au alloys. In the case of pure Cu in contact with the Sn-Pb alloys, two intermetallic layers are observed as follows: Cu_6Sn_5 forms adjacent to the solder alloy, followed by Cu_3Sn adjacent to the Cu substrate. The Cu_6Sn_5 is always observed in optical metallographic cross sections in the as-soldered condition. The Cu_3Sn is only clearly observed after 4 days annealing at 170°C.

Long-term intermetallic growth kinetics for pure Sn and 60Sn-40Pb plated on Cu and Ag has been studied. The data were fitted to Equation 1. The summary of regression analysis results on various substrate and Sn-Pb solders can be seen in Table 2.6. Reviews of the previous work on intermetallic growth kinetics in Sn-Pb solder alloys show that a great deal of work has been done, and some of the findings are potentially useful in the study of new lead-free solder alloys.

Table 2.6 The Growth Rate of the IMC Layer in the Sn-Pb Solder Alloys (Frear, 1991)

System	**T Range [^{o}C]**	**A**	**Q [J/mol]**	**n**	**r^2**
Sn on Cu	20-170	7.18E3	6.523	0.347	0.968
60Sn-40Pb on Cu	20-170	3.56E4	7.941	0.372	0.975
60Sn-40Pb on Phosphor Bronze	80-135	8.63E3	6.206	0.273	0.942
60Sn-40Pb on Cu-Ni-Sn	80-135	2.15E3	6.179	0.192	0.775
Sn on Ag	20-170	8.62E3	6.762	0.416	0.953

Note: T = temperature (°C), Q = Activation energy (kcal/mole), n = constant = time exponent, r^2 = correlation coefficient and A = constant = pre-exponential constant

An experimental study conducted by Harris *et al* (1998) on solid state intermetallic growth in various lead-free solder alloys has been reported. In the study two experimental approaches were carried out: the first involved bulk solder (large volume) and the second reflowing a much smaller volume. The experimental results indicate that the smaller solder volume specimens tend to have planar intermetallic layers, whereas the cast specimens frequently exhibit large deviation from planarity.

A study aimed at understanding the interfacial phenomena in eutectic Sn-Ag solder joints on Cu plate was conducted by (Choi *et al*, 2000). This study shows that the IMC layer generally thickens with increased soldering time and its morphology gradually changes from the initial columnar type into the scallop type in the later stages of the soldering process. When the solder joints are soldered for shorter than 120 seconds and are aged in the solid state, the morphology of IMCs will change into a layer type from the initial columnar type. On the other hand, when the soldering time is longer than 10 minutes, then the grains of the IMCs will maintain a scallop type after ageing.

Other studies on the solid state growth of intermetallic compounds in the Sn-Ag-Cu Alloys have been reported by (Choi *et al*, 2000; Jang *et al*, 2000; Korhonen *et al,*2000; Salam *et al;* 2001; Yoon *et al,* 2000; Vianco *et a,l* 2001; Chi *et al*, 2002; Kang *et al,* 2002; Zeng *et al,* 2002; Choi *et al*, 2002). For example Vianco *et al* (2001) investigated the intermetallic layer growth between the Sn-4.0Cu-0.5Ag solder alloy and Cu substrate. The experiments were done by immersing the Cu coupon into a molten solder bath and the samples were then aged for between 1 to 400 days at temperature between 70°C to 205°C. The inter-metallic compound layers formed between the solder and the substrate were Cu_3Sn and Cu_6Sn_5 and no Ag_3Sn was observed. The growth kinetics of the different inter-metallic compound layers formed is given by the following empirical equations (Vianco *et al* , 2001):

$Cu_3Sn + Cu_6Sn_5$: $$x = 1.7\times10^{-6} + 1.78\times10^{-2}\cdot t^{0.52}\cdot \exp^{\frac{-57700}{RT}} \quad (2.2)$$

Cu_3Sn: $$x = 4.64\times10^{-4}\cdot t^{0.39}\cdot \exp^{\frac{-38400}{RT}} \quad (2.3)$$

Cu_6Sn_5: $$x = 1.7\times10^{-6} + 1.56\times10^{-3}\cdot t^{0.47}\cdot \exp^{\frac{-49200}{RT}} \qquad (2.4)$$

Where x; is the total intermetallic compound layer or individual sub-layer thickness (μm), t: ageing time (sec), R: universal gas constant (8.314J/mol-°K), T: temperature (°K)

Work on solid state growth of the intermetallics between the Sn-3.8Ag-0.7Cu alloy and various metal substrates has been reported by Jang *et al* (2000), Korhonen *et al* (2000), Horsley (2002), Kang *et al* (2002) and Zeng *et al* (2002). In their work, Jang *et al* (2000), Horsley (2002), and Kang *et al* (2002) showed that the intermetallic layer formed between the Sn-3.8Ag-0.7Cu and electroless Ni/Au has a good adhesion and the IMC composition is $(Cu,Ni)_6Sn_5$.

In addition Kang *et al* (2002) showed that the intermetallic growth rate of the Sn-3.8Ag-0.7Cu alloy is much larger than its dissolution rate (some 3 to 10 times larger). Kang *et al* (2002) also found that the intermetallic growth is directly affected by the solder alloy composition and that surface finish had very little effect. In addition the intermetallic growth rates on the electroplated Ni was found to be some 2 (two) to 3 (three) times slower than those on the electroless Ni(P). The IMC growth in various solders alloys aged at 250°C as shown in table 2.7

Table 2.7 IMC Layer Growth in Various Solder Alloys Aged at 250°C (Kang *et al*, 2002)

Solder Surface Finish	Intermetallic Thickness (µm) After 0, 2, 20 min Ageing Time			Total Growth (µm)	Growth Rate (µm/min)
	0 min	2 min	20 min		
Sn-3.5%Ag					
Cu (4µm)	1.7-8.3	1.7-10.0	1.7-13.3	13.3	0.67
Au/Ni(P)/Cu	0.5-5.3	0.7-8.3	1.0-9.7	9.7	0.49
Au/Pd/Ni(P)/Cu	1.0-5.7	2.0-11.3	3.3-8.3	8.3	0.42
Sn-3.8%Ag-0.7%Cu					
Au/Ni(P)/Cu	1.7-5.0	3.0-7.7	5.0-9.3	9.3	0.47
Au/Pd/Ni(P)/Cu	2.3-5.3	3.3-6.7	5.0-11.0	11.0	0.55
Sn-3.5%Ag-3.0%Bi					
Au/Ni(P)/Cu	1.7-7.7	2.3-10.7	3.0-14.0	14.0	0.70
Au/Pd/Ni(P)/Cu	1.5-5.7	2.0-8.3	3.3-13.3	13.3	0.67

The influence of antimony (Sb) on the soldering reaction and growth kinetics of Intermetallic compound (IMC) in Sn–3.5Ag–0.7Cu–*x*Sb (*x*=0, 0.5, 1.0, and 1.5) lead-free solder joints is investigated by (Chen and Li, 2004). The scanning electron microscope (SEM) is used to observe microstructure evolution of solder joint and to estimate the thickness and the grain size of the intermetallic layers. IMC phases are identified by an energy dispersive X-ray (EDX) and X-ray diffractometer (XRD). The results show that some of the Sb powders are dissolved in the β-Sn matrix (Sn-rich phase), some of them precipitate in the form of Ag_3(Sn, Sb), and the rest dissolve in the Cu_6Sn_5 IMC layer. Again it was also observed that both thickness and grain size of IMC decrease when Sb is added.

The growth exponents for both IMC layer and grains were determined by curve-fitting. The results reveal that Sn–3.5Ag–0.7Cu with about 1.0 wt.% Sb solder system exhibits the smallest growth rate and gives the most prominent effect in retarding IMC growth and refining IMC grain size. Based on the thermodynamic and phase diagram analysis, Sb had higher affinity to Sn element, and it will reduce the activity of Sn by forming SnSb compounds, resulting in a decreased driving force for Cu–Sn IMC formation. A heterogeneous nucleation effect for retarding the IMC growth due to Sb addition is proposed.

Systematic experimental work was carried out by Alam and Chan (2005) to understand the growth kinetics of Ni3Sn4 at the Sn–3.5Ag solder/Ni interface. Sn–3.5%Ag solder was reflowed over Ni metallization at 240 °C for 0.5 min and solid-state aging was carried out at 150–200 °C, for different times ranging from 0 to 400 hours. The cross-sectional studies of interfaces have been conducted by using scanning electron microscopy and energy dispersive x ray.

The growth exponent *n* for Ni_3Sn_4 was found to be about 0.5, which indicates that it grows by a diffusion-controlled process even at a very high temperature near to the melting point of the Sn-Ag solder and the activation energy for the growth of Ni_3Sn_4 was determined to be 16 kJ/mol. The solid state interfacial reaction between the BGA Sn-3.5%Ag-0.5%Cu solder and the Au/Ni/Cu bond pad for MEMS applications was investigated at 150-200°C, for different time period ranging from 0 hrs to 400 hrs and compared with that of the Sn-3.5%Ag solder in another study by (Alam *et al,* 2006).

It was found that 0.5 wt% Cu addition plays a strong role on the interfacial reaction products and the reaction kinetics - especially, at a high temperature near the melting point of the solder alloy. While the Sn-3.5%Ag solder reacts with the Au/Ni/Cu metallization simply by forming only one binary intermetallic compound (BIMC), the Sn-3.5%Ag-0.5%Cu solder reacts in a completely different manner

A number of studies (Frear et al, 1987; Schaefer et al, 1996) have indicated that the growth of intermetallic compound layer plays a debasing role in the mechanical strength of solder joints. An early investigation into the effect of temperature on IMC growth was conducted by (So et al, 1996). The objective was to predict the growth of the IMC layer during the life of the solder joint. Chan et al (1996) further investigated the same process parameters (temperature and time) with the main focus this time on the thermal fatigue of surface mount solder joints. The results indicate that during thermal cycling the IMC thickness increases linearly with the square root of cycle number. In another study, Yoon et al (2004) reported on the effect of temperature (isothermal ageing) on intermetallic compound layer growth between Sn-Ag-Cu and Cu substrate. The focus of the study was on the microstructures and thickness of IMC.

A study conducted by Vianco et al (2004) reported on solid state intermetallic compound layer growth between copper and Sn-Ag-Cu solders. The study concerns the solid state growth kinetics of interfacial IMC layers and at high temperatures. Salam et al (2006) carried out a study on IMC formation and growth in Ultra-Fine Pitch Sn-Ag-Cu solder joints. The main objective of the study was to investigate the effect of solder volume on IMC formation and in particular IMC layer thickness. They concluded that the solder joint volume has no significant effect on the total IMC thickness. In a more recent study, Fix et al (2008) investigated the effect of temperature on microstructure changes of lead-free solder joint during long term ageing and vibration fatigue. The results of several investigations reported by the authors did not answer the question of the effect of low temperatures (thermal cycling ageing) on the growth of intermetallic compound layer thickness, hence the need for further work which is presented in this thesis

In a recent study carried out by Guo-kui et al (2008) they compared the growth kinetics of interfacial intermetallic compound (IMC) layer and its effect on the tensile strength of two solder (Sn3.0Ag0.5Cu and Sn0.4Co0.7Cu) joints. The samples were annealed respectively at 85, 120 and 150°C for up to 1,000 hours and were tensile tested and their cross-sections observed by a scanning electron

microscope. The results showed that, for both solder joints, an approximately linear reduction in tensile joint strength with an increase in the IMC layers' thickness occurred. The tensile strength of Cu/Sn3.0Ag0.5Cu solder joints is slightly better than that of Cu/Sn-0.7Co-0.4Cu solder joints under analogous aging conditions. In addition, the growth kinetics of the overall interfacial IMC layer in Sn0.4Co0.7Cu solder joints can be simply described by the classical growth kinetic theory for solid-state diffusion with an activation energy of 2,996.85 J/mol and interdiffusion constant of $4.15\times10^{-17}\,m^2/s$ which are both relatively low, compared with Sn3.0Ag0.5Cu solder on copper with 14,167.8 J/mol and $65.33\times10^{-17}\,m^2/s$ respectively.

In another recent study Shang et al (2009) investigated the microstructure of the eutectic SnBi/Cu interface with transmission electron microscopy to study the growth mechanisms of the intermetallic compounds (IMCs). Although the growth kinetics of the total IMC layer was similar, the individual Cu_3Sn layer grew faster on polycrystalline Cu than on single-crystal substrates. It was found that, on polycrystalline Cu, newly formed Cu_3Sn grains with a smaller grain size nucleated and grew at both the Cu/Cu_3Sn and Cu_3Sn/Cu_6Sn_5 interfaces during reflow and solid-state aging. The consumption of Cu_6Sn_5 to form Cu_3Sn was faster at the Cu_3Sn/Cu_6Sn_5 interface. While on single-crystal Cu new Cu_3Sn grains nucleated only at the Cu/Cu_3Sn interface, the directional growth of the initial columnar Cu_3Sn controlled the advance of the Cu_3Sn/Cu_6Sn_5 interface.

Hodúlová et al (2011) carried out microanalysis on the kinetics of inter-metallic phase formation at the interface of Sn–Ag–Cu–X (X = Bi, In) solders with Cu substrate. Two intermetallic layers are observed at the interface – Cu_3Sn and Cu_6Sn_5. Cu_6Sn_5 is formed during soldering. Cu_3Sn is formed during solid state ageing. Bi and In decrease the growth rate of Cu_3Sn since they appear to inhibit tin diffusion through the grain boundaries. Furthermore, indium was found to produce a new phase – $Cu_6(Sn,In)_5$ instead of Cu_6Sn_5, with a higher rate constant. The mechanism of the $Cu_6(Sn,In)_5$ layer growth is discussed and the conclusions for the optimal solder chemical composition are presented

The studies reported above on solid-state intermetallic growth revealed that the Sn-Cu intermetallic compounds in the bulk solder, the solder/substrate interface and the presence of the Ag_3Sn intermetallic compound in the solder play pivotal roles in the mechanical performance and the reliability of the lead-free solder interconnect. The literature review also revealed that there the IMC layer thickness for both low temperature (example; 25°C, 40°C and 60°C) cycling and high temperature (175°C) isothermal ageing have not been fully exploited

2.6 Previous studies on reflow profile studies

The reflow profile of the eutectic Sn-Ag solder was studied by Yang *et al* (1995). The study found that by increasing the soldering temperature both the amount and the size of the Cu_6Sn_5 intermetallic dendrites in the bulk solder increased. This is because the solubility and diffusivity of copper in the solder increases as the temperature increases, and the dissolved Cu reacts with Sn to form the Cu_6Sn_5 dendrites during cooling. The study also found that due to the higher Sn concentration, the dissolution of Cu into Sn-Ag solder is faster than that into eutectic Sn-Pb solders, confirming the results reported by (Frear, 1991). This leads to the conclusion that Sn-Ag joints will exhibit more Cu_6Sn_5 dendrites than Sn-Pb solders under similar conditions. Another finding of the study is that the thickness of the Cu_6Sn_5 intermetallic layer at the interface increased with soldering temperature and time and that the size and morphology of the Ag_3Sn inter-metallics changed as the cooling rate was changed.

At high cooling rate (water cooling), the Ag_3Sn intermetallic was finely dispersed in the Sn matrix and can only be seen at high magnification (x4000). At a slower cooling rate (air cooling), Ag_3Sn rods are visible at the solder-substrate interface and a coarser eutectic microstructure is observed. Finally, the study suggested that the soldering process should have low reflow temperatures and short reflow times to minimise the formation of these microstructural features.

In yet another study, Lee (1999) investigated the types of defects affected by the reflow profile. The study found that a rapid cooling rate helped to reduce grain size as well as intermetallic growth. However the maximum cooling rate allowed was often determined by the tolerance of the electronics components against thermal shock. The report advised a maximum cooling rate of 4°C/sec. According to the study, the optimum reflow profile features can be summarised as a slow ramp-up rate to a low peak temperature, followed by a fast cooling rate.

The theoretical aspects of Ramp-to-Spike (RTS) reflow profile were presented in a paper by Surakis (2000). The author proposed a Ramp-to-Spike reflow profile without a soak zone. But it is well know that the function of the soak zone is to reduce the large temperature gradient across the assembly so that all parts of the assembly can be heated uniformly. This means that the reflow profile suggested can only be used in the newly developed oven such as forced convection ovens, which are able to provide heat to an assembly gradually and uniformly. The RTS profiles offer some advantages over the traditional reflow profile, such as better wetting, brighter and shinier joints and fewer problems with solderability.

The Sn-4Ag and Sn-3.8Ag-0.7Cu alloys were also studied by Skidmore *et al* (2000) in order to determine which flux chemistries, lead free alloy and reflow profile have the greatest influence on solder joint quality (in terms of good wetting ability, no solder balls, no solder splashed and no voids). The reflow profiles used for the study are shown in Table 2.8. The study showed that the best solder joint was produced by using the Sn-3.8Ag-0.7Cu alloy, and profile no.4 in Table 2.8

Table 2.8 Reflow profiles used in Skidmore *et al* (2000) experiments.

Profile	Preheat Ramp Rate (°C/sec)	Soak Time [Sec] Between 150-175°C	Preheat Ramp Rate (°C/Sec)	Peak Temp (°C)	Time Above Liquidus (217°C)	Cooling Rate (°C/sec)	Profile Description
1	≤3	90-120	≤3	230≤±5	60≤±15	≤4	Low-Temp Conventional profile
2	≤3	90-120	≤3	250≤±5	60≤±15	≤4	High-temp conventional profile
3	≤3	N/A	≤3	225≤±5	90-120	≤4	Low-temp linear profile
4	≤3	N/A	≤2	235≤±5	90-120	≤4	High-temp linear profile

In another study, Suganuma *et al* (2001) suggested that an optimal reflow profile can be obtained by:

1. Lengthening the preheating time.
   The idea here is to minimise the thermal difference across the assembly.
2. Raising the preheating temperature to between 170° and 190°C to reduce the temperature difference between the soak and the peak temperature, which minimises the temperature differential between components.
3. Extending the peak temperature time.

The idea here is to allow more time for the components with large heat capacity to reach the required reflow temperature.

Islam et al (2004) investigated the interfacial reactions of Sn0.7Cu and Sn36Pb2Ag solder on electrolytic Ni layer for different reflow times. It was found that lead-free solders with high Sn content cause excessive interfacial reactions at the interface with under-bump metallization during reflow and that the interface formed after reflow affects the reliability of the solder joint. The traditionally used Sn36Pb2Ag solder was used as a reference. It was also revealed that during reflow the formation of Cu-rich Sn-Cu-Ni ternary inter-metallic compounds (TIMCs) at the interface of Sn0.7Cu solder with electrolytic Ni is much quicker, resulting in the entrapment of some Pb (which is present as impurity in the Sn-Cu solder) rich phase in the TIMCs.

During extended time of reflow, high (>30 at.%), medium (30-15 at.%) and low (<15 at.%) Cu TIMCs are formed at the interface. Again it was revealed that the amount of Cu determined the growth rate of TIMCs and Cu-rich TIMCs had higher growth rate and consumed more Ni layer. By contrast, an important area which was also considered was the growth rate of the Ni-Sn binary intermetallic compounds (BIMCs) in the Sn36Pb2Ag solder joint exhibited slow reaction and the Ni-Sn BIMC was more stable and adherent. The dissolution rate of electrolytic Ni layer for Sn0.7Cu solder joint was higher than for the Sn36Pb2Ag solder joints. The result of the experiment revealed that less than 3μm of the electrolytic Ni layer was consumed during molten reaction by the higher Sn containing Sn0.7Cu solder in 180 min at 250 °C.

Weicheng (2007) investigated voids formation during reflow soldering of BGA. In the investigation it was found that voids are very easily produced in solder joints. The presence of void in solder joints is one of the critical factors governing the solder joint reliability. Moreover voids may degrade the mechanical robustness of the board level interconnection and consequently affect reliability. It was reported that in order to avoid void formation in the solder joints during the reflow soldering of BGA, reduction of oxides in the solder and substrate metallization are to be considered. It was concluded that vacuum reflow technology is valid technology for void-free and lead-free soldering.

In a recent work, Zongjie (2009) carried out soldering experiments of fine pitch quad flat package (QFP) devices with Sn–Ag–Cu and Sn–Cu–Ni lead-free solders by means of a diode laser soldering system, and compared them with the experimental results soldered with Sn–Pb solders and with infrared (IR) reflow soldering method. The results indicate that under conditions of laser continuous scanning mode and fixed laser soldering time, an optimal power is obtained when the optimal mechanical properties of QFP microjoints are achieved. It was revealed that the mechanical properties of QFP micro-joints soldered with a laser soldering system are better than that of QFP microjoints soldered with IR soldering method. The results also indicate that adding rare earth element Ce to Sn–Ag–Cu and Sn–Cu–Ni lead-free solders improves the mechanical properties of QFP micro-joints, and that the optimal amount of Ce is about 0.03%.

In convectional reflow soldering, Sn-Ag-Cu solder is predominantly used and the soldering defects may be reduced if the profile is optimized to the manufacturer's recommended parameters. However, optimization of convectional reflow profiles used was based on Interconnecting and Packaging Electronic Circuits (IPC) and Joint Electronics Device Engineering Council (JEDEC) standards 9JEDEC, 1999).

It is well known that reflow profile influences wetting and microstructure of the initial solder joint, and thus impacts on solder interconnection reliability. The role of reflow profile on tin-lead (SnPb) solder joint performance has been well studied (Lee, 2002; 1999). However, there are some important differences such as melting and peak temperatures must be taken into consideration for Pb-free soldering. A study of eutectic tin-silver (Sn-Ag) reflow profiles has also been reported (Yang, 1995); the study's focus was on the effect of the soldering temperature, soldering time and cooling rate.

In another study, Lee (1999) reported the types of defects caused by the reflow profile. Moreover, authors of (Skidmore and Waiters, 2000) carried out experiments to determine which flux chemistries, lead-free alloys and reflow profiles had the greatest influence on solder joint quality in terms of wetting ability, solder balls, solder splashes and voids. The benefits of ramp-to-spike

(RTS) reflow profile were reported (Suraski, 2000). In another development, Suganuma and Tamanaha (Suganuna and Tamanaha, 2001) discussed the available reflow technology for lead-free soldering.

The effects of reflow profile parameters on intermetallic compound (IMC) thickness and microstructure of Sn-Ag-Cu solder joints were studied (Salem et al, 2004). It was found that the most significant factor in achieving a thin IMC layer and fine microstructure is the peak temperature. Also, the effect of reflow profile on the solder joint shear strength was reported (Pan, 2007). Investigations conducted on the effect of reflow profile and thermal shock on IMC thickness for Sn3.0Ag-0.5Cu alloy was studied (Webster, 2007). Work conducted by Skidmore (2000) revealed that the reflow profile, flux chemistry and lead-free alloy influence solder joint quality in terms of good wettability. Also, they stated that there was no solder balling, no solder splashing and no voiding after the reflow soldering with Sn-3.8Ag-0.7Cu.

A study conducted in (Lee, 2002) indicates that the infrared reflow profile is not optimum for convection ovens and modern solder pastes. However, through the analysis of defect mechanisms, his work revealed that a gentle ramp to about 175°C and a very gradual rise above liquidus, followed by a ramp to a peak temperature of 215°C will result in the highest yields for 95.5Sn-3.8Ag-0.7Cu solder paste. In a study (Suraski, 2000) investigated ramp-to-spike reflow profile without a soak zone. Moreover, Salem et al (2004) investigated two types of reflow profiles, i.e. Ramp-to-spike (RTS) and Ramp-soak-spike (RSS) for Sn-Ag-Cu lead-free solder.

The optimization of reflow profile based on heating factor had been proposed (Gao et al, 2007). The results of the experiment indicated that the most significant factor in achieving a joint with a thin IMC layer and fine microstructure was the peak temperature. The results suggest a peak temperature of 230°C for the Sn-Ag-Cu lead-free solder. The recommended time above liquidus is 40 sec for the RSS and 50-70 sec for the RTS reflow profile respectively. It is reported that the reflow process is the key to achieve a totally well mixed Sn/Ag alloy (Bigas and Cabruja, 2006). In their work, the optimum reflow time used is 20 minutes. The

reflow cycle splits in the following steps: Preheating from 170 to 240 °C at a ramp rate about 0.12 °C/s, followed by 20 min reflow at 240 °C and a cooling step at 25 °C. All the steps performed inside a glycerol bath.

Due to high usage of BGA packages, an investigation of reflow profile optimization for Sn-Ag-cu alloys was conducted. The results show that for each alloy there exists an optimum reflow process window within which one can expect best solder joint reliability performance (Lee, 2009). In another study, Bo et al (2009) reported on reflow profile optimization of micro BGA soldering joints. The results indicated solder joints produced using optimal reflow parameters setting have higher mechanical reliability, and those reflowed farther away from this optimal value have less reliability.

Haseeb and Leng (2011) present data on the effects of Co nano-particles on the interfacial inter-metallic compounds in between lead-free solder and copper substrate. The work shows that the addition of Co nano-particles suppresses the growth of Cu_3Sn but enhances the growth of Cu_6Sn_5.

The studies reported above on solder reflow profiles revealed that the reflow profile is one of the most important factors in determining the soldering defect rate. Therefore it is extremely important to have the reflow profile engineered properly in order to achieve both high yield and high reliability. The goal of setting a reflow profile, that is the relationship between temperature and time, is to obtain the most uniform temperature across the circuit board while minimising heat exposure. In order to achieve this goal, a slow heating rate is one technique for compensating for the inherent large disparity in the heat transfer among the various components.

2.7 Gaps Identified from the Literature Review

From the studies reported above on lead-free solder alloys, solder alloys microstructures, intermetallic compounds formation, and solid-state growth of intermetallic compound layer thickness and reflow profiles for lead free soldering, the following gaps in knowledge have been identified in four key research areas. These are -

a. The effect of pad sizes on inter-metallic compound layer formation and growth for lead-free solder joints under isothermal ageing

b. The cycling temperatures and reflow profiles on inter-metallic growth between Sn-Ag-Cu solder alloy and Cu.

c. The effect of reflow soldering profile parameters on Sn-Ag-Cu solder bumps using Cu substrate

d. The effect of inter-metallic compound layer thickness on the shear strength of 1206 surface mount chip resistor with Nickel plated termination and Sn-3.8Ag-0.7Cu on Cu surface finish.

2.7 Summary

The literature review presented in the first section highlighted the characteristics of lead and lead-free solder alloys used in electronics packaging and assembly. Previous studies on the solder alloy microstructures have been reviewed in the second part of this report. Most of the studies reported in this section are concerned with work on lead-based solder alloys and up-to-date there are very few reports on lead-free solder alloy microstructures. This may due to the fact that the ban on leaded solder alloys only came into force on 1 July 2006. The review of literature on lead-free solder alloy microstructures showed that most of the studies were focused on the need for reducing the intermetallic layer thickness. The review on IMC growth shows that the main areas of interest include the effect of dissolution rate, diffusion and solid state growth on IMC and consequently solder joint reliability. Finally, the review on the effect of reflow soldering profile showed that the studies were focused on understanding the importance of specific parameters such as the peak temperature, soak temperature, time above liquidus and cooling rate. A review of the literature on solder joint metallurgy and microstructure is presented in the next chapter.

CHAPTER III: SOLDER JOINT METALLURGY AND MICROSTRUCTURE

3.1 Introduction

This chapter provides an overview of the fundamentals and basic the concepts used in the study of alloy systems, solder joint metallurgy and microstructure. An understanding of these basic concepts is essential for the understanding of the metallurgy of solder joints; the formation of IMCs, the microstructures and the impact of IMC behaviour on solder joint reliability. This chapter is divided into three main parts. The first part presents the basic concepts used in the study of the microstructure of solder joints; in particular coarsening and precipitation. The second part of the chapter deals with the concepts used in the study of IMC formation and growth, and in particular the principle of diffusion and solid state growth. The final part of the chapter presents some of the important concepts of the solidification process including nucleation and growth, and thermodynamics of reaction.

3.2 Intermetallic Compound Formation

Intermetallic compound is one that is made up of two or more metallic elements, producing a new phase with its own composition, crystal structure and properties (Askeland 1996). The advantage of Intermetallic compounds is that they tend to have a high melting point, stiffness and resistance to oxidation and creep. In solders the intermetallic compounds are dispersed into a softer, more ductile matrix. The Sn-Ag-Cu solder alloy might benefit from the above positive effects because Ag_3Sn and Cu_6Sn_5 intermetallics are present in the alloy (Hwang 2001). The intermetallic compounds are not only present in the bulk solder but also at the interface between the solder and substrate. At the interface, the intermetallic compounds form a strong bond to the metal surfaces. The bonding process is promoted by chemical reactions between the solder and the substrate that form intermetallic compounds.

The bonding function of the IMC generally tends to deteriorate with the time. This deterioration will be faster if the joint is subjected to high temperatures. It has been reported that the thickness of the intermetallic layer could grow to 20μm for the eutectic Sn-Pb solder held at 170°C for thirty days and the fracture toughness can also decrease by a fourfold factor (Morris *et al,* 1994). This implies that although the intermetallic layer may not pose any problems in the as-soldered joint (properly soldered one) but will lead to long-term reliability problems especially when the joint is subjected to high temperatures. It has been suggested that the same problems may also occur in the joints made with the Sn-Ag-Cu lead-free solder alloy.

3.2.1 Diffusion

The study of intermetallic compound in the solder-substrate system would not be complete without an understanding of the basic principles of diffusion. Diffusion can be defined as the mechanism by which matter is transported into or through matter (Brophy *et al,* 1964). Because the movement of each individual atom is always obstructed by neighbouring atoms, its motion is an apparently aimless series of flights and collisions. However the net result of a large number of these events can be an overall specific displacement of the atoms. In fluids, liquids and gases, diffusion mechanisms cause a relatively rapid disappearance of differences in concentration.

In solids, the atoms are more tightly bound to their equilibrium positions. However, there still remains an element of uncertainty caused by the thermal vibrations occurring in a solid which permits some atoms to move randomly. A large number of such movements could result in a significant transport of materials. This phenomenon is called solid-state diffusion. In a pure substance, a particular atom does not remain at one equilibrium site indefinitely. It tends to move from place to place in the material. This movement in pure material is known as self-diffusion. In a mixture of more than one element, such as a Sn-Pb solder alloy, atoms of one element could diffuse through the lattice of the other. This diffusion process is called interdiffusion.

The forces responsible for diffusion can always be analysed thermodynamically. Since diffusion occurs spontaneously, it should be viewed as a process which decreases free energy or increases entropy. Increase of entropy is usually more apparent. Consider this example, interdiffusion of components A and B, where complete solid solubility occurs in the A-B system. A and B are placed in contact and heated to a temperature where diffusion will occurs. If the equilibrium state is a single homogeneous solid solution, A will diffuse into B and vice versa until equilibrium is reached. Thus this process is irreversible and therefore increases entropy.

There are mechanisms by which atoms diffuse as illustrated in Figure 3.1. Figure 3.1a shows vacancy diffusion in which an atom moves to the next lattice site and occupies a vacancy there. In Figure 3.1b an atom moves out of its lattice and becomes an interstitial atom which is free to move. The diffusion mechanism shown in Figure 3.1b is known as interstitial diffusion. In Figure 3.1c atoms in a ring simultaneously move to adjacent lattice sites. In Figure 3.1d two atoms change place directly.

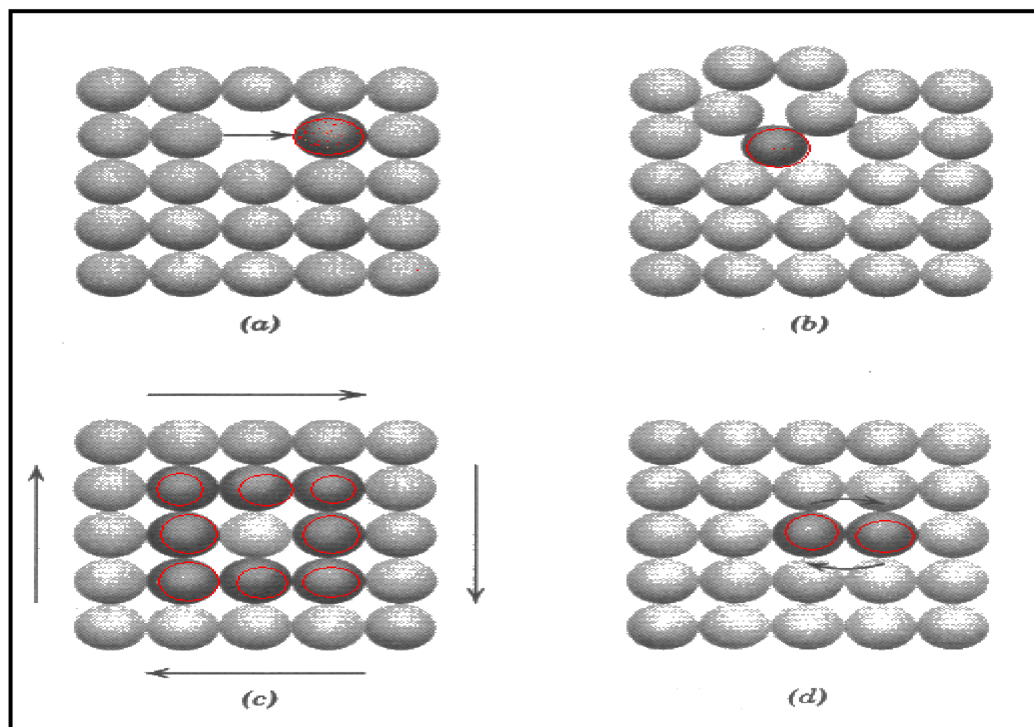

Figure 3.1 Diffusion Mechanisms of an Atom in Solids

Adopted from Brophy et al (1964).

The rate of diffusion can be measured by Flux [J]. Flux is defined as the number of atoms passing through a plane of unit area per unit time (Brophy et al 1964). Fick's first law explains the net flux of atoms, as followed:

$$J = -D \cdot \frac{dc}{dx} \qquad (3.1)$$

Where:

J is the flux (atom.m^{-2}.s^{-1}),

D is the diffusivity or diffusion coefficient (m^2.s^{-1}), and dc/dx is the concentration gradient (atom.m^{-4}).

Concentration gradient (dc/dx) defines how the composition of the material varies with distance. It may be created when two materials of different composition are placed in contact. For example: the concentration gradient builds up in a solid material when is in contact with gas or liquid.

Diffusion coefficient (D) is related to temperature and the relationship is shown in the following Arrhenius equation:

$$D = D_o \cdot \exp^{-\frac{Q}{RT}} \qquad (3.2)$$

Where:

D_o = Diffusion Coefficient (m^2.s^{-1})

Q = Activation Energy (J/mole)

R = Gas Constant = 1.98 Cal/mol/K = 8.31 J/mol/K

T = Temperature (K)

The Arrhenius equation implies that when the temperature of a material increases, the diffusion coefficient will increase; hence the flux of atoms will increase as well. Another implication is that at higher temperatures, the thermal energy supplied to the diffusing atoms permits the atom to overcome the activation energy barrier and more easily move to new lattice sites. At low temperature, diffusion is very slow and may not be significant.

3.2.2. Formation of Intermetallic Compound Layers

When molten solder reacts with the solid substrate, two processes are observed to occur simultaneously (Frear *et al* 1991): the substrate metal dissolves into the molten metal and the active constituent in the solder combines with the substrate metal to form intermetallic compounds on the surface of the substrate metal. The amount of the substrate metal that goes into the solution is related to its solubility in the particular solder and the amount of the intermetallic compound that forms at the surface of the substrate depends more on the solubility of the active element in the base metal. Both processes obviously also depend on the time spent above the solder's liquidus temperature. Note also that additional intermetallics may form in the interface between the solder and the substrate after the solder solidifies since the solid solder may be supersaturated with the substrate metal; hence the reaction process will dominate.

The schematic of the IMC layer formation during the soldering process using Sn-Pb solder alloy is illustrated in Figure 3.2 (Lea, 1991). In the liquid state, the flux of the substrate element (J_S^C) goes to the solder and also the flux of the active element in the solder (J_C^S) goes to the substrate. During that state, an intermetallic layer will form in the interface between the solder and the substrate. When an intermetallic layer is formed, additional fluxes will be present: fluxes of the substrate (J_S^{SC}) and the solder's active-element (J_C^{SC}) through the layer.

In most cases, at the interface between intermetallic [SC] and solder (C), the rate of diffusion of active constituent (C) in the solder is much greater in the intermetallic (SC) than in substrate (S), $J_C^{SC} >> J_C^S$. The reason may be due to the low solubility of tin in the Cu. Thus V_1 is always negative. This implies that the intermetallic grows into the substrate.

At the interface between Substrate (S) and intermetallic (SC), when the solder is in liquid state especially for the eutectic Sn-Pb solder alloy, there is an appreciable solubility of the substrate element in the solder and in general $J_S^C > J_S^{SC}$. Since J_S^{SC} decreases as the thickness z_0 of the intermetallic increases, a steady state condition can be attained where the rate of dissolution of intermetallic at the SC-C

interface (V_2) in equal to its rate of growth at the S-SC interface (V_1). If the volume is limited as it is in the CSP joints, the concentration of substrate in the molten solder rises and hence J_S^C decreases, leading to an increase in V_2 and increase in the steady state thickness of the intermetallic.

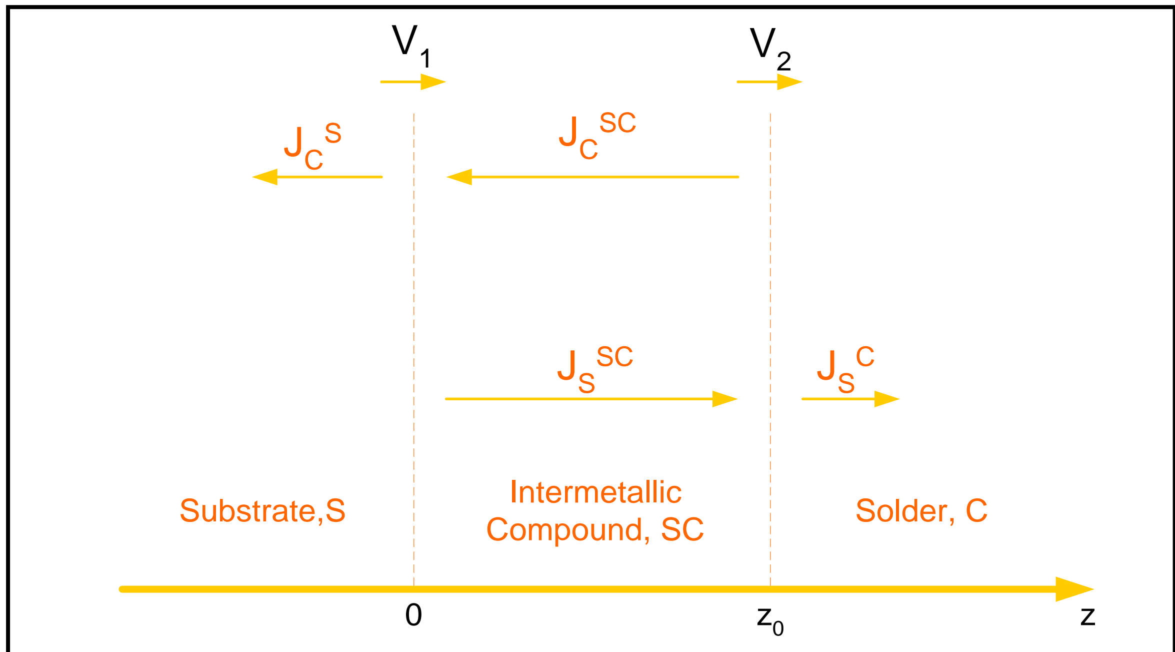

Figure 3.2 Schematic Diagrams Illustrating the Growth of an Intermetallic Compound

(Adopted from Lea, 1988)

The growth of the intermetallic layer can be derived from first Fick's law (Equation 3.1). The rate of thickening of the intermetallic layer is approximately (Lea, *1988*; **Steen, 1982)**

$$\frac{dz_0}{dt} = v_1 - v_2 \propto \left(J_C^S - J_C^{SC}\right) - \left(J_S^{SC} - J_S^C\right) \quad (3.3)$$

Where:

z_0 = thickness of intermetallic compound layer

When the solder is liquid, $J_C^{SC} \gg J_C^S$, so that the growth rate is:

$$\frac{dz_0}{dt} \propto \left(J_C^{SC} + J_S^{SC} - J_S^C\right) \quad (3.4)$$

As time progresses, $\frac{dz_0}{dt}$ reduces to zero and the thickness z_0 is maintained at a constant value.

3.2.3. The Solid State Growth

The schematic of the solid state growth of the intermetallic layer in the Sn-Pb solder joints can be described as follows: At the interface between intermetallic (SC) and solder (C) (as shown in Figure 3.2), the solubility of the substrate (S) in the solder (C) is generally negligible in solid state. Hence the flux of *S* atoms through the intermetallic is much greater than the flux away from the *SC-C* interface into the solder (C). Thus $J_S^{SC} >> J_S^C$, V_2 is positive and the intermetallic grows into the solder.

As it was pointed out earlier in the discussion on the intermetallic formation (section 3.4.2) at the interface between Substrate (S) and intermetallic (SC), the rate of diffusion of active constituent (C) in the solder is much greater in the intermetallic (SC) than in substrate (S), $J_C^{SC} >> J_C^S$. Thus V_1 is always negative. This implies that the intermetallic grows into the substrate.

In summary, in the solid state, $J_C^{SC} >> J_C^S$ and $J_S^{SC} >> J_S^C$, and this means that the growth rate of the intermetallic layer can be derived (from equation 3.3).

$$\frac{dz_0}{dt} \propto \left(J_C^{SC} + J_S^{SC}\right) \quad (3.5)$$

Therefore the layer growth is controlled by the diffusion through the intermetallic layer so that it has a parabolic dependence of thickness on the time.

$$x^2 = Dt \quad (3.6)$$

Where x^2: layer growth and D is the overall diffusivity for the intermetallic layer growth and varies with temperature, according to the Arrhenius equation shown in Equation 3.2.

Another empirical relation for predicting the total intermetallic thickness was later introduced by (Romig *et al,* 1991). In their study, they found that the intermetallic layer does not only grow at a parabolic rate but also experience faster growth rate over an initial period. The following equation is suggested:

$$x(t,T) = x_o + A \cdot t^n \cdot \exp^{-\frac{Q}{RT}} \quad \text{……………………………………………………… (3.7)}$$

Where:

x = total intermetallic thickness at time t and temperature T

x_o = the thickness of intermetallic in the as-soldered condition (at t=0)

A, n = constants

R = Gas Constant = 1.98 Cal/mol/K = 8.31 J/mol/K

Q = activation energy (J/mol)

T = Temperature (K)

The two types of solid-state growth represented by the above equation could be distinguished based on the value of the time exponent n:

- n=1, Linear Growth Kinetics
  Linear growth implies that the growth rate is limited only by the reaction rate at the growth site. Example: Au in contact with eutectic Sn-Pb solder alloy.
- n=0.5, Parabolic Growth Kinetics
  Parabolic growth kinetics applies when layer growth is controlled by bulk diffusion of elements to the reaction interface. Example: Cu in contact with eutectic Sn-Pb solder alloy.

3.3 The Solidification Process

It is important to note that the solder alloy is heated up to its liquid phase during the soldering process and that the liquid solder solidifies as it cools below the liquidus/eutectic temperature. The structure produced during the solidification process affects the mechanical properties and influences the reliability of the solder joint. In particular, the solder microstructures (grain size and shape) and the interface inter-metallic (thickness) may be controlled by solidification. During solidification, the arrangement of the atomic structure of the solder changes from a short-range order to a long-range order or crystal structure. Solidification

requires two steps: nucleation and growth. Nucleation occurs when a small piece of solid forms from the liquid. Growth of the solid occurs as atoms from the liquid are attached to the solid until no liquid remains.

In this section, some of the basic concepts of the solidification process are introduced, with special emphasis on the behaviour in solder materials.

3.3.1. Nucleation and Growth

A material solidifies when the liquid cools just below its melting temperature, because the energy associated with the crystalline structure of the solid is less than the energy of the liquid. The energy difference between liquid and solid is called the volume free energy [ΔG_v]; as the solid grows in size, ΔG_v increases. The changes of the volume free energy as the solid grows bigger are illustrated in Figure 3.3

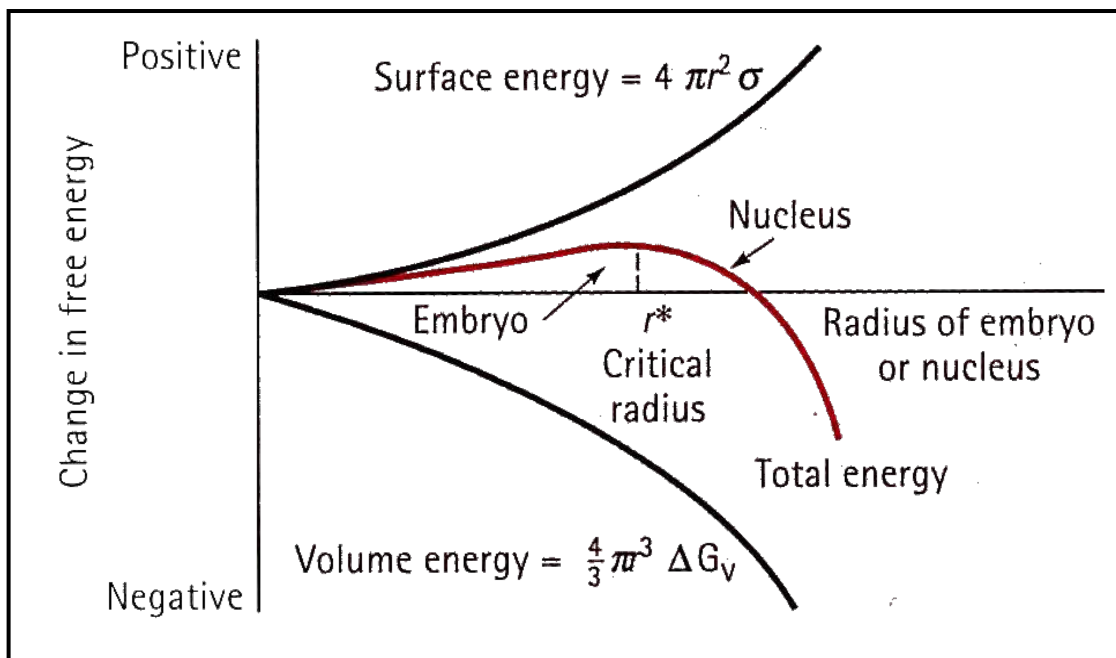

Figure 3.3 The Total Free Energy of the Solid-Liquid System Changes with the Size of the Solid

Adopted from Askeland (1996)

As the solid forms, an interface is created between the solid and the remaining liquid mass. A surface free energy σ □is associated with this interface; the larger

the solid, the greater the increase in surface energy as shown in Figure 3.3. Thus the total change in energy ΔG, as seen in Figure 3.3) is as follows :(**Askeland, 1996)**

$$\Delta G = \frac{4}{3}\pi r^3 \cdot \Delta G_v + 4\pi r^2 \sigma \quad \text{...} \quad (3.8)$$

Where

$\frac{4}{3}\pi r^3$: the volume of a spherical embryo of radius r,

$4\pi r^2$: the surface area of a spherical embryo,

σ : the surface free energy

ΔG : the volume free energy (negative change)

When the solid is very small (less than r* as shown Figure 3.3), further growth causes the total free energy to increase. Instead of growing, the solid prefers to re-melt and cause the free energy to decrease; thus, the metal remains liquid. This small solid volume is called an embryo. If an embryo manages to overcome the barrier, a new nucleus will be created. That is when the solid is larger than r*; further growth causes the total energy to decrease. The solid, that now forms, is stable, nucleation has occurred, and the growth of the nucleus could begin.

3.3.2 Homogeneous Nucleation

As the liquid cools further below the equilibrium freezing temperature, two factors combine to favour nucleation. First, atoms cluster to form larger embryos. Second, the larger volume free energy difference between the liquid and the solid reduces the critical size of the nucleus. Homogeneous nucleation occurs when the undercooling becomes large enough to cause the formation of a stable nucleus. The undercooling is the equilibrium freezing temperature minus the actual temperature of the liquid.

3.3.3 Heterogeneous Nucleation

Except in unusual laboratory experiments, homogeneous nucleation do not occurs in liquid metals. Instead, impurities in contact with the liquid either suspended in the liquid or on the wall of the container that holds the liquid, provide a surface on which the solid can form. A radius of curvature greater that the critical radius is achieved with very little total surface between solid and liquid. Only a few atoms must cluster together to produce a solid particle that has the required radius of curvature. Much less undercooling is required to achieve the critical size, so nucleation occurs more readily. Nucleation on impurity surfaces is known as heterogeneous nucleation (Askeland 1996).

Once nucleated, the solid need a continuous supply of energy to expand it boundary and grow. To minimise this energy, the nucleation tends to occur preferentially at preformed interfaces. In solder joints, for example, the available interfaces include grain boundaries, and the solder-substrate interface. This energy is the driving force for phase growth. It is defined as the fraction of energy of the system that can be converted into mechanical work. Thus, from an energy level standpoint, the phase that offers the largest decrease in free energy is favoured.

In a multi-element system, such as the Sn-Ag-Cu solder joints, the nucleation of an alloy requires more than the overcoming of the energy barrier because of the different constituents of the alloy present at the nucleation sites with appropriate concentrations throughout the period of nucleation. In this condition, the nucleation depends on the spatial distribution of the different constituents at any given time and their ability to diffuse towards the nucleation site.

In the formation of the intermetallic compound, the reaction kinetics varies at different stages of the formation process. In a bulk solder joint, for instance, the constituents are dispersed and required to diffuse at a distance. Hence intermetallic compounds are at a disadvantage during the nucleation step.

As the dimension of the joint becomes smaller, the constituents of the compounds even if present at low concentrations in the solder could diffuse fast enough and contribute to stabilising the nucleation. Hence in a very small solder joint such as flip-chip joints, intermetallic compound layers might grow absolutely thicker in the interface. Detail of the study on the effect of solder pad size on IMC formation is presented in Chapter 5.

3.3.4 Activation Energy

A large class of transformations in materials (although thermodynamically possible) occurs very slowly. Solder joints in electronics products provide an example of such delayed transformation (Sn in a solder alloy and Cu in a substrate can react forming Cu_6Sn_5 or Cu_3Sn intermetallic compounds). However not all of the Sn in a solder alloy can transform spontaneously to the intermetallic compounds when in contact with Cu in a substrate. This apparent lack of spontaneous reaction is in fact just a very slow reaction rate because of the existence and nature of any barriers retarding the reaction (Energy is one of them). The Arrhenius Equation (which is empirically derived) introduces the concept of activation energy, an energy barrier which must be surpassed in order to achieve equilibrium.

The Swedish chemist Arrhenius (1859-1927) developed an expression to describe the increase in rate of chemical reactions with increased reaction temperature. The equation can also be used for a large number of reactions and transformations, both non-chemical and chemical. The Arrhenius Equation is expressed as follows

$$rate = \text{constant} \times e^{-\frac{Q}{RT}} \quad (3.9)$$

Where:

Q = Activation energy([J/mole)

R = Gas constant (8.31 J/mol/K)

T = Temperature (K)

In equation 3.9 the dependence of reaction rate upon temperature was specified by the quantity of the activation energy (Q). The exponential dependence of temperature coincides with that of the Maxwell-Boltzmann Distribution, which specifies the energy distribution of molecules in gases. The Boltzmann relation expresses the probability of finding a molecule at an energy ΔE greater than the energy at a particular temperature, which could be expressed by the following equation:

$$probabiliy \propto e^{-\frac{E}{k \cdot T}} \qquad (3.10)$$

Where:

E = Energy (J/mol)

k = Boltzmann constant (J/mol/K)

T = Temperature (K)

Notice the similarity between the expression in 3.9 and 3.10. This similarity suggests an important property of the rate of a reaction or transformation. It is clear that the reaction rate depends on the number of reacting species that have an amount of energy (ΔE*) greater than the average energy (E_r) of the reactants. The transformation of the energy in such a case is illustrated schematically in figure 3.4, in this figure, the curve represents the energy of a single reacting species as it progresses from the un-reacted condition on the left to the reacted condition on the right. For instance, the reacting species might be an atom diffusing through a crystal lattice in a solder joint. The minimum in Figure (3.4) would be an equilibrium site and the maximum in Figure (3.4) would be the position between the sites, where neighbouring atoms must be pushed aside in order to pass from one site to another. The reaction coordinate would be the physical distance travelled by the atom.

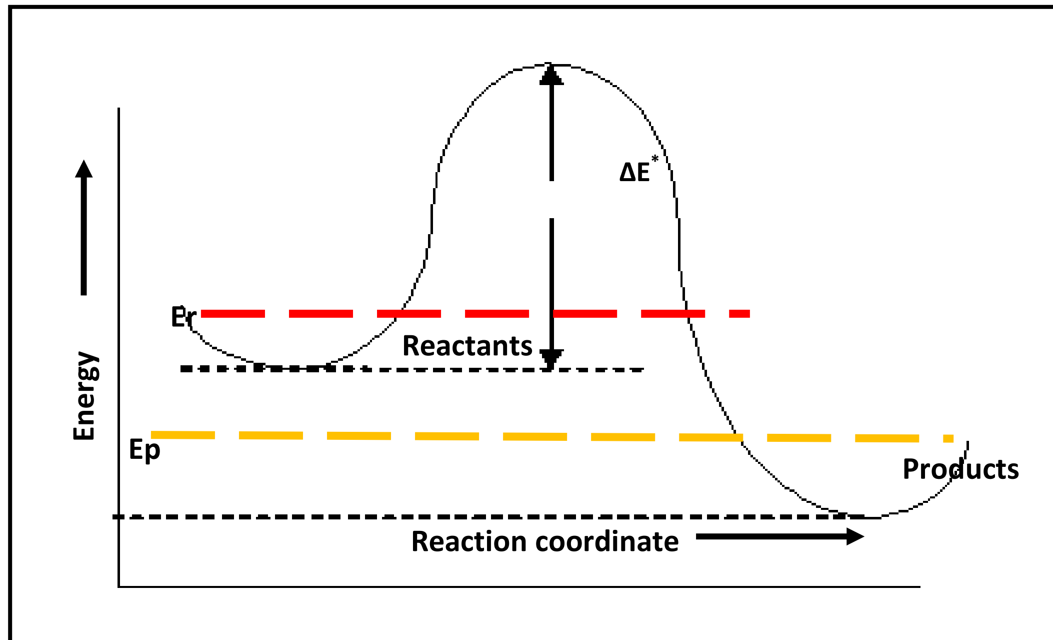

Figure 3.4 Schematic of energy changes from the un-reacted to the reacted state (Adopted from Brophy *et al* 1964.)

If a metal "A" is put in contact with a metal "B" and both are annealed at temperature T_1, atoms from both sides may inter-diffuse and react to form all or some of the equilibrium compounds at the interface. In the solder system between Sn solder alloy and Cu substrate, the Cu_6Sn_5 is the most common intermetallic to form at the interface during as-soldered condition and the Cu_3Sn would only be clearly observed after annealing at 150°C for more than 50 hours (Salam *et al,* 2001).

This phenomenon can be explained from a thermodynamic view point with the following illustration of the growth competition between two compounds. Figure 3.5 shows an example where two distinct paths could be followed by a solid state reaction, leading to the formation of either of two compounds which are in competition. In this situation, the two equilibrium compounds have formation energies ΔG1 and ΔG2. Because ΔG2 is larger than ΔG1, Cu_3Sn is a more stable compound than Cu_6Sn_5 and is hence more likely to grow from an energetic stand-point. However in the real case kinetic rather than energetic considerations will dictate the outcome of the reaction. The faster alloy to nucleate among the two might be the one to form. In Figure 3.5 the kinetic barrier (ΔH1) of nucleation of

the meta-stable compound Cu_6Sn_5 is distinct lower than that (ΔH2) of the more stable alloy Cu_3Sn. Furthermore the greater rate of nucleation of Cu_6Sn_5 does not guarantee that the meta-stable phase would not transform to Cu_3Sn. The meta-stable transformation might occur if the nuclei manage to overcome the kinetic barrier ΔH2. As has been observed in the real case, the Cu_3Sn starts to form after long annealing.

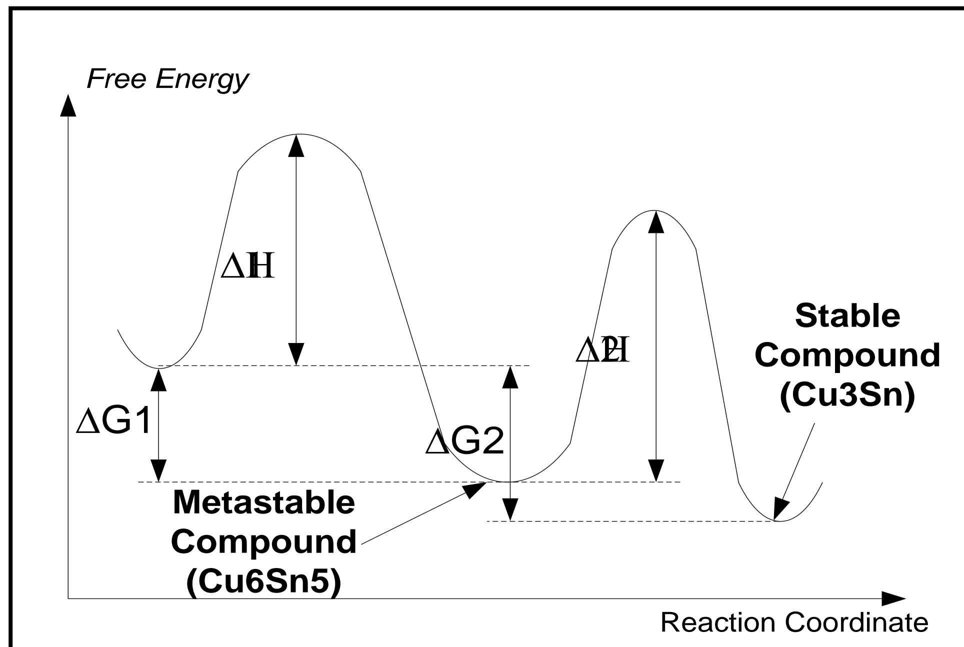

Figure 3.5 Illustration of the Variation of the Free Energy during Growth Competition between a Stable Compound and a Metastable Compound (Adopted from Brophy *et al* 1964.)

3.4 Summary

The understanding of solder joint metallurgy and microstructures is essential in this study of solder joint reliability as bonding between the component, solder and substrate is achieved through a metallurgical reaction. A number of fundamental concepts associated with IMC formation and growth in solder joints have been presented in this chapter. These include diffusion, solid state growth, nucleation and growth amongst others. The experimental procedure and methodology used for the study of IMC layer formation and growth in Sn-Ag-Cu solder joint is presented in chapter 4

CHAPTER IV: EXPERIMENTAL PROCEDURE AND METHODOLOGY

4.1 Introduction

This chapter presents the materials and methods used in this study and in particular the methods used for studying IMC formation and growth in Sn-Ag-Cu lead-free solder joints.The first section of the chapter presents a description of the test vehicles used in various experiments of the study. The second section deals with the experimental equipment used for different parts of the study. The third part presents the stencil printing process employed in the study. The fourth and the fifth sections deal with a description of the reflowed profiling process and the thermal ageing process respectively. The last part presents the metallurgical / metallographic preparation of the test samples and IMC measurement.

4.2. Description of Test Vehicles used in the Study

Four different types of test vehicles were designed and made in-house. The materials used for the test vehicles are those commonly used in the Electronics Manufacturing Assembly for Surface Mount Technology. Type one (1) was designed for experiment on the effect of pad size on IMC layer formation and growth in Sn-Ag-Cu solder joints. A detailed description of the test vehicle is presented in figure 4.1. The test vehicle consists of FR4 PCB single sided 100% copper clad with a thick film metallization. The substrate dimension is (100 * 160 * 1.6) mm. Lead-free solder (96Sn-3.8Ag-0.7Cu) was deposited on five different pad sizes, replicating a typical surface mounted passive component pad sizes, which include (1210) resistor, (1812) inductor, Metal Electron Leadless Face (MELF) resistor, Tantalum C and capacitors D

4.2.1 Type 1 Test Vehicle for evaluation of pad size on IMC

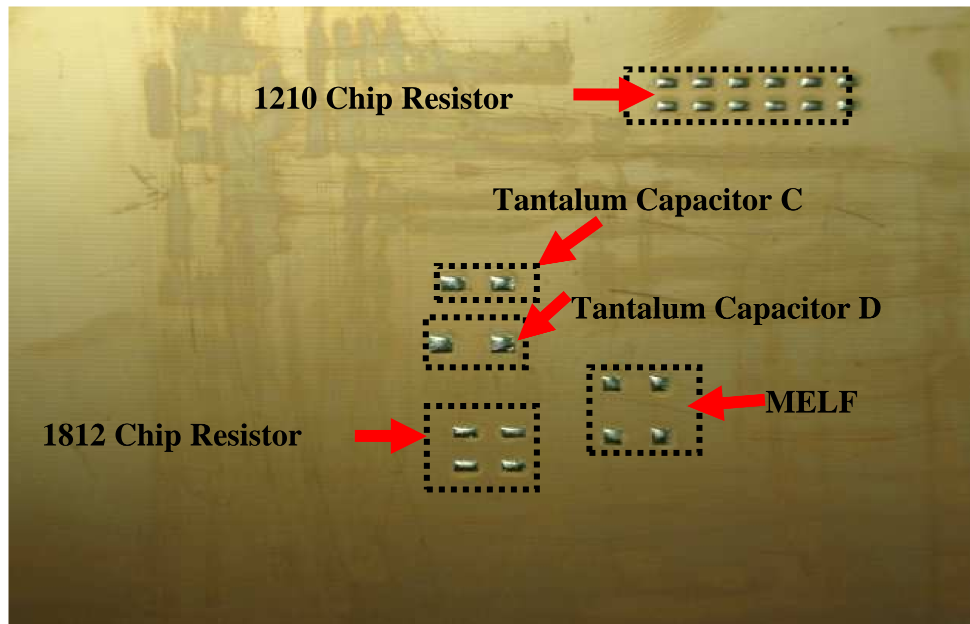

Figure 4.1 Type 1**.** Test Vehicle – For Effect of Pad Sizes on IMC layer Formation and Growth

4.2.2 Type 2 Test Vehicle for ageing temperature and reflow profiles on IMC

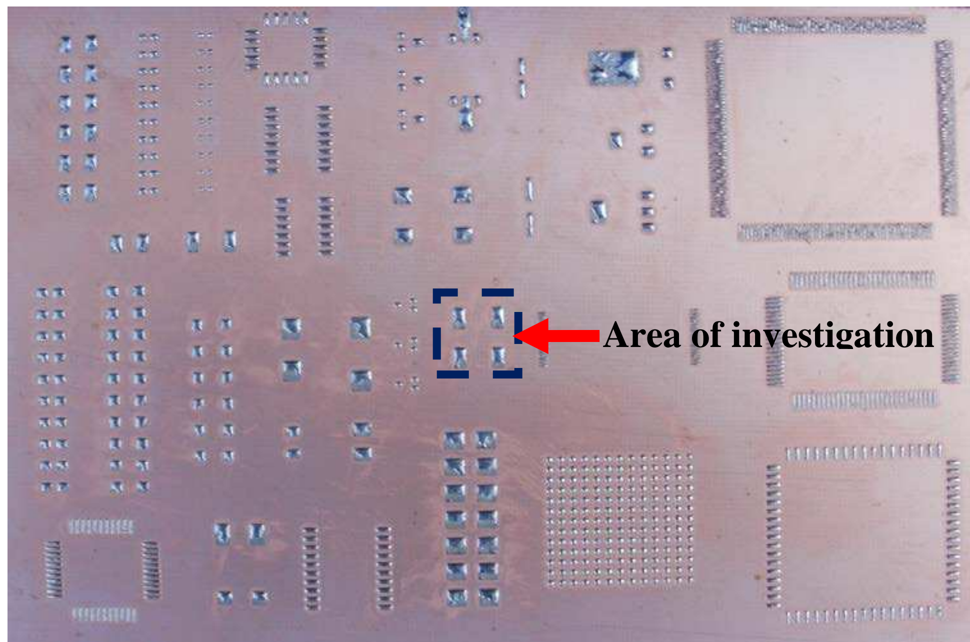

Figure 4.2 Type 2. Test Vehicle – Used for Effect of Ageing Temperatures and Reflow Profiles on Formation and Growth IMC.

The type 2 test vehicle is of different components pad size, pitches and apertures. The area of investigation indicated by green short dashes and has four solder bumps of the same Cu pad dimension (3 x 1.4) mm. Several specimens of solder bumps were made for evaluation of the effect of ageing temperatures and reflow profiles on formation and growth of IMC.

4.2.3. Type 3 Test Vehicle for reflow profile optimization for Sn-Ag-Cu solders bumps

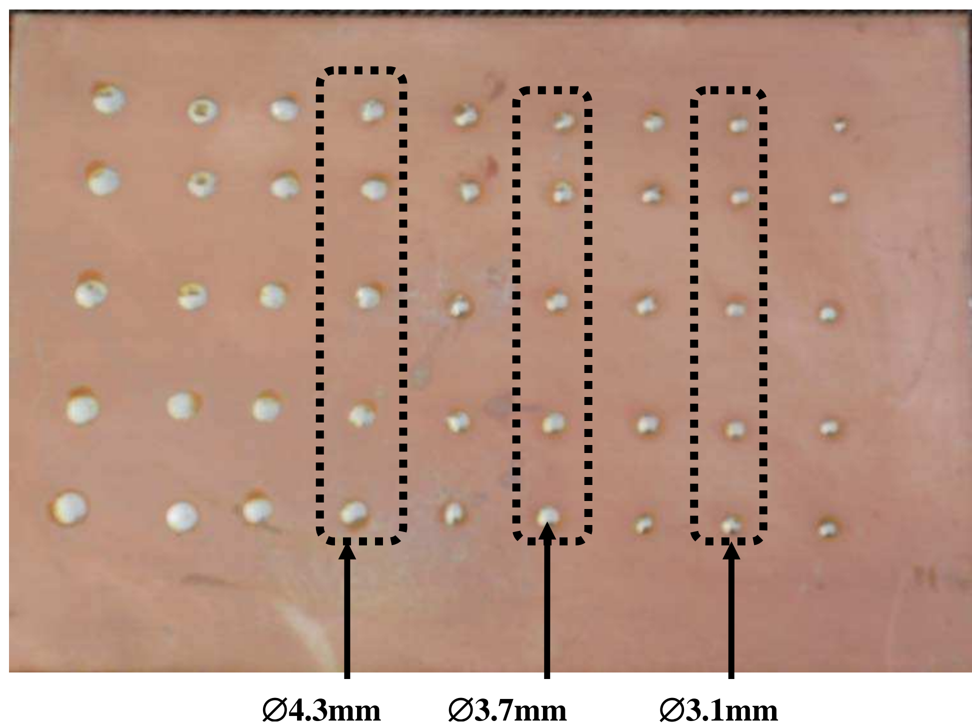

Figure 4.3 Type 3 Test Vehicle – Used for Reflow profile Optimization for Sn-Ag-Cu solders bumps on Cu substrate.

The test vehicles type three (3) consists of forty-five circular solder bumps formed on (160 x 100) mm photo resist copper clad board. The board has different Cu pad sizes with the dimensions of ∅2.5mm, ∅2.8mm, ∅3.1mm, ∅3.4mm, ∅3.7mm, ∅4.0mm, ∅4.3mm, ∅4.6mm and ∅5.0mm. To evaluate the optimization of reflow profile, several specimens of solder bumps were made of the investigated areas as indicated by short dashes. The solder bumps were made by printing the solder paste using a stencil of 0.125mm thick after the bare Cu pads of the test

vehicle had been cleaned using acetone and iso-propanol. The solder paste used for this study is the printing was Sn-3.8Ag-0.7Cu, with a type 3 particle size distribution, 89 wt percent metal content and the particle size distribution of the solder paste was 25-45µm.

4.2.4. Type 4 Test Vehicle for IMC and shear strength of solder joints

The type 4 test vehicle was used for the evaluation of the effect of inter-metallic compound layer thickness on shear strength of 1206 surface mount chip resistors. The 1206 Surface Mount Chip resistors with nickel terminations were placed on the 127cm x 190cm FR-4 Single-Sided PCB. Figure 4.4 shows the different pad sizes used in the study, with fourteen chip resistor joints. A total of forty (40) PCBs were used in this study. The solder paste used for printing was Sn-3.8Ag-0.7Cu, with a type 3 particle size distribution and 89 wt per cent metal content. For the stencil printing; a DEK 260 stencil printer was used as shown in figure 4.5. The printing process parameters used include a pressure of 78.49N/m^2, separation speed of 100%, speed of 50 mm/s and snap off of 0 mm. To achieve good solder wettability in printing, the exposed copper of the FR4 PCB was cleaned with isopropyl alcohol (IPA) to remove surface oxides and contaminates. After the stencil printing process, the "Gold-Plea L20" pick and place machine represented in figure 4.6 was used for placing the components onto the substrates. The substrates were reflowed using a Novostar 2000HT Horizontal Convection Reflow Oven with a 4-stage (preheat-soak-reflow-cooling) as shown in figure 4.7. The temperature profile used for all the samples include: preheat at180°C for 60 sec, soak temperature at180°C for 180 sec, peak reflow temperature at 240°C for 60 sec and cooling at180°C to 100^{0}C for 90 sec and unloaded to cool at 25^{0}C ambient for further processing. Thirty of the specimens were aged in a (Heraeus 4020) climatic chamber as represented in fig 4.11 at 175°C for 100, 200 and 300 hrs to accelerate growth of the IMC layer.

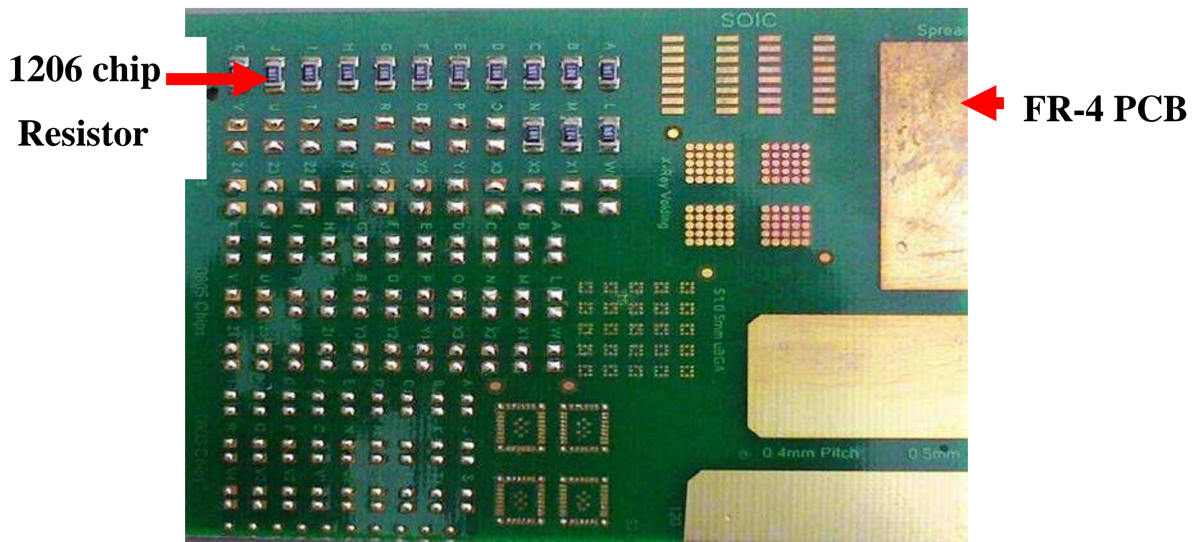

Figure 4..4. Type 4 Test Vehicle - Used for effect of inter-metallic compound thickness on mechanical strength of 1206 surface mount chip resistors with nickel termination

4.3 Experimental Equipment

The main items of equipment used in this study are those that are commonly used for surface mount technology, including:

1. The Stencil printing machine (DEK 260)
2. Pick and place machine (Golden Plea L20)
3. The Reflow soldering machine (Novastar 2000HT Reflow Oven)
4. The Heraeus 4020 temperature cycling chamber
5. Dage-4000PXY Bond tester
6. The Reichert microscope
7. The Scanning electron microscope (JSM5310LV)

4.3.1 Stencil Printing of Solder Paste

The solder paste printing process is one of the critical steps in surface mount manufacturing, affecting directly the yield and quality of assembly, especially in this area of fine pitch technology. Most of the soldering defects encountered after the reflow process such as open/short and bridging problems can have their origins traced back to the defects arising from the solder paste disposition process. Having the correct amount of solder paste deposit on correct location of the

substrate are two essential feature of a good printing process. The printing is usually done by pressing a rubber or metal squeegee against pre-applied solder paste on a stencil with the openings corresponding to the land pattern on the printed circuit board (PCB). The stencil printing parameters employed for the experiments which appeared significantly without defects include; print gap of 0 mm, squeegee speed of 20mm/s, pressure of 8kg, print stroke of 131mm and separation speed 100%.

Figure 4.5 Stencil printing machine (DEK 260 SERIES).

Figure 4.6 Pick and place machine (Gold-Plea L20).

Figure 4.7 Novastar 2000HT Convection Reflow Oven

Figure 4.8 Raddish Electronics SM500CXE Batch Reflow Oven

The Gold- Place L20 in figure 4.6 is an automatic 4-position nozzle changer with 4 nozzles with 32 feeder positions and was employed for components placement. It is user-friendly with window based software including; computer aided design (CAD) conversion software, software for panelised boards and self-diagnostic, error recognition and fault monitoring system. With achievable placement rates up to 3500 cph. Its positional resolution is 0.000125" (3.25 microns) with closed micro step driven motion control of high resolution rotary digital encoders.
The component squaring station enables accurate placement of fine pitch components while protecting fragile leads from damage due to excessive force.

4.3.3 Reflow soldering

The reflow process consists of applying solder paste to a circuit board, placing devices onto the paste, and then conveying the board through a reflow oven with successive heating elements of varying temperature. In the reflow oven each board typically goes through the following stages:

(i) Gradual pre-heating
(ii) Brief duration at high soldering temperature
(iii) Controlled cooling process

The maximum temperature, the rate of heating, the time a device spends at each temperature controlled heating, and controlled cooling are critical parameters for effective process.
Two different types of reflow oven were used in the study, namely:

i. The NOVASTAR 2000HT Horizontal Convection Reflow Soldering Machine (see Figure 4.7)
ii. The Raddish Electronics SM500CXE Batch Reflow Oven (see figure 4.8)

The Novastar 2000HT Horizontal Convection Reflow Soldering Machine is a production scale reflow soldering machine with six different heating zones and one cooling zone. The machine operates on forced convection heating using heating elements which can attain a maximum temperature of 350°C for each of the heating zones. The PCBs are carried on an 1829mm long conveyor belt system, whose speed can be adjusted between 0.05 to 0.99m/min. The machine is

equipped with K type thermocouple terminal and software for programming the reflow temperature.

The Raddish Electronics SM500CXE Batch Reflow Oven is a forced convection batch reflow oven with nitrogen atmosphere capabilities. The oven has a built-in control panel to program the temperature in the chamber. Five heating stages are provided and the maximum temperature produced by each stage is 350°C. The oven also has a gas inlet valve, which will be useful if special gas atmosphere (normally Nitrogen) is needed during reflow.

4.3.4 Temperature profiles

Since different board designs use different types of devices, solder pastes, reflow ovens and circuit boards, no single temperature profile works for all possible combinations. For this reason, it is normal to perform a number of trial runs to help characterise the reflow oven. Figure 4.9 and 4.10 show examples of the reflow profiles obtained for the Novastar 2000HT Convection Reflow Oven and the Reddish Electronics SM500cxe Batch Reflow Oven respectively.

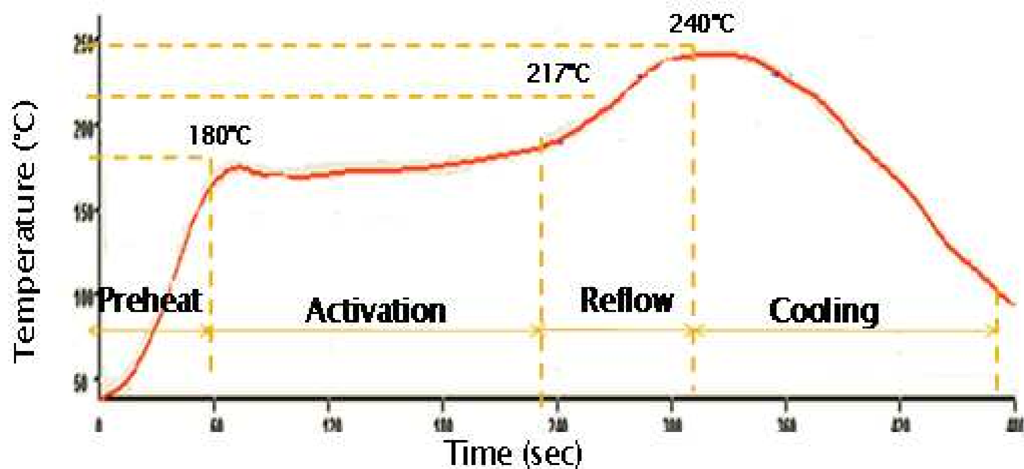

Figure 4.9 Sample of Reflow Profile of Novastar Oven

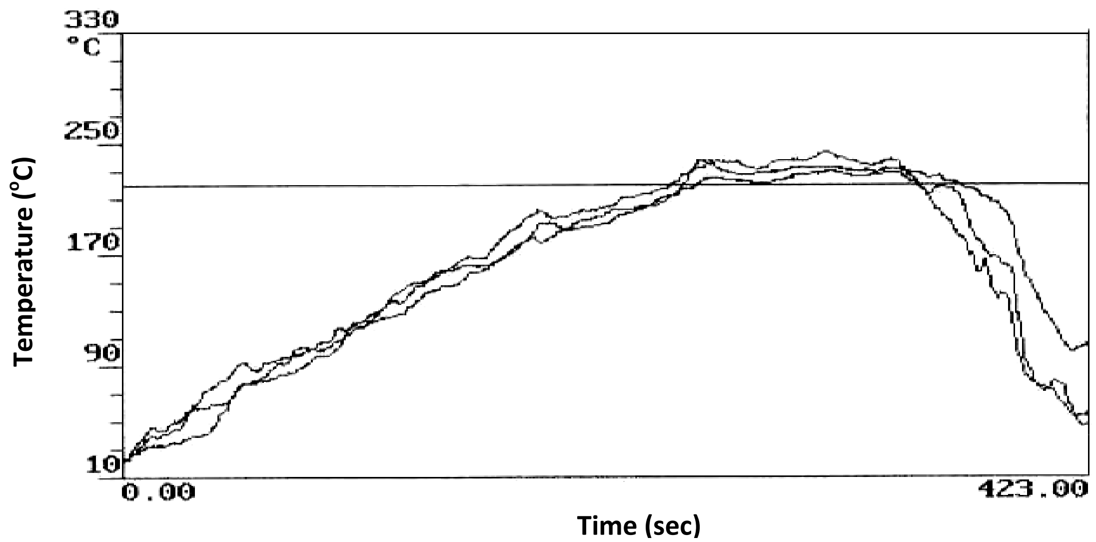

Figure 4.10 Sample Reflow Profile of Raddish Electronics SM500CXE

4.4 Isothermal and temperature cycling ageing

The environmental test chamber shows in figure 4.11 is used for both isothermal and thermal ageing. The temperature of the chamber can be adjusted from -40° to 180°C. It also has a control unit so that the temperature can be programmed to ramp up, cycle between two temperatures or to combine ramping and cycling modes

Figure 4.11 Heraeus 4020 Temperature Cycling Chamber

Figure 4.12 Dage-4000PXY Bond tester

4.5 Evaluation of solder joints shear strength

The evaluation of the shear strength of solder joints was conducted using a shear tester (Dage-4000PXY Bond tester) as shown in figure 4.12. The 4000 bond tester uses patented frictionless load cartridges and air bearing technology which ensures maximum accuracy, repeatability and reproducibility. The shear test methodology involves the precision alignment of the load tool to the bond using both optics and joystick control of an XY stage. The shear height is one of the absolutely critical parameters and therefore shear testing requires automatic touch down of the load tool on the substrate surface and very high precision step back in Z stage. A Test speed (i.e. displacement rates) of 700 μm/s was used throughout the tests. The maximum shear distance employed was 3000μm and a test load of 196.10 N. The shear height and the land speed of the shear test used were 100μm and 500μm/s, respectively.

4.6 Metallographic Preparation of Solder joint Test Samples

The preparation of metallographic sections or micro-sections of solder joints is very much an art. The solders are typically very soft, while the IMC tend to be very hard. The substrate may be either hard or soft depending on the substrate material (for example Au is soft and Cu is relatively hard). The variation in hardness is even greater for joints formed on a thick or thin film metallisation layer on a ceramic substrate. The wide variation in hardness across the joints and substrate interface makes polishing a major challenge. This means that a suitable polish (the grid or the material or the lubricant) must be found for polishing a given joint/substrate combination.

To summarise, the metallographic preparation process consists of the following steps:

1. Cutting
2. Mounting
3. Grinding
4. Polishing

Each of these steps is described briefly in the following sections

4.6.1. Cutting

The cutting process is the first step in the preparation of micro-samples, and it is essential to ensure we have a flat surface, with as little deformation as possible. In this study, a diamond wafering blade was used for cutting the samples and distilled water was used as a lubricant.

4.6.2. Mounting

The samples (type 1, 2 and 3 test vehicles) are embedded in resin to facilitate their handling and to protect the samples from mechanical damage (in particular from abrasive erosion that tears at the soft, ductile copper and solder). For this study, the Sampl-kwick (Buehler) is used for mounting the samples. Sampl-kwick is a translucent acrylic mounting, which has a very fast cure time (typically about 5 minutes) with negligible shrinkage. The mounting process is as follows:

(i) In a small glass, the viscous resin is blended by mixing the powder and the liquid.
(ii) A gentle blending motion is used to minimise the amount of air bubbles produced.
(iii) The blended epoxy resin is allowed to sit for 2 minutes before casting to allow bubbles to rise out of the blend.
(iv) Before casting the resin it is necessary to use support clips in order to prevent the specimen from falling over and SAMPL-KLIP I (Buehler) was utilised for this purpose.

4.6.3. Grinding

Grinding is the first step of material removal and is used for removing damaged or deformed surface material, while introducing only limited amounts of new deformation. The aim is to produce a plane surface in the samples with minimal damage that can be removed easily during polishing in the shortest possible time and this is achieved with steps of successively finer abrasive grit.

The steps in the grinding process can be summarised as follows:

(i) Grinding of the sample with wet abrasive SiC 180 grit until the sample is flat and the sample surfaces are revealed.
(ii) Repeating the grinding with the finer wet abrasive SiC 320 grit for 1 min.
(iii) Finally grinding the sample with the finer wet abrasive SiC 600 grit for 1 min.

4.6.4. Polishing

The polishing process is very similar to grinding, and is used for removing any damage introduced by the previous operations. This is achieved with polishing steps using successively finer abrasive particles. For this study, the diamond paste (1 and 6μm, Buehler) and alumina suspension (Masterprep, Buehler) was used as an abrasive. The polishing cloths used for the diamond paste and the alumina suspension are the Texmet 1000 and the Microcloth (Buehler), respectively. The lubricants used for the diamond polishing and the alumina suspension was Metadi fluid (Buehler) and distilled water, respectively.

4.7 Assessment of the IMC Layer Thickness

To measure the IMC layer thickness, a photomicrograph of the polish surface sample is required, and this can be obtained using an optical microscope or scanning electron microscope (SEM) as shown in figure 4.13 and figure 4.14. The IMC layer is often non planar, determining the layer thickness is often a tedious task. Care must be taken to ensure the measurement is not subjective or depend on the individual taking the measurement.

In this study, the IMC layer thickness was measured using "ISIS" and "image-pro Express" software. The process used for measuring the thickness is as follows: An arc line is drawn on the border of the IMC layer on the IMC photo taken along the joint. The border at the solder side mostly is non planar and the border at the substrate side is often planar. After the arc line has been drawn, the software

calculates the distance between both of the arc lines. The steps are repeated ten times on the same sample. The software then gives ten different measurements: the maximum distance, the minimum distance and the average distance. The IMC layer thickness used in this report is the average thickness calculated by the software.

4.7.1 Measuring with Reichert Microscope

A Reichert Microscope was used for observing and analysing the microstructures of the solder joints after they have been cross-sectioned and metallographically prepared. The Reichert Microscope could provide various magnifications (max: 500x) and a high resolution digital colour camera (JVC) was attached on it so that the magnified image could be digitally saved in a personal computer. The captured image could be further processed using the "Image-pro Express" software. The software has the capability to analyse the captured image, such as measuring the IMC layer thickness.

Figure 4.13 Reichert Microscope

4.7.2 Measuring with Scanning Electron Microscope

With modern scanning electron microscopes it is remarkably easy to generate high quality images with good resolution and depth of focus. Also, once a system has been correctly set up, high quality non-destructive chemical analyses can be obtained in a matter of seconds from an area as small as a few microns. However, to fully appreciate and correctly interpret the images and results requires some understanding of how the scanning electron microscope (SEM) works, and what are its limitations.

Conventional SEM work requires that the specimen be capable of withstanding a high vacuum, be stable under the electron beam, be electrically conductive, and be of suitable dimension to enter the specimen chamber. While these conditions are still necessary for high quality X-ray analysis, by the use of a low vacuum SEM, it is possible to examine unstable specimens without the need for coating. To obtain conventional SEM images, specimens are made conductive by coating with a fine layer of gold by the process of ion sputtering in an argon atmosphere; while for X-ray analysis evaporated carbon is used as a conductive coating.

The electron beam is generated within the electron gun. This consists of a hairpin tungsten filament, which is heated in a vacuum by applying a current of about 2.75 amps; electrons are then generated through thermionic emission. The electrons are then accelerated towards the specimen, through the vacuum in the column, by applying a high voltage potential difference, typically of 20kV between the filament assembly (cathode) and the anode. The beam is then focussed using magnetic electron lenses. Another set of magnetic lenses then deflect the beam, to systematically scan it over the surface of the specimen.

By the interaction of the electron beam and the specimen at the atomic level, various secondary particles are produced by atomic scattering. By using appropriate detectors, these secondary particles are counted, and converted into electrical signals which are then displayed on the CRT as a video signal with a raster scan synchronised with the electron scan rate. Thus the basic image is formed.

The detected particles carry information which describes the nature of the specimen e.g. atomic number, elemental distribution, topography, and chemical characteristics. So, for example, in a backscattered electron image (BEI), when observing grey tones, the brighter areas can be interpreted as having a higher mean atomic number than darker areas. This is a consequence of the differences in electron yield within the specimen. A secondary electron image (SEI) contains more information on topographic features, the brighter areas represent a high slope angle or thin edge feature, whereas darker areas result from flatter features.

When the electron beam is focussed on a single point of interest, and the applied current increased, X-rays are generated from the surface of the specimen. These X-rays have energies which are characteristic of the elements under the beam at that moment. The use of a Si(Li) detector allows these X-rays to be measured and counted. By comparing X-ray signatures from certified laboratory standard materials for each element, non-destructive chemical analysis is possible. X-ray mapping allows the distribution of elements to be presented graphically, and by quantifying the areas, phase distributions and quantities can be calculated. Since all the images generated by the SEM are digital, it is possible to combine the techniques of image analysis and X-ray analysis to produce custom built particle characterisation programs.

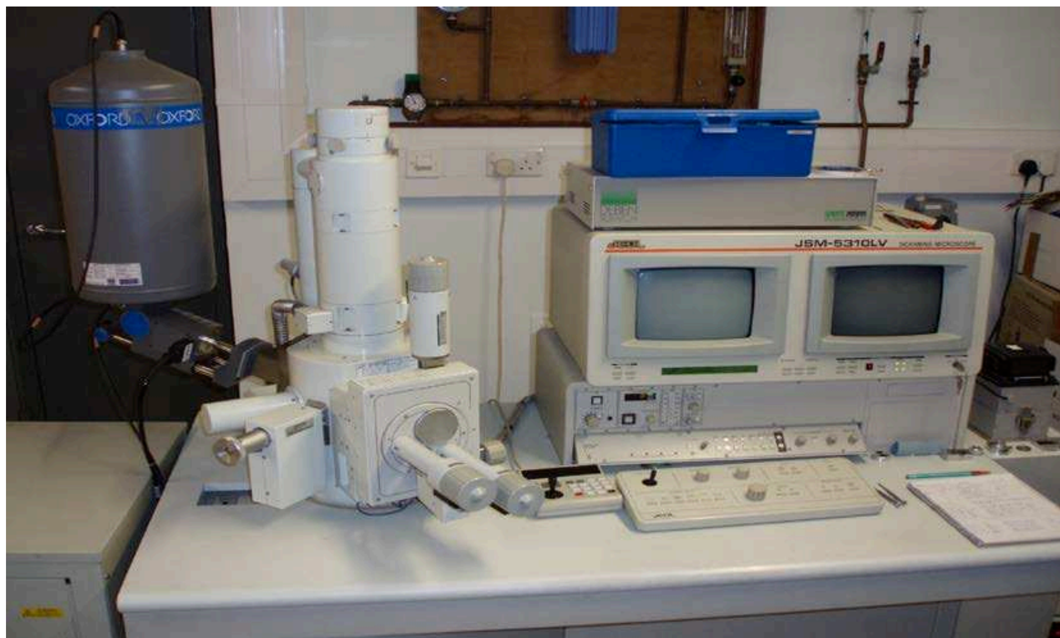

Figure 4.14 JSM5310LV Scanning Electron Microscope

4.8 Experimental Procedures

The experimental procedures for chapter 5, 6, 7 and 8 are briefly outlined in this section:

4.8.1 Experimental procedure of the effect of pad size on IMC layer formation and growth in Sn-Ag-Cu solder joint

As shown in figure 4.1, sixteen (16) test vehicles were prepared for the experiments. Four test vehicles were used for reflow experiment. The remaining twelve (12) test vehicles used in the experiment were isothermally aged for hundred (100), two hundred (200) and three (300) hours respectively. An amount of one hundred and nine-two (192) samples were used for the investigation. In addition, the soldering process parameters used are presented in table 4.1. The pad dimensions of the selected components are shown in table 4.2

Table 4.1: Reflowed soldering process parameters (IPC/JEDEC J-STD-020C)

Parameter	**Temperature (°C)**	**Time (Seconds)**
Preheat	180	120
Soak temperature **Time above liquidus**	180 217	120 150
Peak temperature	245	-
Cooling (°C)	25	90

Table 4.2: Pad dimensions of selected components

Component/Pad	Pad Length (mm)	Pad Width (mm)	Pad Area (mm^2)
B1	2.5	1.4	3.50
B2	3.0	1.4	4.20
B3	2.2	2.2	4.84
B4	3.0	2.0	6.00
B5	3.0	2.4	7.20

4.8.2 Experimental procedure of cycling temperatures and reflow profiles on inter-metallic growth between Sn-Ag-Cu solder alloy and Cu.

In this experimental work, the solder paste was deposited onto the specified volume of FR4 PCB by DEK 260 series stencil printing machine represented in figure 4.5. The printing process parameters used include a pressure of 8kg, separation speed of 100%, speed of 50 mm/s and snap off of (0) mm. To achieve good solder wettability in printing, the exposed copper of the FR4 PCB was cleaned with isopropyl alcohol (IPA) to remove surface oxides and contaminates. After the stencil printing process, the solder bumps formed on the substrates were reflowed using a SM500CXE Convectional Reflow Oven as shown in figure (4.8). Table 4.3 shows the details of reflow profiles (A to E) used to investigate the IMC formation and growth. Based on the applied temperature and time each reflow profile has five distinct zones: Preheat 1, Preheat 2, Preheat 3, Reflow and Cooling.

Table 4.3 Reflow profiles used for specimen types P1and P2.

Profiles	Preheat 1		Preheat 2		Preheat 3		Reflow		Cooling
	T (^{0}C)	t (sec)	T (^{0}C)	t (sec)	T (^{0}C)	t (sec)	T (^{0}C)	t (sec)	t (sec)
A	150	90	180	90	210	180	260	260	150
B	150	90	180	90	250	180	240	260	150
C	150	90	220	90	220	180	240	260	150
D	190	90	180	90	210	180	240	260	150
E	150	90	180	90	210	180	240	260	150

To accelerate the intermetallic growth, all sixty specimens were subjected to thermal cycle ageing using the Heraeus Votsch temperature and humidity chamber represented in (4.11). The temperature cycles (named as T25, T40 and T60) used for ageing the samples are shown in figures 4.15a, 4.16b and 4.17c respectively. The cycles are designed to simulate the "on-off" condition experienced by typical electronics devices. Each sample was aged for duration of 24 hours, although the figures only show one hour profile. While the maximum temperatures for the cycles were different (25, 40 and 60 ^{0}C), the minimum temperature was kept constant at 20 ^{0}C Each of the sixty samples was cross-sectioned and examined with an optical microscope as shown in figure 4.13 to measure the IMC layer thickness. Upon completion of the ageing process, the samples were mounted in epoxy and metallographically polished in preparation for characterisation as stated in chapter 4, section 4.6.

.

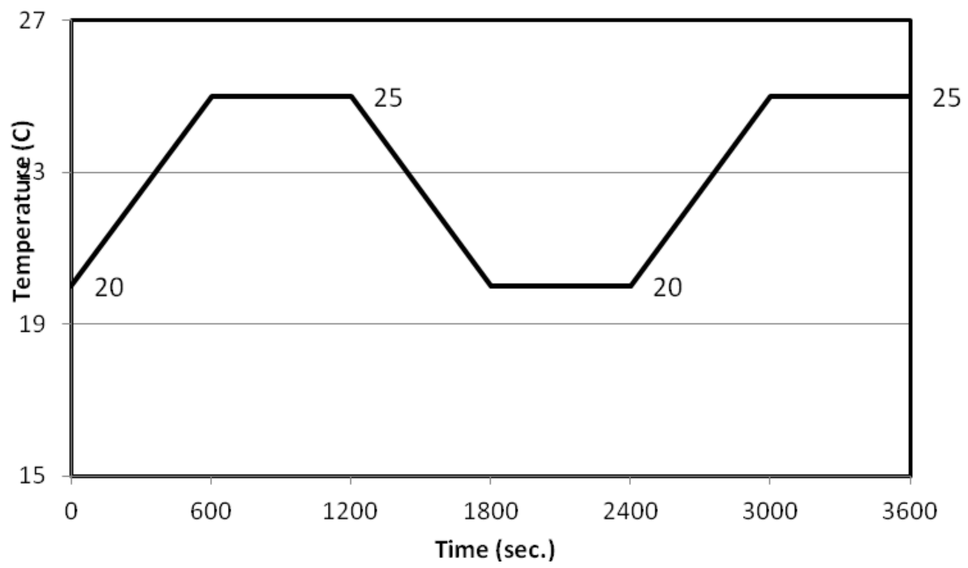

Figure 14.15a Temperature cycle profile, T25 (20°C – 25°C)

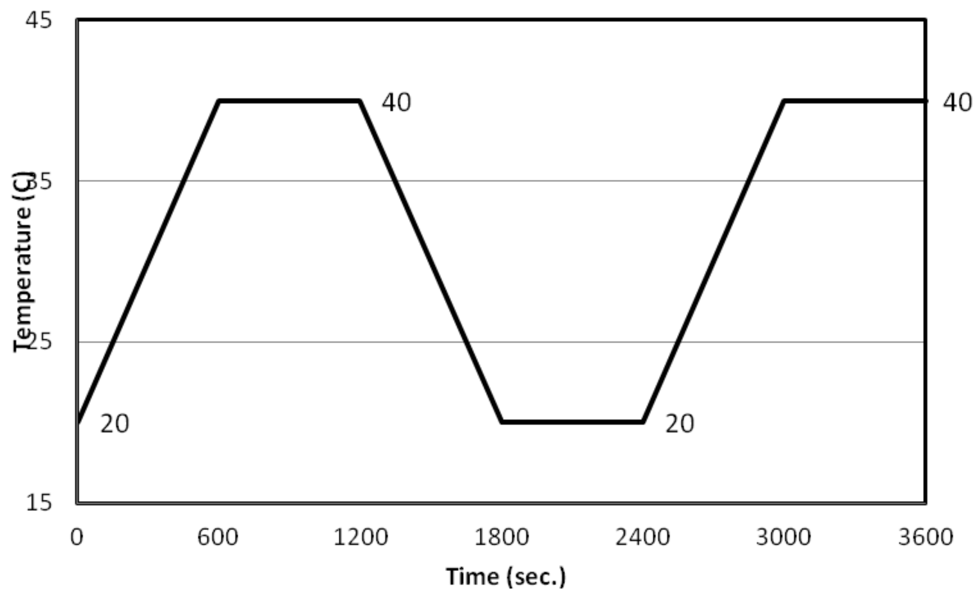

Figure 4.15b Temperature cycle profile, T40 (20°C – 40°C)

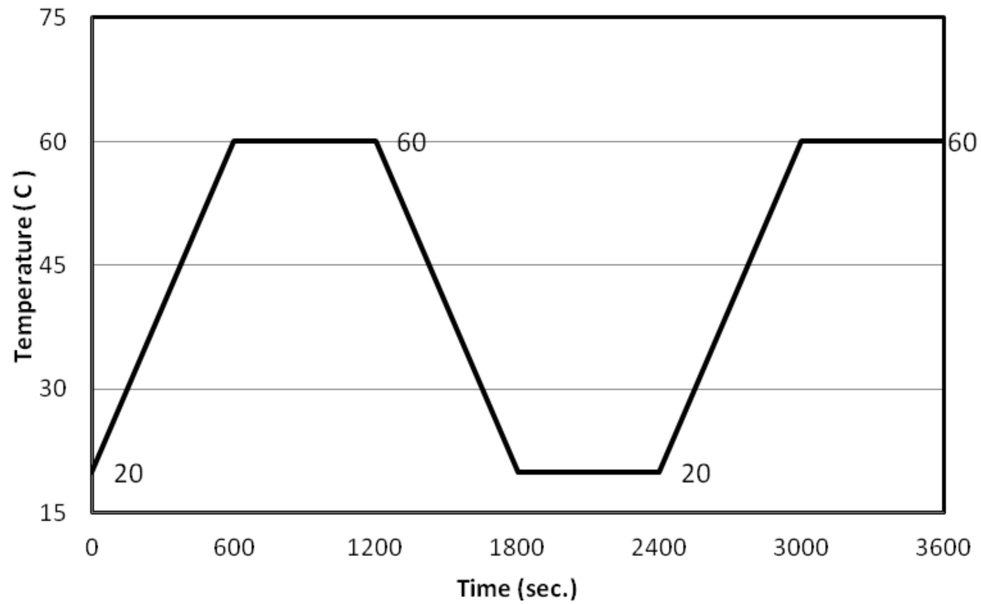

Figure 4.15c Temperature cycle profile, T60 (20°C – 60°C)

4.8.3 Experimental procedure of reflow soldering profiles using full factorial design for Sn-Ag-Cu solder bumps on Cu substrate

Design of experiment is a test or series of tests in which focused changes are made to the input variables of a process so as to observe and identify corresponding changes in the output response (Montgomery, 1997). This commonly used statistical technique assists in the design of new products and processes, optimising existing manufacturing processes, or helps improve existing products. In this experimental work, convectional reflow profiles were studied.
The convectional profiles typically are composed of initial ramp-up as preheat of 3ºC/s until about 150 – 180ºC, then levelling off for a couple of minutes as a soaking zone. This is then followed by the spike zone with relatively 2ºC/s cooling rate after reaching the peak temperature. The typical reflow profile curve is shown in figure 4.9.

4.8.3.1 Factorial design of experiments

A full factorial design of reflow profiles was conducted for solder bumps shown in figure (4.3). The design parameters for a profile include: soak temperature, soak time, time to peak temperature and time above liquidus (TAL). The purpose of the soak temperature and the soak time (Soak profile) is that it brings the entire board up to a uniform temperature. The ramp rate in this zone is slow, almost flat.

The soak profile, also acts as the flux-activation zone for the solder paste. The purpose of the long soak zone is to minimize voids. When TAL is extended above the solder melting point will damage temperature-sensitive components. It also results in excessive intermetallic growth, which makes the solder joint brittle and reduces solder joint fatigue resistance. Furthermore the time to peak temperature is a very critical parameter to be considered because more solids would dissolve in the solder and substrate at peak temperature of a given time.

Component manufacturers face a key development task in order to meet the lead-free requirements. The task is how to make product withstand time-to-peak temperature and higher melting points of most of the lead-free solder pastes. But solder paste manufacturers recommend that enough time and high peak temperature is provided to aid wetting. Meanwhile, component manufacturers advise keeping the lowest peak temperature possible to prevent component damage (Wickham and Hunt, 2001).

In this study, the soak temperature was investigated; the high and low soak temperatures used were 180°C and150ºC respectively. The time to peak temperature employed, which permitted each of the solder volumes to reach the required reflow temperature were 360 seconds for high condition and 240 seconds for low condition.

In an experiment, Skidmore and Waiters (2000) used the ramp-to-spike profile method for optimizing lead-free solder joint quality. The time above liquidus of 90 to 120 seconds which they need used resulted in good wettability, it emerged that there were no solder balls and voids. However, too much heat input above the

solder melting point could lead to excessive intermetallic formation. Therefore, for short duration; time above liquidus used in the experiment was 60 seconds and120 seconds for long duration. Moreover, lead-free flux chemistries contain more rosin / resin which provides greater barriers to compensate for the higher soaking temperature. Therefore, the soak range and length of time must base on the flux chemistry and the melting temperature of the alloy. Due to the flux chemistry of Tin- Silver- Copper (SAC), high soaking time employed was 120 seconds and 60 seconds for low soaking time. In summary, the experiment has four factors with two levels, as detailed in Table 4.4

Table 4.4 Experimental parameters

Factors	High level (+)	Low level(-)
Soak temperature (^{0}C)	180	150
Soak time (Second)	120	60
Time above liquidus (Second)	120	60
Time to peak (Second)	360	240

Let; High level (H) = +, Low (L) level = -, A = Soak temperature, B = Soak time, C = Time above liquidus, D = Time to peak temperature.

4.8.3.2 Assigned parameters of (2^4) full factorial design

Four factors are investigated using 2^4 designs. The factors are soak temperature, soak time, time above liquidus and time to peak temperature. The combination of the factors' data for the experiment is shown in table 4.5

Table 4.5 High and Low signs for the reflow process design

Experiment number	Soak temperature (°C)	Soak time (s)	Time above liquidus(s)	Time to peak temperature(s)
1	L	L	L	L
2	H	L	L	L
3	L	H	L	L
4	H	H	L	L
5	L	L	H	L
6	H	L	H	L
7	L	H	H	L
8	H	H	H	L
9	L	L	L	H
10	H	L	L	H
11	L	H	L	H
12	H	H	L	H
13	L	L	H	H
14	H	L	H	H
15	L	H	H	H
16	H	H	H	H

The main features of the test vehicle are shown in figure (4.3). The procedure for metallographic and microstructure examination can be found in sections 4.6 and 4.7. A total of fifteen (15) test vehicles were constructed under the same environmental conditions. The total number of specimens used for the investigation was one hundred and fifty (150). The experimental test runs were performed by employing the combinations of the reflow profile parameters represented in table 4.6

Table 4.6 Reflow profile parameter combinations.

Experiment number	Soak temperature (°C)	Soak time (s)	Time above liquidus(s)	Time to peak temperature(s)
1	150	60	60	240
2	180	60	60	240
3	150	120	60	240
4	180	120	60	240
5	150	60	120	240
6	180	60	120	240
7	150	120	120	240
8	180	120	120	240
9	150	60	60	360
10	180	60	60	360
11	150	120	60	360
12	180	120	60	360
13	150	60	120	360
14	180	60	120	360
15	150	120	120	360
16	180	120	120	360

The soak temperature, soak time, time above liquidus, cooling rate and peak temperature were identified as optimal reflow factors influencing solder joint quality.([Altera, 2008). In another experimental development, an optimal setting for reflow soldering process in achieving a maximum shear force of lead-free solder joints includes; soak time of 75 seconds, reflow time of 82 seconds and peak temperature of 230°C (Lin et al, 2007).

4.8.4 Experimental procedure of the effect of inter-metallic compound layer thickness on the shear strength of 1206 surface mount chip resistor

To evaluate the effect of IMC layer thicknesses on the shear strength of Sn-Ag-Cu solder joints, several test vehicles were constructed. The test vehicles consist of surface mount chip resistors with nickel termination placed on (127 x 190) mm FR-4, 35μm Cu single sided solder resist probimer printed circuit boards (PCBs) as described in figure 4.4.

The experiment was performed with a total of one hundred and forty samples (140).The 1206 chip resistors were reflowed with the optimum reflow profile suggested in figure 4.9. To investigate the microstructural changes and IMC growth during the ageing period, the specimens were stored in a constant temperature chamber at 175°C for 100, 200 and 300 hours.The fourteen 1206 chip resistors solder joints on each FR-4 PCB were cross-sectioned as described in section 4.5 and the thickness of IMC layer was measured by taking ten measurements on each micrograph of which the average is recorded. The standard deviation of the measured IMC layer thickness was found to be between 0.35 and 0.55.

The solder paste was deposited onto the 1206 chip resistor pad sizes of FR4 PCB by a DEK 260 series stencil printing machine represented in figure 4.5. The printing process parameters used can be found in section 4.3.1. The 1206 chip resistors were placed onto the FR4-PCB as described in section 4.3.2. Both the reflowed soldering and ageing processes carried out are described in section 4.3.3 and 4.4 respectively

4.9 Summary

The experimental procedures and methodology used for various aspects of the studies reported in this thesis has been presented in this chapter. This covers a description of various items of equipment, materials and the test vehicles that were used for conducting the studies. The required reflow soldering parameters for optimal settings of lead-free solder bumps were worked out through conducting several trial tests. The optimal reflow soldering parameters which were significant for minimal intermetallic compound layer thickness include: Soak temperature, soak time, time above liquidus and time to peak temperature. The power-law relation model was used to determine the average thickness of the IMC formed during reflow and isothermal ageing. This model was very useful because it predicts the growth rate constant, the time exponent and reaction time. These factors established that the growth of intermetallic compound layer thickness is by diffusion. The effect of pad sizes on IMC Layer formation and growth is presented in the next chapter.

CHAPTER V: EFFECT OF PAD SIZES ON IMC LAYER FORMATION AND GROWTH

5.1 Introduction

The increasing demands for higher performance, lower cost, and miniaturisation in hand held and consumer electronic products have led to the use of dense interconnections. This has led to the use of smaller solder joints and smaller solderable pad metallisation on the PCB, and in turn led to the use of smaller solder paste deposits on the pads. Although there are a number of reports in the literature on studies evaluating the links between solder paste deposit volumes (and solder joint shape and size), and associated reliability, there are no reports on the effect of solder volume on IMC layer formation and growth.

This chapter presents the results of the study on the effect of pad sizes on intermetallic compound layer formation and growth for lead-free solder joints. The chapter is made up of four main parts. The first part of the chapter describes the solder joints micrographs during reflow and isothermal ageing at 175°C for (100), (200) and (300) hours respectively. The interfacial reaction and solid-state diffusion process were also considered. The second part, presents analysis of IMC compositions using with Electron Dispersive X-ray Spectroscopy. The third part presents the results of the evaluation of the effect of pad size on the IMC layer thickness in the soldered samples. The final part presents the results of the study on IMC layer following isothermal ageing

5.2 Experimental Details

Evaluation of the IMC layers formed in the solder bumps, their shape, microstructure, growth characteristics and uniformity were carried out after isothermal ageing. The details of experimental procedure and the equipment used are presented earlier in chapter 4 (see in sections 4.2.1, 4.3.3 and 4.4).

5.3 Results and Discussion

Section 5.3 presents the results of microstructures, intermetallic compound thickness (IMC) and elemental composition of the as soldered and isothermally aged samples.

5.3.1 The Evolution of Intermetallic Compound Microstructures.

It is now widely accepted that real solids such as solder joints are not continuous media but rather they are micro-composites with complex microstructures. Frear *et al,* (1994) pointed out that it is not possible to construct tractable theories that incorporate the microstructure directly, it is important to recognize that the microstructure exists and that it is responsible for the macroscopic behaviour that is modelled.

The evolving microstructure of Sn-Ag-Cu based alloys on copper substrates has been studied previously (Allen et al, 2004). In an investigation of microstructure of intermetallic compounds conducted by Fix et al (2005) reported that upon soldering, a significant amount of copper from the substrate and nickel from the metallisation of the component dissolves in the liquid solder and changes the solidification morphology of the joint.

The correct interpretation of the microstructure of samples is extremely important when evaluating solder joint cross-sections. The grain structure and intermetallic regions of reflowed joints are often used for failure analysis and assembly process optimization. During soldering, molten solders are drawn into configuration in joints by a process of reactive wetting, which results in the molten solder spreading over the substrate, typically copper and metallisation in conjunction with the metallurgical reaction between them and one or more of the components in the molten solder. The nature of this reaction determines the wettability of the substrate or the metallisation by the solder. Good wettability is characterised by near zero contact angle between the molten solder and the substrate.

The microstructure morphology and the thickness of the intermetallic layer are largely determined by the temperature and time that the molten solder is in contact with the substrate or metallisation. Furthermore, the cooling rate of the molten solder through its freezing point during soldering plus its final chemical composition determines the initial microstructure and properties of the solder in the joint (Chada et al, 2000; Ho et al., 2001; Lee et al, 2002). The following sections present the evolution of solder joint microstructure, for the as soldered and the samples that were isothermally aged at 175°C for 100, 200 and 300 hours respectively.

5.3.2 Evolution of solder joint microstructures after reflow.

Scanning Electron Microscopy (SEM) and Energy Dispersive X-ray spectroscopy (EDS) techniques were employed in the analysis of the microstructure of the reflowed samples. The micrographs of the interfacial intermetallic layer resulting from the five different solder bumps at 240°C peak reflow temperature are shown in figure 5.1 {a – e}. It is clear from these figures that the microstructure of the intermetallic layers indicated formation of scalloped structures. Suh et al (2005) explained that during reaction between molten solder and copper, ripening and growth of the Cu_6Sn_5 scallops take place at the solder/metal interface. This is due to dissolution of the IMC grains during initial reflow process. Also, it was pointed

out that the scallop grow rate is proportional to the cube root of the time and size distribution of Cu_6Sn_5 scallops.

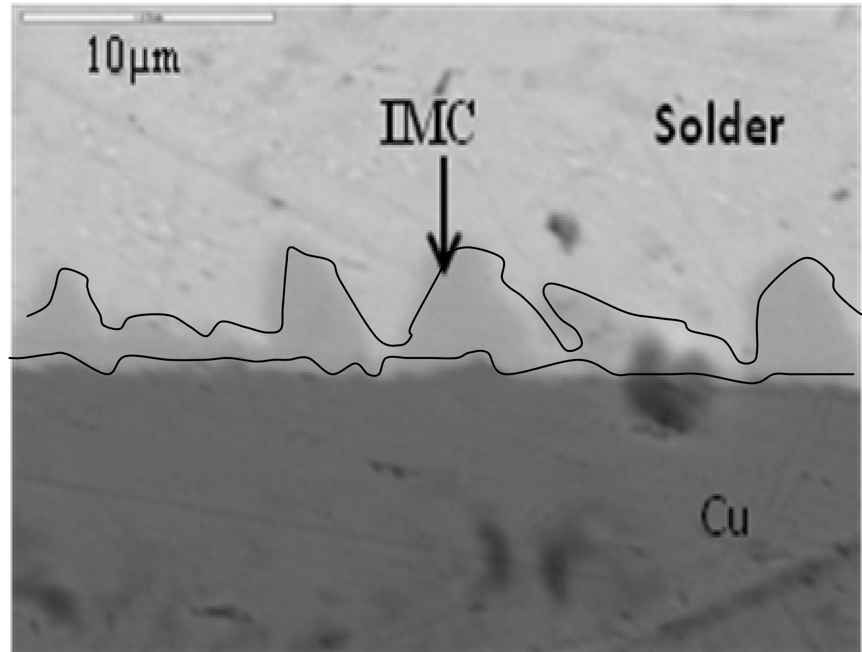

Figure 5.1a Solder joint microstructure on pad (B1) after reflow

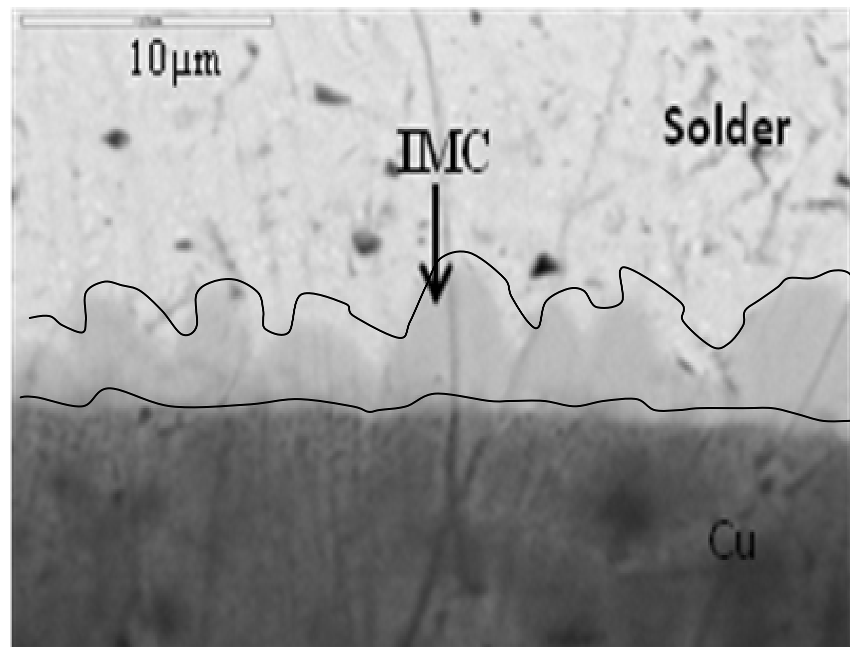

Figure 5.1b. Solder joint microstructure on pad (B2) after reflow

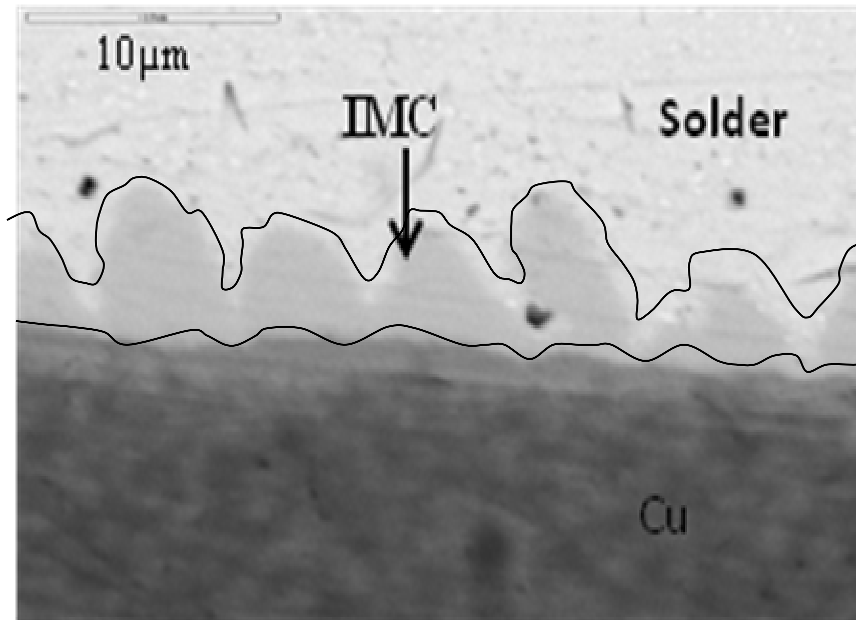

Figure 5.1c Solder joint microstructure on pad (B3) after reflow

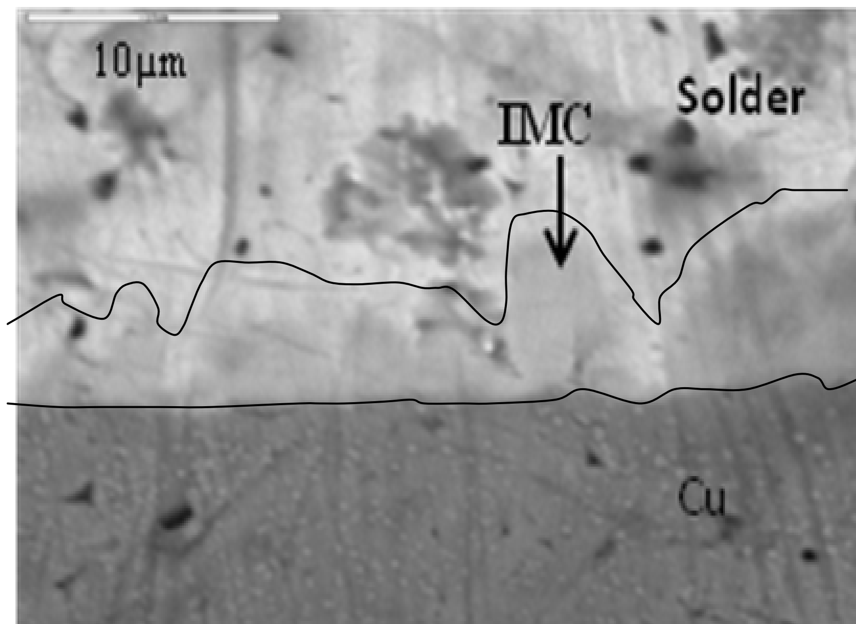

Figure 5.1d Solder joint microstructure on pad (B4) after reflow

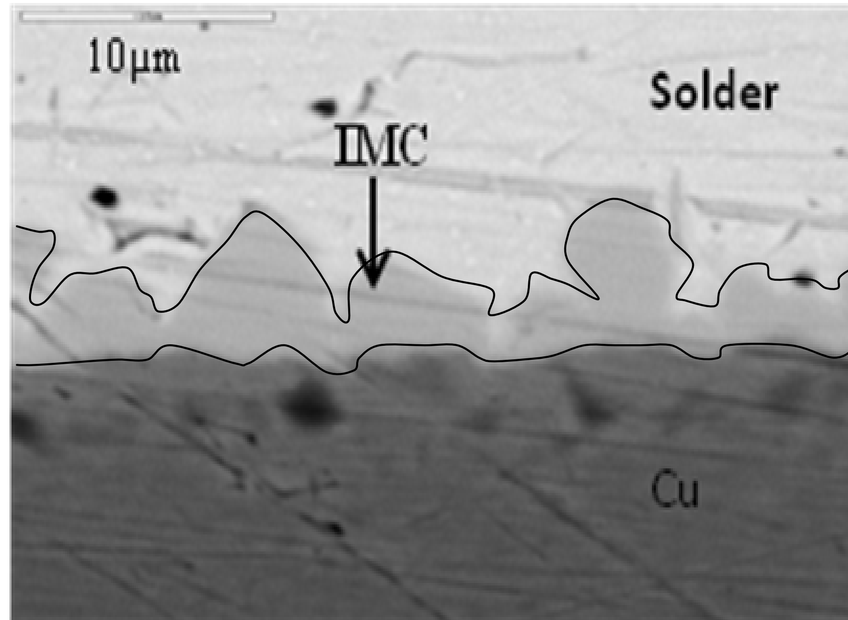

Figure 5.1e Solder joint microstructure on pad (B5) after reflow

5.3.3 Microstructures of IMC after Isothermal Ageing

The IMC formed after soldering continues to grow with time at elevated temperatures by interdiffusion between the elements of the solder and the substrate. The interfacial microstructure depends on the initial state before ageing (governed by the soldering condition).

In this study, it was observed that the IMC morphology and microstructure apparently varied in accordance with the ageing time. The microstructure of the samples for the three isothermal ageing durations for (pad B1) is shown in figure 5.2 (a – c). It is clear from these micrographs that after (100) hours of ageing the initial scallop morphology of the IMC layer changes from scallop-like to planar in the aging process.

This is because during the solid-state aging, the distance of the valley of the scallop is closer to the solder than that of the peak region of the scallop. Since the total (bulk) diffusion coefficients of Cu and Sn through Cu_3Sn are nearly

the same, the required time of Cu atoms reaching the solder or Sn atoms reaching the Cu substrate should be shorter for the valley region of the scallop. This indicates that the growth velocity in the valley region of the scallop-like IMCs is higher than that in the peak region as a result; the whole interfacial layer of the IMCs will tend to become planar with increasing ageing time. Therefore, the thickness of the IMCs increases with time, but with leading to a growth velocity of the IMCs decreasing with time.

The analysis of the samples also shows duplex structure, with Cu_5Sn_6 (η-phase) shows as IMC layer one (1) next to the solder and the Cu_2Sn (ϵ-phase) IMC layer two (2) layer next to the Cu substrate (see in SEM micrographs in Figure 5.2a). After two hundred (200) hours of aging, the intermetallic compound layer became thicker as a function of thermal aging time. After three hundred (300) hours aging, as observed in figure (5.2c), the microstructure of the IMC became more and more planar. Also, IMCs grew with different morphology. The morphologies change during ageing is due to variation of interfacial energy with solder composition. Also during solid-state ageing, the IMC thickness increases because the substrate metal atoms in either the supersaturated solid solution or the precipitated IMCs may diffuse back to the solder-substrate interface, resulting in an additional IMC growth.

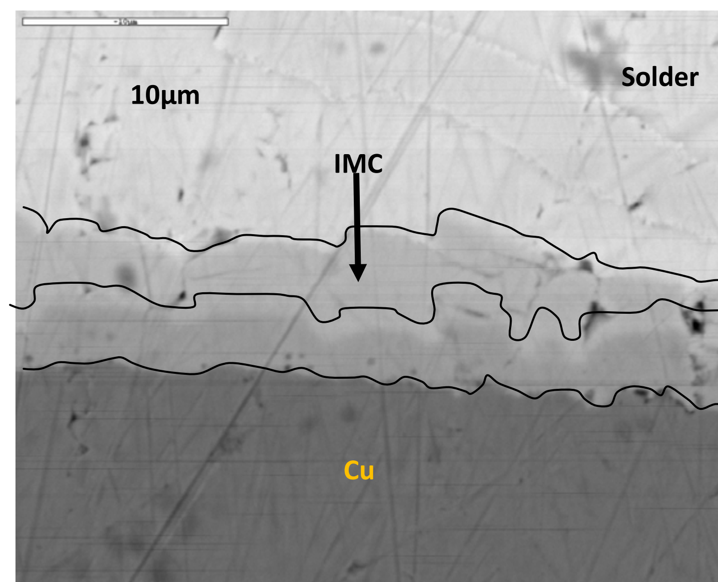

Figure 5.2a Representative of SEM micrograph showing microstructure of B1 after 100 hours isothermal ageing.

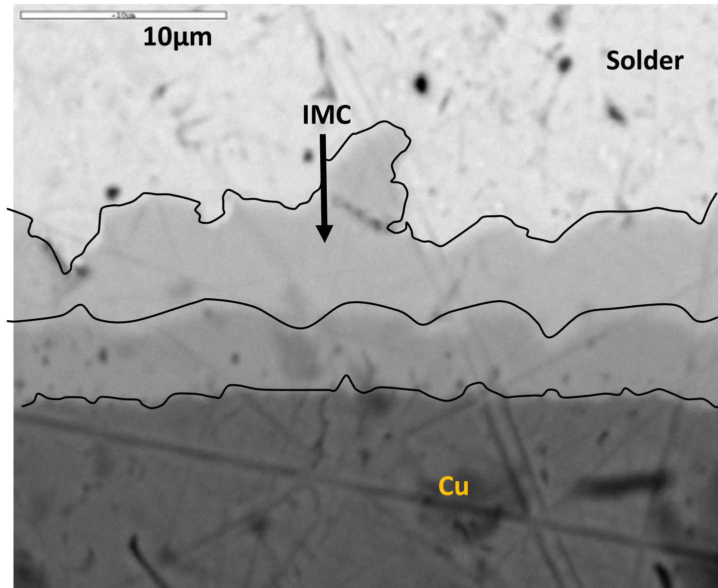

Figure 5.2b Representative of SEM micrograph showing microstructure of B1 after 200 hours isothermal ageing.

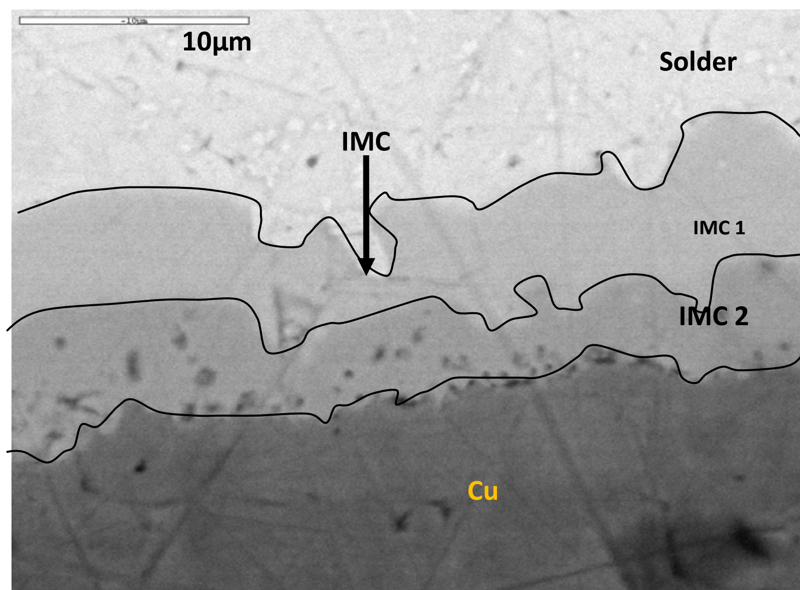

Figure 5.2c Representative of SEM micrograph showing microstructure of B1 after 300 hours isothermal ageing.

5.3.4 Analysis of Intermetallic Compound Layer Composition

In order to determine the elemental compositions, the energy dispersive x-ray (EDX) analysis was conducted on the five different pad sizes. For simplicity, five spotted locations on pad 1 (B1) microstructure of 100, 200 and 300 hours of isothermal ageing at 175°C were used for the elemental analysis as shown in figure 5.3(a- c).

The EDX spectra shown in figure 5.4 (a – c) indicate the intensities of Cu and Sn on the two phases of IMC. The planar continuous IMC that interfaces with the surface of the substrate (pad) is a binary compound made up of Cu-Sn, of which resulted in higher atomic % of Cu than Sn. This is because more Cu atoms dissolved from the substrate, which reacted with the Sn atoms to form the IMC layer. The IMC that interface with the solder was also found to be a binary compound, comprised of Cu-Sn, of which the atomic % of Sn is higher than that of Cu due higher percentage of Sn atoms reacting with small amount of Cu atoms in that layer. However, the Cu-Sn compounds were spotted together with Ag element. After 200 and 300 hours of isothermal ageing, similar ranges, trend and atomic percentage of Cu and Sn were obtained. This might be saturation of the active constituents (Sn and Cu atoms) after reflow and hours of isothermal ageing.

The EDX results of the two main IMC compounds are summarized in Table 5.1 (a – c). The results taken at 100, 200 and 300 hours were organised and grouped under IMC I and II. The IMC I denote the IMC that interfaces with the SAC solder. IMC II denotes the IMC that interfaces with the substrate. The result of EDX on the IMC phases which showed the distribution of Cu and Sn atomic percentages of 0.7%Cu, 3.8%Ag and 88%Sn of the solder alloy and the copper substrate, revealed that the Cu concentration was very high at all the three durations at spot (5) due to the base copper substrate. On the other hand, spot four (4) revealed limited presence Cu concentrations. The composition of intermetallic

compound phase at spot (4) is suggested to be Cu_5Sn_6 while Cu_2Sn is the intermetallic compound phase composition at point (5). The IMC (atomic.%) composition over the ageing period did not show significant changes.

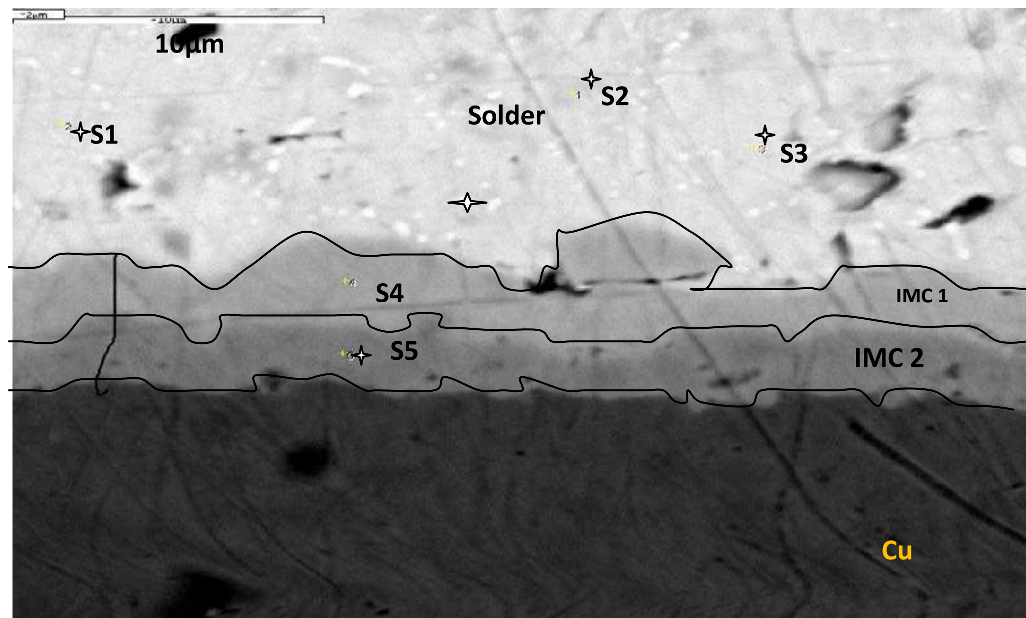

Figure 5.3a. SEM micrograph showing five spotted locations on sample B1 used for elemental and atomic weight percent analysis after 100 hours isothermal ageing

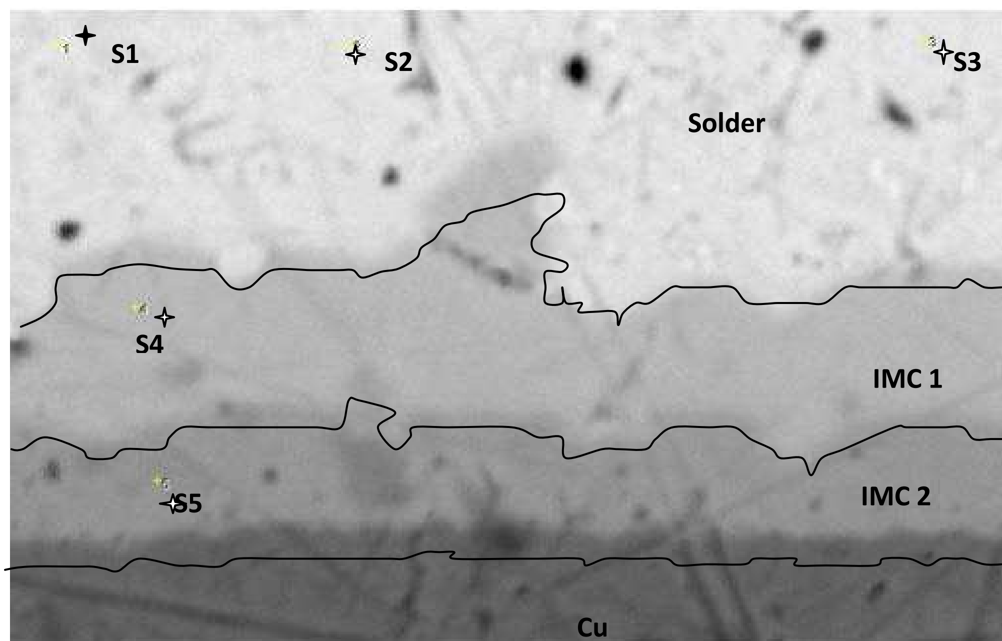

Figure 5.3b. SEM micrograph showing five spotted locations on sample B1 used for elemental and atomic weight percent analysis after 200 hours isothermal ageing

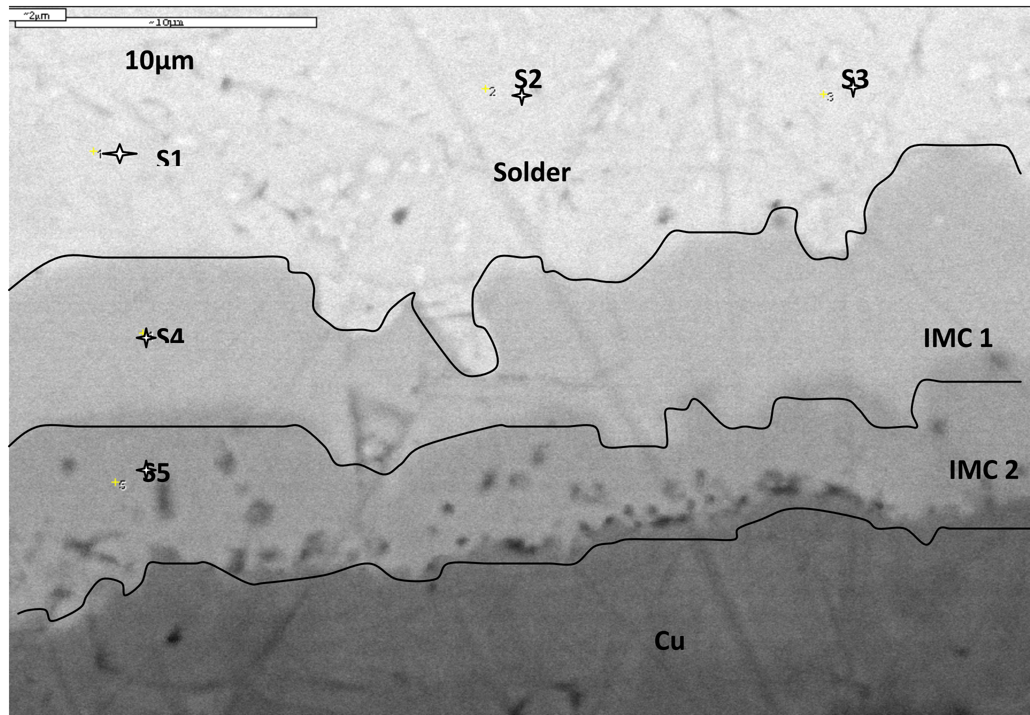

Figure 5.3c. SEM micrograph showing five spotted locations on sample B1 used for elemental and atomic weight percent analysis after 300 hours isothermal ageing

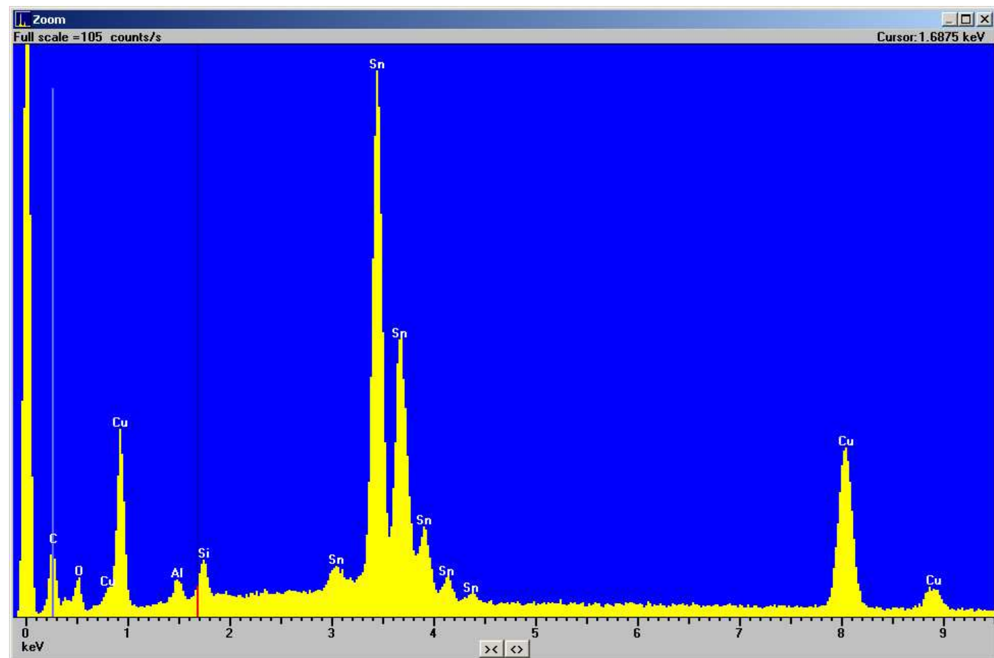

Figure 5.4a EDS spectrum of B1 after 100 hours aging showing intensities of Cu and Sn on IMC form near to the substrate

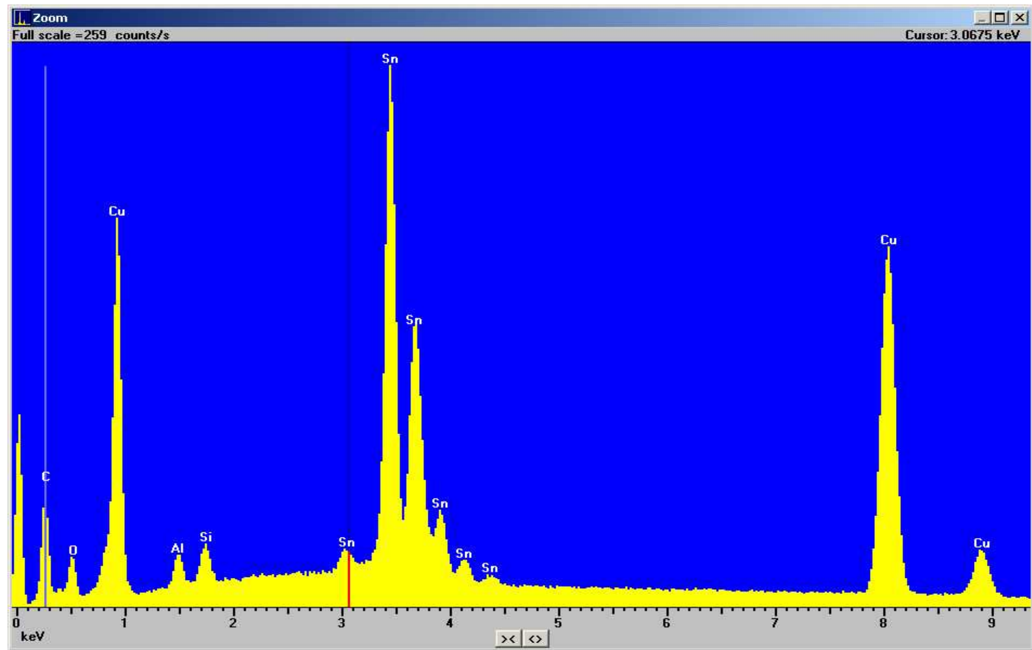

Figure 5.4b EDS spectrum of B1 after 200 hours aging showing intensities of Cu and Sn on IMC form near to the substrate

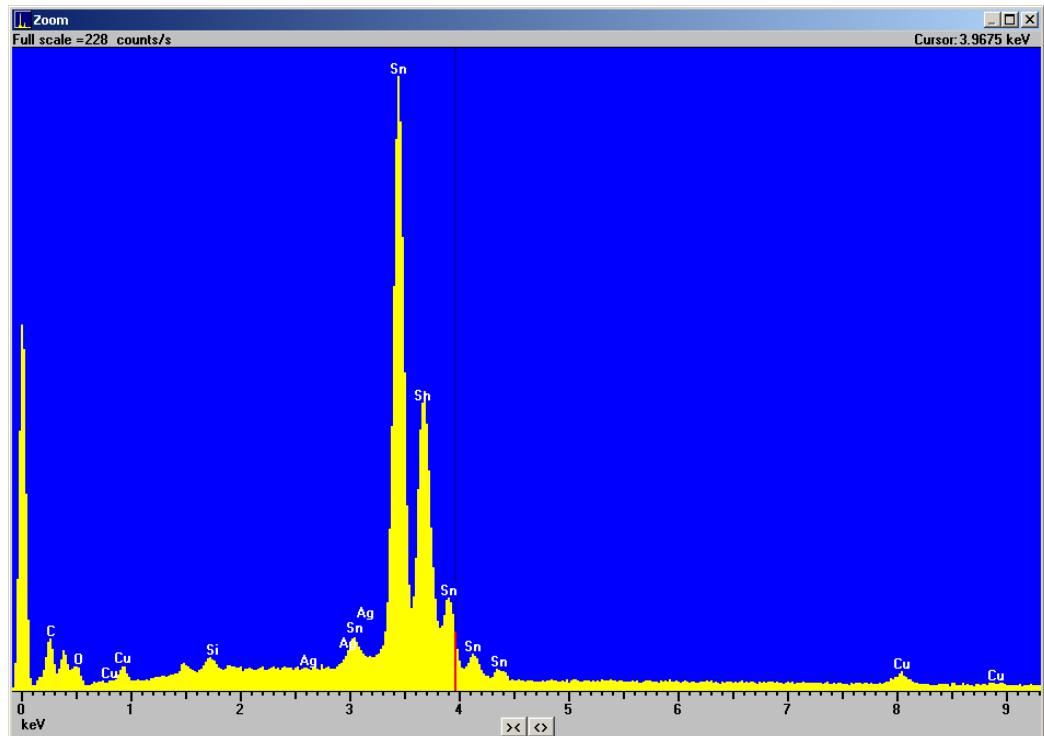

Figure 5.4c EDS spectrum of B1 after 300 hours aging showing intensities of Cu and Sn on IMC form near to the substrate

Table 5.1a The (atomic %) compositions of IMC at solder/Cu interface and the solder matrix at 100 hours of isothermal ageing.

Spectrum	Cu%	Ag %	Sn%
S1	8.21	1.89	89.93
S2	8.79	0.93	90.28
S3	9.758	1.61	90.81
S4	47.691	1.08	51.24
S5	67.08	0.47	32.45

Table5.1b The (atomic %) compositions of IMC at solder/Cu interface and the solder matrix at 200 isothermal ageing.

Spectrum	Cu	Ag	Sn
S1	10.07	1.08	88.86
S2	9.41	1.06	89.53
S3	9.5	0.62	89.88
S4	46.53	0.84	52.63
S5	65.16	0.53	34.32

Table5.1c The (atomic %) compositions of IMC at solder/Cu interface and the solder matrix at 300 isothermal ageing.

Spectrum	Cu	Ag	Sn
S1	9.08	0.55	88.86
S2	9.07	0.54	89.53
S3	8.85	7.35	89.88
S4	47.65	0.84	52.63
S5	66.22	0.43	33.35

5.3.5. Effect of ageing time and temperature on IMC

During natural, temperature cycling or isothermal ageing of an electronic package or assembly, the interface of the solder joint changes by solid-state diffusion, which causes movement of the substrate atoms into the solder, and vice versa. Again, at the interface, the main time-dependent phenomenon occurring is the growth of a layer of intermetallic compound.

The intermetallic compound layer can have a detrimental effect not only on the solderability but also on mechanical properties of the soldered joint because these layers are brittle compared with solder. Furthermore, it is evident that one of the interconnection and solder joint reliability issues is the growth of intermetallic compound layer thickness. Colin Lea (1988) reported that factors affecting the formation and growth of intermetallic compound layer thickness include: time, temperature, type of metallization of the base metal and the solder composition. In this regard, understanding the effect of different ageing times on the growth of IMC is considered in this section of the study.

Solid state growth of intermetallic compound layer as result of solid-state diffusion caused by isothermal ageing between solder and various substrates has been studied comprehensively (Kay and Mackay, 1976). In all cases a parabolic growth rate of thickness (Zo) increasing with the square root of ageing time has been found, but often only after a somewhat faster growth rate over the initial period.

The intermetallic formation and growth during ramp-soak-spike soldering at a peak temperature of 240°C for eight (8) minutes and under solid-state isothermal temperature of 175°C for 100, 200 and 300 hours have been considered in this section of the study. The measured IMC layer thickness resulting from five different pad sizes during reflow process and isothermal ageing conditions are shown in table 5.4 (a-d).

Table 5.2a Measured average values in (μm) of IMC layers of the five different pad sizes after reflow soldering in (μm).

	B1	B2	B3	B4	B5
	4.680	5.541	6.041	5.158	5.605
	4.726	5.103	6.06	4.942	4.965
	4.637	4.311	6.078	5.302	5.337
	5.530	5.330	4.768	5.180	5.675
Average	5.005	5.071	5.736	5.180	5.395

Table 5.2b Measured average values in (μm) of IMC of the five different pad sizes at 175°C for 100 hours

	B1	B2	B3	B4	B5
	5.496	6.632	8.476	6.439	6.741
	6.919	6.680	8.387	5.341	7.531
	6.126	6.688	8.530	6.239	7.245
	6.649	6.876	8.737	8.194	7.252
	7.06	8.053	6.896	8.578	7.745
	6.407	7.672	6.604	8.513	7.802
Average	6.439	7.100	7.938	7.524	7.785

Table 5.2c. Measured average values in (µm) of IMC of the five different pad sizes at 175°C for 200 hours

	B1	B2	B3	B4	B5
	8.933	10.645	11.021	9.856	10.138
	9.915	9.837	9.002	8.595	9.825
	8.047	8.3.365	10.556	8.487	10.537
	10.047	9.467	10.005	10.891	8.618
	8.702	9.964	8.952	9.375	11.633
	9.675	8.814	10.113	11.630	8.825
Average	9.222	9.515	9.941	9.805	9.929

Table 5.2d. Measured average values in (µm) of IMC of the five different pad sizes at 175°C for 300 hours

	B1	B2	B3	B4	B5
	9.514	10.91	12.8	10.741	10.913
	12.347	11.303	11.764	10.829	12.377
	11.413	11.487	12.715	10.868	10.022
	11.029	11.499	10.2	11.175	12.141
	8.226	10.102	11.921	11.044	9.967
	9.4	9.76	12.306	10.987	11.02
Average	10.315	10.843	11.951	10.94	11.02

In order to determine the effect of ageing time on IMC, two factors were considered, namely growth rate constant and the time exponent. These factors are use as indicators to determine the growth characteristics of IMC. To evaluate the effects of the five samples, the power, logarithmic, polynomial and

exponential regression models were engaged. The power regression model exhibited the best fit trend for the experimental data as shown in fig 5.5. The coefficient of determinant (R^2) values and power regression model for sample B1, B2, B3, B4 and B5 are shown in table 5.3. The following is the power regression model used for the growth of IMC layer at 175°C isothermal thermal ageing:

$$Y = kt^n \quad \text{.................................. ………………………….eqn 5.1}$$

Where (Y) denotes the total thickness of the reaction layer; k is the growth rate constant; n is the time exponent and t is the reaction time. For better representation of Eq (5.1), is rewritten into the following logarithmic expression:

$$\text{Log } y = \log k + n \log t, \text{..................... ....eqn 5.2}$$

Where the time exponent (n) actually equal to the slope of Log y vs. log t. However the values of n and k were determined from the power regression analysis by using equation 5.1. Five lines obtained from the five different samples of three different ageing period's at 175°C temperature are nearly parallel to each other which reveal that similar mechanism of IMC growth is operative among 100, 200 and 300. From the n values of the IMC growth as shown in table .5.5, it is believed that it obeys a parabolic growth law.

This is in agreement with work carried out by (Yoon and Jung, 2004; Alam and Chan, 2005; Fix 2008). The results reported by Fix (2008) on the IMC growth of surface mounted chip resistor with a pad size of (2 x 1.2) mm represented as (B6) and of 95.5Sn-4.0Ag-0.5Cu solder subjected to 100, 200 and 300 hours of isothermal ageing exhibited similar results as shown in figure 5.5 and table 5.6. The difference in IMC layer growth might be either solder alloy composition, the thickness of solder deposit or diffusion rate

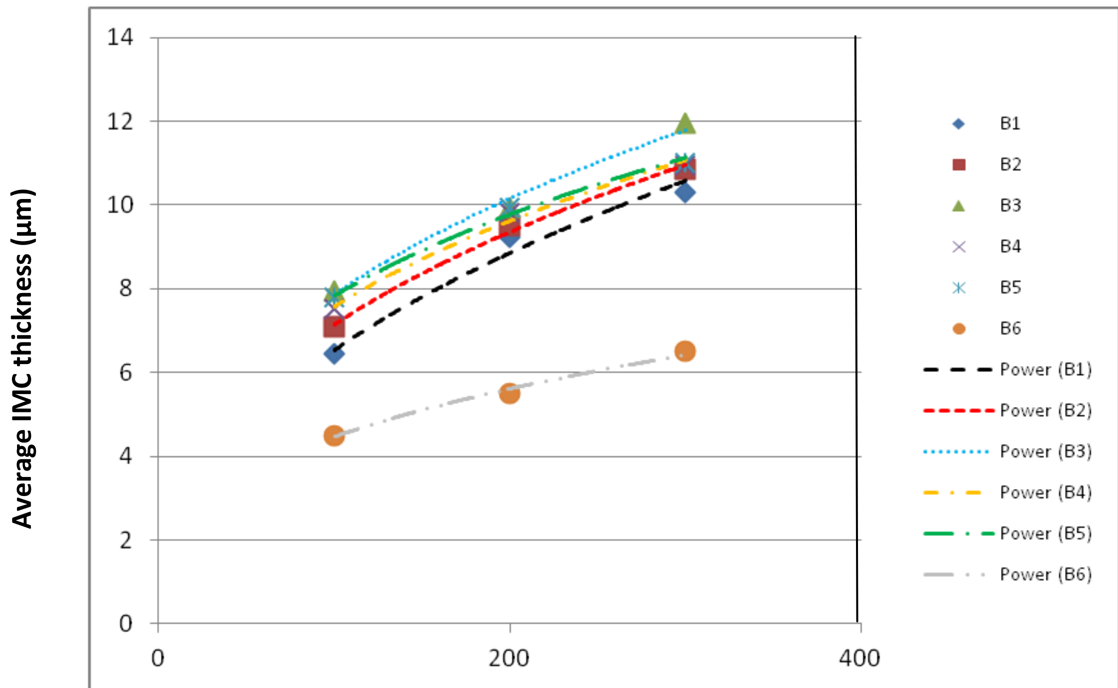

Solid state ageing in (hours) at 175°C

Figure 5.5 Variation of average thickness of IMC as a function of time during solid-state interfacial reactions of Sn-Ag-Cu solder of different Cu pad sizes.

Table 5.3 The coefficient of determinant (R^2) values and power regression model for sample B1, B2, B3, B4 and B5

Sample	**R^2**	**Model equation** $k.t^n$
B1	0.9954	$0.8673t^{0.4385}$
B2	0.9954	$1.1889t^{0.3894}$
B3	0.9915	$1.4511t^{0.3675}$
B4	0.9928	$1.5456t^{0.3452}$
B5	0.9928	$1.7934t^{0.32}$

Table 5.4 The coefficient of determinant (R^2) value and power regression model for sample B6

Sample	R^2	Model equation $k.t^n$
B6	0.9906	$0.9778t^{0.3298}$

(Fix 2008)

Table 5.5 Growth rate constant and time exponent from power regression model of the five samples

Sample (B)	Growth rate constant (k)	Time exponent (t)
B1	0.867	0.438
B2	1.188	0.389
B3	1.451	0.367
B4	1.546	0.342
B5	1.793	0.32

Table 5.6 Growth rate constant and time exponent from power regression model of B6.

Sample	Growth rate constant	Time exponent
B6	0.9778	0.3298

(Fix 2008)

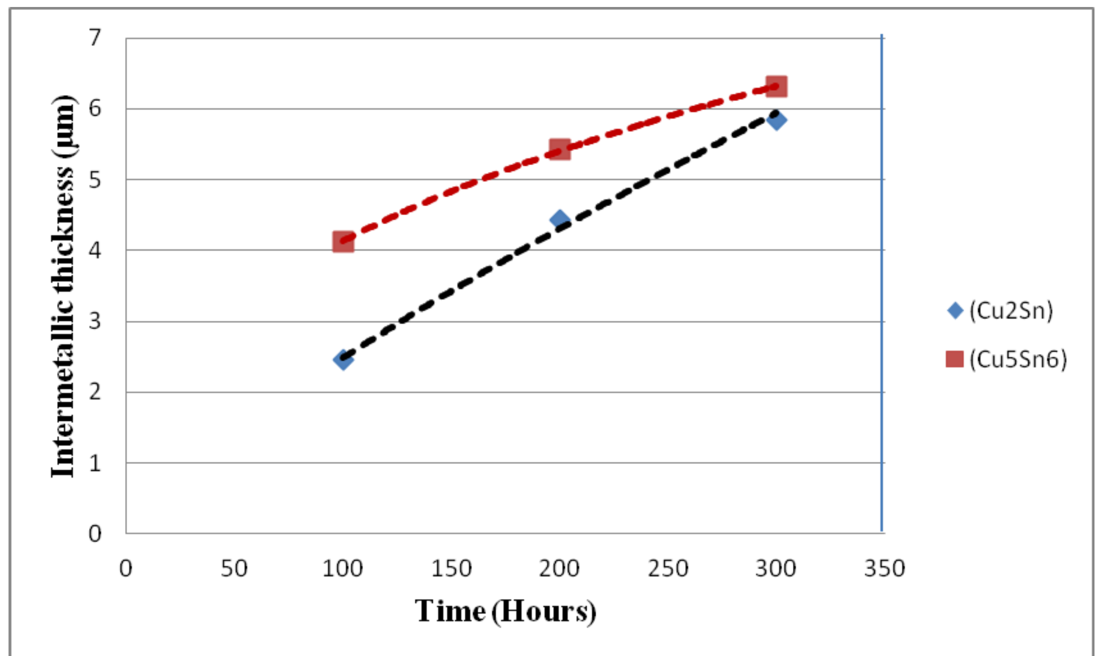

Figure 5.6a. Cu_5Sn_6 and Cu_2Sn intermetallic layers growth of sample B1 aged at 175°C

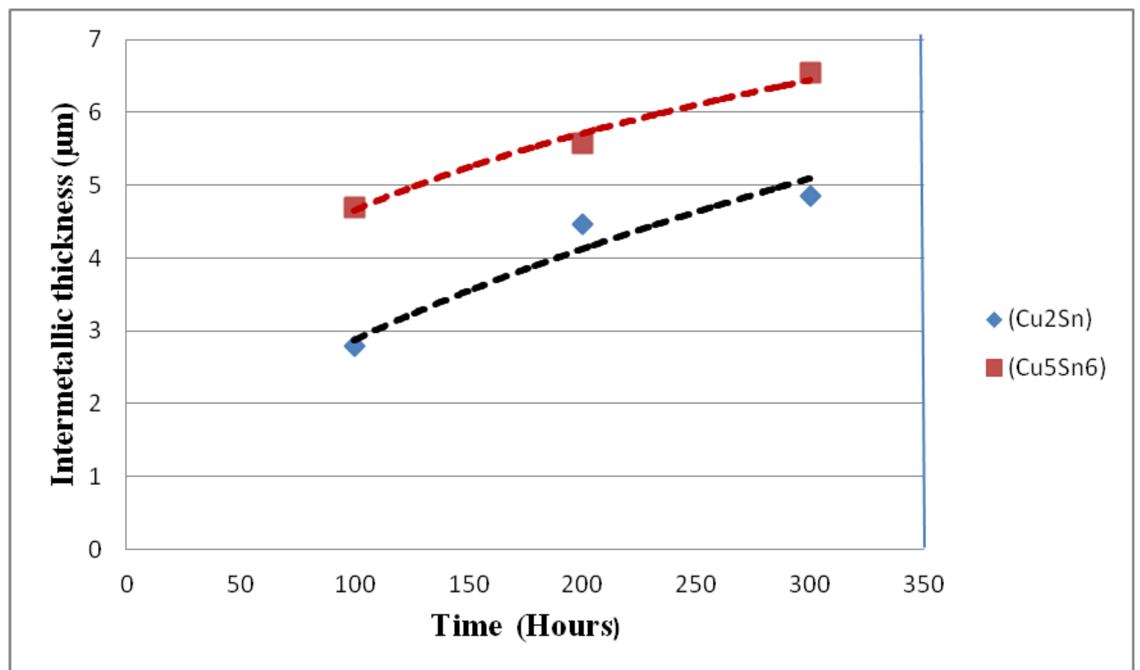

Figure 5.6b Cu_5Sn_6 and Cu_2Sn intermetallic of layers growth of sample B2 aged at 175°C

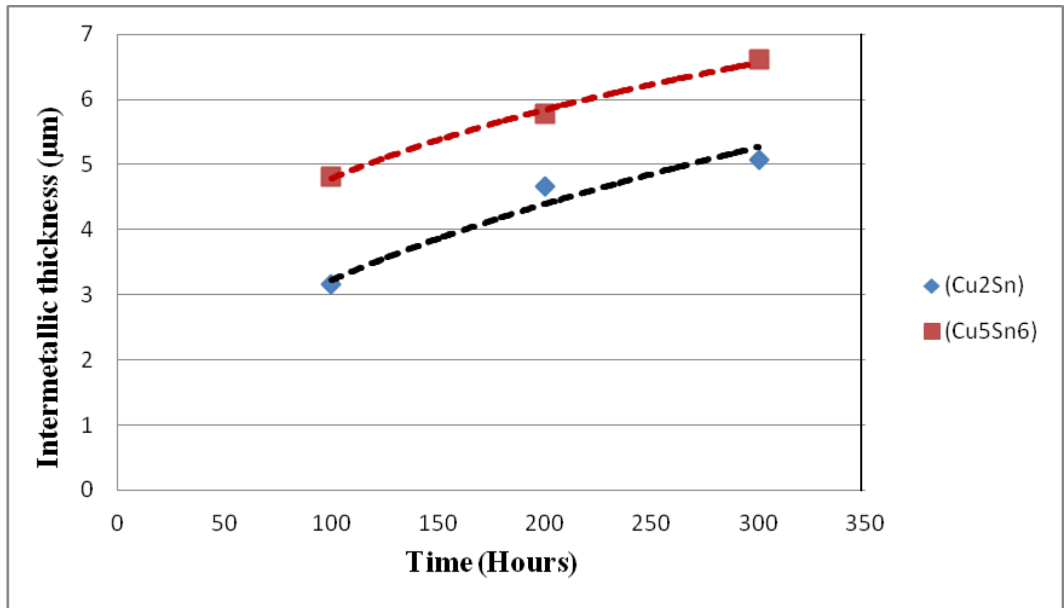

Figure 5.6c Cu_5Sn_6 and Cu_2Sn intermetallic layers growth of sample B3 aged at 175°C

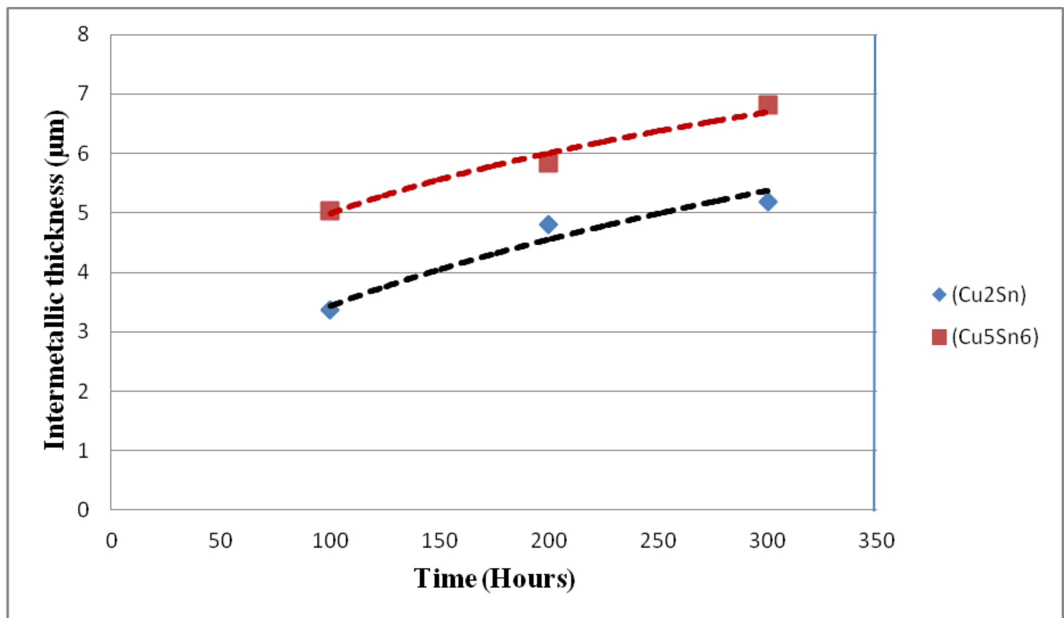

Figure 5.6d Cu_5Sn_6 and Cu_2Sn intermetallic layers growth of sample B4 aged at 175°C

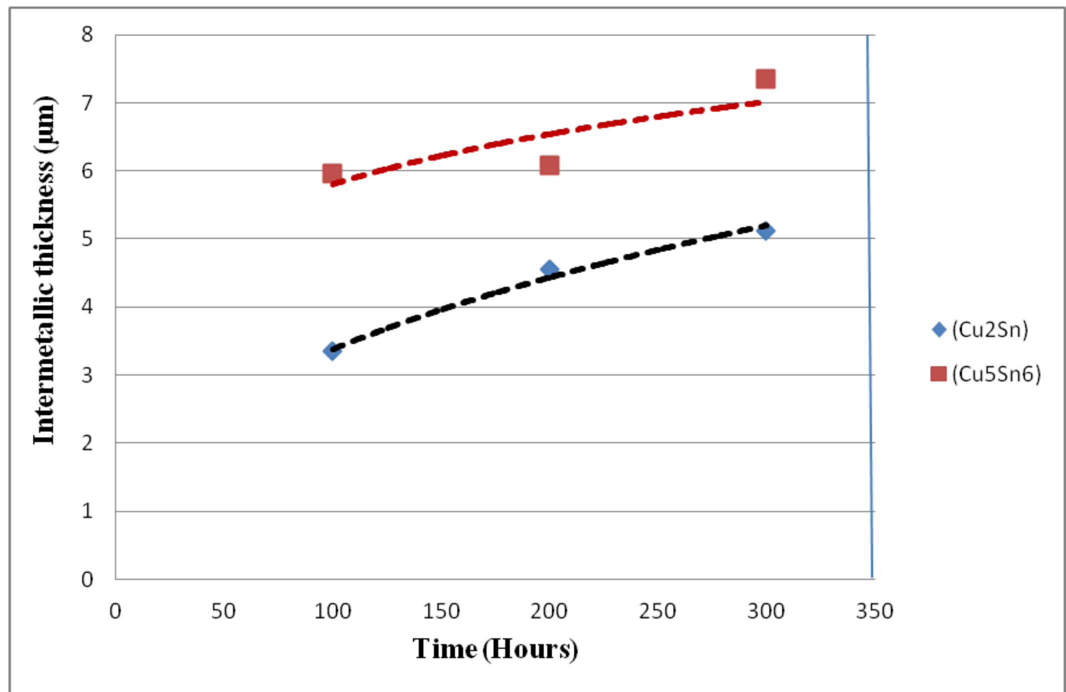

Figure 5.6e Cu_5Sn_6 and Cu_2Sn intermetallic layers growth of sample B5 aged at 175°C

Table 5.9 Growth rate constant and time exponent deduced from power regression model of (Cu_5Sn_6) intermetallic compound

Sample	Growth rate constant	Time exponent	R^2
B1	0.698	0.772	0.998
B2	1.118	0.5927	0.998
B3	1.272	0.575	0.995
B4	1.2505	0.598	0.951
B5	1.2494	0.6123	0.9587

Table 5.10 Growth rate constant and time exponent deduced from power regression model of (Cu_2Sn) intermetallic compound

Sample	Growth rate constant	Time exponent	R^2
B1	0.089	1.4319	0.9634
B2	0.1019	1.3893	0.9521
B3	0.4167	0.8945	0.96
B4	0.4437	0.87	0.9531
B5	0.4792	0.8577	0.96

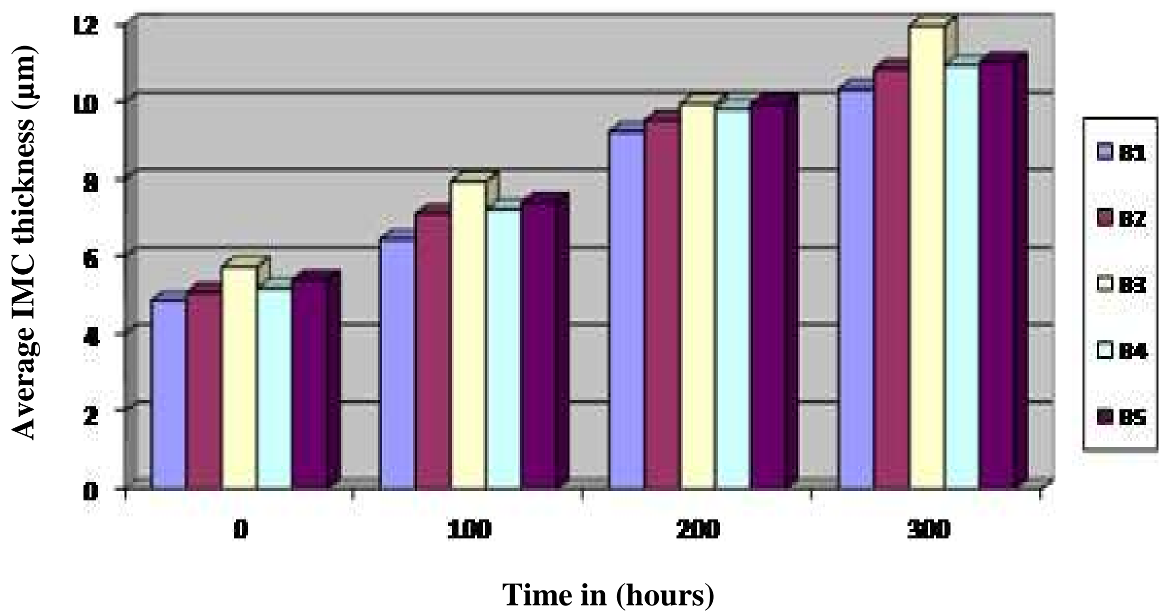

Figure 5.7: Variation of average IMC layer thickness of samples after reflow soldering and isothermal ageing at 175°C

5.4 Discussion of Results

In figure 5.1a the average thickness of IMC layer just after reflow (i.e., before solid–state ageing) was 5.13µm. The formation of IMC layer after reflow indicates a good metallurgical bond between the substrate and the solder alloy. However, it also makes the solder joint brittle, which could lead to crack propagation between the substrate and the IMC formed. After the sample was subjected to 300 hours of isothermal ageing time, the average IMC layer thickness was 10.8µm as shown in figure 5.2c. Thicker IMC layers would facilitate "crack propagation" at solder-substrate interface. The increase in IMC thickness will therefore make the solder joint more vulnerable to failure. The experimental work reported by Karpel et al (2007) confirmed that solder joint eventually fails due to void coalescence and crack propagation through IMC.

The IMC layers growth of sample B1, B2, B3, B4 and B5 is shown in figure 5.6 (a-e). In the five plots, Cu_5Sn_6 is identified by the diamonds and Cu_2Sn by the squares. The power regression model was used for the individual IMC layer growth analysis. The time exponent, growth rate constant and the coefficient of determinant for the IMCs are represented in table 5.7 and 5.8. The slopes of the lines in figure 5.6 (a - e) indicate the rate of IMC growth. As expected, as the time increased the rate of IMC layer growth increased. It was found that IMC growth also obeys the parabolic relation, as in the case of the growth of the total IMC. In all the three durations; 100, 200 and 300 hours of the five samples, the Cu_5Sn_6 grew at a faster rate than Cu_2Sn according to the growth rate constant represented in Table 5.7 and 5.8.

The IMC Cu-Sn layer thickness of the five different pad sizes is represented as B1, B2, B3, B4, and B5 in figure 5.7. The range of IMC growth is between 5.005µm to 5.395µm which is on the five different pad sizes after reflow soldering. The difference in IMC layer thickness of different pad sizes/solder volumes during reflow soldering is due to difference in temperature which exist between the solder volumes (Gao et al 2008). After 100 hours of isothermal

ageing temperature at 175°C, the growth of IMC is between 6.439 μm to 7.785 μm.

The IMC growth during 100 hours of isothermal ageing is due to the inter-diffusion and reaction of Cu and Sn. This reaction appears at the space between Cu_5Sn_6 grains, because the diffusion length through the grains is the shortest (Park, 2010). The interfacial reaction of solder volumes and the five different pad sizes during 200 hours of isothermal ageing showed that there was 7.05% of IMC growth. The growth is attributed to the diffusion rate of Sn and Cu in the solder alloy during the solid-state ageing (Salem et al, 2001). The 300 hours of isothermal ageing on the five different pad sizes and solder volumes exhibited similar effect, with 6.35% of IMC growth. The results show that increasing the solder volume (and solder joint size) does not significantly affect the growth of the intermetallic layer thickness

5.5 Summary

The study of the effect of pad size on intermetallic compound layer formation and growth has been presented in this chapter. Conclusions drawn from the study are as follows:

1. The ratio of the average thickness of IMC layers for the five different pad areas are 1.43: 1.2: 1.18: 0.86: 1.33. These results revealed that there is not much difference in IMC layer thickness of the five different pad sizes. The differences in IMC layer thickness is due to the difference in temperature gradient in the solder volumes.

2. The intermetallic compound layer thickness of the five different pad sizes during 100 hours isothermal ageing showed that the smallest vulome:area solder bumps exhibited thicker intermetallic compound layer of 1.839µm and the largest Volume/Area solder bumps exhibited 1.08µm

3. The intermetallic compound layer thickness of the smallest Volume: Area and the largest volume:area solder bumps after 200 hours are 2.634µm and 1.3508µm respectively. After 300 hours of isothermal ageing, the smallest Volume:area solder bumps exhibited 2.94µm and 1.53µm for the largest Volume: Area solder bumps.

4. The solid state growth of Cu-Sn intermetallic compounds in the solder joints aged isothermally at 175°C for 100, 200 and 300 hours showed that the thickness of IMC layer increases as the ageing time increases.

5. Finally, the results of IMC thickness of volume:area solder bumps of the five different pad sizes for various ageing times revealed that the growth of IMC depends on diffusion of Cu and Sn in the solder joint during solid-state ageing.

The next chapter investigates effect of cycling temperatures and reflow profiles on the intermetallic growth.

CHAPTER VI: EFFECT OF CYCLING TEMPERATURES AND REFLOW PROFILES ON THE INTERMETALLIC GROWTH

6.1 Introduction

This chapter presents a study of the effect of temperature cycling and reflow profiles on the intermetallic growth between Sn-Ag-Cu solder alloy and Cu substrate. In this study, three different temperature cycles were employed to age the Sn-Ag-Cu IMC formed during the convectional reflow soldering.

The chapter is divided into two parts. The first part reports on the effect of reflow profile on intermetallic formation and growth. The second part concerns the investigation of the effect of thermal cycle ageing on intermetallic thickness

6.2 Experimental details

A number of test vehicles were constructed for studying the intermetallic formation and growth. The experiments were conducted with test vehicles of the same solder bump sizes in terms of volume and pad size. The IMC layer thickness were measured and used to evaluate the growth of IMC at the three different temperature cycles. The substrate used in this experiment was FR4 PCB measuring (150 × 160 × 1.6) mm as test vehicle as shown in figure (4.2). Two hundred and forty (240) samples were prepared for the investigation. One hundred and twenty (120) samples were used for solder paste sample P1 and the remaining (120) for sample P2. Both samples P1 and P2 have the compositions of 95.5Sn-3.8Ag-0.7Cu, a melting temperature of 217 ^{0}C and a particle size distribution of 20 – 45µm. In both solder pastes the fluxes used are classified as water-based, rosin-containing, no-clean and halide free. Although the fluxes are classified into the same the categories, there might be some differences in the type and quantity of ingredients that form the flux systems.

6.3 Results

6.3.1 Effect of Reflow profiles on intermetallic formation and growth

As observed by Schaefer et al (1996) and Kim and Jung (2004) the formation and growth of intermetallic layer is mainly controlled by a diffusion mechanism. During the soldering process, interdiffusion of atoms from both solder (95.5Sn-3.8Ag-0.7Cu) and copper substrate is initiated. The Cu at the substrate side starts to diffuse into the solder region and the active Sn constituent at the solder side could also diffuse into the substrate. When the Cu saturation point is attained within the joint, the IMC layer formation can start. Figures 6.2, 6.3 and 6.4 (a and b) show the micrographs of IMC layers for samples P1 and P2.

The microstructures at the Cu pad to bulk solder interface under various thermal conditions are evaluated. The interfacial IMCs of sample P1 and P2 which were thermally cycled within the temperature region of (20 -25ºC) exhibited Cu_6Sn_5 . It followed by increase in IMC thickness at the solder and Cu interface during reflowing within the temperature region of (20 - 40°C) thermal cycling. During thermal cycling of (20 - 60°C) however, IMCs noted for samples P1 and P2 were 1.82μm and 1.4μm respectively. The interfacial thickness of IMCs was found increases with the thermal cycles; however, the growth rate is a function of the thermal aging.

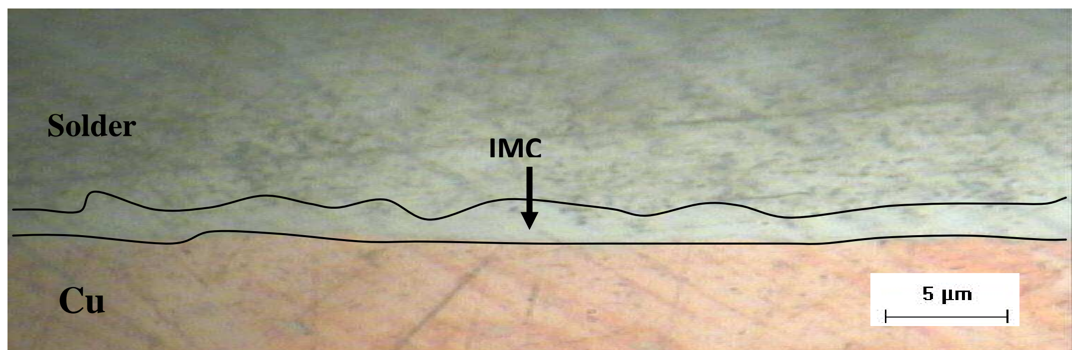

Figure 6.2a IMC Layers aged at 24 hours with T25 temperature cycle for paste sample P1

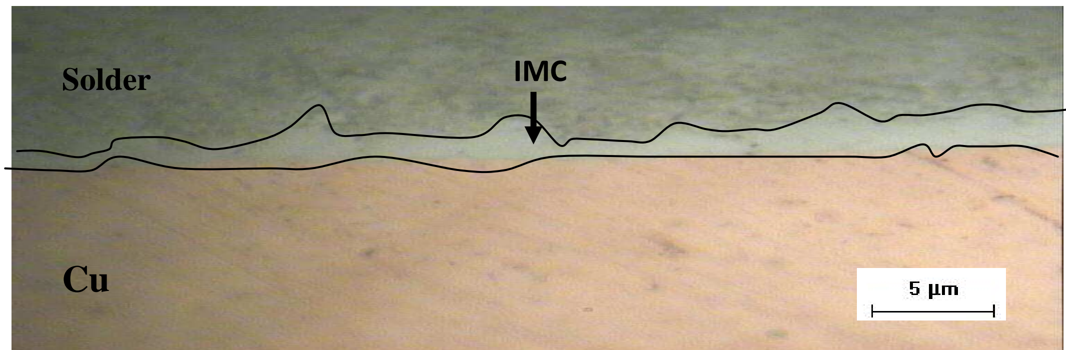

Figure 6.2b IMC Layers aged at 24 hours with T25 temperature cycle for paste sample P2

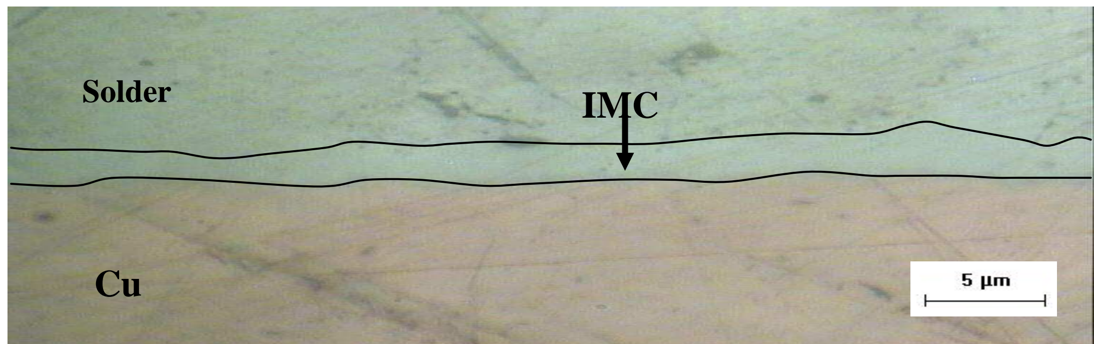

Figure 6.3a IMC Layers aged at 24 hours with T40 temperature cycle for paste sample P1

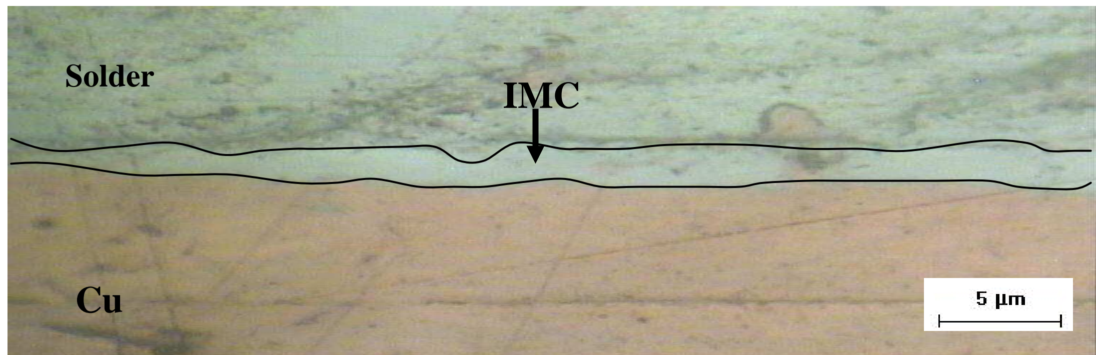

Figure 6.3b IMC Layers aged at 24 hours with T40 temperature cycle for paste sample P2

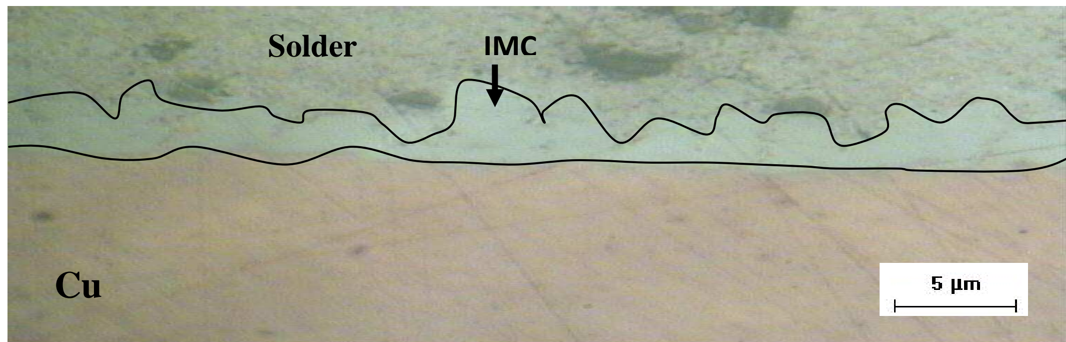

Figure 6.4a IMC Layers aged at 24 hours with T60 temperature cycle for paste sample P1

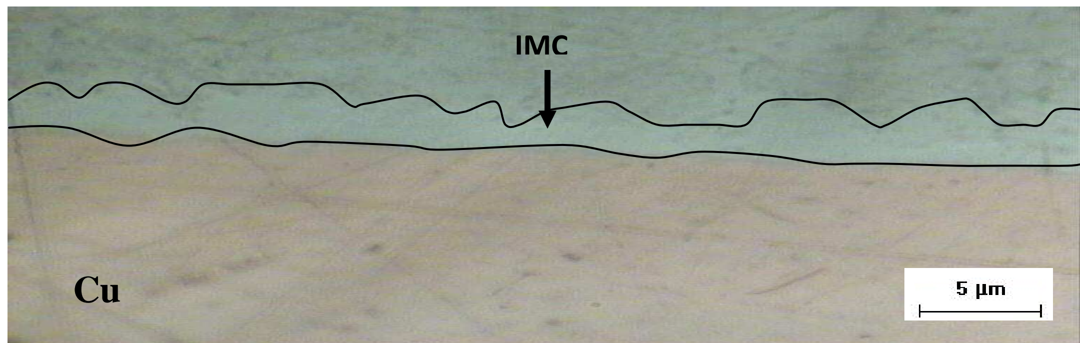

Figure 6.4b IMC Layers aged at 24 hours with T60 temperature cycle for paste sample P2

As shown in table 4. 3, each of the reflow profile is comprised of four time zones and a cooling zone. The profiles are formed by changing the temperatures of the time zones. Profile E is a common type of reflow profile used in the electronic assembly process. Taking profile E as the typical reflow profile, profiles D, C and B are formed by increasing the temperature (by 40 ^{0}C) of preheat 1, preheat 2, and preheat 3 zones respectively. In the case of profile A, the temperature of the reflow zone was set to 260 ^{0}C (20 ^{0}C higher than that of profile E). Temperatures higher than 260^{0}C are avoided as they could damage the reflow oven and the test vehicle.

From the results shown in figures 6.5a and 6.5b, two important observations can be made. Firstly, the intermetallic thickness was found to increase with an increase in temperature of the reflow profile. No matter which zone temperature of the reflow process was increased, the growth of intermetallic layer was observed. This finding strengthens the fact that reflow temperature contributes significantly to the development of intermetallic layer. Secondly, the “reflow” stage was found to be the most influential element in the reflow process and could contribute highly to the growth of intermetallic layer.

This was obvious as profile A (with the highest reflow zone temperature) produced the thickest intermetallic layer. Therefore, care must be taken in setting the reflow zone temperature. The peak temperature in this zone should be high enough for adequate flux action and to obtain good wetting. If the temperature is too low, cold and grainy solder joints will result. However, it should not be too high as this might cause component and board damage or discolouration.

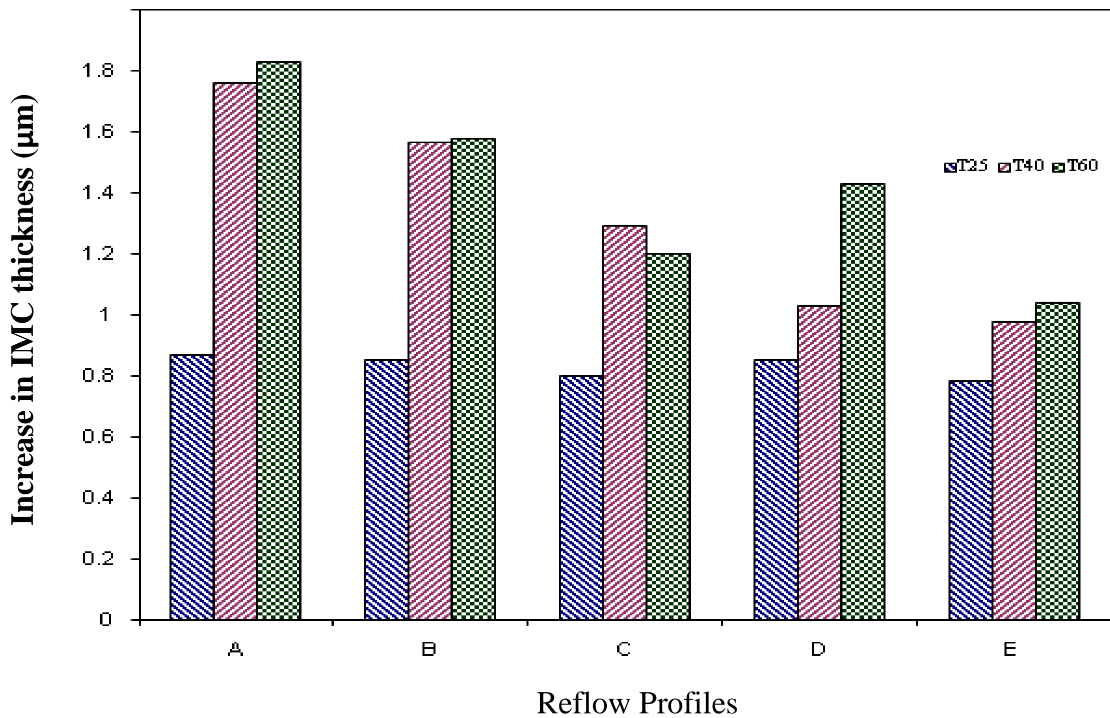

Figure 6.5a IMC thickness for paste P1 as a function of reflow profile and temperature cycle

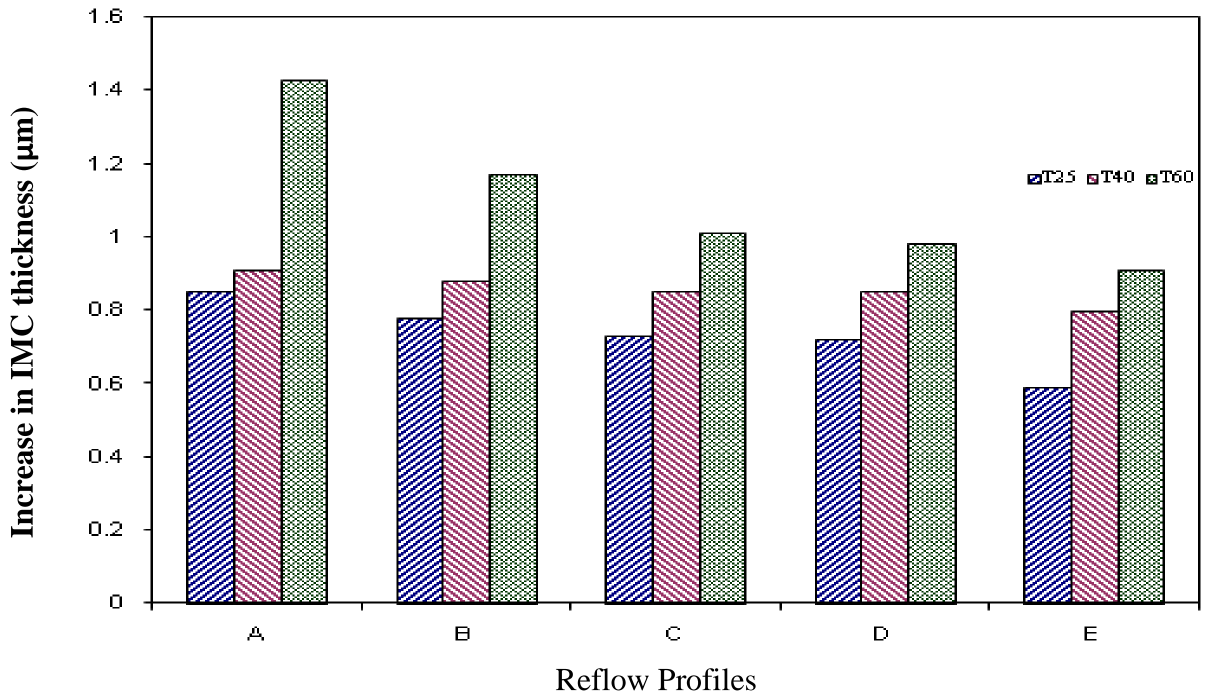

Figure 6.5b IMC thickness for paste P2 as a function of reflow profile and temperature cycle

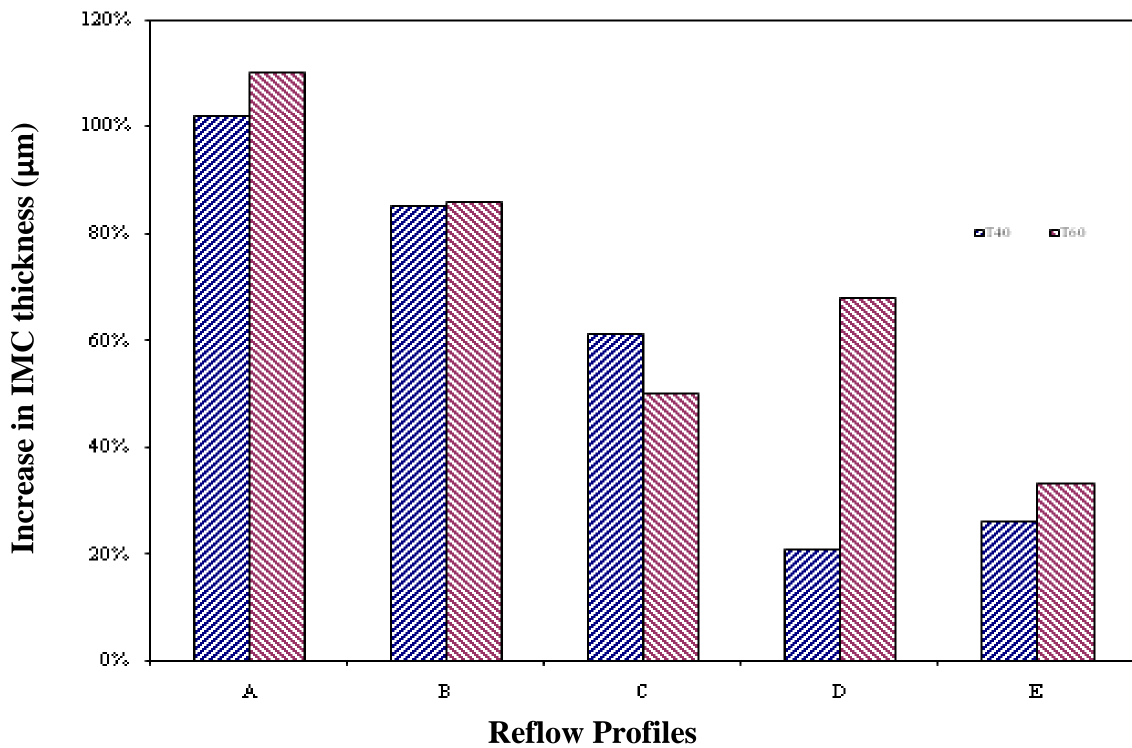

Figure 6.6a Increase in IMC layer thickness of T40 and T60 temperature cycles compared to T25, for paste P1

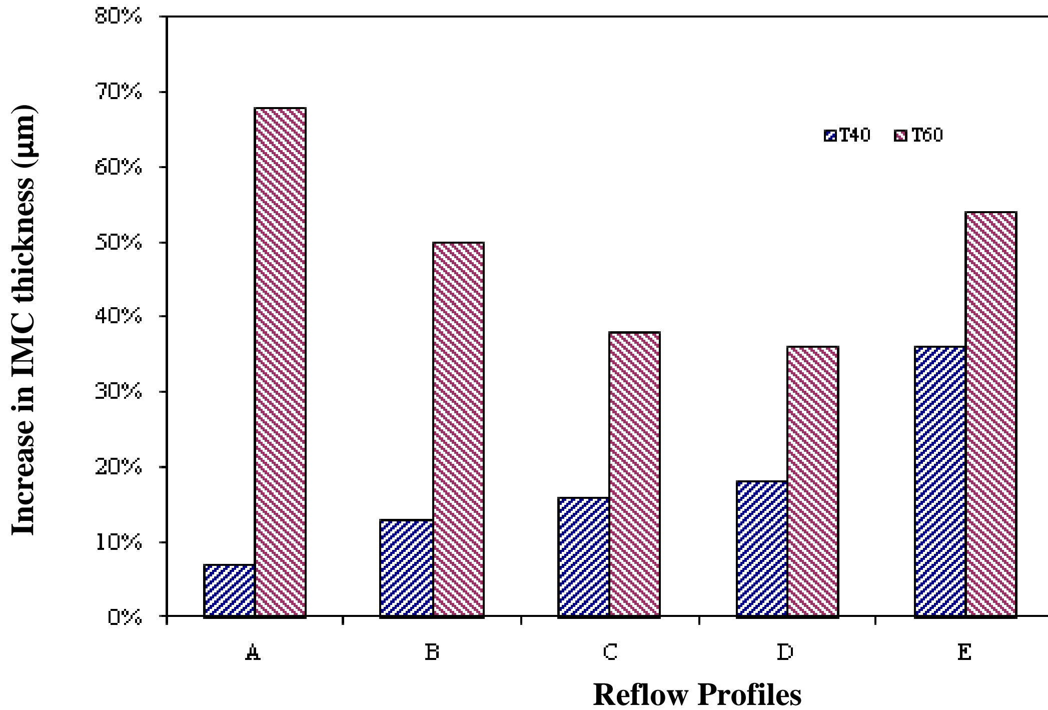

Figure 6.6a Increase in IMC layer thickness with T40 and T60 temperature cycles compared to T25, for paste P2

In addition, the plots figures (6.7a and 6.7b) suggested that the IMC thickness can be successfully fitted into a second order polynomial as shown in equation 6.3. Here, z_0 represents the IMC thickness, T represents the applied thermal cycles. The constants α, β and γ are known as the quadratic coefficient, the linear coefficient and the constant term or free term respectively. Table 2 presents the estimated values of the constants from equation 6.3 for pastes P1 and P2.

$$z_0 = \alpha T^2 + \beta T + \gamma \qquad (6.3)$$

The quadratic coefficient, α indicates which way the fitted curve is bending. The curve would be convex (apex at the bottom, curve opens up) when α is positive and concave (apex at the top, curve opens down) when α is negative. The linear coefficient, β provides the rate of change of IMC thickness with the thermal cycles.

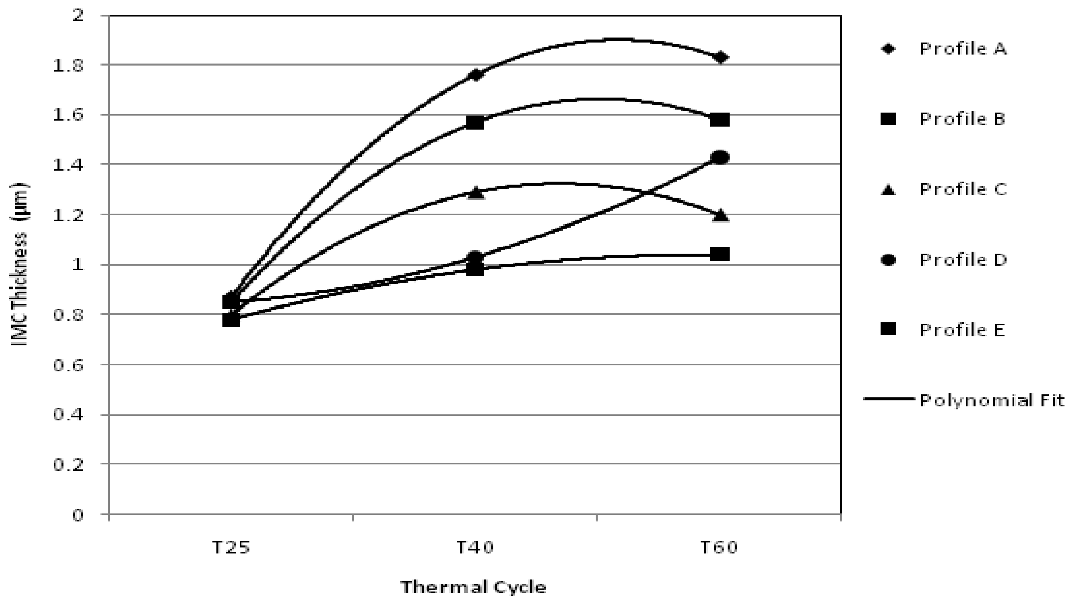

Figure 6.7a. IMC thickness as a function of thermal cycle ageing for different reflow profiles for paste P1

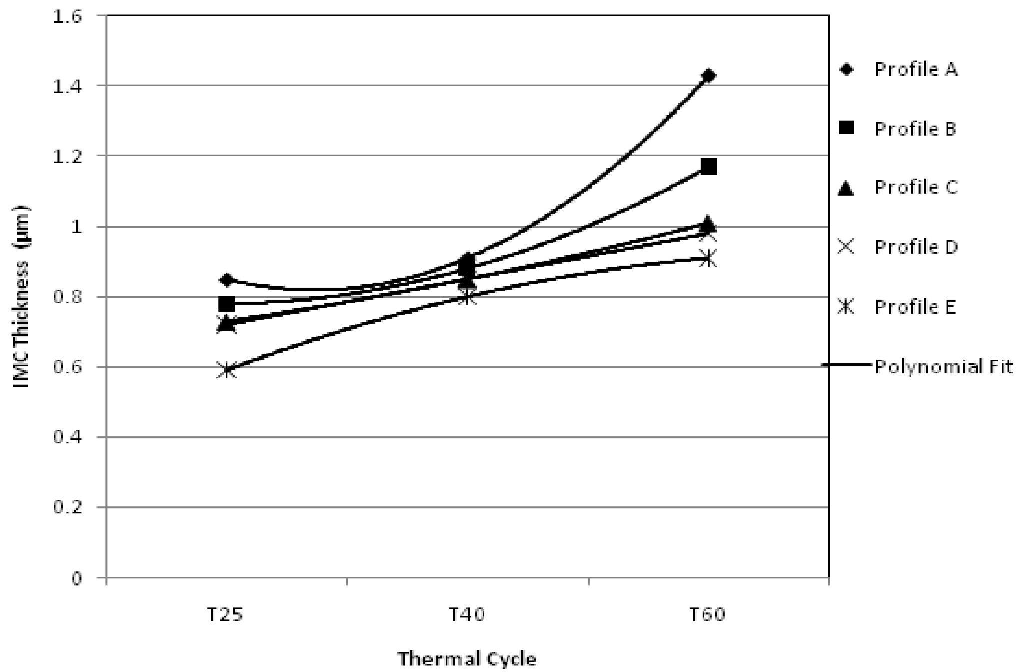

Figure 6.7b. IMC layer thickness as a function of temperature cycle ageing for different reflow profiles for paste P2

Table 6.2 Polynomial model fitted data for pastes P1 and P2

Parameters		Reflow Profiles				
		A	B	C	D	E
α	P1	-0.41	-0.355	-0.29	0.11	-0.07
	P2	0.23	0.095	0.02	1E-14	-0.05
β	P1	2.12	1.785	1.36	-0.15	0.41
	P2	-0.63	-0.185	0.06	0.13	0.36
γ	P1	-0.84	-0.58	-0.27	0.89	0.44
	P2	1.25	0.87	0.65	0.59	0.28

6.4 Discussion of Results

Figure 6.5a shows the IMC layer thickness following the thermal cycling carried out for three different temperature cycling profiles. The first temperature profile (between 20°C and 25°C) did not significantly affect the thickness of IMC layers of the five different reflow profiles. This might be attributed to high activation energy in the as-soldered IMC layer. The second temperature profile (between 20°C and 40°C) had more effect on the thickness of IMC layer of the five different reflow profiles. From figure 6.5a it can be seen that the IMC layer grew only slightly thicker during the thermal cycling possibly due to diffusion of Sn-Cu atoms in the as soldered IMC layer. The third thermal cycling ranged between 20°C and 60°C also exhibited similar effect to the second. The variation in thickness of the IMC layers after thermal cycling are attributed to differences in thickness of IMC layer caused by the reflow temperature and time.

As was expected, both temperature and time had significant effects on intermetallic formation and growth. At high temperature and given enough time, more solids would dissolve at the solder and substrate interface. This would obviously result in thicker intermetallic layer. Figures 6.5a and 6.5b show the growth of intermetallic layer thickness for pastes P1 and P2 as a function of

reflow profile and thermal cycle temperature. Again, as expected, the intermetallic layer thickness was found to increase with increase in the thermal cycle temperature.

Kim and Jung (2004) also observed that the IMC thickness is a function of temperature. The intermetallic layers formed at the interface between solder and the substrates are brittle and is known to adversely impact the solder joint's mechanical integrity, leading to failure at low mechanical stresses.

Taking the thermal cycle T25 as the reference cycle, the increase of intermetallic layer thickness (in percentage) for the other two cycles are presented in figures 6.4a and 6.4b for pastes P1 and P2 respectively. Under the same thermal condition, paste P1 has shown higher intermetallic growth than paste P2. This implies that paste P2 would be more resistant towards intermetallic layer formation. In other words, paste P2 would produce more reliable solder joints for high temperature operating conditions. As mentioned earlier, the main difference between the two paste samples is the flux formulation.

According to Hwang (1989), the composition of a typical flux has some 5 – 20 ingredients and every ingredient plays a role in the final performance of the paste. Therefore, the differences in the IMC thickness observed for the paste samples could be attributed to the difference in flux formulation. Although this finding is of great importance, however, it is not conclusive in the sense that only two solder pastes were used for the investigation. Therefore, it is recommended that further research be carried out with more solder paste samples.

Furthermore, the IMC thickness of paste P1 and P2 presented in figures 6.6a and 6.6b is a function of the applied thermal cycles. For both solder paste samples the IMC thickness was found to increase with increase in thermal cycle temperatures. Fix et al (2008) also observed a similar behaviour although the applied thermal cycles (-40^0C to 125^0C and -40^0C to 150^0C) were different.

6.5 Summary

The study of the effects of cycling temperatures and reflow profiles on intermetallic compound layer growth of Sn-Ag-Cu solder joints have been presented in this chapter. Conclusions drawn from the study are as follows:

1. The study shows that intermetallic compound layer growth occurs at the interface between the solder and substrate and is a function of the reflow profile.

2. The results show that increase in reflow temperature affects the growth of the intermetallic compound layer thickness.

3. The IMCs layer thickness was found to increase with the increase in cycle temperature during ageing.

4. The IMC layer thickness of solder joints of the two lead-free solder pastes with different flux formulation under the same cycle temperatures condition of (20°C – 25°C) resulted in 1.82µm and 1.4µm respectively. The difference in IMC thickness is attributed to the difference in flux formulation.

CHAPTER VII: THE STUDY OF THE EFFECT OF REFLOW SOLDERING PROFILE PARAMETERS ON SN-AG-CU SOLDER BUMPS USING CU SUBSTRATE

7.1 Introduction

The aim of the study presented in this chapter is to determine the optimal reflow soldering profile setting for Sn-Ag-Cu solder and the most significant factor that influences the process. The chapter is made up of three sections. The first section presents the reflow profile parameters and the experimental design used for this study. The second section presents the results from the study. The final section provides conclusions drawn from the investigation

7.2 Full Factorial Design of Experiments (DOE)

Full factorial experiments were designed using four reflow profile factors with two levels for each factor. The interactions between the factors were also considered in the DOE. The chosen reflow profile factors and their corresponding levels are shown in table 7.1. A total of $2^4 = 16$ experiments were performed. A test board was specially designed for this study with solder bumps of three different diameters

Table 7.1 Experimental parameters

Factors	High level (+)	Low level(-)
Soak temperature (^{0}C)	180	150
Soak time (Second)	120	60
Time above liquidus (Second)	120	60
Time to peak temperature (Second)	360	240

Figure 7.1 shows the schematic of the test board. The reflowed solder bumps were cross-sectioned and moulded. Finally, the thickness of IMC layer formed between the solder and the substrate was measured.

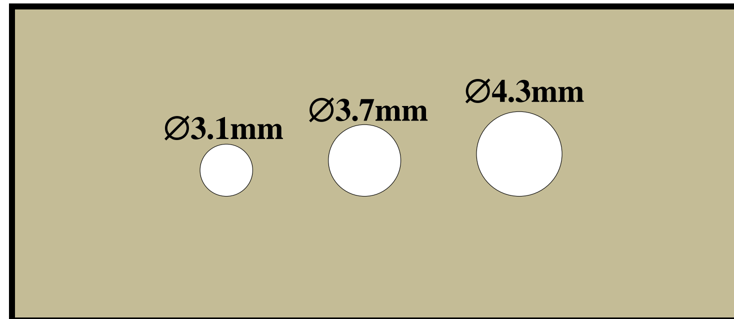

Figure 7.1 Test board with three different sizes of solder bumps

7.2 Results

The results were analysed using different statistical methods namely; normal probability plot of factor effects, pareto plot, optimal plot, and ANOVA. The average responses of ∅ 3.1mm, ∅ 3.7mm and ∅ 4.3mm are shown in table 7.2, 7.3 and 7.4 respectively.

Table 7.2 Average response of ∅ 3.1mm solder bump

	A	*B*	*C*	*D*	*AB*	*AC*	*AD*	*BC*	*BD*	*CD*	*ABC*	*BCD*	*ABD*	*ACD*	*ABCD*	*RESPONSE*
1	-	-	-	-	+	+	+	+	+	+	-	-	-	-	+	1.913767
a	+	-	-	-	-	-	-	+	+	+	+	-	+	+	-	2.211382
b	-	+	-	-	-	+	+	-	-	+	+	+	+	-	-	2.706599
ab	+	+	-	-	+	-	-	-	-	+	-	+	-	+	+	2.168328
c	-	-	+	-	+	-	+	-	+	-	+	+	-	+	-	2.689251
ac	+	-	+	-	-	+	-	-	+	-	-	+	+	-	+	3.173566
bc	-	+	+	-	-	-	+	+	-	-	-	-	+	+	+	3.442325
abc	+	+	+	-	+	+	-	+	-	-	+	-	-	-	-	2.527233
d	-	-	-	+	+	+	-	+	-	-	-	+	+	+	-	3.496837
ad	+	-	-	+	-	-	+	+	-	-	+	+	-	-	+	2.578429
bd	-	+	-	+	+	+	-	-	+	-	+	-	-	+	+	3.729514
abd	+	+	-	+	+	-	+	-	+	-	-	-	+	-	-	3.794570
cd	-	-	+	+	+	-	-	-	-	+	+	-	+	-	+	3.011017
acd	+	-	+	+	-	+	+	-	-	+	-	-	-	+	-	3.475269
bcd	-	+	+	+	-	-	-	+	+	+	-	+	-	-	-	3.816357
abcd	+	+	+	+	+	+	+	+	+	+	+	+	+	+	+	3.515043

Table 7.3 Average responses of ∅ 3.7mm solder bump

	A	*B*	*C*	*D*	*AB*	*AC*	*AD*	*BC*	*BD*	*CD*	*ABC*	*BCD*	*ABD*	*ACD*	*ABCD*	*RESPONSE*
1	-	-	-	-	+	+	+	+	+	+	-	-	-	-	+	2.752402
a	+	-	-	-	-	-	-	+	+	+	+	-	+	+	-	2.360239
b	-	+	-	-	-	+	+	-	-	+	+	+	+	-	-	1.942629
ab	+	+	-	-	+	-	-	-	-	+	-	+	-	+	+	2.291242
c	-	-	+	-	+	-	+	-	+	-	+	+	-	+	-	2.433531
ac	+	-	+	-	-	+	-	-	+	-	-	+	+	-	+	2.850441
bc	-	+	+	-	-	-	+	+	-	-	-	-	+	+	+	3.522220
abc	+	+	+	-	+	+	-	+	-	-	+	-	-	-	-	2.589005
d	-	-	-	+	+	+	-	+	-	-	-	+	+	+	-	3.039264
ad	+	-	-	+	-	-	+	+	-	-	+	+	-	-	+	4.176235
bd	-	+	-	+	+	+	-	-	+	-	+	-	-	+	+	3.210582
abd	+	+	-	+	+	-	+	-	+	-	-	-	+	-	-	4.088654
cd	-	-	+	+	+	-	-	-	-	+	+	-	+	-	+	2.875908
acd	+	-	+	+	-	+	+	-	-	+	-	-	-	+	-	4.833265
bcd	-	+	+	+	-	-	-	+	+	+	-	+	-	-	-	3.555027
abcd	+	+	+	+	+	+	+	+	+	+	+	+	+	+	+	3.903468

Table 7.4 Average responses of ∅ 4.3mm solder bump

	A	B	C	D	AB	AC	AD	BC	BD	CD	ABC	BCD	ABD	ACD	ABCD	RESPONSE
1	-	-	-	-	+	+	+	+	+	+	-	-	-	-	+	2.952164
a	+	-	-	-	-	-	-	+	+	+	+	-	+	+	-	2.13144533
b	-	+	-	-	-	+	+	-	-	+	+	+	+	-	-	2.64351533
ab	+	+	-	-	+	-	-	-	-	+	-	+	-	+	+	2.97028767
c	-	-	+	-	+	-	+	-	+	-	+	+	-	+	-	2.31320167
ac	+	-	+	-	-	+	-	-	+	-	-	+	+	-	+	3.050205
bc	-	+	+	-	-	-	+	+	-	-	-	-	+	+	+	3.15904133
abc	+	+	+	-	+	+	-	+	-	-	+	-	-	-	-	2.17888133
d	-	-	-	+	+	+	-	+	-	-	-	+	+	+	-	2.64726033
ad	+	-	-	+	-	-	+	+	-	-	+	+	-	-	+	3.04652833
bd	-	+	-	+	+	+	-	-	+	-	+	-	-	+	+	3.82079633
abd	+	+	-	+	+	-	+	-	+	-	-	-	+	-	-	4.106975
cd	-	-	+	+	+	-	-	-	-	+	+	-	+	-	+	2.93413433
acd	+	-	+	+	-	+	+	-	-	+	-	-	-	+	-	3.69661367
bcd	-	+	+	+	-	-	-	+	+	+	-	+	-	-	-	3.209963
abcd	+	+	+	+	+	+	+	+	+	+	+	+	+	+	+	3.411821

7.3.1 Analysis of normal probability plot of factor effects

Significant effects may be identified by constructing a normal probability plot of effects. The idea behind this methodology is that all non-significant effects will fall along the straight line representative of the normal distribution. Also, the normal probability plot is a graphically technique for assessing whether or not a data set is approximately normally distributed. The normal probability plots of effects of the three different solder volumes are graphical represented in figure 7.2a, 7.2b and 7.2c respectively. All the effects that lie along the line are negligible, whereas the large effects are far from the line. The apparently negligible effects are combined as an estimate of error (Montgomery, 1997).

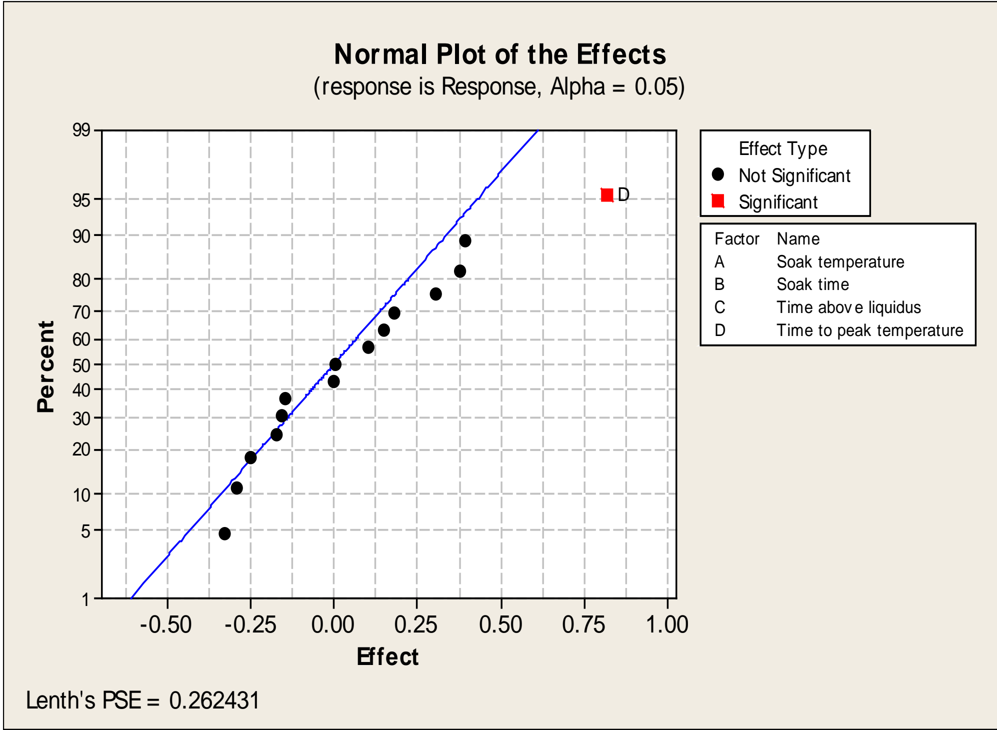

Figure 7.2a Normal probability plots of factor effects of (∅3.1mm)

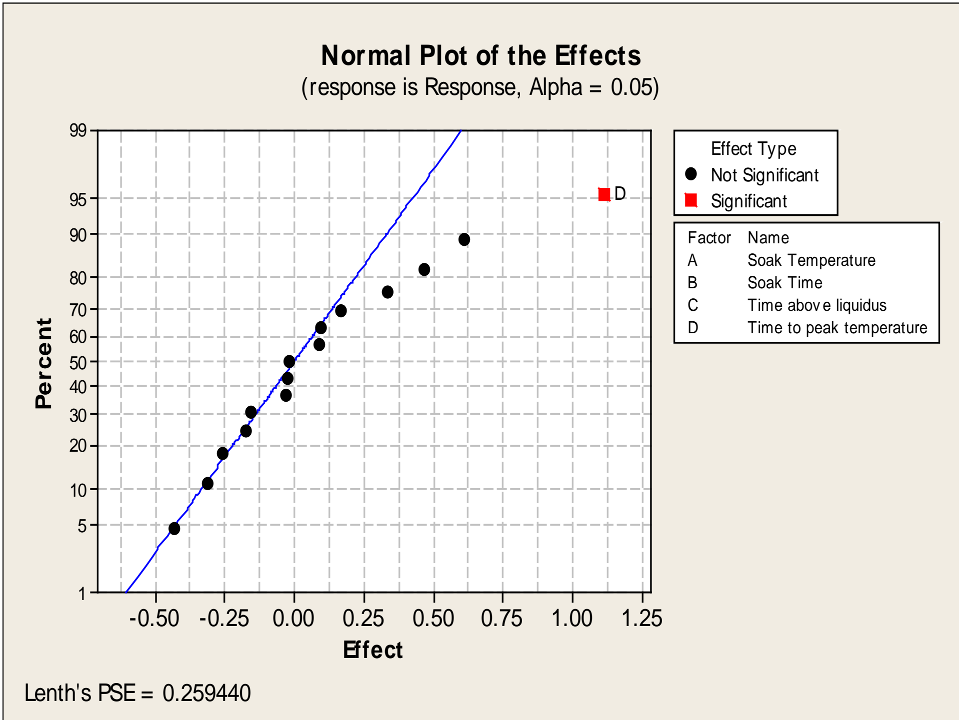

Figure7.2b Normal probability plots of factor effects of (∅3.7mm)

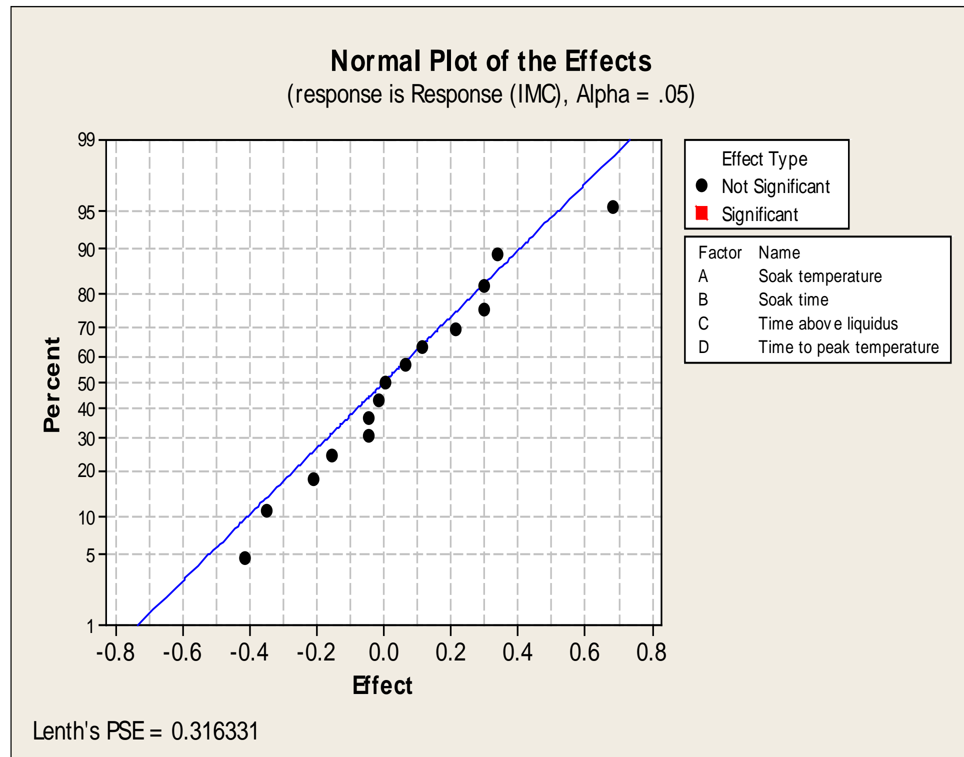

Figure 7.2c Normal probability plots of factor effects of (∅4.3mm)

7.3.2 Pareto Plot Analysis

The Pareto plots represented in figure 7.3a, 7.3b and 7.3c were constructed to compare the relative magnitude and significance of both main and interaction effects. The plot displays the absolute values of the effects and draws a reference line on the chart as shown in figure 7.3a and 7.3b respectively. Any effect that ends beyond this reference line is considered to be potentially important. The Pareto plots of figures 7.3a and 7.3b (for ∅3.1mm and ∅3.7mm solder bumps) indicate that time to peak temperature is the most important factor. The pareto plot for ∅4.3mm solder bump Figure 7.3c showed no significant factor, that is to say, no factor effect crossed the reference line in Figure 7.2c.

However, the time to peak temperature has shown the higher effect than any other factor. According to figure 7.2a, the second and the third influential factors were 'B: soak time' and C: Time above liquidus'. The factor A: Soak temperature failed to show any significant effect. Similarly, the effect of the interactions

between the factors was found to be non-significant. The insignificant interaction effects mean that the interactions do not have much influence on the reflow process and hence can be avoided in any future design of experiments

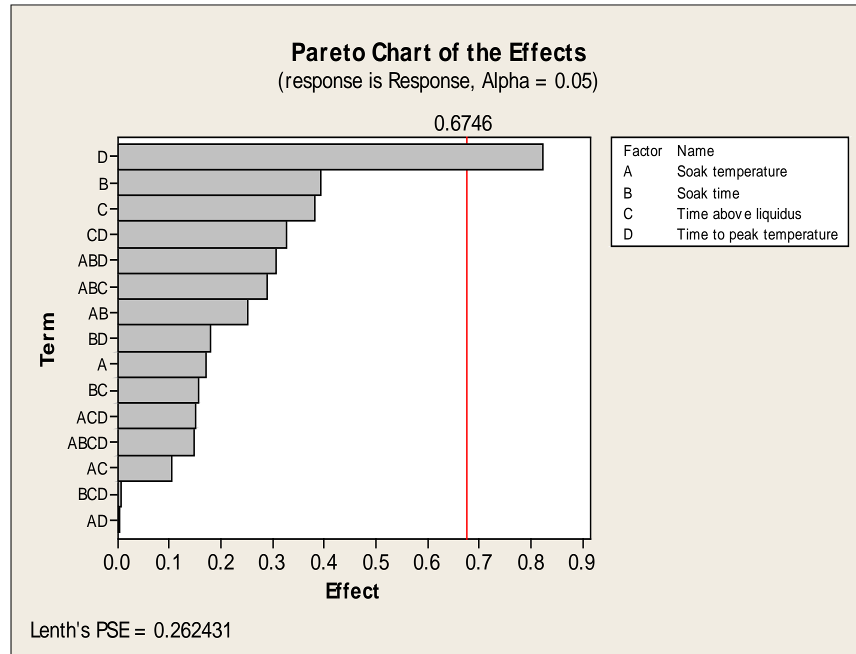

Figure 7.3a Pareto chart of effects of (∅3.1mm)

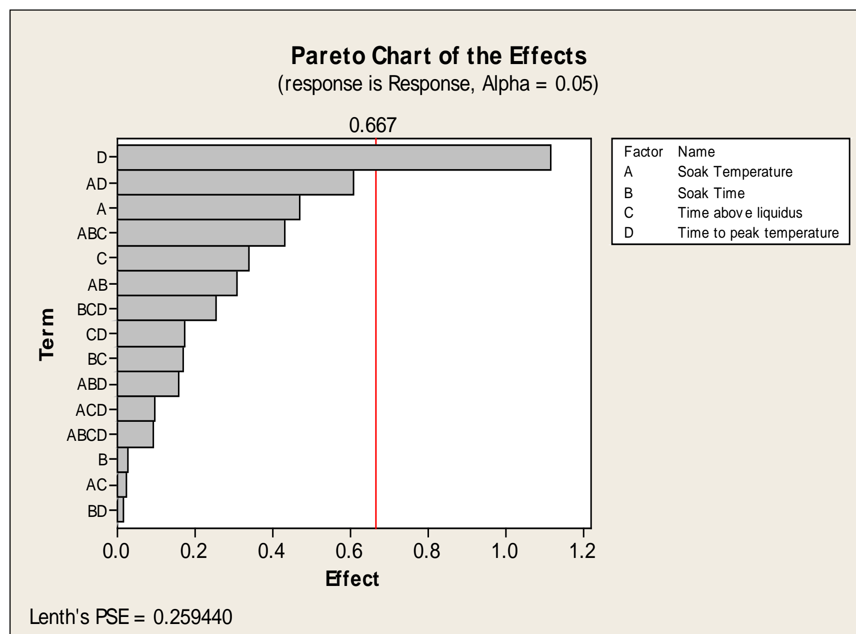

Figure 7.3b Pareto chart of effects of (∅3.7mm)

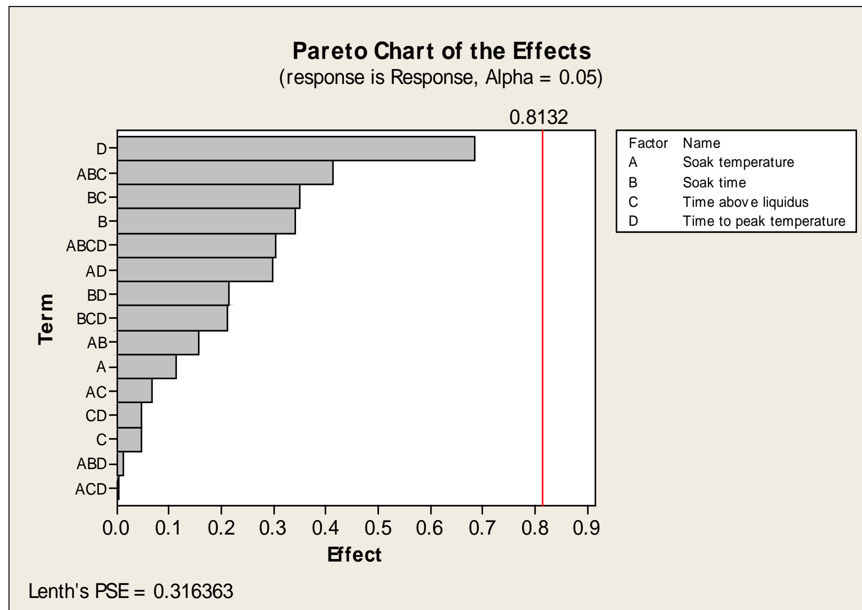

Figure 7.3c Pareto chart of effects of (∅4.3mm)

7.3.3 Optimiser Plot

The optimum operating conditions for achieving desirable reflow soldering were obtained using the response optimiser plot module available in the statistical software, Minitab. The results are presented in figures 7.4a – 7.4c

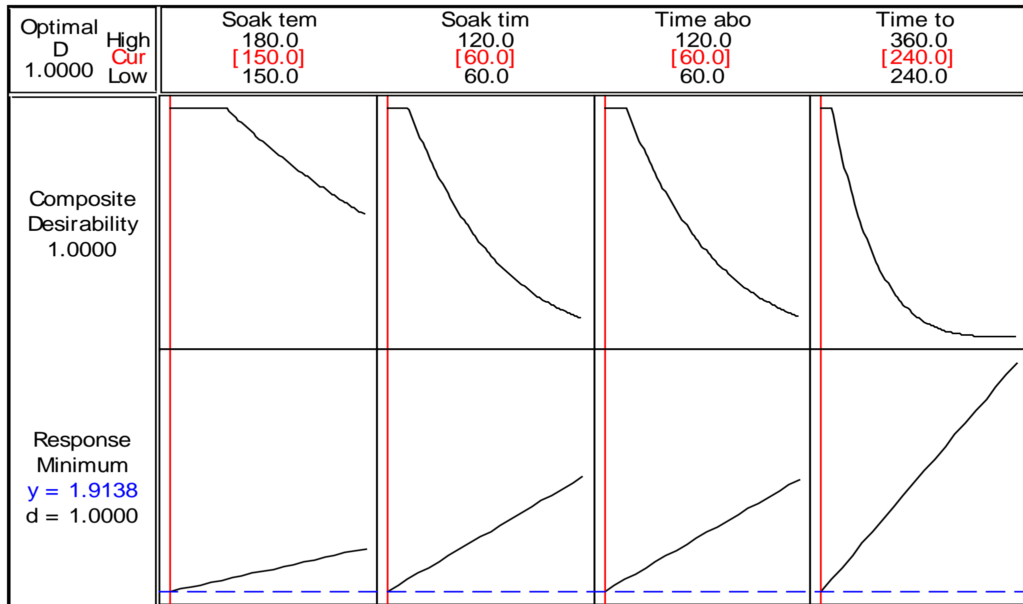

Figure 7.4a Response optimiser plot for (∅ 3.1mm) solder bump

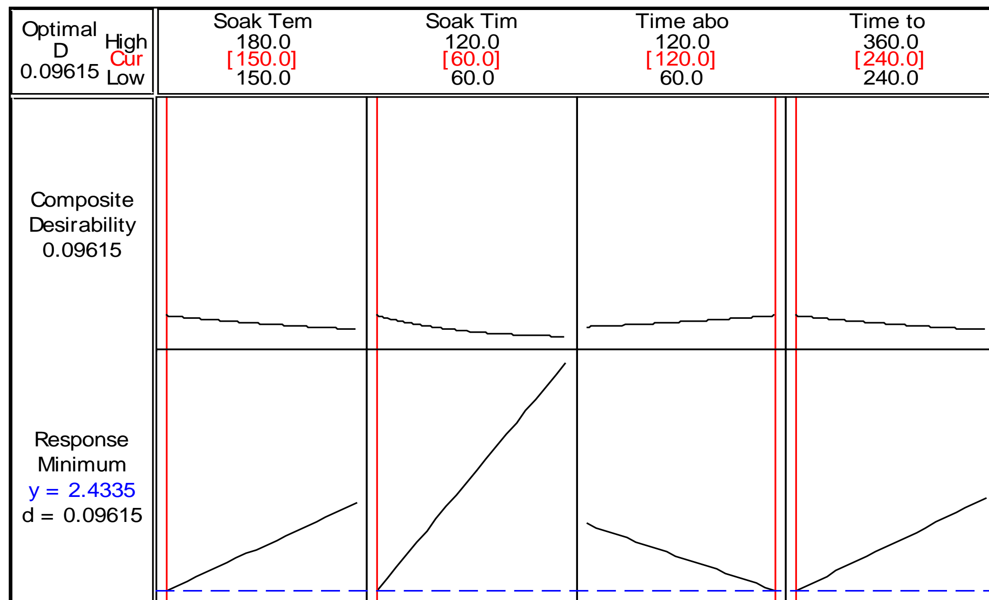

Figure 7.4b Response optimiser plot for (∅ 3.7mm) solder bump

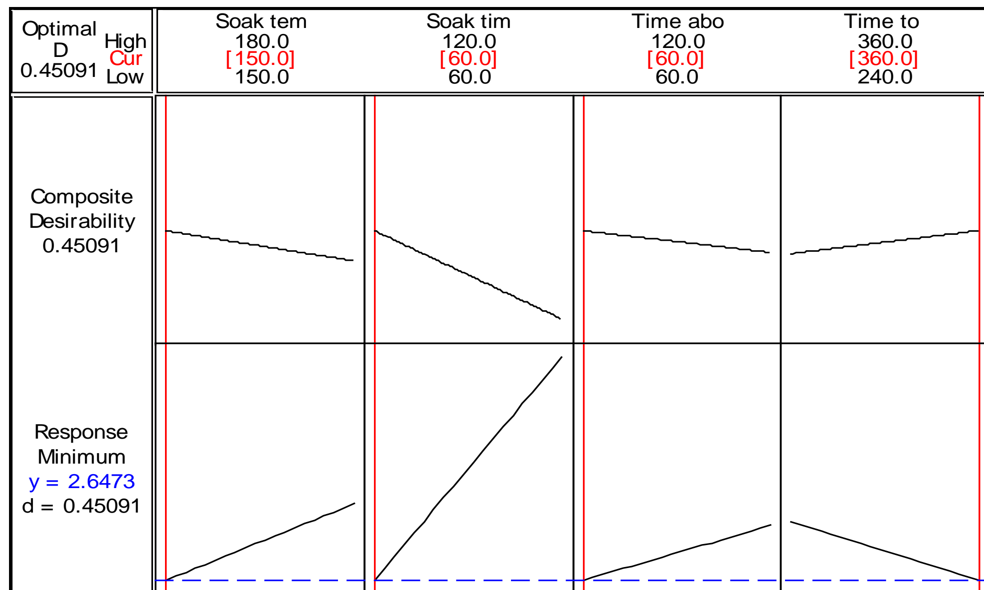

Figure 7.4c Response optimiser plot for (∅ 4.3mm) solder bump

7.3.4 Minitab optimiser parameters reflowed profiles

The Minitab optimiser parameters of the three solder dimensions ∅3.1mm, ∅3.7mm and ∅4.3mm were employed for the reflow profiles represented in figure 7.5a, 7.5b and 7.5c. It was observed that as the solder diameter increased from 3.1 to 3.7mm, the ramp up rate remain unchanged. However, the ramp up rate of ∅4.3mm optimal reflow profile was 2.3°C/sec. This implies that the removal of the flux volatile was slow because of the size of the solder deposit. The three optimal reflow profiles experienced the same peak temperature and cooling rate. But the time to peak temperature of ∅4.3mm solder deposit was the highest as compared to ∅ 3.1mm and ∅3.7mm which resulted to increase in IMC layer thickness.

Table 7.5 Minimum values of Minitab optimiser settings

Solder deposit (∅ mm)	Minimum IMC values in (µm)
(∅ 3.1mm)	1.913
(∅ 3.7mm)	2.433
(∅4. 3mm)	2.647

Table 7.6 Comparison of Minitab optimiser and recommended IPC IMC responses

Solder deposit (∅mm)	IPC Recommended IMC values in (µm)	Optimum profile IMC values in (µm)	% Improvement $\frac{(\mathrm{Re}\,commeded - Optimum)}{\mathrm{Re}\,commended} x100$
3.1	2.389	1.913	24
3.7	2.614	2.433	18
4.3	3.039	2.647	39

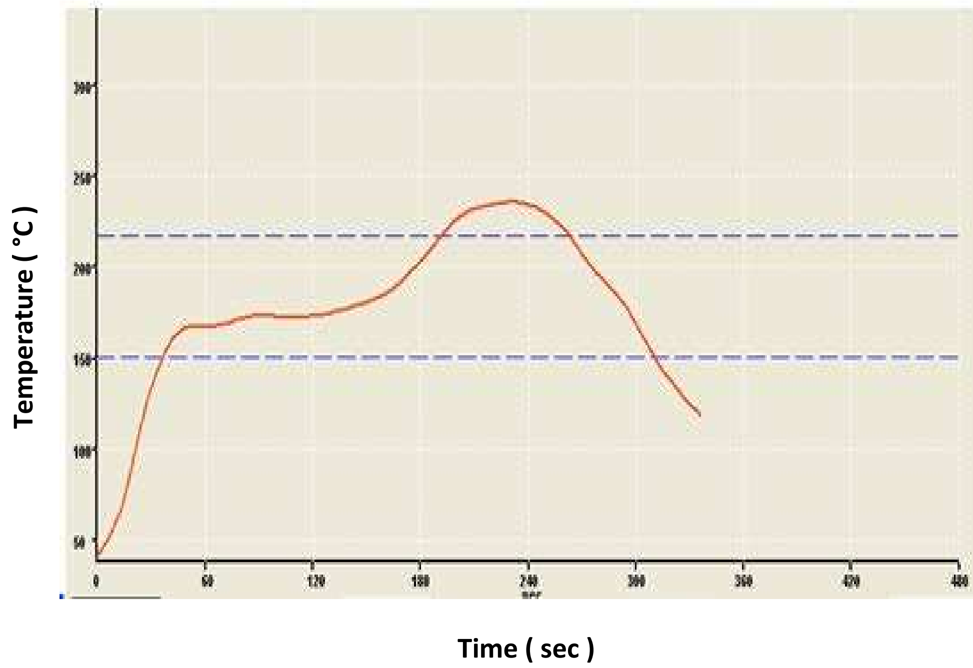

Figure 7.5a Optimal reflow for (∅ 3.1mm) solder bump

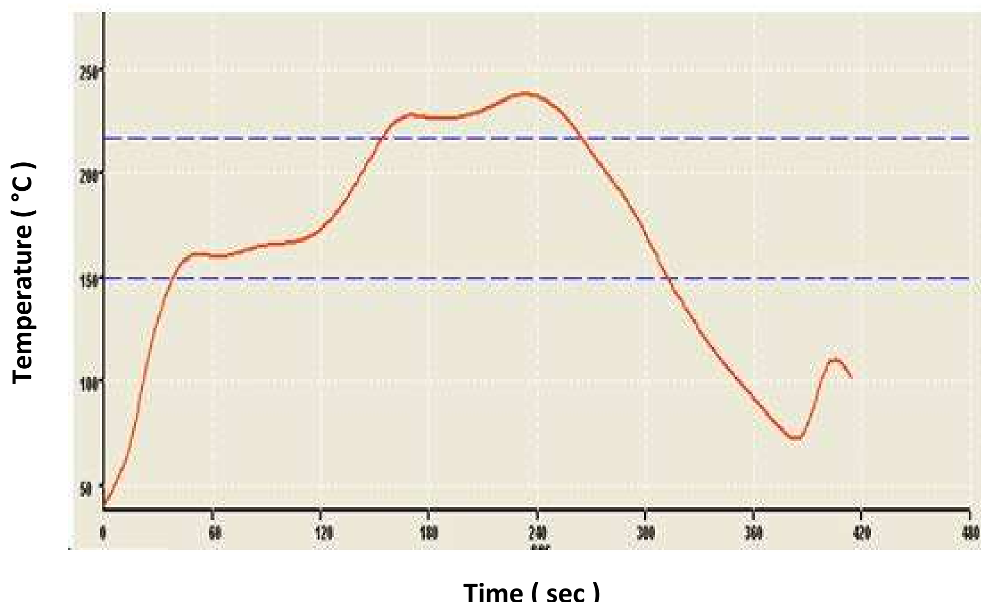

Figure 7.5b Optimal reflow for (∅ 3.7mm) solder bump

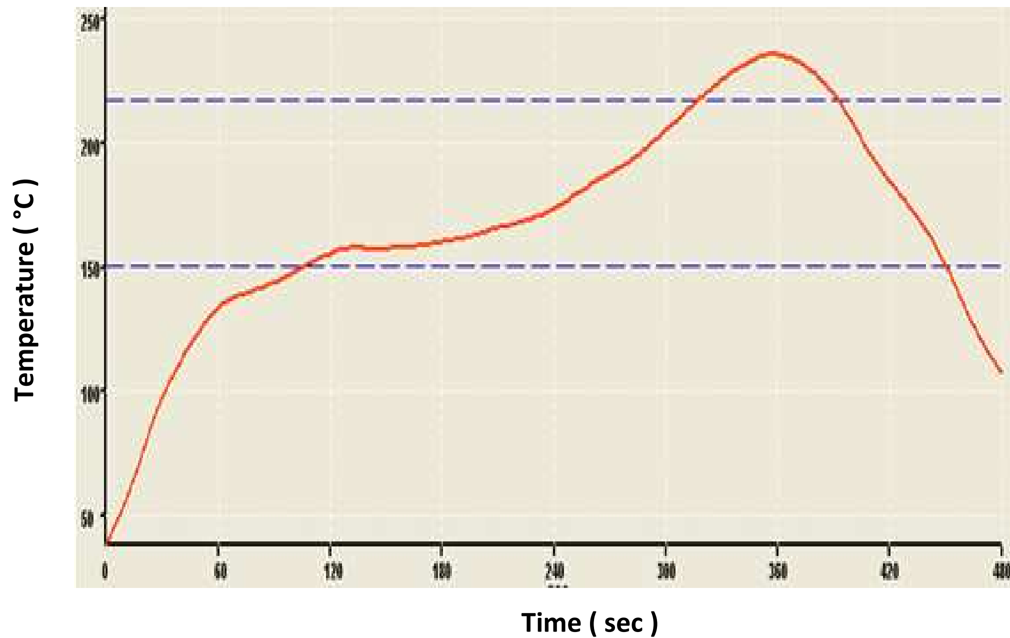

Figure 7.5c Optimal reflow for (∅4.3mm) solder bump

7.3.5 Analysis of variance in the reflow soldering parameters

In order to test for the significance of a factor or an effect, the analysis of variance (ANOVA) was used. Analysis of variance of 2^4 factorial design of the experiment identifies the amount of experimental error and variability in the experiment. (Mira et al, 2006; Wu, 2002; Dahle and Lasky, 2004). The analysis of variance presented in table 7.7, 7.8 and 7.9 summarize the effects estimates and sum of square of the process parameters. The column labelled percentage contribution measures the percentage contribution of each model term.

Table 7.7 Analysis of variance for (∅ 3.1mm)

Source	DF	Seq SS	Adj SS	Adj MS	(%C)
Main Effects	4	4.02769	4.02769	1.00692	68
2-Way Interactions	6	0.95038	0.95038	0.1584	16.19
3-Way Interactions	4	0.80144	0.80144	0.20036	13.65
4-Way Interactions	1	0.08784	0.08784	0.08784	1.49
Residual Error	0				
Total	15	5.86735			

Let DF = Degree of freedom, Seq SS = Sequential sum of square, Adj SS = Adjusted Sum of square, Adj MS = Adjusted mean square and Percentage contribution = (% C)

Table 7.8 Analysis of variance for (∅ 3.7mm)

Source	DF	Seq SS	Adj SS	Adj MS	(% C)
Main Effects	4	6.33922	6.33922	1.58480	65.87
2-Way Interactions	6	2.11459	2.11459	0.35243	21.97
3-Way Interactions	4	1.13563	1.13563	0.28391	11.8
4-Way Interactions	1	0.03431	0.03431	0.03431	0.35
Residual Error	0				
Total	15	9.62374			

Table 7.9 Analysis of variance for (∅4. 3mm)

Source	DF	Seq SS	Adj SS	Adj MS	(%C)
Main Effects	4	2.3998	2.3998	0.6000	50.17
2-Way Interactions	6	1.1534	1.1534	0.1922	24.11
3-Way Interactions	4	0.8643	0.8643	0.2161	18.07
4-Way Interactions	1	0.3652	0.3652	0.3652	7.63
Residual Error	0				
Total	15	4.7827			

7.4 Discussion of Results

The normal probability plot of the effects for ∅3.1mm solder bump reflow soldering process is shown in figure 7.2a. From examination of figure 7.2a, it is evident that time to peak temperature emerged as a significant factor. Similar effect occurred in figure 7.2b; perhaps due to the small difference in solder volume. In figure 7.2c, there was no significant effect on the process, this might due to the size of the solder volume. However time to peak temperature was influential. So, in general, the time to peak temperature was found to be the most significant factor in determining the thickness of intermetallic compound layer irrespective of the bump sizes. In the study, it was expected that time above liquidus and peak temperature would affect intermetallic growth (Harris and Chaggar, 1998**)**. The work reported by Roubaud and Henshall (2001) showed that higher lead-free solder reflow temperature (250°C) did not lead to a significantly higher thickness of IMC layer between the bulk solder and the copper substrate in lead-free assemblies. In view of this finding, the peak temperature of the reflow soldering process for the three different solder volumes was maintained constant.

The results of combination of factors for achieving the desired responses for solder bump Φ3.1mm include; minimizing the Soak time, Soak temperature, Time above liquidus and time to peak temperature. The optimum parameters settings so obtained for achieving optimum reflow soldering for solder bump Φ3.1mm include; Soak temperature of 150ºC, Soak time of 60 seconds, Time above liquidus of 60 seconds, Time to peak temperature of 240 seconds. Also, in figure 7.4a, the optimizer predicted IMC layer thickness of 1.9138µm.The optimum operating conditions for achieving reflow profile settings for ∅3.7mm solder bump is similar to ∅3.1mm solder bump. The only difference is time above liquidus which changed from low to high duration. The difference in Time above liquidus values could be the increase in solder volume. The optimizer predicted IMC layer thickness was 2.433µm as shown in figure 7.4b. The optimum reflow profile setting for ∅4.3mm solder bump include; Soak temperature of 150ºC, Soak time of 60 seconds, Time above liquidus of 60 seconds, Time to peak temperature of 360 seconds. The Minitab optimizer plot figure 7.4c predicted IMC layer thickness of 2.647µm. The time to peak temperature was high at 360 seconds. This is due to the size of solder deposit which undergoes a long melting period before experiencing the peak temperature.

The results obtained from the ANOVA model for ∅3.1mm solder bump as shown in Table 7.5 revealed that main effects really dominate the process, accounting for over 68 percent of the total variability, whereas the 2-way, 3-way and 4-way interactions account for about 16, 1 and 1.49 percent, respectively. The zero percentage residual error is an indication that the experimental set up produced a good replication. Table 7.6 provides estimated effects of the process variables in solder bumps ∅3.7mm. The primary effects contributed to 65% in terms of variability, while 2-way, 3-way, and 4-way interactions contributed to 21.97%, 11.85%, and 0.35% variability respectively. The percentage variability of primary effects of ∅4.3mm was 50.17%, 2-way interactions contributed to 24.11%, while 3-ways interactions was 11.8% and finally, the 4-way interactions contributed 0.35%.

7.5 Summary

The study of the effect of reflow soldering profile parameters on Sn-Ag-Cu solder bumps using Cu substrate has been presented in this chapter. Conclusions drawn from the study are as follows:

1. The results from ANOVA showed that reflow soldering parameters influencing IMC layer thickness are soak temperature, soak time, time above liquidus and time-to-peak-temperature because any variation in magnitude of the soldering parameters affect the IMC layer thickness.

2. The results from the Pareto chart showed that the most significant factor in achieving lower IMC layer thickness is time to peak temperature in reflow soldering process.

3. The results from the optimiser plot response showed that optimum values of the reflow parameters depend on the solder volume. It was also clear that the IMC layer thickness increases as a result of increase in time-to-peak temperature. The time-to-peak temperature affected the growth of IMC layer thickness because the growth of IMC is a function of time and temperature.

CHAPTER VIII: EFFECT OF IMC LAYER THICKNESS ON THE SHEAR STRENGTH OF 1206 CHIP RESISTOR SOLDER JOINTS

8.1 Introduction

This chapter presents the results of the study on the effect of IMC layer thickness on the shear strength of 1206 chip resistor solder joints. The shear strength and the IMC layer thickness during reflow and isothermally aged is investigated. The fracture surfaces of the reflowed and aged solder joints were also investigated.

8.1.2 Reliability of solder joints

The National Electronics Manufacturing Initiative (NEMI) road map shows that solder joints are likely to be used in more vibrant service environments where the stress and strain distributions change with time (Abtew and Selvaduray, 2000; Kim and Tu, 2002). Generally, the solder joints in the Printed Circuit Boards (PCBs) should be made in such a manner that their reliability can withstand complex service conditions. One of the major concerns for the integrity of the solder interconnection is its mechanical properties (Zeng and Tu, 2002).

Obtaining stronger solder joints to meet the heightened requirements, both physical and mechanical properties, for electronics packages and assembly is a priority for the electronics manufacturing industry. In this respect, the Inter-Metallic Compound (IMC) layer thickness is one of the major issues of solder joint reliability (Chan and Yang, 2010).

The formation of an IMC layer signifies good bonding between the solder and substrate, its main disadvantage is that it is also known to be the most brittle part of the solder joint (So and Chan, 1996). These concerns have prompted considerable attention in this area of study.

8.1.3 Effect of reflow and isothermal ageing on solder joint shear strength

Yao et al (2008) asserted that the shear strength of Ni/Au electroplated Cu pads during a number of reflows increased with an increase in Ni content and all joints presented ductile fracture. In a related investigation on interfacial microstructure, it was found that in all composite joints (more than one joints at a point) tested, the shear strengths were approximately equal to non-composite joints (individual joints at different points) and fracturing observed during shear testing of composite joints occurred in the bulk solder, indicating that the SAC–xNi/Ni solder joints had a desirable joint reliability.

In a separate investigation, Ching-Tsung et al, (2008) observed that two different lead-free solders (Sn-8Zn-3Bi and Sn-9Zn-1Al) produced different solder joint strength with Cu pad (4.0±0.3 kg and 2.6±0.1 kg respectively). They both however, exhibited reduced strengths with increasing aging times. For instance, after subjecting the two to ageing at 150 ◦C for 1100 h, the results indicated that the joints' strengths of Sn-8Zn-3Bi and Sn–9Zn–1Al were 1.8±0.3 and 1.7±0.3 kg, respectively with both showing brittle fractures.

Zhao, et al (2009) used three lead-free solder alloys, Sn–3Ag–0.5Cu, Sn–3Ag–0.5Cu–1Bi and Sn–3Ag–0.5Cu–3Bi, each made on a Cu substrate. The experimental results indicate that the addition of Bi delays the propagation rate of IMC layer formation. For the samples aged at 140◦C up to 500h, their shear strength remained at a relatively stable level where the fracture occurs on bulk solder side and the addition of Bi improved the strength level. On the other hand, for the samples aged at 195 ◦C, the shear strengths decreased continuously with aging time, the fracture occurs along the interface between IMC layers and solders.

Surface tension and contact angle of In–31.6Bi–19.6Sn lead-free solder with melting temperature of 61.33°C on a copper substrate and at different reflow temperatures were measured by (Noor et al 2010). It was observed that an increase in reflow temperature improved the shear strength of the In–31.6Bi–19.6Sn/Cu solder joint due to reduced contact angle and larger spreading area. Furthermore, it has also been reported that the strength of the solder joint

decreases with an increasing thickness of IMCs formed at the interface, it is therefore believed that IMC is a potential site for microcracks (Prasah and Sritharan, 2004; Lee and Chen, 2002; Quan et al, 1987; Bang et al 2008).

The shear strength was found to depend on the growth of IMCs and the crack locations of IMCs (Lin and Hsu, 2000). In a study, Bukhari, et al. (2005) evaluated the effects of assembly process parameters and thermal aging. Their results indicate that the effects of thermal aging on solder joint shear strength are much larger than the effects of assembly process variables. In a related study, Oliver, et al. (Oliver et al 2000) investigated the effect of thermal aging on the shear strength of lead-free solder joints and concluded that the shear strength decreases as the aging time increases for a thermally aged Pb-free solder joints

8.1.4 Effect of ageing temperatures on Cu-Sn intermetallic compound

Ageing temperatures have an effect on the interfacial Cu-Sn IMC layer. The growth rate of IMC constituents depends on the interfacial kinetics. Isothermal ageing tests at 70, 120, 155 and 170°C on the interfacial Cu-Sn IMC layer were conducted (Chan et al, 1998). It was reported that the shear fracture in all the solder joints were ductile and largely confined in the bulk solder rather than through the interfacial IMC layer.

However, a linear reduction in joint shear strength was observed with an increase in intermetallic layer thickness up to 5.6µm. Such a reduction in joint strength is due to a continuous removal of Sn from the bulk solder for the growth of interfacial IMC layer and flattening of the solder IMC layer during isothermal aging of the solder joint.

Nano-sized, non-reacting, and non-coarsening $SrTiO_3$ particles have been incorporated into Sn–3.0 wt%Ag–0.5 wt% Cu solder alloys and the interfacial microstructure and the shear strength on Au/Ni metallized Cu pads ball grid array substrates was investigated as a function of the number of reflow cycles and aging time (Fouzder et al, 2011).

The results revealed that the shear strength of solder joints containing $SrTiO_3$ nano-particles exhibited a consistently higher value than those of plain Sn–Ag–Cu solder joints. This was attributed to a second phase dispersion strengthening mechanism and refinement of the IMC. Moreover, the fracture surface of plain Sn–Ag–Cu solder joints was found to exhibit a brittle fracture with a smooth surface while Sn–Ag–Cu solder joints containing $SrTiO_3$ nano-particles showed ductile failure characteristics with rough dimpled surfaces.

8.2 Experimental Details

To evaluate the effect of IMC layer thicknesses on the shear strength of Sn-Ag-Cu solder joints, several test vehicles were constructed. The details of experimental procedure and equipment used is presented in section 4.2.4 in chapter 4, figures (4.4. 4.5 and 4.9) and sections (4.3.1, 4.3.2, 4.4 and 4.5)

8.3 Results

Shown in figure 8.3 and 8.4 are SEM micrographs of the interface between Sn-3.8Ag-0.7Cu solder and 1206 chip resistor on FR-4 PCB with Cu surface finish substrate aged at 175°C for different aging times. Back-scattered electron images of SEM were used to provide clear boundaries of the interfacial layers.

8.3.1 IMC during reflow process

During the reflow process, the Ni surface of the component is exposed to the molten solder. The reaction between the molten solder and Ni layer formed $\{CuNi\}_6Sn_5$ layer at the interface as shown in figure 8.3a. The Cu in the a $(CuNi)_6Sn_5$ layer came from the solder inside because there is no Cu source except the solder. However, the reaction of Cu and Sn in Sn-3.8Ag-0.7Cu determines the formation of $(CuNi)_6Sn_5$ layer(Zhang et al, 2002). The mean thickness of the $(CuNi)_6Sn_5$ layer was approximately 2.6μm.

Again, the interfacial reaction between the substrate (PCB) and the solder during reflow is represented in Figure 8.4a. The formation of a Cu-Sn intermetallic layer in a solder joint during the reflow process arises by interfacial reactions between its constituting species, Sn from the solder and Cu from the copper pad. It was clear from figures 8.3 and 8.4 that the difference of intermetallics measured at component and substrate sides after reflow increased by fifty percent (50%). This might be due to faster reaction between Sn and Cu in both the solder and substrate. Also as expected, the shape of the intermetallic layers at both the component and the substrate sides were scalloped. From figures 8.3a and 8.4a, the intermetallic layer thickness is a function of the reflow time. The interfacial reaction observed in the reflowed samples was similar to previous experiment conducted by (Zeng et al 2001; Li et al 2001). In their work, it was reported that with the presence of Cu in the SnAgCu solder, the formation of Ni_3Sn_4 is suppressed. Instead, the Cu_6Sn_5 forms with some solution of Ni to form $(Cu,Ni)_6Sn_5$.

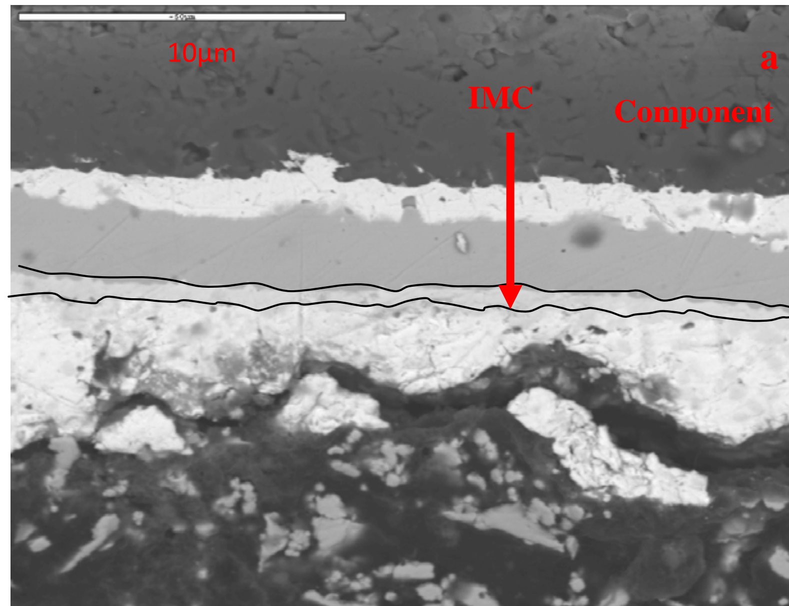

Figure 8.3a SEM micrographs of the Sn-3.8Ag-0.7Cu solder/1206 joints as-soldered

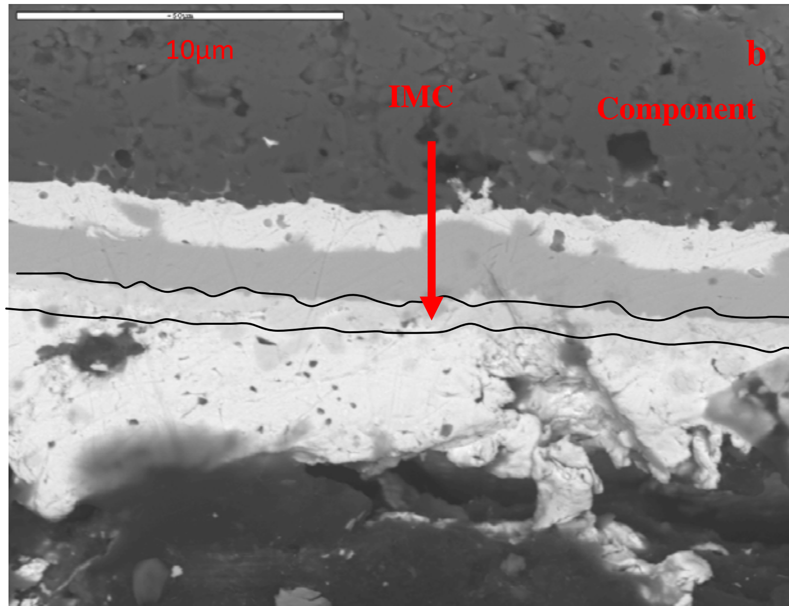

Figure 8.3b SEM micrographs of the Sn-3.8Ag-0.7Cu solder/1206 joints aged at 175 ◦C for 100 hours isothermal ageing

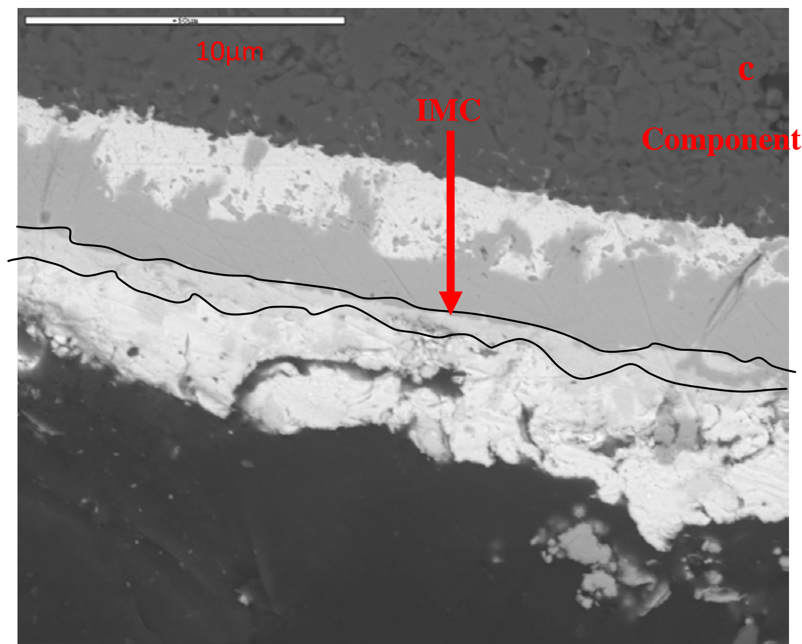

Figure 8.3c SEM micrographs of the Sn-3.8Ag-0.7Cu solder/1206 joints aged at 175 ◦C for 200 hours isothermal ageing

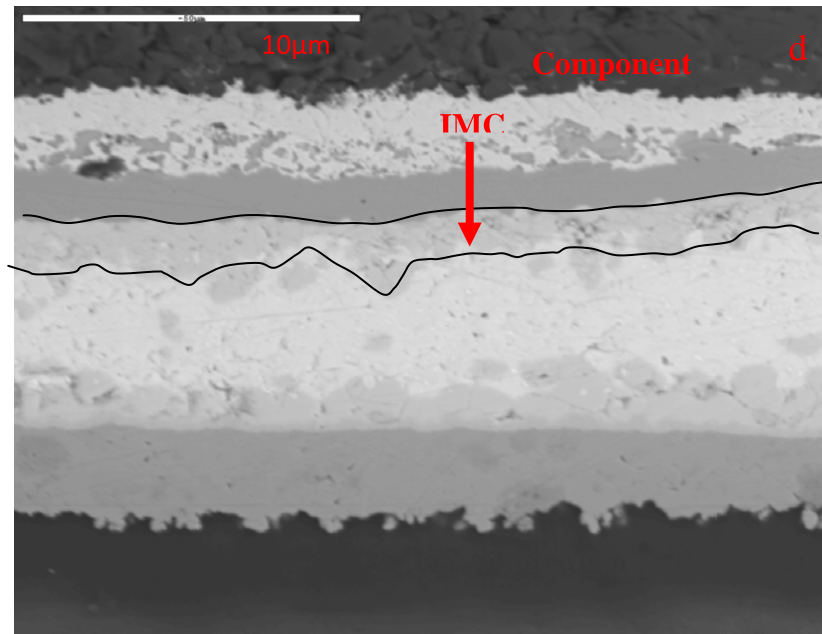

Figure 8.3d SEM micrographs of the Sn-3.8Ag-0.7Cu solder/1206 joints aged at 175 ◦C for 300 hours isothermal ageing

8.3.2 Interfacial reaction between component surface finish and solder deposit during Isothermal ageing.

After isothermal aging at 175°C for 100hours, 200hours and 300 hours the reaction between solder/Ni interface at the component side exhibited SnNiCu intermetallic compound. With an increase in ageing time to two hundred hours (200hrs), IMC layer thickness increased by 20%, as represented in figure (8.3c). In Figure 8.3d, it can be seen that the intermetallic layer grew slightly thicker during the 300 hours of isothermal ageing. The intermetallic compound layer thickness was 7.8µm. The shape of the layer was irregular and uneven scallop.

Also, it was observed that the intermetallic compound atomic percent (at%) composition due to reaction between solder and nickel were similar irrespective of the different ageing times. This observation is similar to work conducted by (Jeon et al, 2003). According to their results, using Sn–0.7Cu solder bump, only $(Cu,Ni)_6Sn_5$ IMC was observed at 175°C for 500 hours. Duplex IMC layers of $(Cu,Ni)_6Sn_5$ and $(Ni,Cu)_3Sn_4$ were observed at 200°C.

8.3.3. Interfacial reaction between substrate and solder deposit

The interfacial reaction between the substrate and the solder formed duplex structures of Cu_5Sn_6 (IMCI) and Cu_2Sn (IMC II) were exhibited as represented in figure 8.4 (b – d). Choi and Lee (2000) in their work observed similar results and stated that the Cu_3Sn (ε-phase) and Cu_6Sn_5 (η-phase) form by the reactions between the Cu substrate and solder deposit.

When the samples were aged continuously at 175°C for a hundred hours (100hrs), it was revealed that IMC layer grew by 9.4% after the reflow soldering process and the IMC morphology changed from scallop-like to planar-like. After 200 hours of ageing, the morphology of the IMC did not change significantly but the thickness of IMC was found to increase by 12.5%.The IMC layer thickness increased by 19.89% after 300 hours of isothermal ageing with more planar-like morphology.

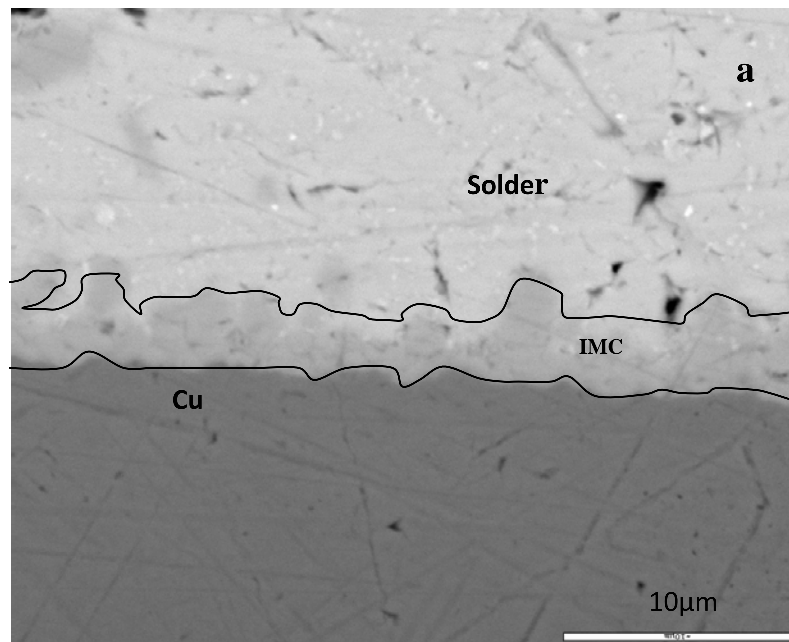

Figure 8.4a SEM micrographs of the Sn-3.8Ag-0.7Cu solder deposit and substrate aged at 175°C as-reflowed

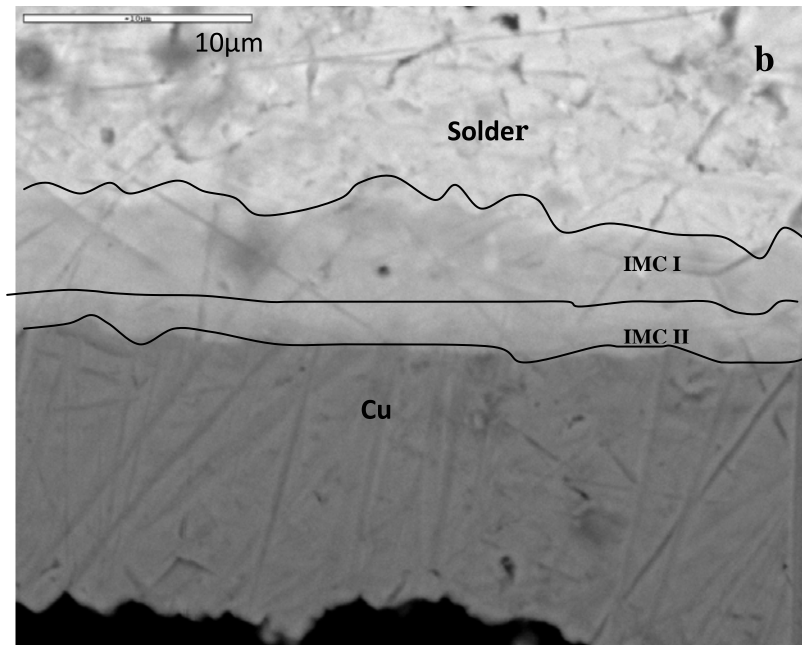

Figure 8.4b SEM micrographs of the Sn-3.8Ag-0.7Cu solder deposit and substrate aged at 175°C for 100 hours

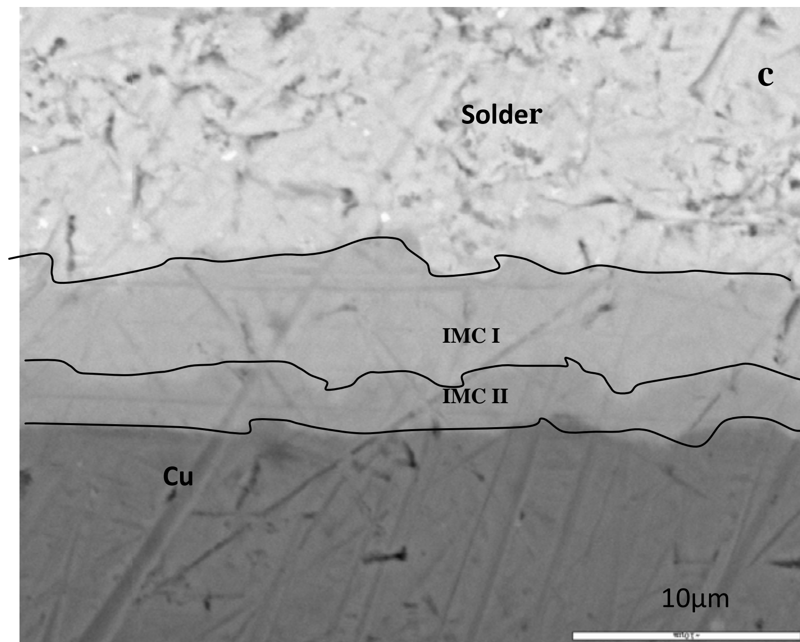

Figure 8.4c SEM micrographs of the Sn-3.8Ag-0.7Cu solder deposit and substrate joints aged at 175°C for 100 hours

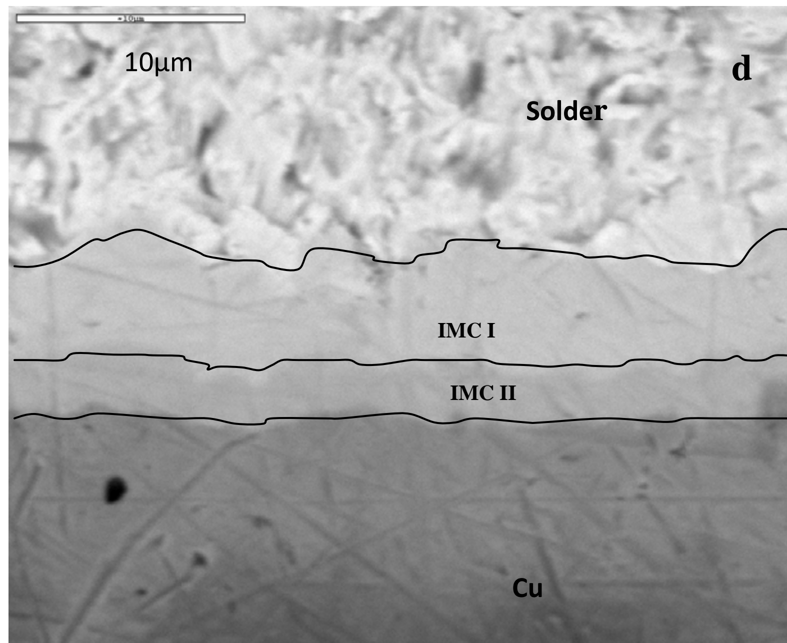

Figure 8.4d SEM micrographs of the Sn-3.8Ag-0.7Cu solder deposit and substate aged at 175°C for 300 hours

Table8.1 IMC layer thickness during reflow and isothermal ageing.

Duration (Hrs)	Component side IMC (µm)	PCB side IMC (µm)	
		L1	L2
0	2.6	5.2	0
100	4.2	6.28	1.14
200	6.3	8.05	1.4
300	7.8	9.4	2.35

Note: L1= IMC1 Average values; L2 = IMC II average values

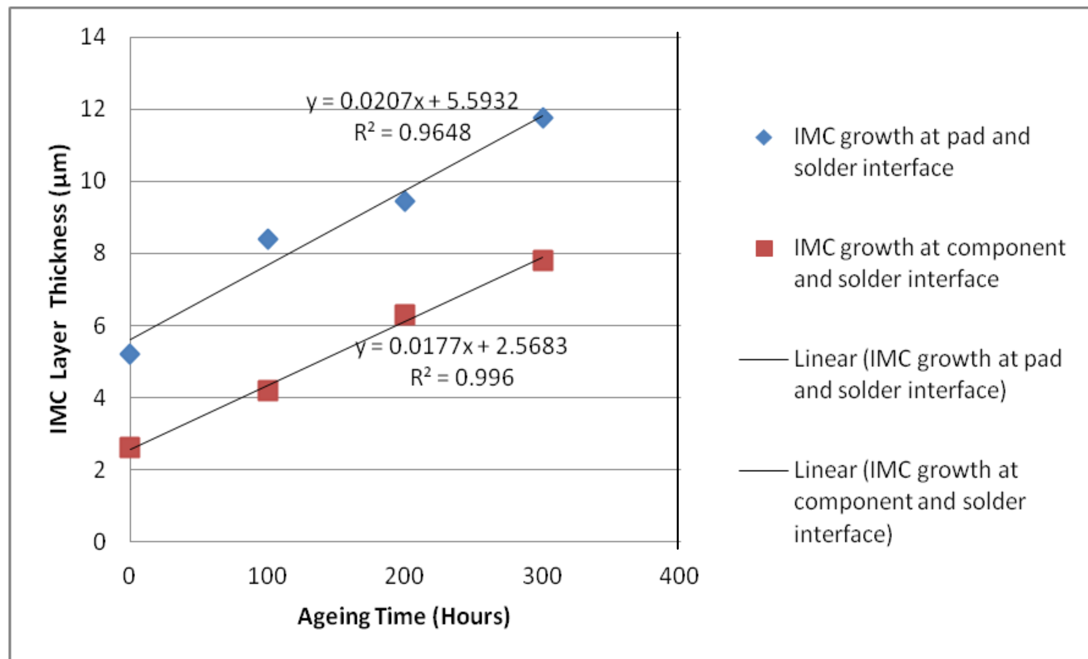

Figure 8.5 IMC thicknesses as a function of ageing time during solid-state interfacial reactions of Sn-Ag-Cu solder with substrate Cu surface finish and component termination of Ni surface finish.

8.3.4 Evaluation of voids percentage in solder deposit

Voids in lead-free solder joints have been a concern to electronic manufacturers. Their prevention in lead-free solder pastes, especially tin-silver-copper has attracted intensive research. Excessive solder voids can create a reliability issue especially in applications where the lead-free assembly will be exposed to isothermal ageing and thermal cycling conditions or in applications where the assembly will be exposed to vibration. Also voids can reduce thermal performance and reduce electrical integrity. Moreover, small voids can in some cases increase reliability by arresting the growth of cracks in a joint. Studies have shown that there is no reduction in reliability when voids are present to up to 25% by volume in the joint [(Wickham, 2007). In this study, the solder deposits subjected to different ageing times were examined for voiding as represented in figures 6 (a – d). The demarcated areas were used for this investigation.

The percentage of voids measured in the reflowed solder deposits was 16.89% volume. This void's percentage is due to volatile components of the paste vaporising and being unable to escape to the surface of the molten metal before solidification occurs (Mackay, 1987). There was a reduction of 1.01% in voids when the solder deposit was isothermally aged at hundred hours (100hrs). This might be attributed to the suppressed reaction of Cu_2Sn formation; the growth of the voids in the solder deposit is also depressed and therefore the size of the voids does not increase with ageing time. Similar phenomena also occurred in both two hundred (200) and three hundred (300) hours ageing with 0.7 and 1.2% percentage reduction in voids respectively.

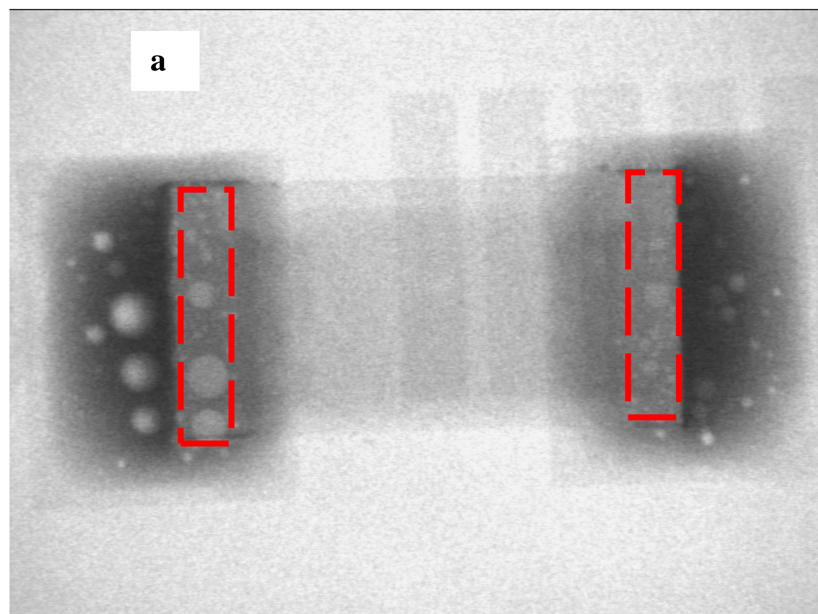

Figure 8.6a X–Ray, Voids in solder deposits as reflowed

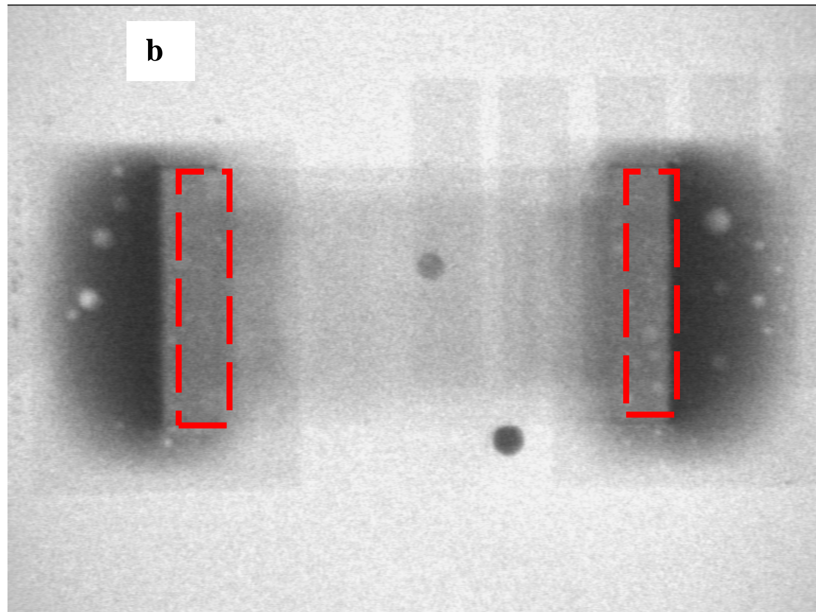

Figure 8.6b X–Ray, Voids in solder deposits after 100 hours isothermal ageing

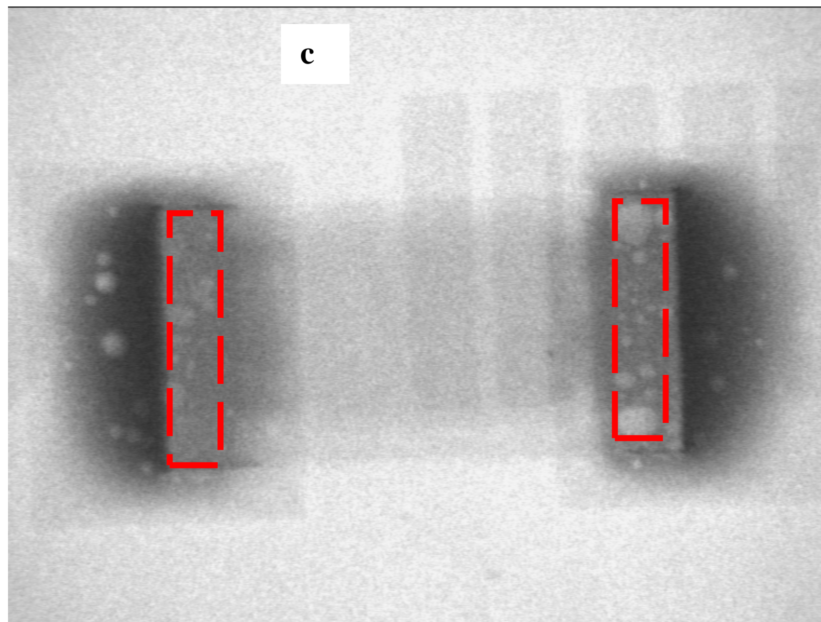

Figure 8.6c X–Ray, Voids in solder deposits after 200 hours isothermal ageing

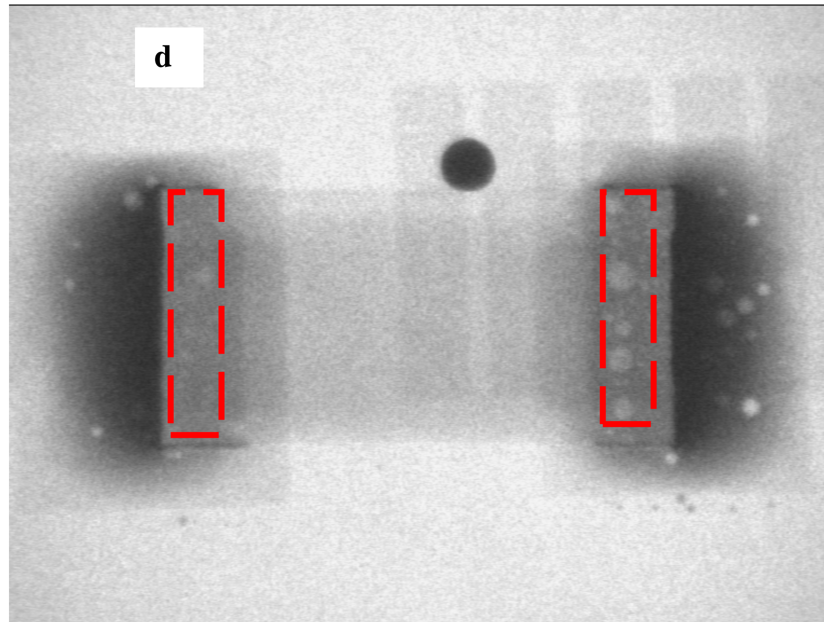

Figure 8.6d X–Ray, Voids in solder deposits after 300 hours isothermal ageing

A comparison between voids percentage in the reflowed and 100 hours aged solder joints showed that the void density in the 100 hours aged solder joint is noticeably less by 1.78% than that of the reflowed solder joint. This reduction might be attributed to percentage of nickel in the solder joint with respect to temperature and time. Mei et al (2005) in their work reported that the condition for the void formation is not certain; the density of the voids at the Cu/solder interface cannot be predicted by only the aging temperature and time; the presence of Ni in either Cu substrate or solder joint might reduce the void density. However, the percentage of voids in the solder joint after 200 hours was 15.58%. The continuous trend of reduction in void percentage could be subjected to greater percentage of Ni atoms migrating from the component side to the substrate as ageing time increases, since Ni atoms suppress the formation and growth of voids. Furthermore, after 300 hours of isothermal ageing, the measured void percentage was 12.68%. Comparatively, the ratio of reduction in void percentage is; 1.4: 1.3: 1.2: 1. The difference in void percentage ratio is 0.1, this is an indication that increases in ageing time and temperature does not have much influence on formation and growth as represented in figure 8.7

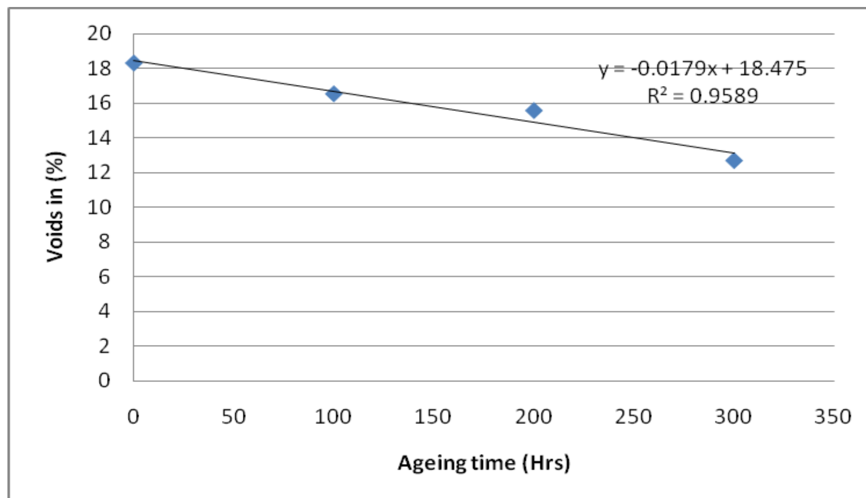

Figure 8.7 Evaluation of voids in solder joint after reflowed and ageing times.

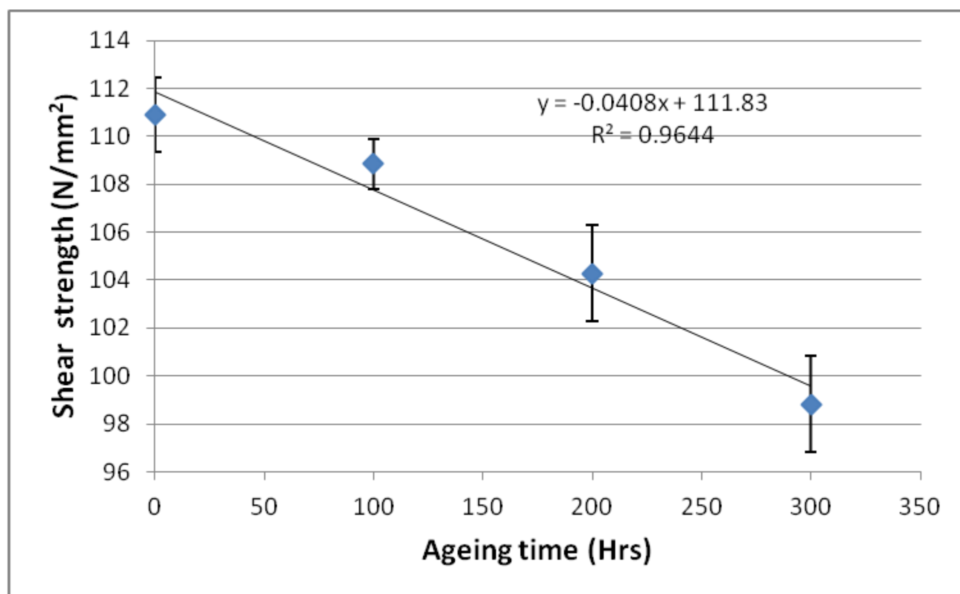

Figure 8.8 Average shear strength of samples reflowed, 100hrs, 200hrs and 300hrs ageing**.**

8.3.5 Fracture surface of FR-4 PCB pad and component termination finish of the solder joints

After measuring the interfacial strength, fractured surfaces of the PCB substrate pads and sheared resistors termination finish were studied under SEM. The sheared fracture surfaces of resistor terminations and the substrate pads of reflowed, 100hrs, 200hrs and 300hrs aged at 175°C are presented in figure 8.8 (a-d) and figure 8.9 (a – d). A Similar fracture surface was noticed more or less, for all the component terminations and the substrate pads. The EDX analysis of the component side reveals a very thin layer of SnNiCu covered the whole component terminations. On the pad side Cu-Sn was detected all over the surfaces.

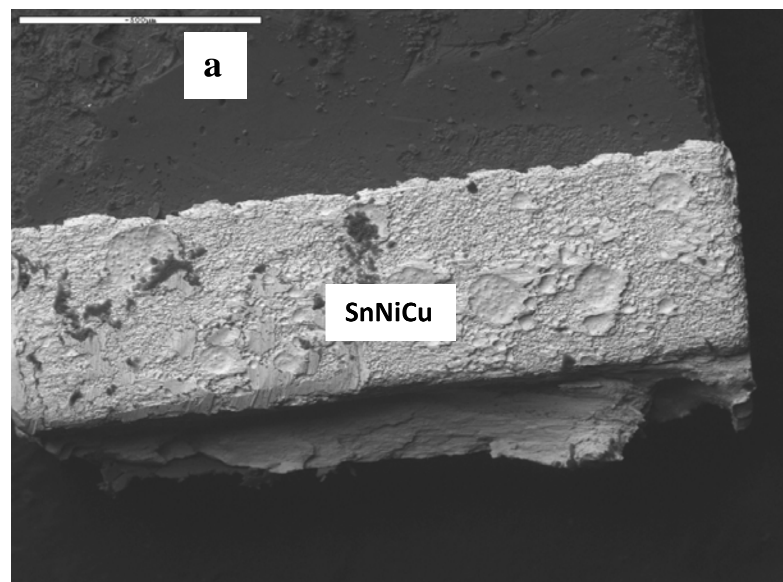

Figure 8.8a Fracture surface of the interface formed between Sn-3.8Ag-0.7Cu solder alloy and component as-reflowed**.**

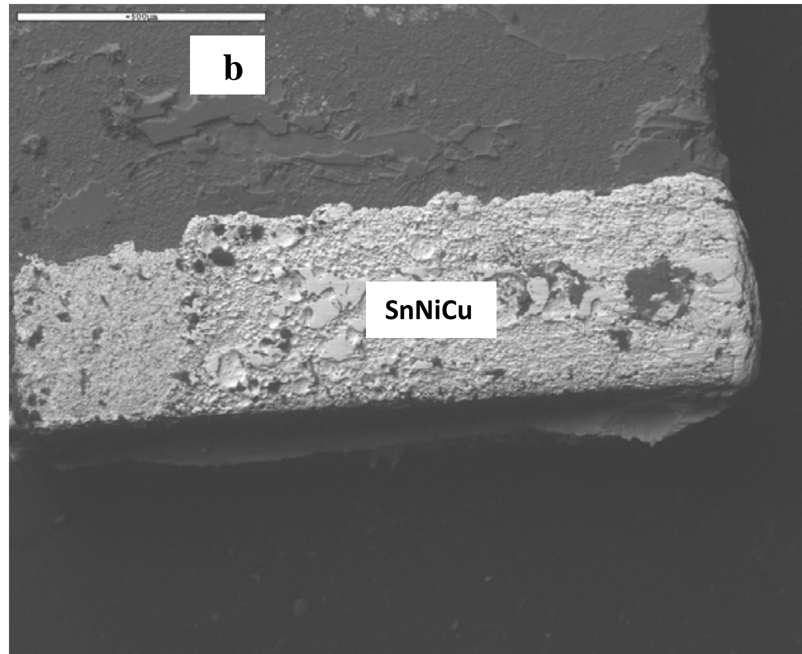

Figure 8.8b Fracture surface of the interface formed between Sn-3.8Ag-0.7Cu solder alloy and component at 100hours of isothermal ageing**.**

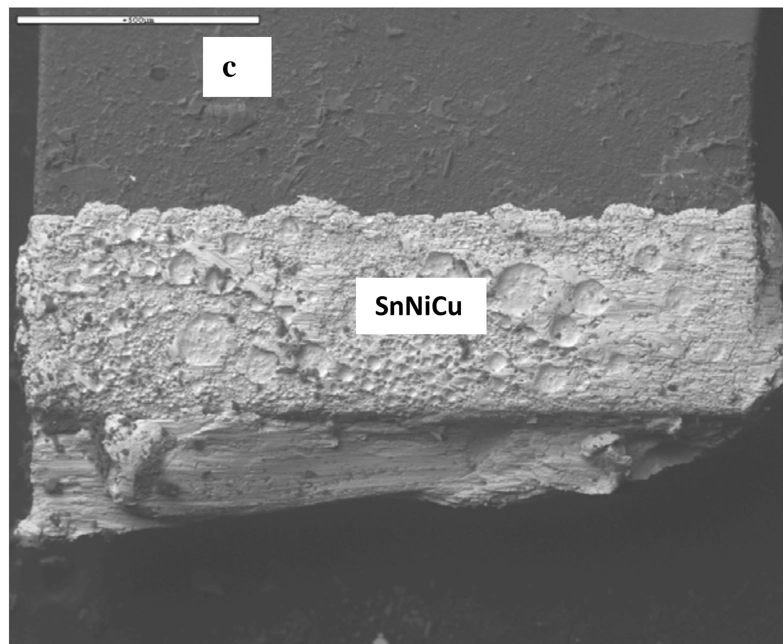

Figure 8.8c Fracture surface of the interface formed between Sn-3.8Ag-0.7Cu solder alloy and component at 200hours of isothermal ageing.

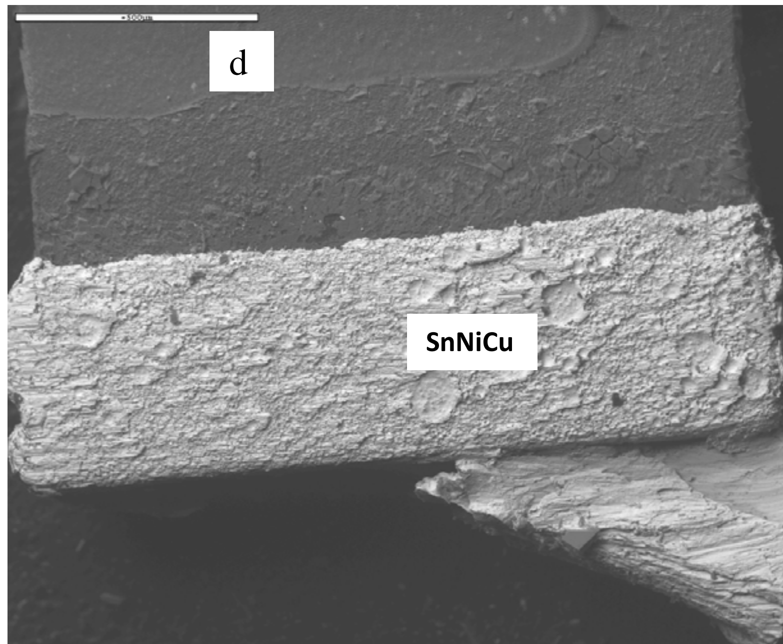

Figure 8.8d Fracture surface of the interface formed between Sn-3.8Ag-0.7Cu solder alloy and component at 300 hours of isothermal ageing**.**

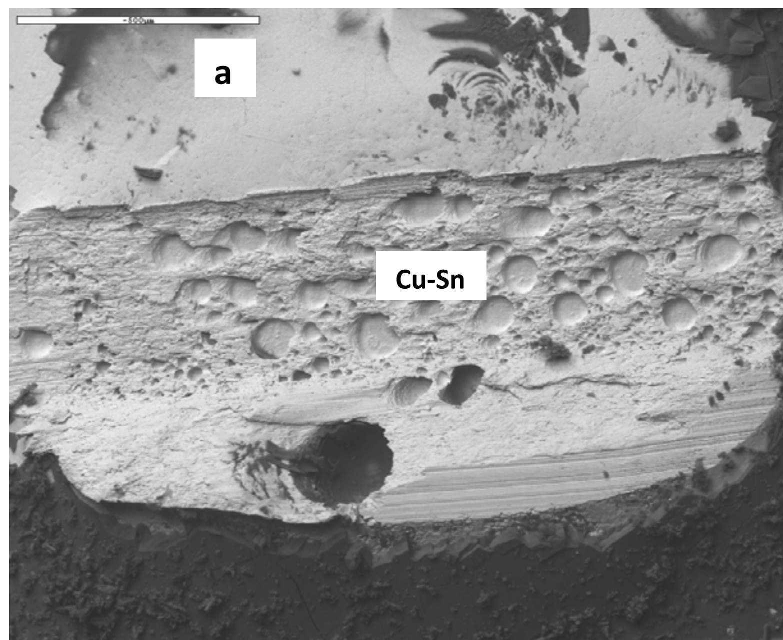

Figure 8.9a Fracture surface of the interface formed between Sn-3.8Ag-0.7Cu solder alloy and pad as-reflowed

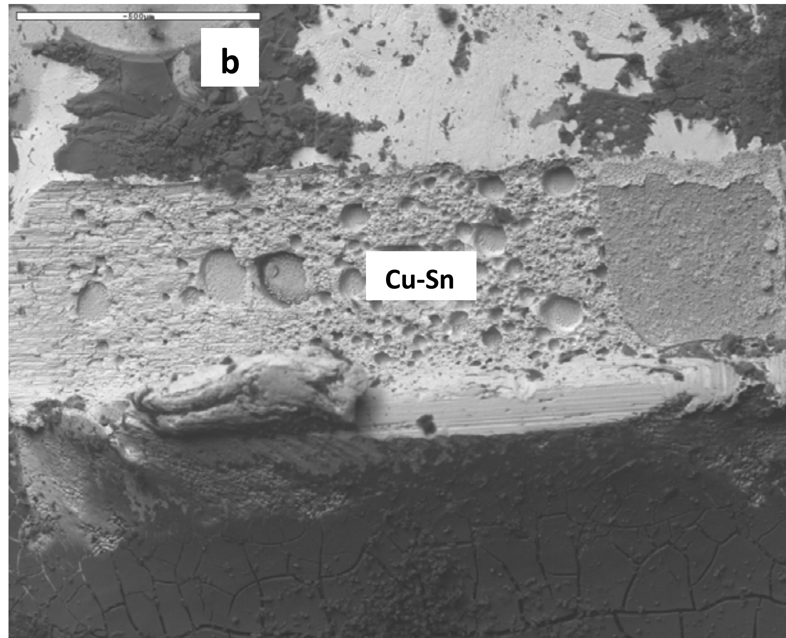

Figure 8.9b Fracture surface of the interface formed between Sn-3.8Ag-0.7Cu solder alloy and pad at 100 hours of isothermal ageing**.**

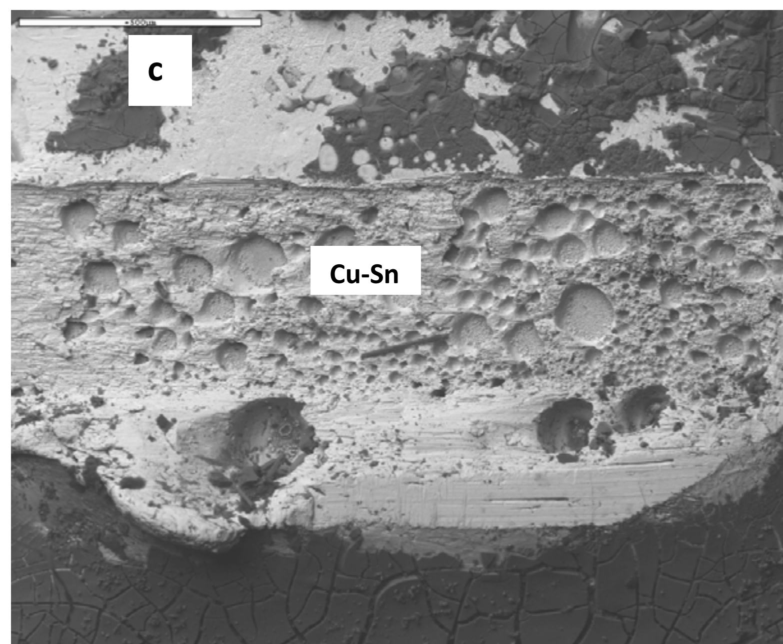

Figure 8.9c Fracture surface of the interface formed between Sn-3.8Ag-0.7Cu solder alloy and pad at 200 hours of isothermal ageing**.**

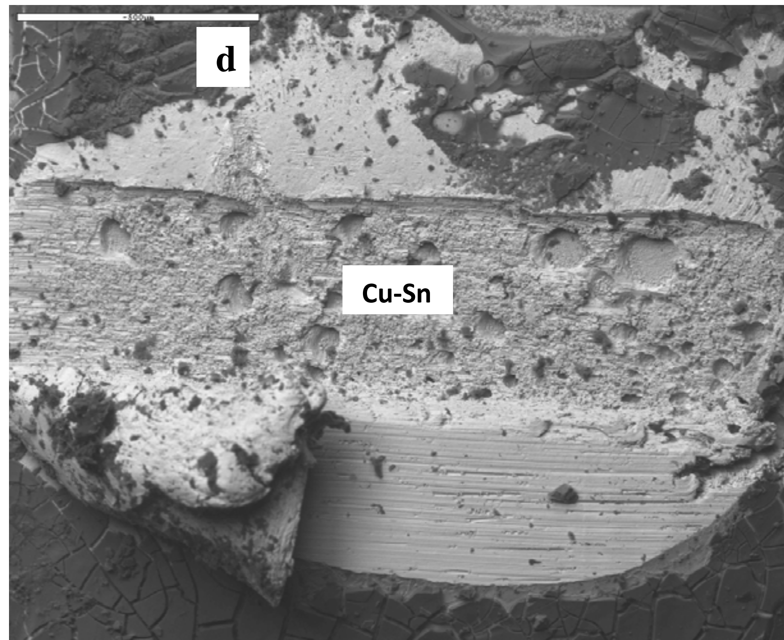

Figure 8.9d Fracture surface of the interface formed between Sn-3.8Ag-0.7Cu solder alloy and pad at 300 hours of isothermal ageing

8.4 Discussion of Results

The growth of the IMC layer at the substrate (pad side) was thicker than that of component side for the isothermal ageing carried out at 175°C. The thickness of the total IMC layer increased from 5.2 to 11.75µm at the pad side, an increase of 39%. On the other hand, the component side increased from 2.6 to 7.8µm, some 50% as shown in table 8.1. The IMC layer growth of both the pad and component sides is shown in fig 8.5.

Comparison of the results of the IMC layer growth for the pad and component side shows that more interfacial diffusion occurred between on the pad side. Also the nickel surface finish of the component termination significantly served as a barrier to the growth of IMC. Figure 8.5 shows the thickness of the total IMC layer as a function of aging times at a constant temperature. The thickness of the interfacial IMC layer was found to increase with ageing time and temperature. The IMC layer thickness of pad and solder interface grew faster than the IMC at the interface of component and solder by 31%. It was reported that excessively

thick reaction layers formed between solder and pad could significantly degrade the mechanical properties of the solder joints (Kin et al 2003; Lee et al 2003).

The shear strength of the joints was examined following ageing at 175°C for different ageing times between Sn–3.8Ag-0.7Cu solder and substrate. The shear strength was measured by performing a typical shear test using the Dage Series 4000 Bond Tester as described in figure 4.4.2. Fifty-six randomly chosen 1206 solder joints were sheared to obtain the average interfacial strength. Figure 8.8 shows the average shear strength of the interfacial reaction of the solder joints. From the graph, it is obvious that an increase in aging time resulted in a decreasing trend in the interfacial strength. It is interesting to observe that there is a reduction of 12%, 10% and 5.5% in shear strength values as the ageing times increased from 0.1333hrs to 300hours. Such a typical trend in shear strength for different ageing times could be attributed to IMC layer thickness and percentage of void in the joints**.**

In the case of fracture surfaces for the reflow reaction time, there was almost 40% of smear area on both component and pad sides. Figures (8.8a and 8.9a) show typical fracture surfaces of reflowed solder joint of Sn–3.8Ag-0.7Cu solder alloy and PCB substrate pad.

After 100 hours of isothermal ageing; few ductile-brittle fractures were observed on both component and pad surfaces as represented in figures 8.8b and 8.9b. The shear strength of the 100 hours sample is 1.82% lower than reflowed shear strength. Moreover, the 200 hours of isothermal ageing solder joint resulted in reduction of shear strength. The fracture surfaces became more brittle as shown in figures 8.8c and 8.9c. Due to it brittle nature, failure can occur at IMC/solder interface. Furthermore, the fracture surfaces of component and pad after 300 hours of isothermal ageing represented in figures 8.8d and 8.9d became more and more brittle, which implies that failure of the joint might occur in IMC/solder interface as well. The EDX analysis reveals that the darker layer on the pad side consists of Cu–Sn IMC whiles at the component side, Sn-Ni-Cu IMC were detected.

8.5 Summary

The study of the effect of IMC layer thickness on the shear strength of 1206 chip resistor solder joints has been presented in this chapter. Conclusions drawn from the study are as follows:

1. The results from the Scanning Electron Microscopy analysis showed that isothermally aged sample at 175°C for 100 hours exhibited an average IMC layer thickness of 7.42µm. Increase in ageing time to 200 hours resulted in IMC layer thickness of 8.45µm. Further increase in ageing time to 300 hours resulted in 11.75µm IMC layer thickness. These results show that the growth of IMC layer thickness increased as the ageing times increase at a constant temperature of 175°C.

2. The results from the Energy Dispersive X-ray analysis showed that the reaction between solder and the component Ni termination during 100, 200 and 300 hours of Isothermal ageing formed SnNiCu at the interface. The Cu in the SnNiCu layer came from the solder side because there is no Cu source except the solder and the atomic percentage (at %) of SnNiCu depends on the ageing time. The formation and composition of IMC in terms of atomic percentage between the solder and the Cu substrate are Cu_5Sn_6 (IMCI) and Cu_2Sn (IMC II).

3. The shear test performed on the solder joints shows that the shear strength varies with ageing time and temperature. The average shear strength of the solder joints after reflow and ageing at 175°C for 100, 200 and 300 hours were 110.88, 108.86, 104.27 and 98.82N/mm^2 respectively. The decrease in shear strength for different ageing is attributed to the brittleness caused by the IMC layer and percentage of void in the joints.

4. Top views of the fracture surfaces after the shear test were examined by SEM; the results of the micrographs showed that regardless of the ageing condition, the fracture occurred at substrate /IMC and IMC/component. Also the brittle and ductile nature of the fracture surface was determined by the shear strength value and the appearance the fracture surfaces.

The conclusions and recommended future work of the thesis is represented in chapter 9.

CHAPTER IX: CONCLUSIONS AND RECOMMENDATION FOR FUTURE WORK

9.1 Conclusions

The conclusions from the work reported in this thesis on the formation and growth of IMC layers and the evaluation of the shear strength of lead-free solder joints are as follows

1. The results from the evaluation of the effect of pad size on IMC layer formation and growth showed that the pad size has very little influence on the growth of the IMC, and that the IMC layer thickness is independent of the pad size.

2. The results from the evaluation of the pad size on IMC layer formation and growth also shows that the growth of IMC depends on diffusion rate, temperature and time according to the power-law model. The significance of these results is that with further miniaturization and reduction in joint size (with IMC layer thickness remaining the same), the ratio of IMC layer thickness to solder joint size will increase and adversely impact the joint reliability.

3. The work carried out on ageing temperatures and reflow profiles of Sn-Ag-Cu alloy and Cu substrate showed the growth of IMC depends on ageing cycle temperature and flux formulation of the solder paste. The results also showed that increase in ageing cycle temperature increases the thickness of IMC layer.

4 The results from the study of reflow soldering profiles using full factorial design for Sn-Ag-Cu solder bumps on Cu substrate showed that the most significant factor in achieving lower IMC layer thickness is time to peak temperature of the reflow soldering process.

5 The results of the study on the effect of IMC layer thickness on the shear strength of Sn-Ag-Cu solder joints showed that there is significant relationship between IMC layer and shear strength, interfacial microstructures and fracture surfaces. The results show that the formation of continuous Cu-Sn and SnNiCu layers lead to weaker interface strength: and that the shear strength of the solder joints decreases with increasing ageing time.

.

9.2 Suggestions for Future Work

1. Traditionally, intermetallic compounds and the thickness of their layers in solder joints are obtain 'destructively' through metallographic sectioning. This prevents further ageing observations and independent joint strength tests. Microfocus X-ray diffraction (XRD) provides an opportunity for a non-destructive technique for identifying and quantifying the intermetallic layers. This technique can give better understanding of how the IMC layers are forming in the solder joints.

2. A full factorial experimental design study on the effect of the various reflow soldering profile parameters is recommended using response surface and contour plots method. The work reported in this thesis only covers four of the six parameters and the full interaction between the parameters have not been carried out.

3. Temperature cycle ageing on 1206 surface mount chip resistor solder joints is recommended for determining the fatigue failure of the solder joints. The work reported in this thesis only covers the evaluation of the shear strength and IMC layer thickness.

4. It is recommended that the work on the effect of Isothermal Ageing on IMC layer growth should be done for the range 100 to 1,000 hours. The work reported in the thesis only covers 100, 200 and 300 hours only. The three data points is unfortunately insufficient draw firm conclusions

5. The experimental work on effect of IMC layer thickness on the shear strength of 1206 chip resistor solder joints, did not examine the effect of IMC layer thickness on the grain structure of the joints and the crack initiation and propagation. Therefore it is recommended that further research is should be conducted in these areas.

Publications

International reviewed **JOURNAL** and **CONFERENCE** articles published during this PhD candidature**:**

1. **P.K. Bernasko**, S. Mallik, N.N. Ekere, and A. Seman and G. Takyi[a], Effect of Ageing Temperatures and Reflow Profiles on the Intermetallic growth between Sn-Ag-Cu solder alloy and Cu. Proceedings of the 11th Electronics Packaging Technology Conference (EPTC 2009), 9 – 11 December 2009, Singapore

2. **P.K. Bernasko**, S. Mallik, N.N. Ekere, and A. Seman and G. Takyi[a], "Evaluating the effect of pad sizes on the inter-metallic layer formation and growth for Sn-Ag-Cu solders on Cu metallization, International Conference on Electronics Packaging (ICEP) 2011, 13-15 April 2011, Nara Prefectural New Public Hall, Nara, Japan.

3. G. Takyi S. Mallik, N.N. Ekere, and **P.K. Bernasko**, "Effect of solder integrity on thermal performance of thermo-electric cooler for 980nm pump laser". Soldering & Surface Mount Technology, Vol. 23, No.2, 2011.

4. **Peter K. Bernasko**, Shefiu S. Zakariyah, Ndy N. Ekere, Sabuj Mallik, [b]G. Takyi "The effects of reflow profiles on Sn-Ag-Cu solder bumps and Cu substrate using full factorial design" Soldering and Surface Mount Technology (submitted journal)

5. **Peter K. Bernasko**, Shefiu S. Zakariyah, Ndy N. Ekere, [a]Sabuj Mallik, G. Takyi "Investigation into Intermetallic Compound Layer Thickness, Voids and Shear Strength of Surface Mount 1206 Chip Resistor" Journal of Electronic Materials (submitted journal)

REFERENCES

Abtew M and Selvaduray G, "Lead-free Solders for Surface Mount Applications", *Chip Scale Review*, September 1998, pp. 29-38.

Abtew, M., Selvaduray, G., Mater. Sci. Eng. R 27 (2000) 95–141.

Alberts Bruce, Dennis Bray, Julian Lewis, Martin Raff, Keith Roberts and James D. Watson, "Molecular Biology of the Cell", *Garland Publishing, Inc.,* 1989, New York.

Altera Corporation, 2008, Reflow Soldering Guidelines for Surface-Mount Devices, 2008, 81 (4), pp 1-10.

Ahat, S., Sheng, M and Luo, L. Effect of static thermal aging and thermal cycling on the microstructure and shear strength of Sn-3.8Ag-0.7Cu solder joints Journal of Materials Vol. 16, pp2914-21, 2001.

Alam M. O, Chan Y. C and Hung K. C, Journal of Electronic Materials 31, 1117 (2002).

Alam, M. O., Chan, Y. C., and Tu, K. N., Journal of Applied Physics Vol. 94, 7904, 2003.

Allen, S. L., Notise, M.R., Chromik, R.R and Vinci, R.P. Microstructural evolution in lead-free solder alloys: Part I. +II, Journal of Resistance. Vol. 19, 5, pp 1417-31, 2004.

Askeland DR(ed.), The Science and Engineering of Materials, 3rd edn., Chapman & Hall, UK, 1996, pp. 281-337.

Bader S, Gust W, Hieber H. Rapid formation of intermetallic compounds by interdiffussion in Cu-Sn and Ni-Sn systems. Acta Metall Mater, Vol 43, (1), pp 329 – 337, 1995.

Bang, W.H., Moon, M.-W., Kim, C.-U., Kang, S.H., Jung, J.P., Oh, K.H., Journal of Electronic Materials 37 (4) (2008) 417–428

Bauer BD and O'Neill MP, "Are you ready for lead-free solder paste?" SMT's guide to Lead free Soldering, June 2000, pp. 11-12.

Bergman LK and Tazi Mo, "Critical steps of BGA rework and repair", *Surface Mount* Technology Magazine, v 11, n 8, Aug. 1997, pp. 50, 52-53.

Bigas, M. and Cabruja, E. (2006), "Characterisation of electroplated Sn/Ag solder bumps", Microelectronics Journal, Vol 37 No 3, pp. 308–316.

Biocca, P., 2002, Developing a Reliability lead-free Surface Mount Technology Assembly Process, Kester Des Plaines IL, USA

Bjorn Dahle and Ronald C. Lasky, Ph.D., PE, 2004, Optimizing Your Reflow Profile for Maximum Productivity and Profitability, APEX, Anaheim CA.

Bo, Tao; Zhouping, Yin; Han, Ding; Yiping, Wu; (2009), Reflow profile optimization of BGA solder joints considering reflow temperature and time coupling, Soldering & Surface Mount Technology, Vol, 24, no.4, pp 38 – 44

Biocca P, "Global Update on Lead-free Solders," *Proc. Surface Mount International*, San Jose, CA, 1998, pp. 705-709.

Boulanger R, "Assembly Processes", in Coombs CF Jr (ed.), Printed Circuits Handbook, McGraw-Hill, 5th edition, 2001, pp. 41.3-41.33.

Brophy JH, Rose RM and Wulff J, The Structure and Properties of Materials, Volume II: Thermodynamics of Structure, John Wiley & Sons, USA, 1964. pp. 62-97

Bukhari, S., Santos,D.L., Lehman, L.P., and Cotts, E., " Continued Evaluation of the Effects of Processing Conditions and Aging Treatments on Shear Strength and Microstructure in Pb- free Surface Mount Assembly," Proceedings of the SMTA Pan Pacific Microelectronics 2005 Symposium

Chan, Y.C., So, Alex C.K., Lai, J.K.L., Growth kinetic studies of Cu–Sn intermetallic compound and its effect on shear strength of LCCC SMT solder joints ,Materials Science and Engineering B55 (1998) 5–13

Chan, Y.C., Yang, D., Failure mechanisms of solder interconnects under current stressing in advanced electronic packages, Progress in Materials Science, Volume

55, Issue 5, July 2010, Pages 428-475

Chia, J., Cotterell, B., Chai, T., Mater. Sci. Eng. A417 (2006) 259–274.

Chi C, Chang HS, Hsieh KC and Chung CL, “Interfacial microstructure of Pb-free and Pb-Sn solder balls in the ball-grid array package,” *Journal of Electronic Materials*, v 31, n 11, November 2002, pp. 1203-1207.

Choi WK, and Lee HM, “Effect of Soldering and Aging Time on Interfacial Microstructure and Growth of Intermetallic Compounds between Sn-3.5Ag Solder Alloy and Cu Substrate,” Journal of Electronic Materials, Vol.29, No.10, 2000, pp.1207-1213.

Choi WK, Kang SK and Shih DY, “A study of the effects of solder volume on the interfacial reactions in solder joints using the differential scanning calorimetry technique,” *Journal of Electronic Materials*, v 31, n 11, Nov. 2002, pp. 1283-1291.

Dalrymple TW and Milkovich C, “Rework process for microBGA and CSP components”,

Surface Mount Technology Magazine, v 14, n 7, Jul. 2000.

Date, M., Shoji, T., Fujiyoshi, Sato M.K., Tu, K.N., Scripta Mater. 51 (2004) 641–645.

Dwinell JF Sr, “On rework: The case for duplicating the production thermal profile”, *Surface* Mount Technology Magazine, v 11, n 10, Oct. 1997, pp. 52-53.

Ferry J, “Who's afraid of lead-free rework?” *Circuits Assembly*, v 13, n 11, Nov. 2002, pp. 24.

Fix A. R., Lopez, G. A., Brauer, I., Nuchter, W. and Mittemeijer, E.J , Microstructural evolution and mechanical properties of SnAgCu alloys, Journal of Applied Physics, Vol. 100, 4, pp.043519-1-8.

Fix, A. R., Nuchter, W. and Wilde, J., “Microstructural changes of lead free solder joints during long term ageing, thermal cycling and vibration fatigue”, *Soldering and surface mount technology,* Vol. 20, no 1, (2008), pp 13-21.

Fouzder, Tama., Shafiq, Ismathullakhan., Sharif, Y.CA., Yung, W.K.C., Influence of SrTiO3 nano-particles on the microstructure and shear strength of Sn–Ag–Cu solder on Au/Ni metallized Cu pads, Journal of Alloys and Compounds 509 (2011) 1885–1892

Frear, D., Grivas, D., Morris, J. W Jr, "The effect of Cu6 Sn5 whisker precipitates in bulk 60Sn 40Pb solder", *Journal of Electronics materials*, Vol.16, no 3, (1987), pp 181,

Frear D, Morgan H, Burchett S and Lau J (ed.), The Mechanics of Solder Alloy Interconnects, Van Nostrand Reinhold, New York, 1994, pp. 42-86.

Frear DR, Solder Mechanics: A State of the Art Assessment, TMS, Minerals Metals Materials, Pennsylvania, USA, 1991, pp. 29-104.

Gao F, Mukherjee S, Cui Q, and Gu, Z, Department of Chemical Engineering and Nanomanufacturing Center, University of Massachusetts Lowell, One University Avenue, Lowell, Massachusetts 0185

Gapal, Sekharan., Jafri Mohd Rohani, Sha'ri Mohd Yusof and Zailis Abu Bakar, 2006, Optimazation of Solder Paste Printing Parameters Using Design of Experiments, Journal Teknologi; 43 (A), 11-20.

Gao, Jin Gang., Wu, YiPing., Ding, Han., (2007) "Optimization of a reflow soldering process based on the heating factor", Soldering & Surface Mount Technology, Vol.19 Iss:1, pp.28 – 33

Gao, Jin Gang., Wu, YiPing., Ding, Han and Wan, Nian Hong., Thermal profiling: a reflow process based on the heating factor, Soldering & Surface Mount Technology, Vol. 20, No. 4, 2008 pp. 20–27

Ghosh G, "A Comparative Study of the Kinetics of Interfacial Reaction between Eutectic Solders and Cu/Ni/Pd Metallization," *Journal of Electronic Materials*, Vol.29, No.10, 2000, pp. 1182-1193.

Gowda A, Srihari K and Primavera A, "Lead-free Rework Process for Chip Scale Packages", Proceedings of SMTA/NEPCON East Conference, Boston, USA, June 2001.

Guo F, Choi C, Lucas JP and Subramanian KN, "Microstructural characterisation of reflowed and isothermally-aged Cu and Ag particulate reinforced Sn-3.5Ag composite solders", *Soldering & Surface Mount Technology,* vol.13, no.1, 2001, pp. 7-18.

Hamilton, C., and Snugovsky, P., (2007), "A Study of Copper Dissolution During Lead Free PTH Rework Using a Thermally Massive Vehicle", SMTA International (2007).

Handwerker C, "Lead-free Solders: A Change in the Electronics Infrastructure", *Circuitree*, September, pp. 2-4.

Handwerker C, "NIST Research in Lead- Free Solders: Properties, Processing, Properties, Processing, Reliability", 2002, on-line www.seas.ucla.edu/eThinFilm/P freeWorkshop/pdf.

Harris PG and Chaggar KS, "Role of intermetallic compounds in lead-free soldering", Soldering & Surface Mount Technology, no.30, MCB Univ Press Ltd, Oct 1998, pp. 38-52.

Haseeb A.S.M.A. LengTay See Effects of Co nanoparticle addition to Sn–3.8Ag–0.7Cu solder on interfacial structure after reflow and ageing, Intermetallics, Volume 19, Issue 5, May 2011, Pages 707-712

Hodúlová Erika, Palcut Marián, Lechovi Emil, Šimeková Beáta and Ulrich Koloma

Kinetics of intermetallic phase formation at the interface of Sn–Ag–Cu–X (X = Bi, Solders with Cu substrate *Journal of Alloys and Compounds*, *Volume 509, Issue 25*, *23 June 2011*, *Pages 7052-7059*

Horsley RM, "Microstructural Characterisation of Solder Joints using the Sn-Ag-Cu Eutectic Alloy in a No-clean Surface Mount Technology (SMT) Assembly Process", PhD thesis, University of Salford, UK, 2002, pp. 168.

Hwang, J. S. (1989), Solder Paste in Electronics Packaging, Van Nostrand Reinhold, (1989).

Hwang JS (ed.), Environment-friendly Electronics: Lead-free Technology, Electrochemical Publications, Isle of Man, British Isles, 2001, pp. 231-243.

Hwang JS, "Lead free solder: the Sn/Ag/Cu system", *SMT magazine,* July 2000, pp. 18-21. International Technology Roadmap for Semiconductors (2005).

Izuta, G., Tanabe, T., Suganuma, K., (2007), "Dissolution of Sn-Ag-Cu System Lead-Free Solder", *Soldering &Surfac Mount Technology*, Vol. 19 No. 2, pp. 4-11.

Jang JW, Frear DR, Lee TY, and Tu KN, "Morphology of interfacial reaction between lead-free

solders and electroless Ni-P under bump metallization," *Journal of Applied Physics*, Vol.88, No.11, Dec 2000, pp. 6359-6363.

JEDEC/Electronic Industries Alliance, Inc. Moisture/Reflow Sensitivity Classification for Non Hermetic Solid State Surface Mount Device (J-STD-020A), New York: JEDEC/Electronic Industries Alliance, 1999

Jeng, S.T., Chang, H.H., Lai, Y.S., Tsai, T.Y., Microelectron. Reliab. 49 (2009) 310–317.

Jeon, Y.D., Ostmann, A. H., Paik, Reichl, K.W., in IEEE Proceeding of the Conference on Electronic Components and Technology, 2003, pp. 1203–1208.

Jien-Ming Chen, Chin-Fu Kuo, Di-Bao Wang, Chin-Wen Huang, Shang-Ching Sun, Yu-Sheng Hsieh, Wu-Zhong Zhon, Low Bias Voltage and High Sensitivity CMOS Condenser Microphone Using Combined Stress Relaxation Design, 5th International Microsystems Packaging Assembly and Circuits Technology Conference (IMPACT), 2010

Jirsa, Jan; Dusek, Karel; Studies of Surface Mount Technology and Its Risk Analysis, Electronics Technology, 34th International Spring Seminar, Czech Republic, 2011

Kang SK, Shih DY, Fogel K, Lauro P, Yim MJ, Advocate GG, Griffin M, Goldsmith C, Henderson DW, Gosselin TA, King DE, Konrad JJ, Sarkhel A and Puttlitz KJ, "Interfacial reaction studies on lead (Pb)-free solder alloys," IEEE Transactions on Electronics Packaging Manufacturing, vol.25, no.3, July 2002, pp. 155-161

Karpel, A., Gur, G., Atzmon, A., Kaplan, W. KNS Joint Publication with Technion University, J. Material Science, 2007.

Kim, D. and Jung, S., " The effect of isothermal aging on the thickness of intermetallic compound growth betweeen low melting point solders and Ni-plated

Cu substrate" Journal of Electronic Materials, Vol. 33, no.12, (2004), pp.1561-1566.

Kim JS, Kang M and Lee SB, "Recrystallization during the discontinuous precipitation of beta Sn in 95Pb-5Sn and 85Pb-15Sn solder alloys," *Scripta Materialia*, vol. 38, no. 11, May 1998, pp. 1677-1684.

Kim KS, Huh SH, Suganuma K, "Effects of cooling speed on microstructure and tensile properties of Sn-Ag-Cu alloys", *Materials Science and Engineering A*, vol. 333, no. 1-2, August 2002, pp. 106-114.

Kim, H.K., Tu, K.N., Appl. Phys. Lett. 67 (1995) 2002–2004.

Kim, K.S., Huh, S.H., Suganuma, K., J. Alloys Compd. 352 (2003) 226.

Kivilahyi, J. K. Journal of The Materials Metals & Material Society, Vol 54, pp 52 (2002).

Korhonen TM, Su P, Hong SJ, Korhonen MA and Li CY, " Reactions of Lead-free Solders with CuNi Metallizations," *Journal of electronic materials*, vol.29 no.10, 2000, pp.1194-1199.

Lea C (ed.), A Scientific Guide to Surface Mount Technology, Electrochemical Publications, Scotland, UK, 1988, pp. 329-377.

Lead-free Soldering R&D Committee, "Challenges and Efforts Towards Commercialization of Lead-free Solder – Road Map 2000 for Commercialization of Lead-free Solder – ver 1.2", the Japan Electronic Industry Development Association (JEDEC), on-line: www.leadfree.org.

Lee NC, "Optimizing the reflow profile via defect mechanism analysis," Soldering & Surface Mount Technology, vol.11, no.1, 1999, pp. 13-20.

Lee YG and Duh JG, "Interfacial morphology and concentration profile in the unleaded solder/Cu joint assembly", *Journal of Materials Science: Materials in Electronics*, vol.10, no.1, Chapman & Hall Ltd, Netherlands, 1999, pp. 33-43.

Lee T, “Electromigration and Solid State Aging of Flip Chip Solder Joints and Analysis of Sn Whiskers on Lead Frame,” PhD Thesis, University of California, USA, 2001, pp. 64-70.

Lee, N. C. Reflow Soldering Processes and Troubleshooting, 2002, pg. 239, Newnes, Boston

Lee, N. C, Reflow Soldering Processes and Troubleshooting SMT, BGA, CSP, and Flip Chip Technologies, Newnes Publishing, pg 2001

Lee, H.-T., Chen, M.-H., Materials Science and Engineering A333 (2002) 24–34.

Lee, J., D.,Park, Moon, J., Lee,Y., Shin, D., Kim, Y., J. Electron. Mater. 29 (2000) 1264–1269

Li GY, and Chan YC, “Ageing effects on shear fatigue life of solder joint between Pd/Ag conductor and Sn/Pb/Ag solder”, *Proceedings of the Electronic Technology Conference*, EPTC, IEEE, Singapore, 1997, pp. 102-107.

Li, M., Zhang, F., Chen, W.T., Zeng, K., Tu, K.N., Balkan, H., Elenius, P. Interfacial microstructure evolution between eutectic SnAgCu solder and Al/Ni(V)/Cu thin films, J. Mater Res, 2001

Lin, Yu-Hsin., Deng, Wei-Jaw., Shie, Jie-Ren., and Yang, Yung-Kuang., 2007, Optimization of reflow soldering process for BGA packages by artificial neural network, Department of Industrial Engineering and Management, Ming Hsin University of Science and Technology, Hsinchu, Republic of China.

Lin, Ching-Tsung., Hsi, Chi-Shiung., Chang, Moo-Chin Wang Tao-Chih., Liang Ming-Kann., Interfacial microstructures and solder joint strengths of the Sn–8Zn–3Bi and Sn-9Zn–lAl Pb free solder pastes on OSP finished printed circuit boards, Journal of Alloys and Compounds 459 (2008) 225–231

Lin KL, Hsu KT. Manufacturing and materials properties of Ti/Cu/electroless Ni/solder bump on Si. IEEE Trans Comp Packag Technol 2000;23:657–60

Liu, P. P., Liu, J., J. Alloys Compd. 462 (2008) 73–79.

Madeni J. C and Liu **S,** Center for Welding, Joining and Coatings Research, Metallurgical & Materials Engineering Department, Colorado School of Mines, U.S.A. March, 2011

Mackay, C. A., Some Causes of Problems with Existing SMT Solder Creams and Possible Improvements, Circuit World, Vol.13, No.3, pp.4 –7 (1987)

Marshall JL, Fosterm LA and Sees JA, "Microstructural Influence on the Mechanical Properties of Solder", in Frear DR, Morgan H, Burchett S and Lau J (ed.), Mechanics of Solder Alloy Interconnects, Van Nostrand Reinhold, New York, 1994, pp. 42-86.

Massalski, T.B., Okamoto, H., Subramanian, P.R., Kacprzak, L., Binary Alloy Phase Diagram, second ed., ASM International, Materials Park, OH, 1990, pp. 1442–1446.

Ming-Yi Tsai; Hsu, C.H.J.; Wang, C.T.O.; Investigation of thermomechanical behaviors of flip chip BGA packages during manufacturing process and thermal cycling, Components and Packaging Technologies,Volume: 27 , Issue3, , Page(s): 568 – 576, 2004

Mira, Manuel., Zhang, James Z., Ball, Aaron K., 2006, Lead-Free Reflow Oven Parameters Optimization, Proceedings of IJME-INTERTECH Conference.

Miric, AZ and Grusd A, "Lead-free Alloys", *Soldering and Surface Mount Technology*, v.10, no.1, 1998, pp. 19-25.

Mizoguchi S, "Chapter 11: Structural Control of Casting," Cramb A (ed.), The Making, Shaping and Treating of Steel, 11th Edition - Casting Volume, the AISE Steel Foundation, Pittsburgh, USA, 2003, pp. 11.1-11.4.

Montgomery, D.C. (1997), Design and Analysis of Experiments, Fourth Edition, John Wiley & Sons, Inc., New York, pp. 101–245.

Moon KW, Boettinger WJ, Kattner UR, Blancaniello FS, and Handwerker CA, "Experimental and Thermodynamic Assessment of Sn-Ag-Cu Solder Alloys", *Journal of Electronic Materials*, Vol. 29, No. 10, 2000, pp. 1122-1136.

Morris JW Jr., Goldstein JLF and Mei Z, "Microstructural Influence on the Mechanical

Properties of Solder", in Frear DR, Morgan H, Burchett S and Lau J (ed.), Mechanics of Solder Alloy Interconnects, Van Nostrand Reinhold, New York, 1994, pp. 7-43.

Nakamura Y and Sakakibara Y, "Microstructure of solder joints with electronic components in lead-free solders," *Soldering & Surface mount Technology*, vol.10, no.1, 1998, pp.10-12.

NCMS (National Centre for Manufacturing Sciences), "Lead-free Solder Project – Final

Report", NCMS, August, 1997.

NCMS (National Centre for Manufacturing Sciences), "Lead-free, High-temperature Fatigue resistant Solder – Final Report", NCMS, 2001.

Nguty TA, Ekere NN, Philpott JD and Jones GD, "Rework of CSP: the effect on surface intermetallic growth", *Soldering and Surface Mount Technology*, Vol. 12/3, 2000b, pp. 35-38.

Noor, Ervina Efzan Mhd., Sharif, Nurulakmal Mohd., Kuan, Cheong., Ariga, Yew Tadashi., Hussain, Ahmad Badri Ismail Zuhailawati., Wettability and strength of In–Bi–Sn lead-free solder alloy on copper substrate, Journal of Alloys and Compounds 507 (2010) 290–296

Ohnuma I, Miyashita M, Anzai K, Liu XJ, Ohtani H, Kainuma R and Ishida K, "Phase Equilibria and the Related Properties of Sn-Ag-cu Based Pb-free Solder Alloys. Journal of Electronic Materials., Vol. 29, No.10, 2000, pp.1137-1144.

Oliver, J.R., Liu, J., and Lai, Z. "Effect of Thermal Ageing on the Shear Strength of Lead-free Solder Joints," Proceedings of the 2000 International Symposium on Advanced Packaging Materials, pp. 152-156.

Ott L (ed.), An Introduction to Statistical Methods and Data Analysis, PWS-Kent, Boston, USA, 1988, pp. 131, A3

Ourdjini, A.; Hanim, M.A.A.; Koh, S.F.J.; Siti Aisha, I.; Tan, K.S.; Chin, Y.T.; Effect of Solder Volume on Interfacial Reactions between Eutectic Sn-Pb and Sn-Ag-Cu Solders and Ni(P)-Au Surface Finish, 31st International Conference on Electronics Manufacturing and Technology, 2006

Ožvold, M., Hodúlová, E., Chriaštelová, J., Janovec, J., . Turna M Slovak University of Technology, Faculty of Materials Science and Technology J. Bottu 24, 91724 Trnava, Slovak Republic

Pan, J., Toleno, B.J., Chou, T. and Dee, W.J. (2006), "The effect of reflow profile on SnPb and SnAgCu solder joint shear strength", Soldering & Surface Mount Technology, Vol. 18 No. 4, pp. 48-56.

Pandher, R., Athavale, **S.,** Proceedings of Electronic Packaging Tecknology Conference, (EPTC (2006), pp. 708 – 716.

Prakash, K.H., Sritharan, T., Materials Science and Engineering 379 (2004) 277.

Prasad S, Carson F, Kim GS, Lee JS, Jeong TS and Kim YS, "Reliability of Lead-free BGA Packages", *Proceedings of IMAPS 2000 Conference*, Chicago, 2000a.

Prasad S, Carson F, Kim GS, Lee JS, Rouband P, Henshall G, Kamath S, Garcia A, Herber R and Bulwith, "Board Level Reliability of Lead-free Packages" *Proceeding of the 2000 Surface Mount Technology Association (SMTA) Conference*, 2000b.

Quan, L.K., Frear, D., Grivas, D., Morris, J.W., Journal of Electronic Materials 16 (3) (1987) 203–208.

Ranjit KR, "Design of Experiments using the Taguchi Approach," 1st edn., John Wiley and Sons, USA, 2001, pp. 95-135.

Richard BP, Levoguer CL, Hunt CP, Nimmo K, Peter S and Cusack P, "An Analysis of the Current Status of Lead-free Soldering", Department of Trade and Industry Report, April 2000.

Richards B and Nimmo K, "An Analysis of the Current Status of Lead-free Soldering – Update 2000", *Department of Trade and Industry*, on-line: www.leadfree.org.

Romig AD Jr., Chang YA , Stephens JJ, Frear DR, Marcotte V and Lea C, "Chapter 2: Physical Metallurgy of Solder-Substrate Reactions," in Frear DR, Jones WB and Kinsman KR (ed.), Solder Mechanics, TMS, 1991, pp. 54-55

Roubaud, P. and Henshall, G. (2001), “Thermal fatigue resistance of Pb-free second level interconnect”, Proceedings of the SMTA International

Rupprecht H, “Array package rework - Lead free throws a curve”, *Circuits Assembly*, v 13, n 7, Jul. 2002, pp. 30-34.

Salam B, Ekere NN and Rajkumar D, “Study of the interface microstructure of Sn-Ag-Cu lead free solders and the effect of solder volume on intermetallic layer formation,” Proceeding 51st ECTC, 2001, pp. 471.

Salam, B., Ekere, N. N, and Durairaj, R., “A study of Intermetallic compounds (IMC) formation and growth in Ultra-Fine pitch Sn-Ag-Cu lead free solder joint”, *Proc 1st Electronics System Integration Technology Conf.*, Dresden, Germanay, September 2006, pp. 988 – 994.

Salam, B., Virseda, C., Da, H., Ekere, N.N. and Durairaj, R. (2004), “Reflow profile study of the Sn-Ag-Cu solder”, Soldering & Surface Mount Technology,Vol.16 No. 1, pp.27-34.

Schaefer, M. W., Laub, J. M., Sabbe, J. M., and Fournelle, R. A., “A Numerical Metho for Predicting Intermetallic layer thickness developed during the formation of solder joints”, Journal of Electronic materials, Vol. 25, no. 6, (1996), pp 992-1003

Schaefer M, Laub W, Fournelle RA and Liang J, “Evaluation of Intermetallic Phase Formation and Concurrent Dissolution of Intermetallic During Reflow Soldering”, in Mahidrana RK, Frear DR, Sastry SML, Murty KL, Liaw PK and Winterbottom W (ed.), Design and reliability of solders and solder interconnects, the Minerals Metals and Materials Society, TMS, 1997, pp. 247-257.

Shina, S, Eaton W, "Using Circuit Simulation with Taguchi Design of Experiment Techniques to Optimize the Performance of a Digital Half-adder Integrated Circuit", Quality Progress, *Journal of Quality Engineering*, Vol. 5, Number 4, 1993, pp. 589-600.

Skidmore T and Waiters K, “Optimizing Solder Joint Quality-Lead Free,” *Circuits Assembly*, April 2000, pp. 17-22.

So, C. K., and Chan, Y. C., "Reliability Studies of Surface Mount Joins- Effect of Cu-Sn Intermetallic Compounds", *IEEE Trans-CPMT-B*, Vol. 19, no. 3, (1996), pp. 661 – 668. Stafford JW, "Semiconductor Packaging Technology", in Coombs CF Jr (ed.), Printed Circuits Handbook, McGraw-Hill, 5th edition, 2001, pp. 2.1-2.22

Sriyarunya, A.; Tondtan, J.; Kittidacha, W.; Tukiman, H.; Backward compatibility of solder alloys with chip scale package, 12th Electronics Packaging Technology Conference (EPTC), 2010

Steller, A.; Pape, U.; Dudek, R.; Solder joint reliability in automotive applications: Analysis methods and assessment criteria, 3rd, Electronic System-Integration Technology Conference (ESTC), 2010

Suganuna H and Tamanaha A, "Reflow Technology", *SMT magazine*, issue: February 2001, pp.65-70.

Suganuna H, and Tamanaha A, "Reflow Technology", *SMT magazine*, February 2001, pp.65-70.

Suraski D, "The benefits of a Ramp-to-Spike Reflow Profile," *SMT magazine*, April 2000, pp.64-66.

Tseng, A.; Lin, M.; Hu, B.; Chen, J.W.; Wan, J.M.; Lee, S.; Yi-Shao Lai*;* Advanced QFN Surface Mount Application Notes Development*,* 12th Electronics Packaging Technology Conference (EPTC), 2010

TU, P. L., Chan, Y. C. and Lia, J. K. L, "Effects on intermetallic compounds on the thermal Fatigue of the surface mount solder joints". *IEEE Trans-CPMT-A*, Vol. 20, no l, (1997), pp. 87 – 93.

Vianco PT, Hlava PH, Kilgo AC, and Rejent JA, "Intermetallic Compounds," in J.S. Hwang (ed.), Environment-friendly Electronics: Lead-free Technology, Electrochemical Publications, Isle of Man, UK, 2001, pp. 436-464.

Vianco, P. T., Rejent, J. A. and Hlava, P. F., "Solid-state Intermetallic compound layer growth between copper and 95.55Sn-39Ag-0.6Cu soldering" *Journal of electronic materials*, vol. 33, no. 9, (2004), pp. 991 – 1004

Warwick, M. E. and Muckett, S. J., “Observations on the growth and impact of Intermetallic, compounds on Tin-coated substrates”, *Circuit World* , Vol 9, no.4, (1983), pp 5-11.

Webster, J., Pan, J. and Toleno, B.J. (2007), “Investigation of the lead-free solder joint shear performance”, Journal of Microelectronic and Electronics Packaging, Vol. 4 No. 2, pp. 72-7.

Wei YY and Duh JG, “Effect of thermal ageing on (Sn-Ag, Sn-Ag-Zn)/PtAg, Cu/Al_2O_3 solder joints”, *Journal of Materials Science: Materials in Electronics*, vol. 9, no. 5, Chapman & Hall Ltd, London, Oct 1998, pp. 373-381.

Wickham M and Hunt C, “Thermal Profiling of Electronic Assemblies”, National Physical Laboratory (NPL) Report MATC (A)050, September 2001, on-line: http://www.npl.co.uk/ei/publications/abstracts.html#-13

Wickham, Martin., Voiding: Occurrence and Reliability Issues with Lead-free, National Physical Laboratory, U.K.

Wiese S, Schubert A, Walter H, Dudek R, Feustel F, Meusel E and Michel B, “Constitutive Behaviour of Lead-free Solders vs. Lead-containing Solders – Experiments on Bulk Solder and Flip-chip Joints”, Proceeding of the 2001, Electronic Components and Technology Conference (ECTC), 2001, pp. 890-902.

Wu, Y.P. (2002), “Heating factor – a quantitative parameter of reflow profile”, Modern Surface Mounting Technology Information, June, pp. 63-6.

Yang W, Felton LE, and Messler RW Jr., “The effects of soldering process variables on the microstructure and mechanical properties of eutectic Sn/Ag/Cu solder joints,” *Journal of electronic materials*, vol.24, no.10, 1995, pp. 1465-1472.

Yao, Pei., Liu, Ping., Liu, Jim., Interfacial reaction and shear strength of SnAgCu–xNi/Ni solder joints during aging at 150C, Microelectronic Engineering 86 (2009) 1969–1974

Ye LL, Lai Z, Liu J and Tholen A, “Microstructural Coarsening of Lead-free Solder Joints during Thermal Cycling”, Proceeding of the 2000, Electronic Components and Technology Conference (ECTC), 2000.

Yoon SW, Park CJ, Hong SK, Moon JT, Park LS and Chun HS, "Interfacial Reaction and Solder Joint Reliability in Pb-free Solders in Lead Frame Chip Scale Packages (LF-CSP)," Journal of Electronic Materials, vol.29, no.10, 2000, pp. 1233-1240.

Yoon, J. W. and Jung, S. B., "Effect of Isothermal ageing on Intermetallic compound layer growth at the interface between Sn3.5Ag-0.75Cu solder and Cu substrate " Journal of Material Science, vol. 39, (2004), pp 4211-4217

Zhang, F., Li, M., Chum, C.C., Tu, K.N., Influence of substrate metallization on diffusion and reactions at UBM/solder interface across a solder joint. J. Mater. Res. (2002)

Zhao. Jie., Cheng, Cong-qian., Qi, Lin., Chi, Cheng-yu., Kinetics of intermetallic compound layers and shear strength in Bi-bearing, SnAgCu/Cu soldering couple, Journal of Alloys and Compounds 473 (2009) 382–388

Zhaozhi, Li; Sangil, Lee; Lewis, Brian J; Houston, Paul N.; Baldwin, Daniel F.; Stout, Gene; Tessier, Ted; Evans, John L.; Sensitivity analysis of Pb free reflow profile parameters toward flip chip on silicon assembly yield, reliability and intermetallic compound characteristics, Proceedings of 60th Electronic Components and Technology Conference, Las Vegas, NV, USA, June, 2010

Zeng, K., Vuorinen ,V., Shang, J.K Intermetallic reactions between lead-free SnAgCu solder and Ni(P)/Au surface finish on PWBs, in: Proceedings of the 5th Electronic Components and Technology Conference, Orlando, FL, Piscatway, USA, IEEE, 29 May-31 June 2001, pp685 690.

Zeng,K., Tu, K.N., Mater. Sci. Eng. R 38 (2002) 55–105.

Zeng K, Vuorinen V and Kivilahti JK, "Interfacial reactions between lead-free SnAgCu solder and Ni(P) surface finish on printed circuit boards," IEEE Transactions on Electronics Packaging Manufacturing, v 25, n 3, July 2002, pp. 162-167